

Membrane Based Biogas Upgrading Processes

Von der Fakultät für Maschinenwesen
der Rheinisch-Westfälischen Technischen Hochschule Aachen
zur Erlangung des akademischen Grades
eines Doktors der Ingenieurwissenschaften genehmigte Dissertation

vorgelegt von
Marco Scholz

Berichter:

Univ.-Prof. Dr.-Ing. Matthias Wessling

Prof. Eric Favre, Ph.D.

Tag der mündlichen Prüfung: 11. Oktober 2013

Diese Dissertation ist auf den Internetseiten der Hochschulbibliothek online verfügbar.

Danksagung

Eine Dissertation ist nie das Ergebnis eines Einzelnen. Vielmehr entsteht eine solche Arbeit in enger Zusammenarbeit vieler Personen. Allen die zum Gelingen der vorliegenden Arbeit beitragen haben, möchte ich herzlich danken. Besonderer Dank gilt:

- Prof. Dr.-Ing. Matthias Wessling für die Möglichkeit am Lehrstuhl für Chemische Verfahrenstechnik zu promovieren, für die Betreuung der Arbeit, für viele Ideen, die diese Arbeit bereicherten.
- Prof. Dr.-Ing. Thomas Melin für die Betreuung und die wertvollen Diskussionen zu Beginn meiner Zeit am Institut.
- Prof. Dr.-Ing. Eric Favre für die Begutachtung der vorliegenden Arbeit und interessante Diskussionen.
- Herrn Dr. Torsten Brinkmann (Helmholtz Zentrum Geesthacht) für eine hilfreiche Diskussion zur Modellierung in Aspen Custom Modeler.
- Herrn Mirko Skiborowski (RWTH Aachen) für zahlreiche Diskussionen und Hilfestellungen bei der Modellierung in GAMS.
- Meinen Büro- und Arbeitskollegen Thomas Harlacher, Marc Ajhar, Sebastian Koester und Johannes Völler-Blumenroth für eine stets sehr gute Zusammenarbeit.
- Meinen langjährigen, studentischen Hilfskräften Michael Alders, Stephan Kempkes, Theresa Lohaus und Felix Stockmeier für ihren unermüdlichen Einsatz.
- Den Abschlussarbeitern Christoph Frevert, Sebastian Falß, Sabrina Dahmen, John Linkhorst, Valentin Stelzer, Robin Sluzalek, Seval Varlik, Theresa Lohaus, Ludger Wolff, Gregor Rudolph, Florian Weiß, Jonas Lölsberg, Leo Meyer-Schickerrath, Burkhard Ohs, Julian Niebel, Tankred Schmitt und Dennis Kloss für ihren starken Einsatz und hohe Motivation, die mit ihren Beiträgen wesentliche Ergebnisse zu dieser Arbeit beigesteuert haben.
- Meinen Eltern Martina und Martin Scholz, sowie meiner Schwester Teresa Scholz, die mich schon während des Studiums unterstützt und bestärkt haben.
- Meiner Frau Kathrin und meiner Tochter Charlotte Martina, die immer ein großer Rückhalt sind und stets für einen angenehmen Ausgleich zur Arbeit sorgen.

Vielen Dank!

Aachen, im Dezember 2013

Marco Scholz

*Für Kathrin und Charlotte
Für meine Eltern Martina und Martin und meine Schwester Teresa*

Abstract

Biogas which mainly consists of methane and carbon dioxide is generated by digesting organic wastes, energy crops, manure and sewage. It is mainly used in combined heat and power engines to generate electricity. However, significant amounts of heat are produced along with the electricity which often cannot be used. Thus, upgrading of biogas which is the separation of carbon dioxide from the methane rich gas is more efficient and the product gas can be injected in the natural gas grid.

Conventional biogas upgrading techniques require significant amounts of energy, to regenerate solvents and adsorption materials or to supply low temperatures for cryogenic distillation. Gas permeation membranes are an interesting alternative to conventional gas separation technologies. Due to their moderate energy requirements, their simple and modular installation, gas permeation membranes are most favorable applied to biogas upgrading in the agricultural production.

Gas permeation membranes are also permeable for the gas components to be rejected. In order to obtain high product gas purities and high product recoveries at the same time intelligent multistage gas permeation layouts are required. Due to the infinite number of possible process configurations generic process development most likely results in sub-optimal process designs. Therefore, a superstructure optimization model was used to identify the most promising membrane based process configuration including the optimal process conditions. In addition, the optimal membrane material was determined inherent Robeson's upper bound characteristics. The optimal process layout was converted into a rigorous dynamic process simulation to investigate changes in the process conditions. A process control scheme was determined which maintains the product gas purity over a wide range of variations in the process conditions. The rigorous model of the hollow fiber gas permeation module was implemented in Aspen Custom Modeler and it accounts for non-ideal effects such as Joule-Thomson cooling, concentration polarisation, real gas behavior and pressure losses. Often membranes unfold their full potential when they are combined to conventional gas separation equipment. Hence, the performances of hybrid gas separation systems are compared to conventional biogas upgrading techniques.

The simulation and optimization models developed within this work at hand are not limited to the application of biogas upgrading. An adaptation to other gas separation application can easily be done. Thus, these models allow for a fast, optimal and reliable design of gas permeation processes and they build a valuable fundament for future work.

Zusammenfassung

Biogas besteht hauptsächlich aus Methan und Kohlenstoffdioxid und wird bei der Fermentation organischer Reststoffe, Energiepflanzen, Gülle und Klärschlämmen gewonnen. Oftmals wird das Biogas direkt in Blockheizkraftblöcken verstromt, wobei erhebliche Wärmemengen anfallen, die häufig ungenutzt an die Umgebung abgegeben werden. Eine Alternative zur direkten Nutzung des Biogases, ist dessen Aufbereitung. Dabei wird hauptsächlich Kohlenstoffdioxid vom Methan getrennt, um den Brennwert des Gases zu erhöhen und um ein Produktgas zu erhalten, das als Erdgassubstitut ins Erdgasnetz eingespeist werden kann.

Zum Betrieb konventioneller Biogasaufbereitungsverfahren sind erhebliche Energiemengen erforderlich, um Lösemittel oder Adsorptionsmaterialien zu regenerieren oder um tiefe Temperaturen für eine destillative Trennung bereitzustellen. Gaspermeationsmembranen stellen eine interessante Alternative zu konventionellen Biogasaufbereitungsverfahren dar. Insbesondere der einfache und modulare Aufbau sowie moderate Energieverbräuche machen ein membranbasiertes Biogasaufbereitungsverfahren besonders attraktiv für den Einsatz in landwirtschaftlichen Biogasanlagen.

Gaspermeationsmembranen sind auch für die bevorzugt zurückgehaltenen Gase durchlässig. Um hohe Produktgasreinheiten und hohe Produktgasausbeuten zu erhalten, ist eine intelligente Verschaltung mehrerer Membranstufen erforderlich. Durch die Vielzahl möglicher Prozesskonfigurationen und Prozessparametern führt eine auf Erfahrung basierende Prozessauslegung zu suboptimalen Prozessen. In dieser Arbeit wurde die Methode der Superstrukturoptimierung auf Gaspermeationsprozesse angewandt, um eine optimale Verschaltung von Gaspermeationsstufen und optimale Betriebsparameter zu identifizieren. In einem weiteren Schritt wurde ein optimales Membranmaterial ermittelt und hinsichtlich einer Markteinführung bewertet. Das optimale Biogasaufbereitungsverfahren wurde in ein rigoroses Prozessmodell überführt, um dynamische Prozesssimulationen durchzuführen. Anhand dieser Simulationen wurde ein Regelkonzept für das optimale Biogasaufbereitungsverfahren ermittelt. Zur rigorosen Untersuchung von Gaspermeationsmodulen wurde ein Modell für Hohlfasermembranen in Aspen Custom Modeler implementiert. Das Modell berücksichtigt nicht-ideale Effekte, die beim Betrieb von Gaspermeationsmodulen beobachtet werden. Zu nennen sind: Der Joule-Thomson Effekt, Konzentrationspolarisation, Realgasverhalten und Druckverluste zu beiden Seiten der Membran. Oftmals entfalten Membranen ihr Potential in Kombination mit konventionellen Gastrennprozessen. Daher wurden hybride Gaspermeationsprozesse konventionellen Gasseparationsprozessen gegenübergestellt. Abschließend wurde ein Strukturoptimierungsmodell für das gesamte Biogasaufbereitungsverfahren erstellt, das neben der Abtrennung von Kohlenstoffdioxid, die Separation von Wasserdampf und Schwefelwasserstoff vom methanreichen Gasstrom berücksichtigt.

Die in dieser Arbeit entwickelten und implementierten Simulations- und Optimierungsmodelle sind nicht auf Biogasaufbereitungsprozesse beschränkt. Eine Übertragung auf andere Gastrennprobleme ist leicht möglich. Somit bilden die Prozess- und Optimierungsmodelle eine wertvolle Basis zur schnellen, optimalen und verlässlichen Auslegung von Gaspermeationsprozessen.

Contents

| | | |
|----------|--|-----------|
| 1 | Introduction | 1 |
| 1.1 | Process design methodology | 3 |
| 1.2 | Outline | 9 |
| 2 | Reviewing the state of the art in biogas upgrading | 11 |
| 2.1 | Introduction | 12 |
| 2.2 | The potential of biogas in the energy supply of the future | 13 |
| 2.3 | Process description | 13 |
| 2.4 | State of the art biogas upgrading processes | 15 |
| 2.5 | Membranes for biogas upgrading | 19 |
| 2.5.1 | Selectivity, permeability and permance | 19 |
| 2.5.2 | Membrane materials | 20 |
| 2.6 | Membrane modules | 21 |
| 2.7 | Operating membrane modules | 22 |
| 2.8 | Gas permeation processes | 24 |
| 2.8.1 | Driving force generation | 24 |
| 2.8.2 | Conceptual process design | 27 |
| 2.8.3 | Process equipment | 27 |
| 2.8.4 | Single stage gas permeation processes for biogas upgrading | 29 |
| 2.8.5 | Multistage processes | 32 |
| 2.8.6 | Hybrid processes | 34 |
| 2.8.7 | Upgrading combined with utilization in combined heat and power engines | 36 |
| 2.9 | Installed membrane based biogas plants | 37 |
| 2.9.1 | Membrane based upgrading plants in research and development | 37 |
| 2.9.2 | Commercial membrane based upgrading plants | 37 |
| 2.10 | Future perspectives | 39 |
| 2.11 | Conclusions | 39 |
| 3 | Modeling of hollow fiber gas permeation modules | 41 |
| 3.1 | Introduction | 42 |
| 3.2 | Mathematical description of fundamental equations | 43 |
| 3.2.1 | Material balance | 43 |

| | | |
|----------|---|-----------|
| 3.2.2 | Energy balance | 45 |
| 3.3 | Mathematical description of non-ideal effects | 45 |
| 3.3.1 | Real gas behavior | 46 |
| 3.3.2 | Pressure losses | 47 |
| 3.3.3 | Joule-Thomson Effect | 47 |
| 3.3.4 | Concentration polarization | 48 |
| 3.4 | Additional relevant non-ideal effects | 51 |
| 3.5 | Application of the model in process simulation | 52 |
| 3.6 | Membrane module | 52 |
| 3.7 | Results and discussion | 53 |
| 3.7.1 | Model validation | 53 |
| 3.7.2 | Case studies to evaluate model performance | 55 |
| 3.8 | Pressure dependent permeance | 60 |
| 3.9 | Conclusions | 62 |
| 4 | Structural optimization of a membrane based biogas upgrading process | 65 |
| 4.1 | Introduction | 66 |
| 4.2 | Process model | 68 |
| 4.2.1 | Unit operation models | 70 |
| 4.2.2 | Economics | 72 |
| 4.2.3 | Robeson Plot | 73 |
| 4.3 | Results and Discussion | 76 |
| 4.3.1 | Model validation | 76 |
| 4.3.2 | Superstructure optimization with commercial membranes | 76 |
| 4.3.3 | Identifying the optimal selectivity and permeance | 78 |
| 4.4 | Conclusions | 84 |
| 4.5 | Appendix | 85 |
| 5 | Dynamic simulation and control | 87 |
| 5.1 | Introduction | 88 |
| 5.2 | Upgrading process | 89 |
| 5.3 | Process model | 90 |
| 5.4 | Process control schemes | 92 |
| 5.5 | Results and Discussion | 93 |
| 5.5.1 | Control scheme 1 | 94 |
| 5.5.2 | Control scheme 2 | 102 |
| 5.5.3 | Comparing control scheme 1 and scheme 2 | 104 |
| 5.5.4 | Start up of the process | 105 |

| | | |
|----------|--|------------|
| 5.6 | Advanced control schemes | 106 |
| 5.7 | Conclusion | 107 |
| 6 | Membrane hybrid processes for biogas upgrading | 109 |
| 6.1 | Introduction | 110 |
| 6.2 | Upgrading process | 111 |
| 6.3 | Process description | 111 |
| 6.3.1 | Hybrid process with pressurized water scrubbing | 111 |
| 6.3.2 | Hybrid process with amine scrubbing | 112 |
| 6.3.3 | Hybrid process with cryogenic separation | 113 |
| 6.3.4 | Combination of a gas permeation process and a combined heat and power engine | 115 |
| 6.3.5 | Benchmark processes | 115 |
| 6.4 | Process model | 116 |
| 6.4.1 | Unit operation models and model parameters | 116 |
| 6.4.2 | Economic parameters | 117 |
| 6.5 | Results and discussion | 119 |
| 6.5.1 | Investment costs | 121 |
| 6.5.2 | Operating costs | 121 |
| 6.5.3 | CH ₄ recovery | 122 |
| 6.5.4 | Specific upgrading costs | 123 |
| 6.5.5 | Comparison to conventional technologies | 125 |
| 6.6 | Conclusion | 126 |
| 7 | Superstructure optimization of biogas upgrading processes | 129 |
| 7.1 | Introduction | 130 |
| 7.2 | Process equipment for biogas purification | 130 |
| 7.3 | Process model | 131 |
| 7.4 | Results and discussion | 133 |
| 7.4.1 | Base case | 133 |
| 7.4.2 | Amine process | 140 |
| 7.4.3 | Combined simulation | 142 |
| 7.4.4 | Remarks | 142 |
| 7.5 | Conclusion | 142 |
| 7.6 | Appendix | 144 |
| 7.6.1 | Absorption processes | 144 |
| 7.6.2 | Pressurized water scrubbing | 148 |
| 7.6.3 | Amine scrubbing | 152 |

| | | |
|----------|---|------------|
| 7.6.4 | Glycol scrubbing | 156 |
| 7.6.5 | Membrane process | 159 |
| 7.6.6 | Adsorption processes | 159 |
| 7.6.7 | Drying with silica gel | 161 |
| 7.6.8 | Desulfurization with iron chelates | 162 |
| 7.6.9 | Desulfurization with activated carbon | 163 |
| 7.6.10 | Compressor | 164 |
| 8 | Conclusion and outlook | 167 |
| 8.1 | Summary biogas upgrading | 168 |
| 8.2 | Summary process design | 169 |
| 8.3 | Outlook | 172 |
| | Bibliography | 175 |

Chapter 1

Introduction

Mother nature is fascinating. She converts the most disgusting and foul-smelling material, animal excrement, into one of the most valuable product widely used in our every day life: methane.

The electrical energy supply in western countries is mainly based on fossil fuels such as oil, natural gas and coal, and on nuclear energy production. Natural resources, including uranium, will decline within the near future and the combustion of fossil fuels trigger the greenhouse effect [1]. Hence, a transition to use renewable energy resources has to be made. Technologies to use solar and wind power are available and they often convert these energies directly to electrical energy. Due to strong fluctuations in solar and wind power, electrical energy storage is mandatory, but these technologies are not profitable, yet.

An alternative to solar and wind power is the usage of biogas as a renewable energy resource generated in the agricultural production, in sewage plants and from landfills [2]. Biogas which mainly consists of CH_4 and CO_2 can be used to drive gas engines, combined heat and power cycles, and gas turbines. In contrast to solar and wind power, biogas is produced continuously and it can easily be stored in the natural gas grid after upgrading the raw biogas. In Germany the storage capacity of the natural gas grid is 217 TWh. With an average natural gas consumption of 106 GW, the natural gas grid could provide gas more than 2000h, without being replenished [3]. Hence, an enormous energy storage is already available.

To inject biogas into the natural gas grid the heating value of the gas has to be increased significantly. Gas components such as CO_2 , H_2S and water vapor have to be removed from CH_4 to meet the natural gas standard and to avoid corrosion [4]. Various techniques for conventional gas separation are available to selectively bind CO_2 and to obtain a CH_4 rich product gas which is ready for grid injection. In biogas upgrading chemical and physical absorption, and adsorption technology are applied to separate CO_2 and CH_4 [5]. Recently, gas permeation membranes are also used [2].

Compared to conventional gas separation techniques gas permeation processes are easy to operate, robust and have a small footprint. Moreover, gas permeation membranes do not only remove CO_2 , the ability to permeate H_2S and H_2O is even higher so that these gases could be removed from CH_4 in one single step. Thus, they are an ideal technology for on-farm biogas upgrading. In Germany, more than 93 % of the biogas is generated in the agricultural production [6]. Until now most of the biogas is burned in decentral on-farm combined and heat power engines [7] but often the generated heat cannot be used and consequently the total plant efficiency is low.

Providing an optimized membrane based upgrading process could support the application of biogas upgrading rather than using combined heat and power engines. The upgraded biogas, which is injected to the natural gas grid, can be used in central, efficient and large scale combined heat and power cycles or gas turbines.

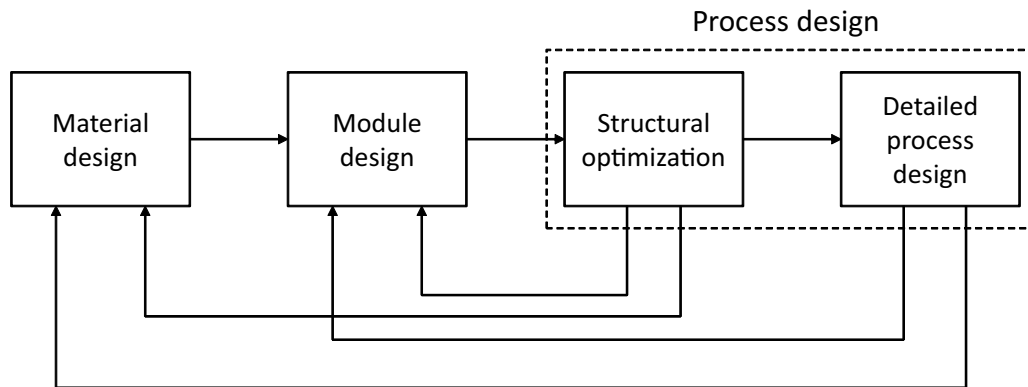


Figure 1.1: Process design methodology in gas permeation. The process determines the material and module design. Appropriate process design can be accomplished by performing a structural optimization first and a detailed process design subsequently. The results from process simulation can be used to define objectives in module and material development.

In this thesis at hand a membrane based biogas upgrading process is developed. Various software tools have been designed and implemented to design, analyze and optimize biogas upgrading processes. The software tools developed within the frame of this work are not limited to the separation of biogas upgrading. They can easily be applied to other gas separation applications for instance the polishing of natural gas, nitrogen and oxygen supply from air and to helium recovery and production.

1.1 Process design methodology

To design a membrane based biogas upgrading process, the methodology illustrated in Figure 1.1 is applied. The four stage procedure starts with selecting an appropriate membrane material and choosing an adequate type of membrane module. Subsequently, the characteristics of the membrane and the module are applied in process design. Performing structural process optimization prior to detailed process design supports the design of the most profitable process configuration. The findings of the process design steps can give an useful indication for future material and module development. In the following section, the process design procedure is described in detail focusing on structural optimization and detailed process design. Extensive literature is available for the selection of the membrane material [8–11] and the type of membrane module [12–14].

The heart of a membrane based separation process is the membrane itself. Membrane materials have to provide adequate permeances and selectivities, and the material has to be mechanically, thermally and chemically stable. Minor components in the feed gas may destroy the membrane material [15] and high carbon dioxide partial pressure may plasticize the membrane material [16]. Although many different materials have been identified to have appropriate separation properties for common gas separations, only nine materials are commercially applied in gas permeation processes [9]. Various

materials such as carbon nanotubes and inorganic membranes have selectivities which are much higher than for conventional polymeric materials. However, these materials cannot economically be manufactured in large quantities, yet. Thus, the crucial issue in material selection is to identify a membrane material with high selectivities and high permeances which is either easy to manufacture or already commercially available.

Membranes are assembled in gas permeation modules. Three different types of modules are common in gas permeation: hollow fiber, spiral wound and envelope type modules. When the raw gas is free of dust and particles, hollow fiber modules are commonly used due to their high packing density. Particles may block the hollow fibers and reduce significantly the separation performance [17]. In contrast, spiral wound and envelope type modules are more tolerant to contamination by particles or dust. The modules operate in counter current, co current or cross flow. In most gas permeation applications counter current flow is preferred, as the driving force for permeation is higher compared to other flow regimes. Details on the various module designs as well as on the operation of membrane modules can be found in [12–14].

The selection of a process configuration is a crucial step in designing gas permeation processes. Here a reliable and cost efficient design have to be found in order to compete with conventional gas separation technologies. The process design can be distinguished into two steps which are the structural optimization and the detailed process design. However, the structural optimization of gas permeation processes is often not performed. Thus, only suboptimal processes are designed and the membrane based separation does not unveil its full potential.

The structural optimization identifies the most economic process configuration by determining the number of membrane stages, the recycles and the connections between the various membrane stages and the compression equipment, respectively. In addition, the optimal process conditions are determined [18, 19]. In particular, the process pressures on the feed and permeate side of the gas permeation stages are calculated. Typically, short cut models for the involved unit operations are applied to perform the optimization. Two different optima can be distinguished which are the economic and the energetic optimum. However, the economic optimum is of higher practical relevance as the energy demand can often be reduced by providing more membrane area. For an economic evaluation capital costs and operational costs, have to be considered together with the sales of the product. Optimizing gas separation process can either be performed by minimizing the process costs or by maximizing the process profit. Constraints such as the purity of the product gas and the required product recovery have to be specified. The optimization model is either a mixed integer nonlinear program (MINLP), in case that process streams exist or not, or it can be a nonlinear (NLP) program when process stream can be split into various streams.

Two strategies to solve such a mathematical program can be distinguished which are i) the applications of solvers which are able to solve the mathematical program directly [20] and ii) the application of evolutionary algorithms [21] which is based on stochastic optimization. Both methods are used to search for the optimal solution in large spaces (for many sets of parameters). Stochastic methods do

Table 1.1: Commercial process optimization software.

| Software | Supplier |
|----------|----------------------------------|
| GAMS | GAMS Development Corporation |
| AMPL | AMPL Optimization LLC |
| AIMMS | Paragon Decision Technology B.V. |
| GLPK | Open source |

not guarantee to identify the global optimum, while direct solution do. Biegler and Grossmann [22] mentioned four methods to solve mixed integer nonlinear problems which are the branch and bound, the generalized benders decomposition, the outer-approximation and the extended cutting plane method. Algorithms to apply these methods are available in a small family of computer codes: GAMS, AMPL, α -ECP and MINOPT. Details on that methods can be found in [22].

The final step of the proposed process design procedure is to size the equipment and to determine the process conditions as precisely as possible. Accordingly, the application of rigorous models for the involved unit operations is mandatory. While short cut models applied in structural optimization typically neglect energy balances, these should be included in the rigorous models to monitor the process temperatures and their effect on the separation performance. Process conditions in which condensation may reduce the separation performance of the gas permeation modules can be detected. The detailed process design analyzes whether critical process conditions such as explosive mixtures are expected during operation. The detailed process design should also survey the process performance for changed process conditions. Variations in the feed flow rate and composition have a strong impact on process performance. Hence, sensitivity analyses over a broad range of process conditions should be performed to identify critical conditions. Finally process control strategies can be established to maintain the required product gas purities for changed feed conditions.

Table 1.1 shows common software packages and the software suppliers which can be applied in structural optimization. All these packages provide a structured framework to develop general data organization. Transforming the problem statements, methods for solving these problems can be applied using sophisticated solvers [23, 24]. Remarkably, the problem formulation is independent of the applied solver so that different solvers can easily be used to calculate the problem. Generally, programs to solve MINLPs do not provide physical and chemical property data. If these properties have to be included in the optimization the respective equations have to be implemented in the model. Accordingly, the complexity of the model increases and often simplified short cut models are used in process optimization. As the software packages to solve nonlinear mixed integer problems are not dedicated to chemical process engineering, only limited tools for process evaluation are available. In GAMS for instance sensitivity analysis can be performed. However, cost and energy evaluation are not facilitated and the user has to program the equations himself.

Table 1.2: Evaluation of gas permeation models.

| | Marriott | Datta | Qi | Kookos | Uppaluri | Lababidi |
|----------------------------|----------|-------|------|--------|----------|----------|
| Multicomponent | + | + | + | + | + | - |
| Real gas | - | - | - | - | - | - |
| Pressure loss bore side | + | + | - | - | - | - |
| Pressure loss shell side | + | + | - | - | - | - |
| Concentration polarization | + | - | - | - | - | - |
| Energy balance | + | - | - | - | - | - |
| Permeance (T,p) | - | - | - | - | - | - |
| Reference | [25] | [26] | [27] | [28] | [29] | [30] |

Table 1.3: Commercial process simulators in chemical process engineering.

| Software | Supplier |
|-------------|-----------------------------|
| Aspen Plus | Aspen Technology Inc. |
| Aspen Hysys | Aspen Technology Inc. |
| UNISiM | Honeywell Process Solutions |
| CHEMCAD | ChemStations Inc. |
| PRO/II | Simulation Sciences |

Table 1.2 lists various studies performed recently on the optimal design of gas permeation network configuration. Most models applied in structural optimization of membrane networks are simple and only the basic mass transfer equations together with mass balances are taken into account. The energy balance and pressure losses are often neglected and constant permeances are assumed. However, for structural optimization detailed models are not necessary as they would increase the computing efforts and detailed calculation of the energy balance is only required if strong temperature effects and their influences are expected (high Joule-Thomson coefficients together with high transmembrane pressures). A detailed description on the superstructure methodology and the respective software packages to solve mixed integer nonlinear problems can be found in [19, 25, 29]. Commonly, five commercial process simulation packages are available for computer-aided detailed process design. Table 1.3 presents these software packages. Most processes in chemical industry involve conventional process equipment. The underlying balances for mass, momentum and energy are only dependent on the process equipment. Hence, it is reasonable to implement these equations

and provide the set of equations in model libraries [31]. These models can be used for numerous sets of compounds and process configurations. In contrast, the physical and thermodynamic properties of the fluids are highly dependent on the substances to be involved and the process conditions. Therefore, these data are provided by extensive property databases [31, 32]. The parameters of various equations of state and Gibbs free energy models determine the physical properties.

Models for process equipment such as heat exchangers, pumps, compressors, distillation columns and absorption columns are available in the aforementioned model libraries. The underlying model equations are usually programmed in FORTRAN- or C-subroutines.

Models for gas permeation modules are not available in commercial process simulation softwares [33]. Models of other membrane based separation technology (e.g. reverse osmosis, pervaporation) are also not provided, since membrane technology is often not considered as state of the art separation technology. Nevertheless, gas permeation models can be incorporated in common process simulation. Applying user defined models is supported by predefined interfaces between the process simulation package and common software development tools. Concerning the Aspen Plus[®] simulation software, user defined models can be programmed in

- Aspen Custom Modeler[®] [12],
- FORTRAN
- or in Microsoft-Excel[®].

Using Aspen Custom Modeler[®] to program a user defined model of a gas permeation module is convenient since the model can either be applied to process simulation or be used as a stand alone model for analyzing gas permeation modules. In Aspen Custom Modeler[®], thermodynamic properties can be applied and the model validation as well as first studies on single stage processes can easily be performed. Implementing the gas permeation model in FORTRAN or Microsoft-Excel[®] is a simple alternative to apply these models in process simulation. By importing user defined models in the Aspen Plus[®] environment, these models can be used in the same way as any other model in the Aspen Plus[®] model library.

Process simulation software supports process development by providing tools for process analysis and design:

- Sensitivity analysis
- Sizing process equipment
- Cost evaluation
- Determining energy demand

Analyzing the influence of process parameters or design parameters on the process performance can be investigated by sensitivity analysis. Here, the parameters are varied within a predefined range and

Table 1.4: Evaluation of gas permeation models.

| | Coker | Marriott | Kalids | Giglia | Davis | Katoh | Makaruk | Mota | Rautenbach | Scholz | Ohlrogge |
|------------------------|-------|----------|----------|--------|-------|-------|---------|------|------------|--------|----------|
| Multicomponent | + | + | + | - | + | + | + | + | + | + | + |
| Real gas | + | - | - | - | - | - | - | - | - | + | + |
| Pressure loss bore | + | + | + | + | - | + | + | - | - | + | + |
| Pressure loss shell | - | + | - | - | - | - | + | - | - | + | + |
| Concentr. polarization | - | + | - | - | - | - | - | - | - | + | + |
| Energy balance | + | + | - | - | + | - | - | + | - | + | + |
| Permeance (T,p) | - | - | + | - | - | - | + | - | - | + | + |
| Flowsheet integration | - | - | - | - | + | - | - | - | + | + | + |
| Reference | [34] | [35, 36] | [37, 38] | [39] | [40] | [41] | [42] | [43] | [44] | [45] | [33] |

their influence on key performance indicators is calculated. The sensitivity analysis is a powerful tool to monitor the impact of changes in composition and flow rates. Constraints can be included while solving the equations to determine the size of process equipment. Economic evaluation packages are available along with most commercial process simulation packages. In Aspen Icarus[®] for instance, operating costs and investment costs can be estimated. For gas permeation equipment the user has to provide this data, since neither models for gas permeation modules nor data to estimate process costs are available. The energy demand of conventional process equipment is calculated along with the balances for mass, momentum and energy. In Aspen Plus[®] the calculation method (e.g. isentropic, polytropic) as well as the equipments efficiencies for determining the energy demand of compressors can be specified.

Various gas permeation models have been programmed for the application in process simulation. Table 1.4 lists and evaluates these models. Most gas separation processes involve more than two gas species to be separated. Therefore, it is mandatory that models for process simulation are capable of calculating multicomponent gas mixtures. Non-ideal effects such as pressure losses, Joule-Thomson cooling, real gas behavior and concentration polarization may have a remarkable impact on the separation performance. The Joule-Thomson Effect can be calculated with the energy balance. The permeance of molecules through polymeric membranes is dependent on temperature and pressure. Hence, Table 1.4 presents whether the models include these effects. The models are also evaluated in terms of integration in conventional process simulators. Therefore, it is evaluated whether the models were applied in process simulation or if any information is given on the flowsheet integration.

Table 1.4 shows that most models can calculate multicomponent mixture and that the calculation of pressure losses on one side of the membrane are taken into account.

1.2 Outline

Figure 1.2 illustrates the structure of the thesis. In Chapter 2 the current state of the art in biogas upgrading is presented. Here, the boundary conditions for the subsequent chapters are set. Furthermore, an overview on membrane based biogas upgrading is given including examples for multistage gas permeation processes.

In order to analyze the gas permeation process a detailed model of a hollow fiber gas permeation module was developed and implemented in Aspen Custom Modeler which is presented in Chapter 3. The model is based on the conservation equations for mass, energy and momentum. Non-ideal effects such as concentration polarization and real gas behavior are accounted for to realistically reflect the separation performance of the gas permeation module. The model is extended and applied in Chapter 5 to analyze the dynamic behavior of the membrane based upgrading process. Moreover, it is used in the steady state process simulation to investigate membrane hybrid processes in Chapter 6. Chapter 4 presents the application of a superstructure optimization model for gas permeation processes. The model was implemented in the General Algebraic Modeling System (GAMS). The process configuration, the required membrane areas and the process pressures are determined simultaneously, by maximizing the profit of the upgrading process. In addition, the model is extended to identify the optimal CO_2/CH_4 selectivity with respect to the upper bound of the Robeson plot. Hence, a simultaneous optimization of process layout, equipment sizes, process conditions and membrane material is performed. For commercial membrane materials a three stage gas permeation process is the most profitable process configuration, while a two stage process is optimal when the membrane selectivity is optimized together with the process layout. The three stage membrane process is analyzed in detail in the subsequent chapters.

In Chapter 5 the dynamic behavior of the three stage gas permeation process is analyzed with regard to changing feed conditions. The dynamic process model including a multistage compressor and process control equipment was set up in Aspen Plus Dynamics. The feed flow rate and the CH_4 content in the feed gas are varied during dynamic simulation. Two different process control schemes to maintain the product gas purity are proposed and analyzed. Both process control schemes operate by changing the pressure on the permeate side of the gas permeation stages. Using the proposed process control schemes, changes in the feed conditions can be compensated within short periods so that product purity is maintained.

Chapter 6 presents a study on membrane hybrid processes which was performed in Aspen Plus. Gas permeation membranes are combined with conventional biogas upgrading techniques to merge the advantages of both technologies. Combinations of gas permeation with amine absorption, pressur-

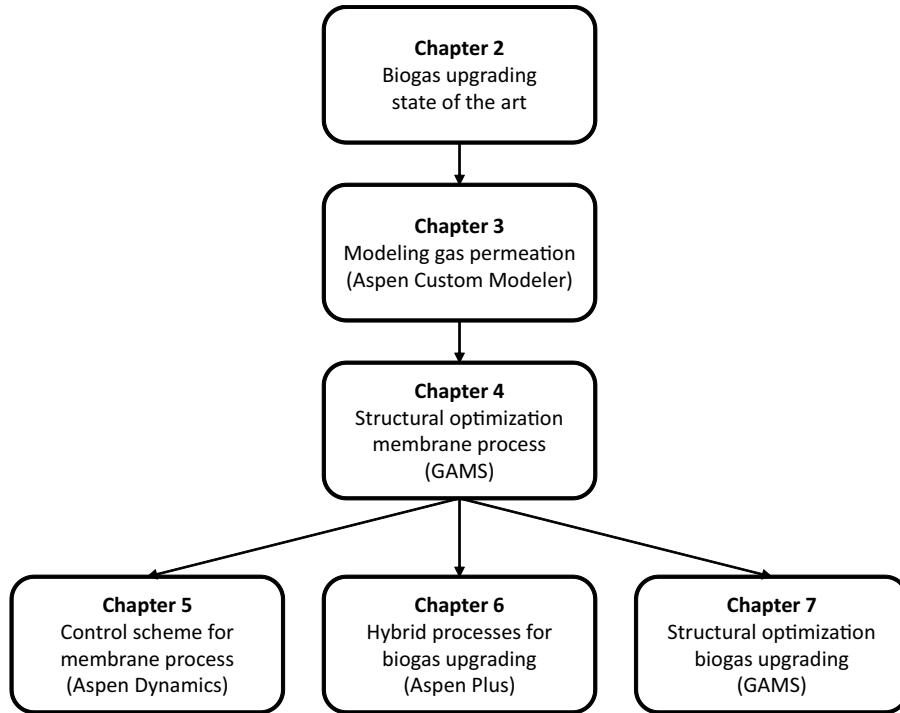


Figure 1.2: Structure of the dissertation.

ized water scrubbing and cryogenic separation are investigated. An additional process which uses the permeate of the gas permeation stage to drive a gas engine is analyzed. In general, the application of a single stage gas permeation membrane improves the upgrading process for conventional gas separation techniques. The three stage gas permeation process is used as a benchmark for the membrane hybrid processes.

Finally in Chapter 7, a process optimization for the entire biogas upgrading process is performed using GAMS. Models of unit operations for CO₂ removal, desulfurization and gas drying have been implemented. A process optimization identifying the most profitable process configuration together with the optimal unit operations and process conditions is presented. Key parameters such as electricity and steam costs have a remarkable impact on the optimal process configuration and process profitability. Sensitivity analyses are conducted to evaluate the impact of electricity, steam and membrane costs as well as of membrane selectivity, feed flow rate and CH₄ content in the feed gas on the optimal process configuration.

Chapter 2

Reviewing the state of the art in biogas upgrading

Parts of this chapter have been published in: Renewable and Sustainable Energy Reviews.

Title: *Transforming Biogas into Biomethane using Membrane Technology.*

DOI: 10.1016/j.rser.2012.08.009.

2.1 Introduction

The transition from a fossil-based energy supply to energy generation from renewable resources is mandatory but still pending [46]. Using biogas generated from organic substances can support this transition [6]. In Europe, the biogas production in 2007 was 69 TWh (for comparison: 600 MW coal fired power plant 5 TWh) [47] but the economic potential has not been exploited, yet [48].

Biogas is either used in combined heat and power engines (CHP) or it is used as a natural gas substitute by removing CO_2 from CH_4 . Today, most biogas plants operate by combusting the gas on-farm in CHPs, which is inefficient when the produced heat cannot be utilized. Hence, the electrical power efficiency is less than 40 % [5, 49, 50].

Upgrading the raw biogas, which is often referred to as biomethane, and supplying this gas to the natural gas grid, seems an attractive alternative to its utilization in CHPs. Biomethane can be used for both energy generation and as feedstock for the chemical industry [51]. In contrast to on-farm CHPs, the supply of biomethane to the natural gas grid and the subsequent utilization of the gas in combined large size heat and power cycles is more efficient as the generated heat is utilized by customers demanding large quantities of heat, such as district heating or industrial customers [52]. Recently, first biogas upgrading plants were installed in Europe and in the US [53, 54] using technologies from the chemical process industry and natural gas treatment to remove CO_2 from CH_4 . These technologies are well established but have drawbacks such as the large size of the equipment and high energy demand. Membrane technology is an alternative to conventional gas separation processes as gas permeation membranes address the aforementioned drawbacks.

Thus, the present study is a review of membrane based biogas upgrading systems. As shown in Figure 2.1, membrane processes have to be designed with a multiscale approach. Appropriate membrane materials, as well as an efficient module and process design, determine the competitiveness with conventional separation technology. In this study, various membrane materials will be presented. Commercial gas permeation module suppliers and their corresponding module designs will be identified. The main focus of the present study is the membrane based process design which includes single and multistage gas permeation processes as well as hybrid processes in which gas permeation modules are combined with conventional separation equipment. Ultimately, a reflection on the future perspectives of membrane based biogas upgrading will be presented.

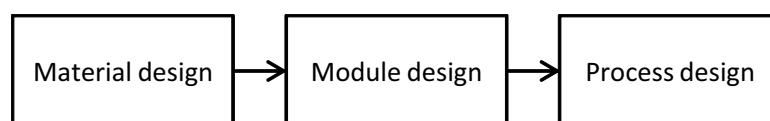


Figure 2.1: Characteristics of membrane process design. First a membrane material has to be selected. Then an adequate module has to be chosen, and finally the module has to be integrated into the process.

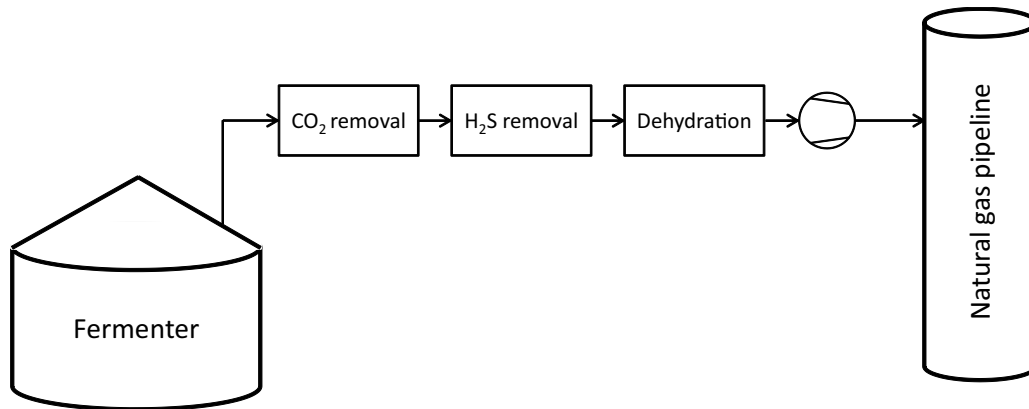


Figure 2.2: Biogas upgrading process illustrating the required separating and polishing steps from the fermenter to the natural gas grid. CO_2 , H_2S , and H_2O have to be removed before the gas is injected into the pipeline.

2.2 The potential of biogas in the energy supply of the future

Biogas is generated by the digestion of organic matter in:

- Sewage plants
- Landfills
- Industrial wastes
- Agricultural production

Hence, biogas can be used as an energy source in industrialized as well as in developing countries. The world energy demand in 2050 will be more than 1000 EJ/a. Resch et al. [55, 56] report that the bioenergy use in 2004 has been 50 EJ. However, they distinguished between four different energy potentials, which are the theoretical, the technical, the realizable, and the mid-term potential. For energy supplied by biomass, they report a theoretical potential of 2900 EJ and a technical potential of 250 EJ. McKendry [57] note that biomass has currently a share of 10 % to 14 % in the world's energy supply. Other studies report that bioenergy will contribute 10 % to the future energy supply [58]. The share of biogas is expected to be 25 % of the total bioenergy [59].

Although the contribution of biogas to the future energy mix seems to be marginal, it is an important energy source in some regions [60–62]. In contrast to solar and wind based energy supplies, biogas is produced continuously, so that it can be used for a base load energy supply.

2.3 Process description

The size of biogas plants in rural areas is limited by the economics of transporting the material for digestion [7, 63]. Typical biogas plants generate raw gas flow rates of less than $4000 \text{ m}^3(\text{STP})/\text{h}$ [5].

Table 2.1: Mole fractions of biogas components ([53]) prior to the upgrading. The typical range of biogas composition is given. As H₂O will condense during the interstage cooling, the mole fractions change significantly.

| Compound | Typical range |
|--------------------------|---------------|
| CH ₄ | 0.45–0.75 |
| CO ₂ | 0.25–0.55 |
| H ₂ O | 0.031 |
| N ₂ | 0.0001–0.05 |
| O ₂ | 0.0001–0.02 |
| H ₂ S | 0.000006–0.02 |
| Organic sulfur molecules | < 0.00002 |
| NH ₃ | < 0.000006 |
| Benzene, toluene, xylene | < 0.000001 |
| Siloxanes | < 0.0000007 |

The raw gas leaves the fermenter at approximately ambient pressure and a temperature of 30°C. Figure 2.2 shows the process steps in biogas upgrading. The biogas is generated in a fermenter and leaves the fermenter saturated with H₂O. The most important cleaning step is CO₂ removal, which is referred to as upgrading the biogas. In addition, H₂O and H₂S have to be removed. Subsequently, the upgraded and cleaned biogas is compressed and injected into the natural gas grid as a natural gas substitute. The sequential arrangement of the various process steps shown in Figure 2.2 depends on the corresponding upgrading technology [5].

Table 2.1 illustrates the raw biogas composition. The raw biogas consists mainly of CH₄ and CO₂ and the composition is highly dependent on the biogas source and the applied substrate for fermentation [64, 65]. Minor components such as H₂S or NH₃ are generated during fermentation and these components also have to be removed before the upgraded gas is fed to the natural gas grid.

In order to inject the gas into the natural gas grid, the gas has to be purified and it has to meet the corresponding pipeline specifications. Table 2.2 presents the pipeline specifications for natural gas injection in the US, in Austria, and in Germany. In the UK, no standard has yet been developed [66]. In the US the CO₂ content is specified, which has to be lower than 2 vol-%, while in Germany the Wobbe-Index is used to control the gas quality.

Table 2.2: Pipeline specifications when supplying upgraded biogas to the natural gas grid: German, Austrian, and US standards.

| | Unit | Germany | Austria | US |
|--|-------------------|----------------|-------------|-----------|
| Wobbe index | $\frac{kWh}{m^3}$ | 15 (12.8–15.7) | 13.25–15.72 | |
| Upper heating value | $\frac{kWh}{m^3}$ | 8.4–13.1 | 10.7–12.8 | |
| Lower heating value | $\frac{kWh}{m^3}$ | | | 9.8–11.4 |
| O ₂ dehydrated gas networks | mol-% | < 3 | < 4 | < 0.2–1 |
| O ₂ not dehydrated gas networks | mol-% | < 0.5 | < 0.5 | < 0.2–1 |
| H ₂ S | mol-% | < 0.0003 | < 0.0004 | < 0.00037 |
| H ₂ O | | < dewpoint | < dewpoint | < 120 ppm |
| CO ₂ | mol-% | | | < 2–4 |
| Ref. | | [4, 67] | | [68, 69] |

2.4 State of the art biogas upgrading processes

Conventional CO₂ separation equipment is well established in the chemical industry. Processes such as physical and chemical absorption as well as adsorption are used in biogas upgrading [70]. In amine absorption processes an absorption column and a desorption column are combined so that the amine solution can be regenerated continuously by heating the amine solution. Hence, the CO₂ is stripped from the amine solution.

The advantage of amine scrubbing is that high CH₄ purities (> 95 %) and low CH₄ losses (< 0.1 %) are achieved [5, 53]. However, the application of amine scrubbing is energy intensive, as steam has to be supplied to regenerate the amine solution. Furthermore, the amine solution is sensitive to impurities of H₂S and thus H₂S has to be removed before the raw gas enters the absorption column. The amine scrubber operates at ambient pressure and the product gas is obtained at this low pressure, so that a subsequent compression is required for gas grid injection. Amines are toxic and malfunction of the upgrading plant may harm the environment and have an impact on the humans and animals at the site. In addition, absorption columns are voluminous. The equipment size is not a crucial issue for biogas upgrading processes at agricultural sites in terms of footprint. However, the equipment size determines the capital costs.

In the pressurized water scrubbing process two columns, one absorption column and one desorption column, are required. CO₂ is absorbed in the H₂O at elevated pressures. The H₂O is regenerated by decompressing the H₂O and by feeding a stripping gas to the desorption column. Accordingly, no heat is required to remove the CO₂ from the H₂O.

The pressurized water scrubbing process operates using only H₂O as a solvent, which is more secure

than applying chemical solvents. The absorption process operates at elevated pressures so that the product gas is already pressurized. Since water scrubbers operate basically at pressures of less than 10 bar, the upgraded gas has to be compressed to grid pressure. Since H_2S cannot be completely removed from the H_2O in the regeneration some of the H_2O has to be removed in order to prevent accumulation of sulfur components in the solvent. The selectivity of absorbing CO_2 and CH_4 is limited, which results in significant CH_4 losses.

In addition to the liquid separation processes, adsorption can be applied to capture CO_2 on solid surfaces [71–73]. In general, adsorption is a discontinuous process, but the application of multiple adsorption vessels transforms the discontinuous process into a continuous process. While one vessel is adsorbing the CO_2 molecules from the bulk CH_4 stream, the other adsorption vessels are regenerated. To adsorb CO_2 molecules, the raw gas has to be compressed. The loaded vessels are regenerated by lowering the pressure in the vessel and the adsorbed molecules desorb. Two types of adsorption mechanism can be used to separate CO_2 and CH_4 , which depend on the solid material. Both rate limited and equilibrium limited adsorption are applied in industrial scale separation systems [74].

Using pressure swing adsorption, gases with high CH_4 purities ($> 98\%$) are produced [5]. However, significant CH_4 losses are unavoidable since some CH_4 also adsorbs on the solid surface. Some pressure swing adsorption suppliers have optimized the system using six vessels, and obtain CH_4 recoveries higher than 98% [5]. The system is rather complex and it requires intensive control and maintenance due to its moving parts (control valves). As the pressure swing adsorption operates at moderate pressure, the purified gas has to be compressed in an additional compressor. Furthermore, there is a tradeoff between CH_4 purity and CH_4 recovery [53].

In order to obtain high purities for both gas components CO_2 and CH_4 , cryogenic separation can be used [75, 76]. However, this separation technique requires large quantities of energy as the gas mixture is chilled down to less than -80°C . The boiling point of CH_4 is at -162°C and the sublimation of CO_2 is at -78.5°C (both at standard pressure). The required CH_4 purity for natural gas grid injection is 96% , but the CH_4 purity obtained from cryogenic separation is significantly higher, which is inefficient. Moreover, cryogenic separation requires large processing equipment. Accordingly, cryogenic separation is not used in biogas upgrading.

Detailed information on conventional upgrading equipment is available in [5, 77]. Table 2.3 compares the various conventional upgrading processes in terms of electrical and thermal energy demand as well as in terms of specific upgrading costs. The energy demand corresponds to the flow rate of the product gas. The specific upgrading cost is related to the energy content of the product gas.

The aforementioned analysis of conventional process equipment for biogas upgrading indicates the following main drawbacks:

- The processes are energy intensive.
- The CH_4 rich product gas is at low pressure.
- Complex systems involving several process steps are required to remove CO_2 , H_2S , as well as

Table 2.3: Comparing conventional upgrading equipment for CO₂ removal. Pressure swing adsorption (PSA), chemical absorption using amine scrubbing, and physical absorption applying pressurized water scrubbing are compared. The data is adapted from a technical report by Fraunhofer Umsicht [5]. * including compression up to 7 bar. ** referred to the product gas

| | unit | PSA | Amine absorption | Water absorption |
|----------------------------|--------------------------|--|---|--|
| Energy demand (el.)* | kWh/m ³ (STP) | 0.25 | 0.15 | 0.25 |
| Energy demand (th.) | kWh/m ³ (STP) | 0.7–0.75 | 0.3–0.8 | - |
| Specific upgrading costs** | Euro cent/kWh | 1.31 | 1.35 | 1.25 |
| Product pressure | bar | 4-7 | 1.1 | 4-7 |
| CH ₄ recovery | - | 0.97 | 0.999 | 0.98-0.99 |
| Supplier | | CarboTech Eng. (D) Cirmac (NL) QuestAir (CAN) Verdesis (CH) | DGE (D) Cirmac (NL) MT-Biomethan (D) CarboTech (D) | Flotech (S, NZ) Malmberg (S) YIT(S) RosRoca (D) |

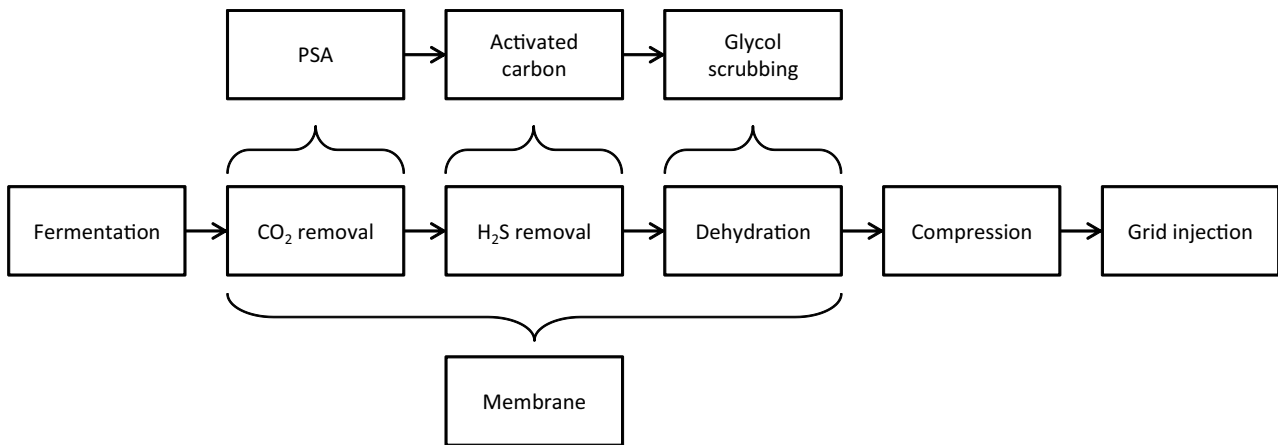


Figure 2.3: The various unit operations in biogas upgrading are shown from the fermenter to the natural gas grid. Generally, each individual separation is done by one individual unit. The membrane system can perform the three separation steps in one step, which is an advantage compared to conventional equipment for CO₂ removal.

H₂O, hence reducing the robustness of the system.

- Large equipment sizes.
- Associated materials such as water, amines, or activated carbon are required.

Membrane based gas separation seems able to address these drawbacks. Typical advantages of gas permeation processes are [78, 79]:

- High energy efficiency
- Low capital costs
- Robustness of the process
- Ease of operation and maintenance
- Small footprint due to high packing densities of membranes in compact modules
- Product gas already at natural gas grid pressure.

A membrane based separation plant is mainly designed to remove CO₂ from the CH₄ bulk. However, trace components in the raw biogas such as H₂S or H₂O permeate even faster through the membrane than CO₂ [80]. Therefore, gas permeation membranes could remove CO₂, H₂S, and H₂O in one step if sufficient driving force for permeation is provided. Figure 2.3 shows that in conventional biogas upgrading processes, the removal of single gas components is performed by individual units.

2.5 Membranes for biogas upgrading

Membrane based biogas upgrading is an alternative to conventional upgrading technologies. In the recent past, gas permeation membranes have frequently been applied to natural gas treatment [9, 69, 79–84]. Therefore, it is reasonable to adapt these membrane processes to biogas upgrading [85, 86], since the gas mixtures involved are similar. However, the process conditions in natural gas treatment and biogas upgrading are different. The natural gas is under pressure when it leaves the natural gas field whereas in biogas upgrading, the raw gas has to be compressed to the pipeline pressure.

Basically, two entirely different membrane processes can be applied for separating CO₂ and CH₄ which are the application of gas permeation membrane [15, 77, 87–89] and membrane contactors [90–92], respectively. Since conventional membrane based gas separation is commonly done by gas permeation, the present study focuses on gas permeation membranes as this technology is already mature and is frequently applied.

2.5.1 Selectivity, permeability and permance

In gas permeation two type of membranes can be distinguished, dense and porous membranes. While porous membranes are only applied in a handful of applications, dense polymeric membranes dominate the gas permeation market. The separation of gases through polymeric membranes is determined by the solution diffusion mechanism, which is based on the solution of the gas molecules at the membrane surface of the feed side, the diffusion of the gas molecules through the membrane and the desorption of the gas molecules at the permeate side of the membrane. Remarkable differences in the solution and diffusion coefficients for different gas species allow for a separation of these gases. The permeability P of a gas species j takes both effects into account:

$$P(j) = S(j) \cdot D(j) \quad (2.1)$$

S and D are the solubility and diffusivity of the gas molecules, respectively. However, the permeability does not take the membrane thickness into account and thus it only reflects the material properties. For a technical application of a gas permeation membrane the permance Q which is

$$Q(j) = \frac{P(j)}{\delta} = \frac{S(j) \cdot D(j)}{\delta} \quad (2.2)$$

is more important as it reflects the membrane properties by taking the membrane thickness δ into account. The selectivity α of a membrane is the ratio of the permeabilities for two different gas species i and j

$$\alpha(i,j) = \frac{P(i)}{P(j)} = \frac{Q(i)}{Q(j)} \quad (2.3)$$

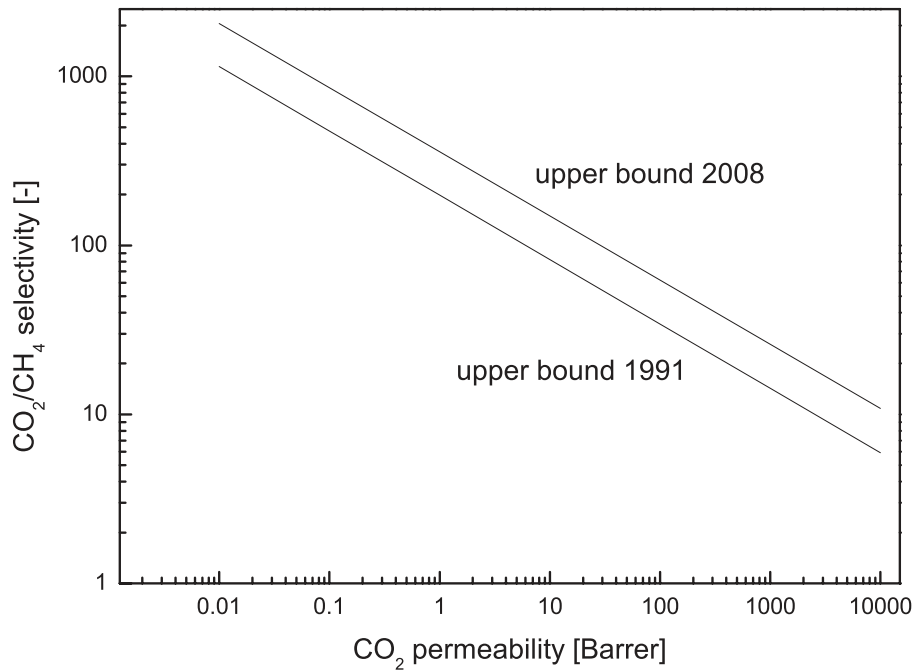


Figure 2.4: Robeson's upper bound curves for CO₂ and CH₄ separation in 1991 and 2008.

and it characterizes the separation performance of the membrane. For multicomponent gas mixtures the selectivity is often reported with respect to the slowest permeating gas species.

Process design aims for both high selectivity and high permeance. However, there exist an inevitable trade-off between these two parameters which was extensively analysed by Robeson. He published trade-off curves for a handful of important gas separations in 1991 and 2008. Figure 2.4 shows both upper bounds for the separation of CO₂ and CH₄.

2.5.2 Membrane materials

The membranes in biogas processes have to withstand harsh process conditions as significant quantities of H₂S and H₂O are present and the gas is pressurized. Thus, the membrane material has to be chemically resistant to those gases. Furthermore, the membrane material has to withstand pressures of more than 25 bar and temperatures of more than 50°C.

Various membrane materials are able to separate CO₂ and CH₄ and both polymeric as well as inorganic materials can be used. However, in industrial scale gas separation, only polymeric membrane materials are applied [9], due to their low manufacturing cost compared to inorganic materials.

Basu et al. [93] have compiled and reviewed current membrane materials for CO₂/CH₄ separation. Table 2.4 presents these materials, their permeability P and CO₂/CH₄ selectivity. The membrane materials are evaluated in terms of technology maturity. Here, materials which are commercially available and which are manufactured in large quantities are referred to as commercial. Materials which have recently been developed and are still under investigation are labeled as research.

Table 2.4: Membrane materials suitable for biogas upgrading were analysed by Basu et al. [93]. The permeability is presented in Barrer. Polymers as well as mixed matrix membranes (MMM) can be applied. In contrast to polymeric membranes which are commercially available, mixed matrix membranes have not reached this stage yet and are under investigation.

| | Material | CO ₂ (Barrer) | α (CO ₂ /CH ₄) | Development |
|---------|------------------------------------|--------------------------|--|-------------|
| Polymer | CA | 6.3 | 30.0 | commercial |
| Polymer | EC | 26.5 | 1.4 | commercial |
| Polymer | PC | 4.2 | 32.5 | commercial |
| Polymer | PDMS | 2700.0 | 3.4 | commercial |
| Polymer | PI | 10.7 | 42.8 | commercial |
| Polymer | PMP | 84.6 | 5.8 | commercial |
| Polymer | PPO | 75.8 | 6.9 | commercial |
| Polymer | PSf | 5.6 | 22.4 | commercial |
| MMM | CNT-PDMS | 190.0 | 5.6 | research |
| MMM | silica nanoparticles-PSf (10 % np) | 9.2 | 24.5 | research |
| MMM | SWNT-PSf(10 % SWNT) | 5.2 | 18.4 | research |
| MMM | Cu-BPY-HFS -PI(30 wt) | 10.4 | 27.5 | research |

Many of the recently developed materials show outstanding permeability and selectivity data, such as SAPO-34 membranes [94–96]. However, it is difficult to manufacture these materials in industrial scale quantities [96] and it is not expected that these materials can be manufactured in industrial scale quantities within the next few years.

Polymeric membrane materials are commonly applied in gas permeation. The most frequently applied and suitable membranes for natural gas treatment are polyimides and cellulose acetate membranes [69, 97]. However, cellulose acetate membranes are sensitive to H₂O. Without pretreatment, cellulose acetate membranes are unsuitable for biogas upgrading [69].

2.6 Membrane modules

For gas permeation, three types of modules exist: hollow fiber, spiral wound, and envelope type modules [12]. Table 2.5 presents and evaluates the various types of gas permeation modules.

Due to the high packing densities, the application of hollow fiber and spiral wound modules is common. The gas is compressed before it enters the membrane system. The compression equipment has to be protected from particles as well as liquids and the corresponding components are removed prior to compression. Hence, hollow fiber modules can be used in biogas upgrading processes

Table 2.5: Comparison of hollow fiber, spiral wound, and envelope type gas permeation modules. Adapted from [14].

| | Unit | Hollow fiber | Spiral wound | Envelope |
|-----------------------------|--------------------------------|--------------|--------------|----------|
| Packing density | m ² /m ³ | < 10000 | 200–1000 | 30–500 |
| Approximate area per module | m ² | 300–600 | 20–40 | 5–20 |
| Costs for module | US-\$/m ² | 2–10 | 10–50 | 50–200 |
| Pretreatment requirements | | high | fair | minimal |

Table 2.6: Comparison of different membrane module designs to be applied to gas permeation. The suppliers labelled with * are no longer active in the field of gas permeation.

| Supplier | Module type | Polymer |
|---------------------------------|---------------|--|
| Air Liquide Medal | Hollow fiber | Polyimide, polyaramide |
| Air Products | Hollow fiber | Polysulfone |
| Cameron former Natco Cynara | Hollow fiber | Cellulose acetate |
| GMT Membrantechnik | Envelope type | Poly(ethylene oxide)-poly(butylene therephthalate) |
| Evonik | Hollow fiber | Polyimide |
| IGS Generon Membrane Technology | Hollow fiber | Tretrabrome polycarbonate |
| Kvaerner Membrane Systems * | Spiral wound | Cellulose acetate |
| MTR Inc. | Spiral wound | Perfluoro polymer, silicone rubber |
| Parker | Hollow fiber | Polyphenylene oxide |
| Praxair * | Hollow fiber | Polyimide |
| Sihi GKSS | Envelope type | Silicon rubber |
| UBE Membranes | Hollow fiber | Polyimide |
| UOP former Grace | Spiral wound | Cellulose acetate |

without further pretreatment. Table 2.6 depicts the membrane module suppliers for treating natural gas streams with the module type and the polymer used to separate CO₂ and CH₄, respectively.

2.7 Operating membrane modules

Operating gas permeation modules is accompanied by various physical effects which may influence the module performance and should be considered when designing gas permeation plants. Figure 2.5 depicts these effects. The permeation of a gas from the pressurized side of a membrane to the unpressurized side can be considered as an isenthalpic decompression of the gas. As the pressure changes due to permeation and the composition of the gas is constant, the temperature has to change (Joule-Thomson Effect). Details on the Joule-Thomson Effect were reported by Coker

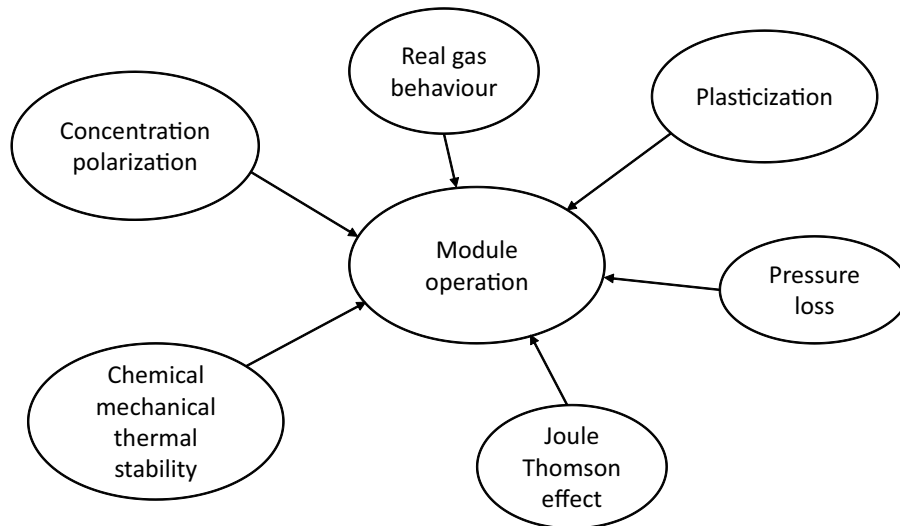


Figure 2.5: Various thermodynamic and physical phenomena influencing module performance in the gas permeation process.

et al. [34], Gorissen [98], Welsch [99] and Scholz et al. [45]. The Joule–Thomson Effect results in significant cooling of both the raw gas on the feed side of the gas permeation module and the gas on the permeate side. The lower temperature in the module influences the thermodynamic behavior of the gas as well as the mass transfer through the membrane [98]. The lower temperature may result in the condensation of gases. The mass transfer of gas molecules through the polymeric membrane materials increases with increasing temperature, while the selectivity decreases with increasing temperature. As permeance decreases with decreasing temperature, a larger membrane area is required to obtain the pipeline purity of the product gas.

Pressure losses in gas permeation modules are common. On both sides of the membrane, pressure losses reduce the driving force of permeation. In general, these pressure losses are small. Nevertheless, pressure losses are pronounced at subambient pressure on the permeate side of the module. A detailed analysis of pressure losses in hollow fiber gas permeation modules was reported by Rautenbach et al. [100] and Scholz et al. [45].

Due to the selective permeation of gas molecules, the retained gas species molecules accumulate at the membrane surface. This phenomenon is referred to as concentration polarization [13, 101, 102]. It is highly dependent on the flux of the components through the membrane and the higher the flux, the more pronounced is the concentration polarization. Concentration polarization reduces the mass transfer through the membrane. Both the process selectivity as well as the flux are reduced. Concentration polarization occurs in the porous support of the membrane and in the boundary layers. Details on the effects of concentration polarization can be found in [45, 101, 102]. The permances of commercially available membrane materials for CO_2/CH_4 separation are generally moderate so that concentration polarization will not be an issue in biogas upgrading.

Since the biogas is delivered at high pressures to the natural gas grid, the real gas behavior of the gas components has to be taken into account [45]. In particular, CO_2 has a pronounced real gas

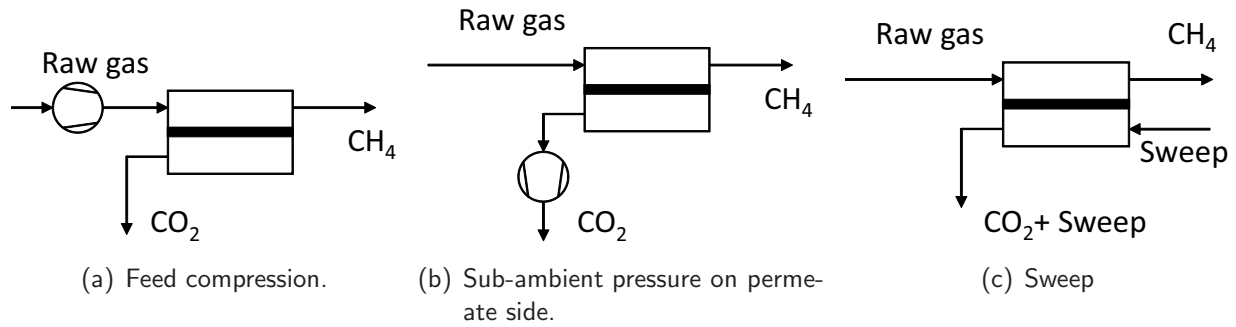


Figure 2.6: Driving force generation concepts for gas permeation.

behavior which reduces the permeation of CO_2 . This effect increases with increasing pressure. More information on the influence of real gas behavior on gas permeation can be found in [103].

It is a well known fact that high CO_2 partial pressure causes significant sorption of CO_2 in the polymer matrix, translating to increased polymer chain mobility [16, 104–107], which is referred to as plasticization. Thus, the mass transport for all gas species through the membrane increases. Moreover, plasticization significantly reduces the selectivity of the gas permeation material. Hence, it is essential to apply polymers with high selectivities as well as high plasticization resistance.

2.8 Gas permeation processes

2.8.1 Driving force generation

In gas permeation, the driving force of permeation is the partial pressure difference Δp_j of the gas components from the feed side to the permeate side,

$$\Delta p_j = x_j \cdot p_F - y_j \cdot p_P. \quad (2.4)$$

Thus in gas permeation, three different methods can be applied to generate the driving force: feed compression, a vacuum on the permeate side, and the application of a sweep gas on the permeate side. Figure 2.6 illustrates these methods. On the left side of Figure 2.6, a gas permeation process is presented in which the feed is compressed and the permeate side operates at ambient pressure. The feed gas which is fed to the gas permeation module remains pressurized as it flows through the module and leaves the module upgraded as retentate stream. Hence, the natural gas pipeline pressure is generated by the compressor, which provides the driving force for permeation.

The central part of Figure 2.6 depicts a gas permeation process which applies sub-ambient pressure on the permeate side of the gas permeation module to provide the driving force of permeation. This process configuration is particularly efficient if small amounts of gas have to be removed from the bulk streams and the components to be removed permeate quickly through the membrane. However,

the generated pressure ratio is limited, due to a minimum applicable pressure of 0.2 bar for large scale vacuum pumps [108]. Moreover, the upgraded biogas is not pressurized and an additional compressor is required to supply the gas at natural gas grid pressure.

Using a sweep stream on the permeate side can be used to generate the driving force of permeation, which is shown on the right hand side of Figure 2.6. Here, the permeate stream is diluted, so that the concentration of the fast permeating components is reduced [109]. The raw gas, the product gas, or an inert gas can be used as sweep gas and it has to be chosen carefully as it influences the process economics. However, using a sweep stream can be inefficient if the permeate is the product since the sweep gas contaminates the permeate stream.

Applying only a sweep gas operation is inappropriate, as only a limited driving force is generated. The maximal applicable driving force by using a sweep gas is

$$\Delta p_j = x_j \cdot p_F - \underbrace{y_j \cdot p_P}_{\approx 0} \quad (2.5)$$

For sweep gas operation, the last term in Eq. (2.5) is approximately 0. Hence, the driving force is linearly dependent on the feed pressure. Without applying any pressure on the feed side, the driving force is limited to a mole fraction of the respective gas components in the feed gas. Assuming a pure gas on the feed side at atmospheric pressure, only a driving force of 1 bar is generated. In addition, the feed gas is not pressurized, so the compression has to be done prior to grid injection. However, using a sweep gas in combination with feed gas compression may be beneficial if an appropriate sweep gas is available [109].

Using feed compression may be efficient since then the product gas is already pressurized. However, as the raw gas contains significant quantities of CO₂, it is also compressed and the corresponding energy is lost when the gas permeates through the membrane. To compare the different methods of generating a driving force, the required energy to drive the process has to be evaluated.

Figure 2.7 depicts the specific energy demand for a single stage gas permeation process as a function of the CO₂ mole fraction in the feed gas. Here, the feed gas is considered as a binary mixture of CH₄ and CO₂. In order to compare the operation in which subambient pressure on the permeate side is used to the compression of the feed gas, a product CH₄ mole fraction of 96 % is specified. The specific energy demand is the ratio of the compressor load P_{el} and the product flow rate $\dot{n}_{product}$:

$$\text{specific energy demand} = \frac{P_{el}}{\dot{n}_{product}} \quad (2.6)$$

The compressor efficiency is assumed to be 0.72. If subambient pressure on the permeate side is applied, the pressure is assumed to be 0.2 bar and the feed pressure is 1.1 bar. When compression of the feed side is applied to generate the driving force, the feed pressure in the gas permeation module is 10 bar. In both cases, the pressure losses of the membrane module are neglected as the

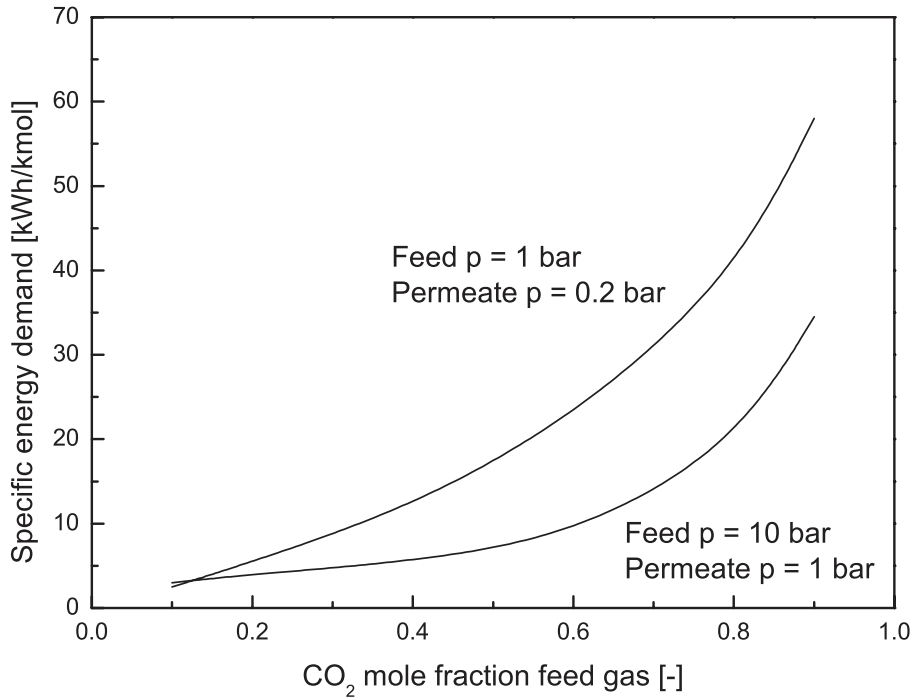


Figure 2.7: The specific energy demand is plotted as a function of the mole fraction of CO₂ in the feed gas. A high pressure operation on the feed side with a pressure of 1 bar at the permeate side is compared to using a sub-ambient pressure of 0.2 bar on the permeate side with a feed gas pressure of 1 bar.

pressure losses are low [45]. The permeate pressure is fixed at an ambient pressure of 1 bar.

Figure 2.7 shows that applying subambient pressure on the permeate side is favorable for CO₂ mole fractions in the feed of less than 15 %. If the CO₂ mole fraction is higher than 15 %, feed compression should be applied. For both a subambient pressure on the permeate side and applying high pressures on the feed side, the specific energy demand strongly increases with increasing CO₂ load in the feed gas. Concerning biogas upgrading, in which the feed gas typically consists of 30 %–50 % CO₂, compression of the feed gas is beneficial.

In conclusion, when upgrading biogases containing CO₂ mole fractions of more than 20 % feed gas, compression should be applied. However, this is a rough estimate and should be used only as an indicator. Three aspects have been neglected. First, a membrane based biogas upgrading process would not consist of a single stage process, as CH₄ losses are pronounced and strongly degrade the economic efficiency of the process. Second, the compressors are modeled as single stage compressors without interstage cooling. Normally, a three stage compressor with interstage cooling would be applied if the gas is to be pressurized up to 16 bar. Biegler et al. [110] gave a rule of thumb for determining the number of compressor stages N :

$$\frac{P_k}{P_{k-1}} = \left(\frac{P_n}{P_0} \right)^{\frac{1}{N}}. \quad (2.7)$$

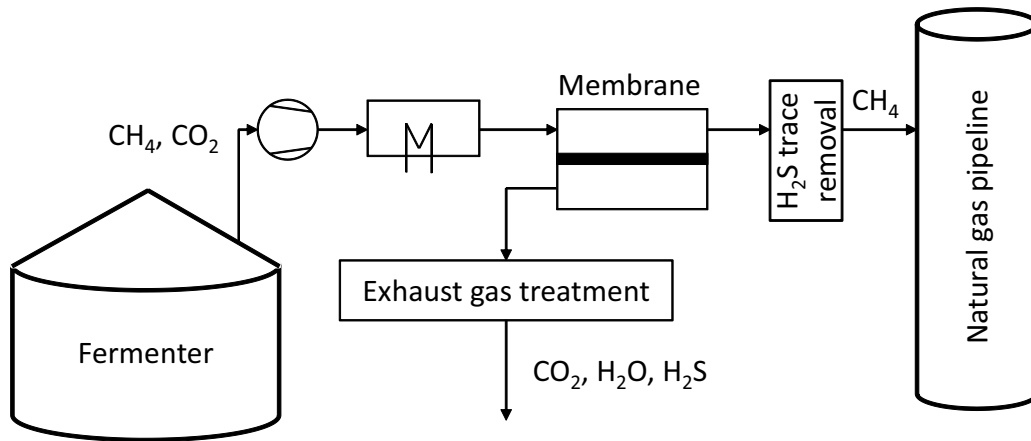


Figure 2.8: The process equipment for a membrane based upgrading process. The raw gas leaving the fermenter is pressurized up to the grid pressure by a multistage compressor using interstage cooling. Subsequently, the gas temperature is controlled in a heat exchanger to protect the gas permeation membrane from high temperatures. In the gas permeation system, the raw gas is split into a CO_2 rich stream which is referred to as the permeate, and a CH_4 rich stream, which is the retentate. The permeate stream is fed to an exhaust gas treatment unit which captures the components not to be fed to the environment.

Here, $\frac{P_k}{P_{k-1}}$ is the pressure ratio per compression stage, which ranges typically between 1.15:1 and 4:1 (see Table 2.7) and $\frac{P_n}{P_0}$ is the pressure ratio for the entire compression. Third, using subambient pressure on the permeate side delivers the product gas at 1.1 bar. Hence, an additional compressor has to supply the pressure to inject the gas into the natural gas grid.

2.8.2 Conceptual process design

Figure 2.8 presents the basic flowsheet of the membrane based biogas upgrading process and the required unit operations when gas permeation membranes are applied. The raw gas is compressed to the required pipeline pressure. The pressure is slightly higher than the pipeline pressure in order to overcome the pressure losses in the upgrading equipment and the piping system. Subsequent to the compression, the gas flows to a heat exchanger to control the gas temperature and to avoid high temperatures in the membrane system. Then the gas enters the membrane system to purify the gas. A fine desulfurization unit lowers the H_2S level when the membrane system is not able to achieve the required H_2S level. Finally, the purified CH_4 enters the natural gas grid.

2.8.3 Process equipment

By upgrading biogas using gas permeation modules, at least four process steps are required, using as equipment: compressors, membrane modules, a heat exchanger upstream of the gas permeation

Table 2.7: Comparison of various compressors which could be applied for generating the driving force. These compressors are evaluated in terms of pressure level, flow rate, and resistance against acidic gases. Adapted from [111].

| | Axial | Centrifugal | Reciprocal |
|------------------------------------|------------|-------------|------------|
| Pressure 25 bar | – | + | + |
| Flow rate 100–2000 $\frac{m^3}{h}$ | + | – | + |
| Pressure ratio | 1.15:1 | 1.7:1–3.1:1 | 3:1–4:1 |
| Particle tolerance | – | – | – |
| Liquid tolerance | – | – | – |
| Changes in gas composition | – | – | + |
| Efficiency | up to 90 % | 83 % | 80 %–92 % |
| Appropriate for biogas | – | – | + |

modules, and the off gas treatment. The membrane modules have explicitly been described in Section 2.6. There are various types of compressors for generating the driving force: axial, centrifugal, and reciprocal compressors. These compressors are frequently applied in the process industry as well as in the energy generation industry. However, the application of these compressors are limited by the pressure level to be generated and by the gas flow rate to be compressed. As the process conditions may be harsh, due to elevated H_2S and H_2O concentrations at high pressures, the compressors have to be resistant to these gases.

Table 2.7 summarizes the criteria which have to be met by the compression equipment in order to compress raw biogas streams. Typical raw gas flow rates of industrial scale biogas upgrading plants range from 100 $\frac{m^3}{h}$ to 2000 $\frac{m^3}{h}$.

A heat exchanger is required to control the gas temperature at the gas permeation module inlet. Due to the compression of the gas prior to the membrane system, the gas temperature increases significantly and hence, the membranes have to be protected against high temperatures. In general, both plate heat exchangers as well as shell and tube heat exchangers can be used. Due to the higher packing density and the application at high pressures of more than 20 bar, it is recommended to use a shell and tube heat exchanger in biogas upgrading.

The exhaust gas leaving the membrane based biogas upgrading system consists mainly of CO_2 . However, significant amounts of H_2S , H_2O , and CH_4 are present in the off gas, which cannot be fed to the ambient. The off gas has to meet strict environmental standards [5] and particularly, the CH_4 content has to be reduced.

The CH_4 content in the off gas determines the selection of the appropriate exhaust gas treatment method. At low CH_4 concentration (< 2 %), a thermal oxidation can be applied to reduce the CH_4 content [5]. At low CH_4 concentrations, the combustion has to be supported by a combustible gas. At elevated CH_4 (2 % – 6 %) concentrations, either a thermal or a catalytic oxidation can be used.

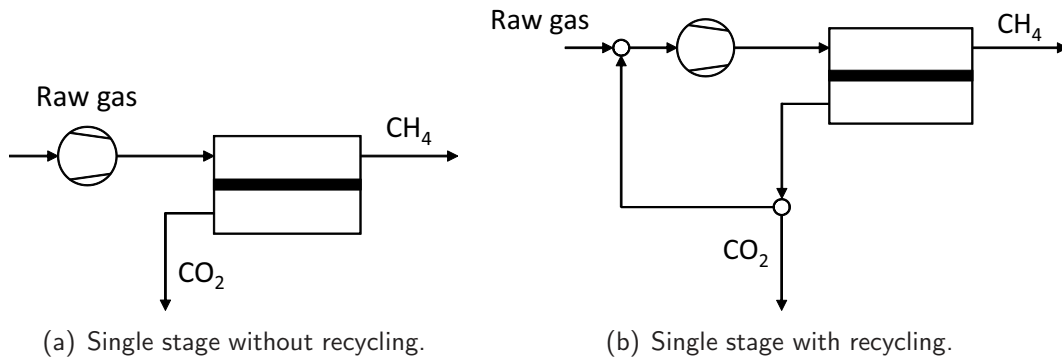


Figure 2.9: Single stage membrane based biogas upgrading process using feed compression. Process a) the permeate flows to the ambient. Process b) the permeate is partially recycled to enhance the CH_4 recovery.

Various tailor-made burners have recently been developed, e.g., the FLOX[®]-burner and the catalytic combustion system ZETECH4[®] (CarboTech, Germany) [5]. For driving the FLOX[®]-burner (e-flox GmbH, Germany), a CH_4 concentration of more than 7 % is required. At low CH_4 concentration, of less than 0.4 %, the recuperative and the catalytic burner of Caverion (Caverion GmbH, Germany) is able to reduce the CH_4 content.

2.8.4 Single stage gas permeation processes for biogas upgrading

Figure 2.9 illustrates two single stage gas permeation processes for upgrading biogas. The process on the left hand side is the most simple gas permeation process to remove CO_2 from CH_4 . However, the CH_4 losses by applying this process are high and determined by the membrane selectivity. The process on the right side shows a single stage process with a partial recycling of the permeate stream. Applying this process, the CH_4 recovery increases significantly [97]. Nevertheless, the CH_4 recovery is limited and cannot reach values of more than 95 % if a CH_4 purity of 96 % has to be achieved. In addition, the partial recycling of the permeate stream drastically increases the flow rate through the compressor and hence increases the energy demand for driving the separation process. Details on single stage processes were investigated by Jaeschke and Ajhar [89].

Figure 2.10 illustrates the trade-off between CH_4 recovery and CH_4 purity. Here, the CH_4 purity is plotted as a function of CH_4 recovery for CO_2/CH_4 selectivities ranging from 20 to 100. The CH_4 product mole fraction increases with decreasing CH_4 recovery. However, the separation performance is dependent on the membrane selectivity. The higher the selectivity, the higher the CH_4 product mole fraction for a specific CH_4 recovery. If a CH_4 recovery of 96 % is considered, the CH_4 mole fraction in the retentate is 66 % for a selectivity of 20 and 79 % for a selectivity of 40. However, for 96 % CH_4 recovery, the CH_4 product mole fraction is 91 % for a selectivity of 80 and 93 % for a selectivity of 100. Thus, the effect of membrane selectivity is less pronounced when high selectivities are considered. Today, commercially available membrane materials have CO_2/CH_4 selectivities of

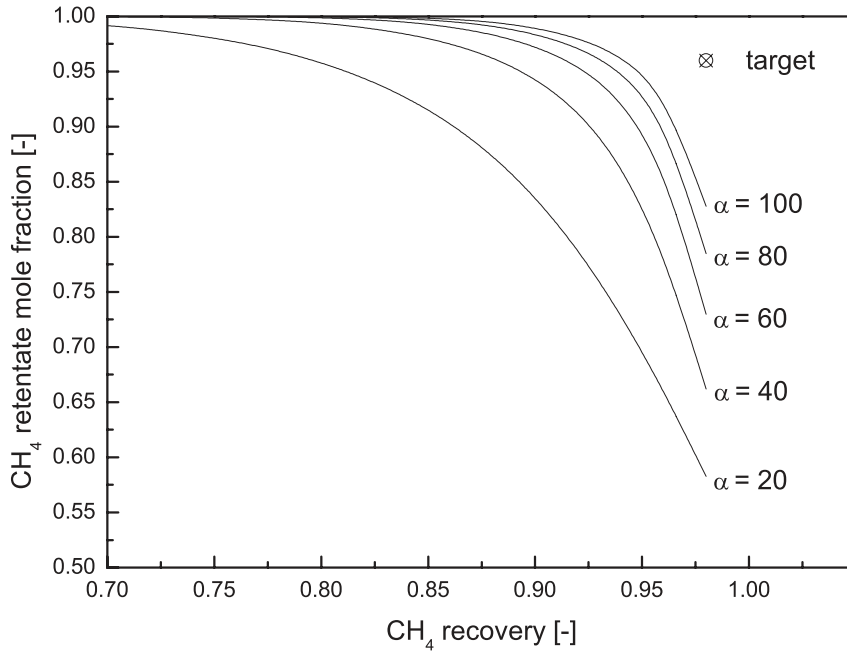


Figure 2.10: Trade-off between CH₄ purity and CH₄ recovery for the separation of 50 % CO₂ and 50 % CH₄. The curves are presented for CO₂/CH₄ selectivities ranging from 20 to 100. The target value for biogas upgrading is illustrated.

about 20 [69]. Furthermore, to take advantage of highly selective membranes, high pressure ratios have to be provided which is energy demanding [112]. Hence, membranes with selectivities of more than 100 cannot effectively be applied.

The permeate mole fraction of CO₂ depends on the pressure ratio, which is the ratio of the feed pressure p_F to the permeate pressure p_P :

$$\phi = \frac{p_F}{p_P} \quad (2.8)$$

Figure 2.11 shows the permeate mole fraction of CO₂ as a function of the applied pressure ratio. The simulations were performed for a binary mixture of CO₂ and CH₄ with mole fraction of 50/50. The permeate pressure is 1 bar and the retentate purity of CH₄ is fixed at 96 %. The dashed line in Figure 2.11 depicts the interface between the regime in which the gas permeation process is selectivity controlled and the region where the pressure ratio most significantly influences the CO₂ mole fraction in the permeate. This interface between the two regions is specified at a value of 90 % of the permeate mole fraction of CO₂ at an infinite pressure ratio which can be determined by [13]:

$$y_{CO_2} = \frac{\alpha x_{CO_2}}{1 - x_{CO_2} + \alpha x_{CO_2}} \quad \text{at } (\phi = \infty). \quad (2.9)$$

Here, x_{CO_2} is the CO₂ mole fraction on the feed side of the gas permeation module and α the membrane selectivity. In Table 2.8 these values are determined for various CO₂/CH₄ selectivities.

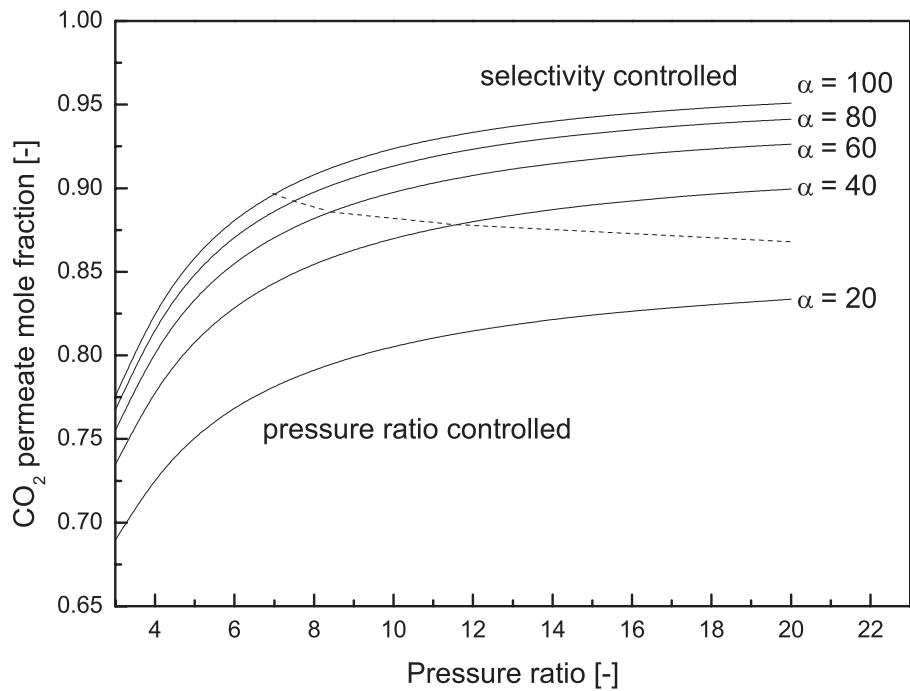


Figure 2.11: Permeate mole fraction of CO_2 as a function of pressure ratio for selectivities ranging from 20 to 100. The dashed line specifies the interface between the regions where the operation is selectivity controlled and where pressure ratio controlled.

Table 2.8: Calculation of the maximal CO_2 mole fraction in the permeate at an infinite pressure ratio. 90 % of the maximal value indicate the interface between the pressure ratio controlled regime and the selectivity controlled regime.

| Selectivity | max. CO_2 | 90 % of max. CO_2 |
|-------------|--------------------|----------------------------|
| 20 | 0.952 | 0.857 |
| 40 | 0.976 | 0.878 |
| 60 | 0.984 | 0.885 |
| 80 | 0.988 | 0.889 |
| 100 | 0.990 | 0.891 |

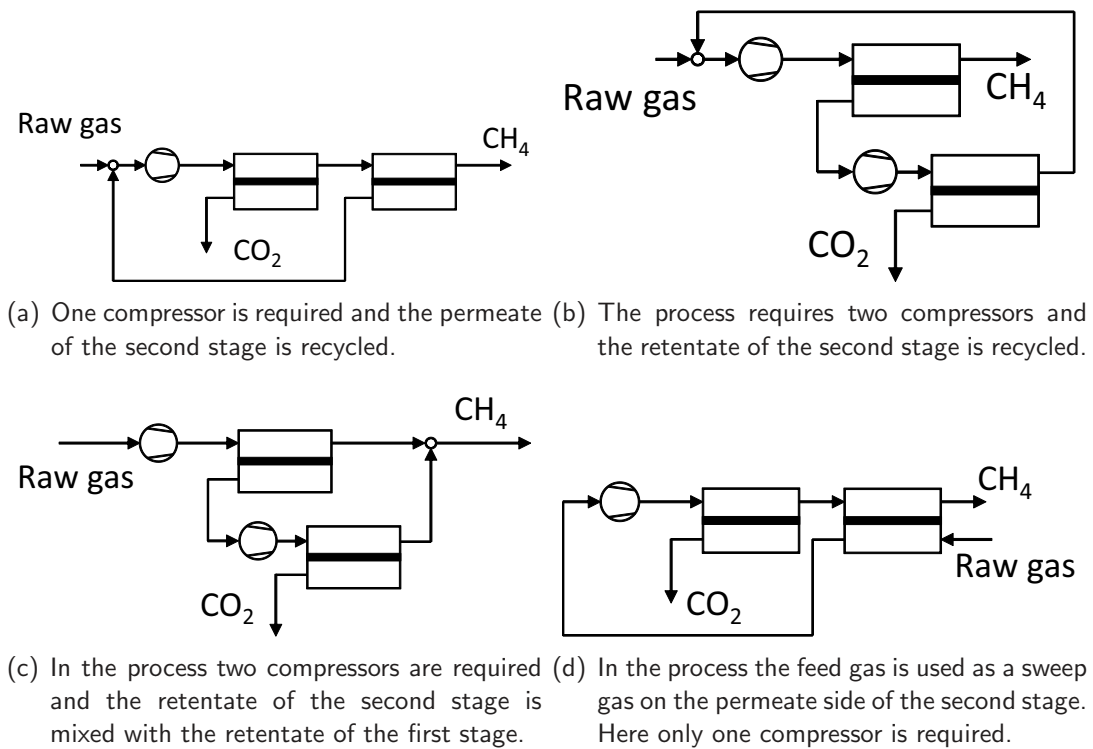


Figure 2.12: Two stage processes for biogas upgrading.

For biogas upgrading, where pressure ratios of more than 16 and selectivities of more than 40 are used, it is likely that the gas permeation module operates in the selectivity controlled region. However, applying single stage gas permeation processes is inefficient, due to significant CH_4 losses. Multistage gas permeation processes can be applied to tackle this drawback.

2.8.5 Multistage processes

Applying various membrane stages in a multistage system is a strategy to obtain high product purity and simultaneously increase the CH_4 recovery of the upgrading system. Figure 2.12 depicts four different two stage upgrading processes. In process a), the first stage removes CO_2 from the raw biogas gas. However, the CH_4 purity of the gas leaving the first gas permeation stage is lower than the required CH_4 purity for grid injection. In order to purify the CH_4 stream, a second membrane stage is applied, which controls the product purity. However, the permeate stream of the second gas permeation stage contains significant amounts of CH_4 and this stream is recycled to enhance the CH_4 recovery.

In process b), which was investigated by Deng et al. [49], the required CH_4 purity is obtained in one step. However, significant amounts of CH_4 permeate through the membrane and a second gas permeation stage is applied to recover CH_4 . A second compressor is required to generate the driving force of permeation for the second gas permeation stage. The CH_4 rich stream of the second stage

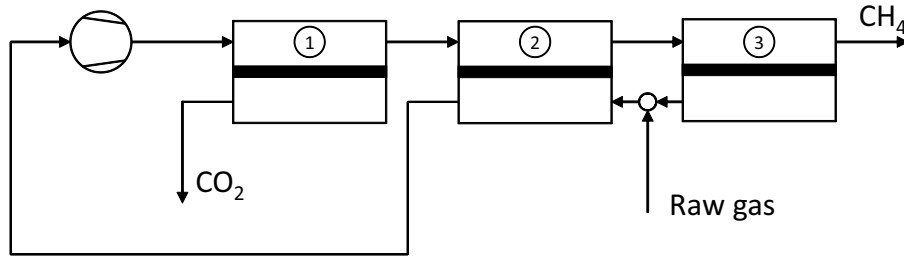


Figure 2.13: Flowsheet of a three stage gas permeation process proposed by Makaruk et al. [42]. Here, the feed is used as a sweep gas to increase the driving force by mixing the permeate of the third stage and the raw gas.

is recycled to the first stage compressor and is mixed with the raw gas.

Process c) is related to process b) [49]. Here, the CH_4 rich stream obtained from the second membrane stage is purified to meet the required purity for grid injection. This stream is mixed with the CH_4 rich stream from the first stage.

In process d) both using a sweep stream as well as compressing the raw gas are applied to generate the driving force of permeation. Here, the raw biogas is used as a sweep gas to increase the driving force in the second membrane stage. This process design is similar to that of process a). The application of the sweep stream is only useful if the CO_2 mole fraction of the permeate of the second stage is higher than the CO_2 mole fraction of the feed stream. Hence, the sweep gas reduces the CO_2 mole fraction on the permeate side of the second stage. The driving force increases and less membrane area is required.

Figure 2.13 shows a three stage biogas upgrading process [42]. This process is similar to process d) in Figure 2.12. The unpressurized raw gas is mixed with the permeate of the third stage. It is important that mixing the raw gas stream with the permeate improves the process by diluting the permeate stream of the second stage. Accordingly, less membrane area is required without increasing the recycle stream.

In Figure 2.14 a three stage membrane process is shown which was recently patented by Evonik Industries [113]. In this process polymeric membranes are applied which have CO_2/CH_4 selectivities of more than 50. In the first stage the bulk of CO_2 is removed from CH_4 . The retentate of the first stage is fed to a second stage in which the final CH_4 purity is adjusted. The permeate of the second stage contains significant amounts of CH_4 . To increase the CH_4 recovery the permeate stream is recycled and mixed with the raw gas stream. In order to further increase the CH_4 recovery the permeate of the first stage which contains only a small fraction of CH_4 is fed to a third gas permeation stage. Here, the CO_2 permeates through the membrane and it leaves the process as exhaust gas. The retentate stream which is enriched in CH_4 is recycled and mixed with the raw gas stream. The driving force for permeation in the third membrane stage is generated by a pressure control valve which adjusts the pressure on the permeate side of the first stage and the pressure on the feed side of the third stage simultaneously.

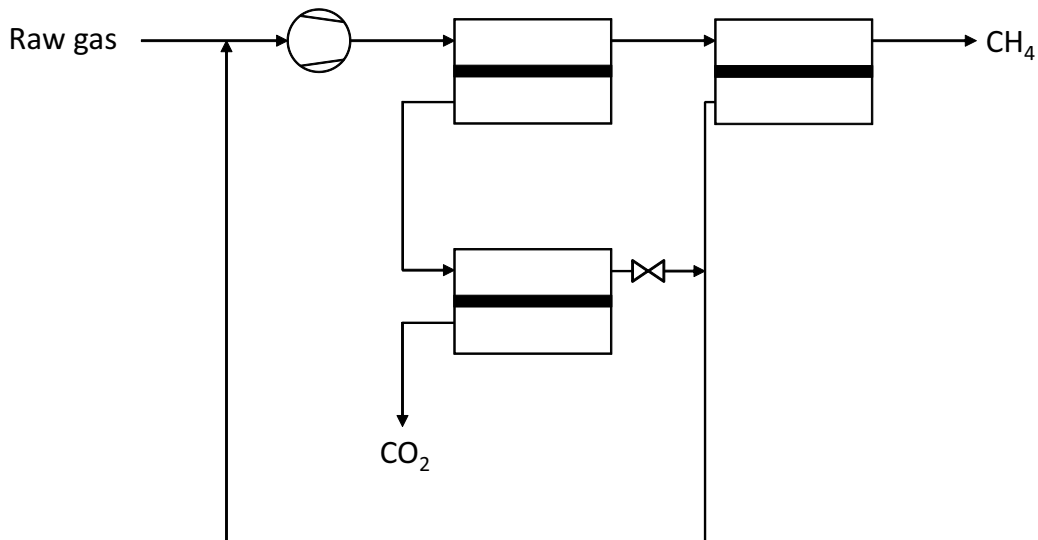


Figure 2.14: Three stage process in which CH_4 purities of more than 96 % and CH_4 recoveries of more than 99 % can be realized.

By applying this process CH_4 recoveries of more than 99 % can be obtained while the CH_4 purity is higher than 96 %. The high CH_4 recovery is generally obtained on cost of the increased recycle stream. However, an increased membrane selectivity reduces the recycle stream. In fact, process data such as specific energy demand for industrial size upgrading plants based on the three stage membrane configuration will be available soon. Thus, we will not include it in the following evaluation (see Tab. 2.9).

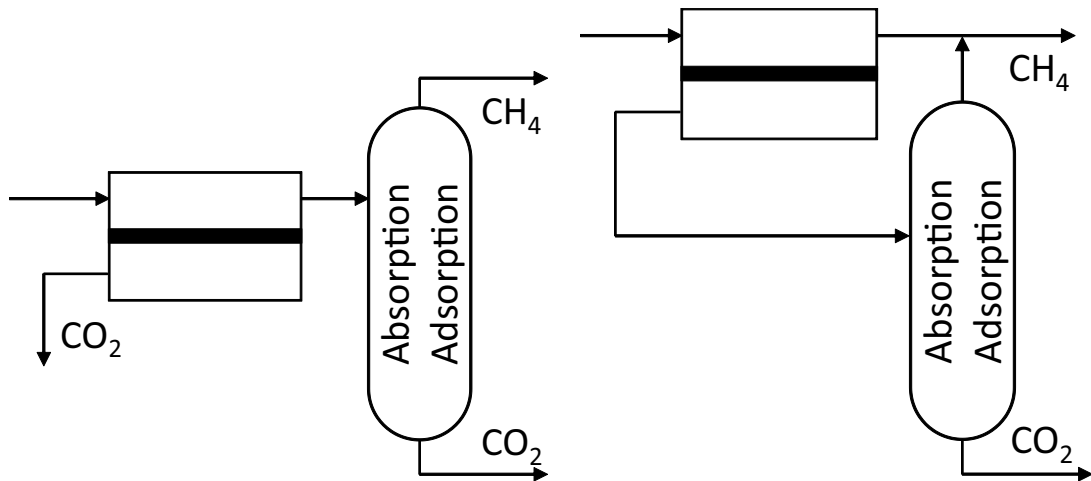
Table 2.9 evaluates the various multistage processes in terms of CH_4 recovery, specific energy demand, specific membrane area requirement, as well as in terms of specific upgrading costs. Process b) from Figure 2.12 has the lowest upgrading costs and the highest CH_4 recovery. Compared to conventional process technology presented in Table 2.3 the membrane processes consume slightly more energy than the conventional processes. The specific upgrading costs are higher than the upgrading costs for conventional upgrading equipment. Nevertheless, using a membrane system the product gas is supplied at natural gas grid pressure so that no additional compression is required. In conventional processes, the gas is supplied at low to moderate pressure. Thus, the energy and the costs for compression to grid pressure are not included in the specific energy demand and the upgrading costs. Therefore, the total upgrading costs including the compression to grid pressure should be used to compare the different technologies and thus membrane based systems become more attractive.

2.8.6 Hybrid processes

Gas permeation processes are quite efficient for moderate purification of gases [79]. To obtain high purity products from a gas permeation stage requires either a large membrane area or strong driving forces, which translates to significant operational costs. Hybrid processes in which membrane

Table 2.9: Various gas permeation upgrading processes are compared in terms of energy demand, CH₄ recovery, required membrane area, and specific upgrading costs. Permeance of CO₂ 66.67 GPU; Permeance of CH₄ 2.08 GPU.

| | CH ₄ recovery | Specific energy kWh/m ³ | Specific area m ² h/m ³ | Upgrading costs US-\$/m ³ | Supply pressure bar | Ref. |
|------------------------------------|--------------------------|---------------------------------------|--|---|------------------------|------|
| Single stage | 0.855 | 0.277 | 1.70 | 0.228 | 20 | [49] |
| Two stage (Figure 2.12 process a)) | 0.957 | 0.318 | 1.92 | 0.220 | 20 | [49] |
| Two stage (Figure 2.12 process b)) | 0.997 | 0.286 | 1.69 | 0.201 | 20 | [49] |
| Two stage (Figure 2.12 process c)) | 0.973 | 0.295 | 1.57 | 0.206 | 20 | [49] |



(a) Hybrid process in which the membrane removes the bulk of CO_2 and the conventional process equipment further polishes the gas stream. (b) The conventional gas separation equipment is used to recover the CH_4 lost in the permeate of the membrane stage.

Figure 2.15: Hybrid processes for biogas upgrading.

technology is combined with conventional gas separation equipment may be superior to the individual processes in which only one single technology (i.e. amine scrubbing, membrane technology) is applied [69].

Figure 2.15 illustrates two hybrid processes for biogas upgrading. In process a), the gas permeation stage is used to perform the bulk separation of CO_2 and CH_4 so that only moderate CH_4 purities are obtained from the membrane stage. The conventional process equipment downstream of the gas permeation stage polishes the CH_4 stream. Two exhaust gas streams enriched in CO_2 are generated. In process b), the gas permeation stage is applied to obtain the CH_4 purity in a single membrane stage. However, as demonstrated in Section 2.8.4, the permeate stream contains significant quantities of CH_4 , which should be recovered. The permeate stream from the membrane stage flows to the conventional gas separation equipment. Here, the size of the equipment is small, as the permeate stream is generally less than 50 % of the raw gas stream. The recovered CH_4 can be pressurized and mixed with the product from the gas permeation stage.

2.8.7 Upgrading combined with utilization in combined heat and power engines

Gas permeation processes can be linked efficiently with combined heat and power engines [114]. Here, the permeate of the membrane stage contains CH_4 for driving the combined heat and power engine. This option is quite promising, as the heat generated at the engine can be used efficiently for heating the fermentation process. A detailed investigation of such a process was recently carried out by Makaruk and Harasek [114].

2.9 Installed membrane based biogas plants

Although membranes show remarkable performance in upgrading biogas, only a limited number of membrane based upgrading plants have been installed. Table 2.10 lists the plants which have been installed in the last few years in Europe and the US. In principle, two categories of biogas upgrading plants are distinguished: commercial plants and plants installed for research.

2.9.1 Membrane based upgrading plants in research and development

In 1989, Rautenbach and Welsch [87, 115] constructed a biogas upgrading plant which operated for more than two years at a landfill in Germany. The flow rate of the raw gas was $200 \text{ m}^3(\text{STP})/\text{h}$ and the gas was supplied to the natural gas grid at 35 bar. Polyimide hollow fiber modules (UBE Industries) with an area of 700 m^2 were installed. They analyzed various multistage processes and identified a two stage cascade with a recycle of the second step permeate as a simple and reliable upgrading process (see Figure 2.12 process a)). In addition, they analyzed the influence of the Joule–Thomson Effect on the permeation performance.

Stern et al. [15] built a membrane based biogas upgrading plant which was installed to upgrade gas generated by a municipal waste water treatment plant. The flow rate was $3.4 \text{ m}^3(\text{STP})/\text{h}$ and the CH_4 mole fraction of the feed gas was 63 % balanced with CO_2 and small amounts of organic compounds. However, the raw gas was compressed to 55 bar to supply both the pressure to drive the separation process and the required grid pressure. A single stage process was implemented, to investigate the separation performance of the gas permeation modules.

Makaruk and Harasek [114, 116] presented experimental results from a gas permeation plant which produces natural gas substitute for utilization as fuel gas and for grid injection. A two stage membrane cascade was installed with recycling of the second stage permeate (see Figure 2.12 a)). The upgrading plant produces $100 \text{ m}^3(\text{STP})/\text{h}$ of biomethane with a CH_4 purity of 98 %.

2.9.2 Commercial membrane based upgrading plants

In Europe only a limited number of membrane based biogas upgrading plants exist. Recently, some plants were installed using polymeric membrane materials. In the US, various membrane based upgrading plants were installed by Air Liquide. Here, a short overview of the existing plants is given. The first commercial gas permeation based biogas upgrading facility in Europe was installed in 1990 in Collendoorn (The Netherlands). The raw gas is produced from a landfill and $25 \text{ m}^3(\text{STP})/\text{h}$ are injected into the natural gas grid. Hollow fiber membranes (Cirmac) produce a moderate CH_4 purity of 88 %.

In 2010, Bebra Biogas installed a two stage biogas plant in Kisslegg-Rahmhaus (Germany) with a

Table 2.10: Installed membrane based biogas upgrading plants. Flow rates labelled with * refer to the raw gas flow rate.

| Country | Location | Operating since | Product flow rate [m ³ /h] |
|-----------------|---------------------|-----------------|---------------------------------------|
| The Netherlands | Collendoorn | 1990 | 25 (today 375) |
| The Netherlands | Beverwijk | 2006 | 80 |
| US | Raeger (PA) | 2006 | 4721* |
| US | Johnson City (TN) | 2006 | 2361* |
| Austria | Bruck an der Leitha | 2007 | 100 |
| US | Kersey (PA) | 2007 | 14164* |
| US | Imperial (PA) | 2007 | 7082* |
| US | Cairnbrook (PA) | 2007 | 4721* |
| US | Davidsville (PA) | 2007 | 2361* |
| US | Oklahoma City (OK) | 2008 | 2361* |
| US | Church Hill (TN) | 2008 | 2361* |
| US | Winder (GA) | 2008 | 7082* |
| US | Atlanta (GA) | 2009 | 8263* |
| US | Seattle (WA) | 2009 | 18886* |
| Germany | Kisslegg-Rahmhaus | 2010 | 300 |
| The Netherlands | Witteveen | 2010 | 200 |
| US | Pittsburgh (PA) | 2010 | 4721* |
| US | New Orleans (LA) | 2010 | 10623* |
| Austria | Wiener Neustadt | 2011 | 120 |
| US | Athens (TN) | 2011 | 3541* |
| US | San Diego (CA) | 2011 | 2361* |
| US | Fresno (CA) | 2011 | 2361* |
| Norway | Lillehammer | 2012 | 30 |
| UK | Poundbury | 2012 | 650 |
| Germany | Sachsendorf | 2012 | 150 |
| Switzerland | Pratteln | 2012 | 210 |
| Germany | Zeven | 2012 | 250 |

capacity of 300 m³(STP)/h upgraded biogas. A CH₄ purity of 98.7 % is achieved and the plant operates at feed pressures of 5–7 bar. The CH₄ mole fraction in the permeate ranges between 3 % to 8 %. Prior to the gas permeation stage, the gas is dehydrated by condensation and the H₂S is removed by activated carbon. Two stage compression equipment is installed.

In the US, the first membrane based upgrading plant was installed in 1993 at a landfill in Los Angeles County with a capacity of 2600 m³/h raw gas. The product gas is used as fuel and has a CH₄ purity of 97.5 %. The membranes were provided by UOP (SeparexTM).

2.10 Future perspectives

We expect that membrane based biogas upgrading will be frequently used as a future upgrading technology due to

- An enhanced acceptance of membrane technology by biogas users, plant designers, and gas suppliers, caused by the currently installed reference plants.
- Easy and robust operation as well as the energy efficiency of the gas permeation system.
- High CH₄ recoveries, of more than 99.5 %.
- Improved membrane materials with selectivities higher than 60 and adequate permeances.
- Exploration of the biogas upgrading market for small upgrading plants (< 100 m³(STP)/h) where membrane based biogas upgrading is particularly efficient.
- The general trend to exchange combined heat and power engines by upgrading equipment.
- The great potential of biogas utilization in India [117–121] and Brazil [122–124]

Research challenges in membrane based biogas upgrading include:

- Stability against minor components such as H₂S
- Plasticization of polymeric membrane materials at elevated CO₂ partial pressures

2.11 Conclusions

In this current study concepts for membrane based biogas upgrading processes are presented. The biogas upgrading process as well as conventional upgrading processes and their characteristics are presented as a benchmark for the membrane process. Gas permeation processes have outstanding properties which make them superior to conventional gas separation equipment in biogas upgrading.

However, single stage membrane processes are not able to upgrade the raw biogas economically and limits of the gas permeation process are discussed in detail. Nevertheless, the typical trade-off between product gas purity and CH₄ recovery can be dismantled by applying multistage gas permeation networks. Here, high CH₄ purities as well as high CH₄ recoveries can be obtained at the same time.

The increased application of membrane based biogas upgrading in the future is expected. The development of polymeric membrane materials which are easy to manufacture and have high CO₂/CH₄ selectivities will fuel the application of gas permeation membranes. In addition, many small scale on-farm combined heat and power engines will be replaced by biogas upgrading equipment as the generated heat cannot be used efficiently. Ultimately, gas permeation systems are an excellent technology to upgrade biogas as the upgraded gas is delivered at natural gas grid pressure and no additives such as organic solvents are required to purify the raw biogas.

Chapter 3

Modeling of hollow fiber gas permeation modules

Parts of this chapter have been published in: Industrial & Engineering Chemistry Research.

Title: *Modeling Gas Permeation by Linking Non-Ideal Effects.*

DOI: 10.1021/ie202689m.

3.1 Introduction

Models for process simulation are important for analyzing how small changes in gas processing efficiency translate to significant improvements in cost-effectiveness. Exactly predicting the operation of gas permeation modules requires the simulation of non-ideal module behavior.

Within the past decade, many studies have modelled gas permeation processes. For example, Ohlrogge compiled and compared various gas permeation modules [125]. Most of these cited models focus individually on particular non-ideal effects such as concentration polarization, the Joule-Thomson Effect, real gas behavior and pressure losses.

The phenomenon of concentration polarization has been extensively investigated by Mourgues and Sanchez [101]. They note that concentration polarization becomes significant when the gas permeation membrane has selectivities of 100 and permeances of higher than 1000 GPU for the faster permeating component. Their model, however neglects real gas behavior and assumes isothermal conditions. This model also cannot be used in flowsheeting software such as Aspen Plus[®] to perform more complex process simulation.

A few studies reported about Joule-Thomson cooling in gas permeation [98]. Rautenbach and Dahm [88] investigated temperature in gas permeation modules for separating CO₂ and CH₄. Coker et al. [34] programmed a model to analyze the Joule-Thomson Effect also for CO₂/CH₄ separation but it cannot be applied in process simulators. Pressure losses on the shell side of the gas permeation module are also not considered.

Pressure losses along the flow channels of feed and permeate are either modelled using Hagen-Poiseuille type of differential equation [37, 78, 126, 127], using experimental data [36] or are neglected [40]. When pressure losses are taken into account the pressure on the shell side of hollow fiber gas permeation modules is often assumed to be constant [37].

Often conventional gas permeation models assume ideal gas behavior [39, 44] for each gas component to be separated. A few studies analyze the influence of real gas behavior on module performance [33, 103, 128]. However, the latter study focuses on modelling envelope type gas permeation modules.

As shown above, conventional gas permeation models are either unsuitable for process simulation or often do not account for non-ideal effects as a whole. Thus, this current study presents a new model which addresses these problems: it can be used in process simulation and it considers all of the aforementioned non-ideal effects together. The applied equations for a hollow fiber gas permeation module have been programmed using Aspen Custom Modeler[®] (ACM). Up to now only a temperature dependent permeance is implemented. The pressure and composition dependence of permeance can easily be included by providing a polynomial interpolation of mixed gas data.

Using this comprehensive model, we quantify in two studies how the accumulation of non-ideal effects influence the simulation results for the module performance. The simulation results are verified by mixed gas membrane separation data and by literature data published by Pan [129].

Table 3.1: Model parameters for the simulation of a hollow fiber membrane module.

| Model parameters |
|-------------------------------------|
| Outer fiber diameter |
| Porous support thickness |
| Fiber length |
| Fiber packing density |
| Heat transfer coefficient |
| Number of fibers |
| Permeance of each component |
| Activation energy of each component |

3.2 Mathematical description of fundamental equations

The model of a hollow fiber membrane module was programmed in Aspen Custom Modeler[®] (version 2006.5) which is part of the Aspen Tech simulation engine. Designed to simulate steady-state, this model can simulate multicomponent mixtures and can be extended to a dynamic simulation model. The model parameters include geometric as well as material properties summarized in Table 3.1. Module properties such as the pure gas permeances, the activation energy for the temperature dependent permeance, and the heat transfer coefficient have to be obtained from experimental analysis.

3.2.1 Material balance

The ACM model is based on ordinary material balances for each gas component. Both counter-current flow as well as co-current flow conditions can be modeled with the presented model. Since counter-current flow is often advantageous over co-current flow [12], this whole study deals with counter-current operation. The differential mole balances for the retentate and the permeate are:

$$\frac{d\dot{n}_R}{dx} + \dot{n}'' W = 0 \quad (3.1)$$

$$\frac{d\dot{n}_P}{dx} + \dot{n}'' W = 0 \quad (3.2)$$

whereby, \dot{n}_R and \dot{n}_P refer to the molar flow rate on the retentate side and the molar flow rate on the permeate side, respectively. The flux through the membrane is designated by \dot{n}'' . In Figure 3.1

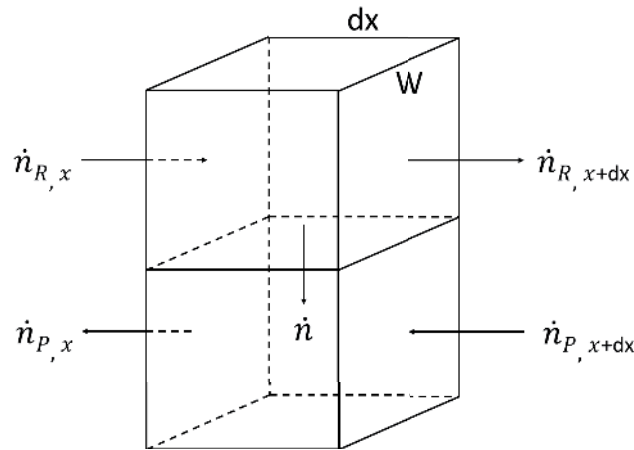


Figure 3.1: Material balance for the retentate side and the permeate side of the gas permeation module.

W delineates the width of the module that is quantified as:

$$W = nof \cdot \pi \cdot d \quad (3.3)$$

Whereby the term nof and d designate the number of hollow fibers and the outer fiber diameter, respectively. The material transfer through the membrane \dot{n}'' is modeled by applying the solution diffusion model and by assuming:

- Pressure-independent permeances
- No coupling of the permeating species
- Equal chemical potentials between gas and membrane phase

Accordingly, the flux of component j is:

$$\dot{n}_j'' = Q_j (x_j p_F - y_j p_P) \quad (3.4)$$

The empirical determined permeance Q_j and the partial pressure difference specify the mass transfer of the component j through the membrane. Here, x_j and y_j delineate the mole fraction of the gas components on the retentate side and on the permeate side, respectively, whereby p_F is the feed pressure and p_P is the pressure of the permeate side.

3.2.2 Energy balance

As thermodynamic effects may accompany gas permeation processes [10], it is essential to include the energy balance describing the temperature along the membrane module. The counter-current energy balance for the retentate side and for the permeate side are:

$$\underbrace{\frac{d\dot{H}_R}{dx}}_{\text{ret. enthalpy}} + \underbrace{\dot{n}'' W h_{Mem}}_{\text{perm. enthalpy}} + \underbrace{k(T_R - T_P)W}_{\text{heat transfer}} = 0 \quad (3.5)$$

$$\frac{d\dot{H}_P}{dx} + \dot{n}'' W h_{Mem} + k(T_R - T_P)W = 0 \quad (3.6)$$

Here, \dot{H}_R and \dot{H}_P delineate the enthalpy of the gas on the retentate side and the enthalpy of the gas on the permeate side, respectively. The temperatures on the feed side and on the permeate side are T_R and T_P , respectively. The molar enthalpy of the flow permeating through the membrane is h_{Mem} .

Both Equations 3.5 and 3.6 are based on three different phenomena: the change in enthalpy along the hollow fiber, the heat transfer through the membrane due to temperature difference on both sides of the membrane and the enthalpy transferred by permeation.

The transferred heat depends on the heat transfer coefficient k of the membrane material (mainly the porous support layer) which has to be determined experimentally or is available in literature. The temperature and pressure to determine the molar enthalpy of the permeating stream are assumed to be equal to the temperature and pressure on the feed side [34].

3.3 Mathematical description of non-ideal effects

By operating gas permeation membrane modules, various non-ideal effects may be observed. In this current study, the following non-ideal effects are considered:

- Real gas behavior, in particular, upon applying pressures of more than 10 bar [125]
- Pressure losses on the bore side and shell side of the module [17]
- The Joule-Thomson Effect if significant amounts of CO₂ permeate through the membrane [34]
- Concentration polarization in case of high permeable membranes

Depending on the separation process, these effects have to be taken into account to accurately describe the module performance. The real gas behavior depends on the gas components involved

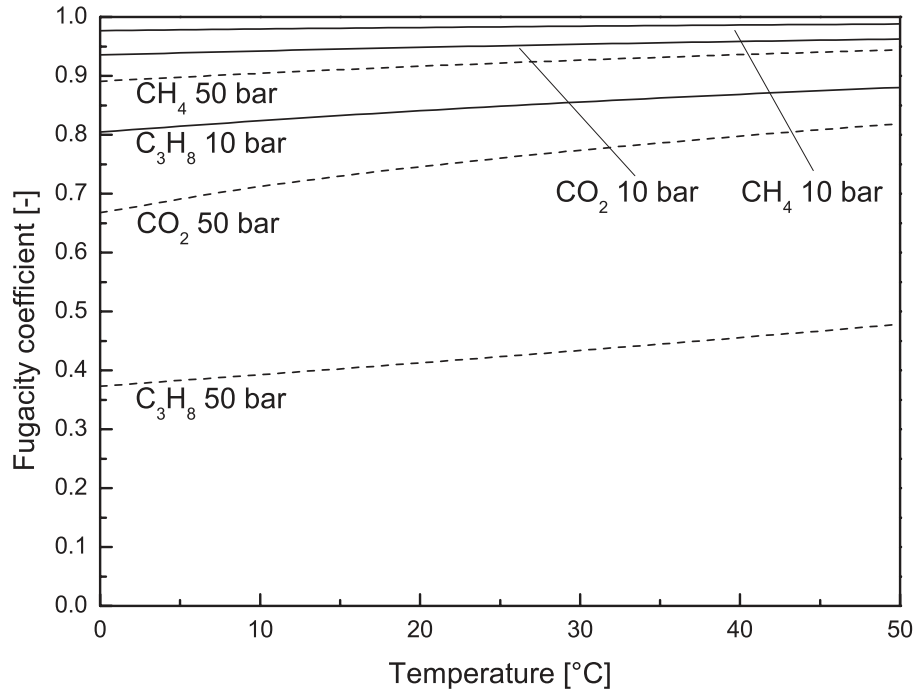


Figure 3.2: Fugacity coefficients of CH₄, CO₂ and C₃H₈ as a function of temperature at a pressure of 10 bar and 50 bar.

and reduces the driving force by decreasing the partial pressure of that component. Generally, the real gas behavior adversely affects separation performance, because the driving force of permeation is reduced for the various gas components. Hence, larger membrane areas are required for separation. Pressure losses on both sides of the membrane also reduce the driving force of permeation. Moreover, significant temperature changes of the gas are caused by the Joule-Thomson Effect. By reducing the gas temperature, the membrane selectivity increases whereas the permeances decrease. Concentration polarisation negatively influences the separation performance and may limit module performance.

3.3.1 Real gas behavior

Real gas behavior is incorporated in the model by calculating the fugacity coefficients. Accordingly, the mass transfer is assigned as:

$$\dot{n}_j'' = Q_j (\varphi_{j,R} x_j p_F - \varphi_{j,P} y_j p_P) \quad (3.7)$$

Whereby, $\varphi_{j,R}$ and $\varphi_{j,P}$ delineates the fugacity coefficient of each gas component on the retentate side and on the permeate side, respectively.

Real gas behavior considers interactions of the gas molecules. It can be determined by calculating the fugacity coefficients which are determined by an ACM procedure. Using the procedures in ACM

an equation of state or an activity model must be specified. For permanent gases the Soave-Redlich-Kwong Equation of State is applied [125, 130]. Figure 3.2 shows the fugacity coefficients of CH₄, CO₂ and C₃H₈. It can be seen that CO₂ and C₃H₈ distinctly exhibit real gas behavior whereas CH₄ shows ideal gas behavior. At higher pressures the fugacity coefficients decrease strongly.

3.3.2 Pressure losses

Pressure losses on both sides of the membrane can significantly reduce the driving force. The pressure losses are calculated by assuming laminar flow in the bore of the fiber and on the shell side of the module [13, 17]. The pressure losses are calculated by:

$$\frac{dp_b}{dx} = -\xi \frac{\rho}{2 \cdot d_{id}} v^2 \quad (3.8)$$

$$\frac{dp_s}{dx} = -\xi \frac{\rho}{2 \cdot d_{hyd}} v^2 \quad (3.9)$$

The terms p_b and p_s represent the pressure of the bore side and the shell side, respectively. The terms d_{id} and d_{hyd} delineate the inner fiber diameter and the hydraulic diameter of the shell side, respectively. The gas velocity is designated by v and ρ refers to the gas density.

By assuming laminar flow on both sides of the membrane, the friction factor ξ can be calculated by:

$$\xi = \frac{64}{Re} \quad (3.10)$$

Whereby Re is the Reynolds number. Hereby, Equation 3.10 is valid for Reynolds numbers lower than 2300. Typical gas velocities range from 0.01 – 0.38 $\frac{m}{s}$ on the permeate side and 1.5 – 1.7 $\frac{m}{s}$ on the retentate side. Thus, since the Reynolds number is 220, the assumption of laminar flow is valid.

3.3.3 Joule-Thomson Effect

The permeation of a gas through a membrane can be compared to an isenthalpic decompression which is accompanied by a change in temperature from the feed to the permeate side and is characterized by:

$$h_R(x_R, T_R, p_F) = h_P(y_P, T_P, p_P) \quad (3.11)$$

Here, h_R and h_P delineate the molar enthalpy on the retentate side and on the permeate side, respectively. Table 3.2 depicts the Joule-Thomson coefficients for various gases. In particular, since

Table 3.2: Joule-Thomson coefficients at 30 °C and 10 bar [131].

| Constituent | Joule-Thomson coefficient [$\frac{K}{bar}$] |
|-------------|---|
| H_2 | -0.03 |
| N_2 | 0.20 |
| O_2 | 0.26 |
| CH_4 | 0.42 |
| CO_2 | 1.05 |
| C_3H_6 | 1.95 |
| C_3H_8 | 2.03 |

CO_2 has a high Joule Thomson coefficient, applications involving CO_2 at high feed pressures are prone to large temperature changes in the module.

The permeance and the selectivity of the membrane material are dependent on temperature [10] and the Joule-Thomson Effect may change the temperature in the gas permeation module. Permeance as a function of temperature is described by using the following Arrhenius type equation [8, 13, 132].

$$Q_j(T) = Q_{j0} \cdot \exp\left[-\frac{E}{\mathfrak{R}} \cdot \left(\frac{1}{T} - \frac{1}{T_0}\right)\right] \quad (3.12)$$

Where E is the activation energy and \mathfrak{R} is the molar gas constant. The reference permeance Q_{j0} is determined at the reference temperature T_0 . With regard to glassy polymer membranes, it is a well-known fact that higher temperatures lead to reduced selectivities and increased permeabilities. Reduced temperatures may also cause condensation of condensable gas components. Condensation have to be avoided since acidic gases might dissolve in the condensate and could attack the membrane material. Furthermore, a liquid film or droplets on the membrane surface would induce an additional mass transfer resistance, thereby reducing the flux through the membrane.

A physical property database in ACM can be used to monitor phase changes in the membrane module. The dew point temperatures as well as the gas temperatures are determined this way.

3.3.4 Concentration polarization

Concentration polarization may significantly reduce module performance by increasing the flow through the membrane of the retained components and decreasing the respective flow of the preferentially permeating components. Figure 3.3 illustrates that concentration polarization occurs in the boundary layers as well as in the porous support. Figure 3.3 also shows the variables presented in the following equations. Concerning asymmetric membranes, it is assumed that the active membrane

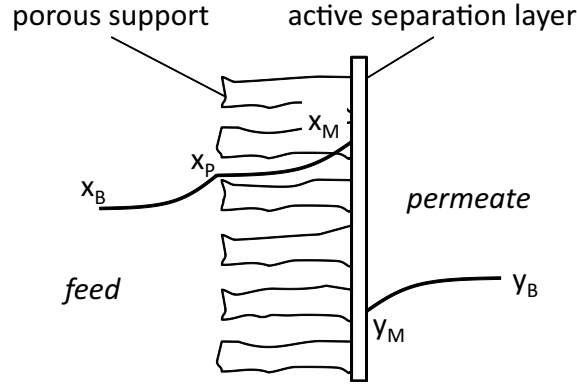


Figure 3.3: Concentration polarization considering bore side feed and the active membrane layer on the outer fiber diameter.

layer is located at the outer circumference of a hollow fiber. In addition, it is assumed that the feed enters the bore of the fiber. The bore side feed configuration is used to avoid maldistribution of the feed gas. Using outside-in operation, the gas flowing around the fibers would suffer from preferential flow through less dense fiber packings. Inside-out operation is preferred when the retentate is the product gas and when high product purities are required. In low pressure applications (<15 bar), feeding the gas to the bore side is commercial practice for instance in separating O_2/N_2 [100, 132, 133]. For high pressure application (>15 bar) the gas is fed on the shell side of the gas permeation module due to the mechanical stability of the hollow fibers.

The governing equations to determine the concentrations at the membrane surface are based on differential mass balances in the boundary layers and in the porous support. These balances are presented by Melin and Rautenbach [13]. Within the boundary layers, the diffusion coefficient and the boundary layer thickness can be replaced by the mass transfer coefficient k which is specified by Sherwood correlations [13]. The bulk concentration $x_{j,B}$ and the concentration at the surface of the porous support $x_{j,P}$ are linked by the following equation:

$$\frac{x_{j,B} - x_j^*}{x_{j,P} - x_j^*} = \exp\left(-\frac{\dot{n}''}{c_{Tot} \cdot k_j}\right) \quad (3.13)$$

Whereby, x_j^* and c_{Tot} delineate the local mole fraction of each gas component in the membrane and the total concentration of gas molecules in the gas phase, respectively. The local mole fraction of a gas component in the membrane is determined by the ratio of the flux of the respective component through the membrane and the total flux of all gas components through the membrane.

$$x_j^* = \frac{\dot{n}_j''}{\sum_{j=1}^n \dot{n}_j''} \quad (3.14)$$

The mass transfer coefficient k_j on the feed side is calculated by the following Sherwood correlation:

$$Sh_{Feed} = \frac{k_j \cdot d}{D_j} = 1.62 \left(Re_{Feed} \cdot Sc_{Feed} \cdot \frac{d}{L} \right)^{\frac{1}{3}} \quad (3.15)$$

The terms Re_{Feed} and Sc_{Feed} designate the Reynolds number and the Schmidt number on the retentate side of the gas permeation module. Here, d and L refer to the inner fiber diameter and the length of the fiber, respectively.

The permeating molecules passing through the feed side boundary layer subsequently enter the pores of the porous support layer. Concentration polarization exists in the porous support, and the concentration profile of the various gas components within the porous support is determined by a differential mass balance. Since the thickness δ of the porous support is known, there is no need to use a Sherwood correlation for determining this. Equation 3.16 shows the concentration on the membrane surface $x_{j,M}$ to be dependent on the concentration at the interface of the porous support $x_{j,P}$

$$\frac{x_{j,P} - x_j^*}{x_{j,M} - x_j^*} = \exp\left(-\frac{\dot{n}'' \cdot M}{\delta_M \cdot \varepsilon \cdot D_j}\right) \quad (3.16)$$

whereby, M is the molar weight, δ_M is the support thickness, and the terms ε and D_j delineate the porosity of the porous support and the diffusion coefficient of component j , respectively. The diffusion coefficients are available in the Aspen Properties[®] database. The diffusion coefficients are determined by the Dawson-Khoury-Kobayashi model for pressures higher than 1 atm. For pressures lower than 1 atm the Chapman-Enskog-Wilke-Lee model is applied. Detailed information on the correlations to determine the diffusion coefficients can be found in the Aspen Properties help [32] which uses the data published by Bird et al. [134].

Analogous to the calculation of the concentration polarization at the feed side, the mass transfer through the membrane determines the concentration profile on the permeate side:

$$\frac{y_{j,M} - x_j^*}{y_{j,B} - x_j^*} = \exp\left(-\frac{\dot{n}''}{c_{Tot} \cdot k_j}\right) \quad (3.17)$$

Here, the terms $y_{j,M}$ and $y_{j,B}$ designate the permeate concentration at the membrane surface and the bulk concentration on the permeate side, respectively. The mass transfer coefficient k_j on the permeate side is calculated by Sherwood correlation:

$$Sh_{Per} = 1.62 \left(Re_{Per} \cdot Sc_{Per} \cdot \frac{d_{hyd}}{L} \right)^{\frac{1}{3}} \quad (3.18)$$

Whereby, Re_{Per} and Sc_{Per} delineate the Reynolds number and the Schmidt number on the permeate side. Concerning the shell side of the hollow fiber gas permeation module a hydraulic diameter d_{hyd}

is determined. Since the boundary layer thickness δ is much smaller than the outer fiber diameter, it is reasonable to use the balances for flat sheet membranes.

Equations [3.13, 3.16 and 3.17] indicate that concentration polarization depends on the flux through the membrane. The higher the flux the more pronounced the influence of concentration polarization is. In the following we present membranes with low flux levels but high selectivity as described in Visser et al. [16].

3.4 Additional relevant non-ideal effects

Multicomponent mass transport in glassy polymer membranes is often affected by three phenomena [104, 105, 135]: (a) competitive sorption at low feed pressures and a resulting mutually affected transport of the gases, (b) penetrant induced plasticization at high feed pressures and (c) frame of reference effects. These three effects are not considered in this study. Chern et al. [136] have evaluated the influence of feed pressure and composition-dependent permeance by applying the dual-sorption model. They compared the dual-sorption model to constant permeance data and found that a roughly 5 - 14 % change in most of the process variables. However, an appropriate mass transfer model to include the pressure and composition dependence of the permeance can easily be incorporated in the presented model by using a polynomial interpolation of mixed gas permeation data.

Al-Juaied and Koros [135] present a model which takes the frame of reference into account. They report that the diffusion of the gas molecules through the membrane is accompanied by a convective flow of gas molecules which is referred to as bulk flux. The influence of the bulk flux is pronounced when the sorption of gas molecules in the polymer is significant (high pressure). As a result of the non-selective bulk flux the selectivity of the membrane is reduced at elevated pressures. The mathematical description of the frame of reference effects can account for the pressure dependence of the selectivity in the separation of CO_2 and CH_4 [135] as well as in the separation of C_3H_6 and C_3H_8 [137]. Mathematically, the bulk flux contribution can be accommodated as well in the equation describing the membrane transport. In this current study it is of no relevance since the membrane swelling is low.

Additionally, minor components like water or higher hydrocarbons may effect membrane properties and in particular the permeances [138]. However, the selectivity is only influenced when the reduction of permeance is different for the various gases. Gales et al. [139] have reported on the effect of volatile organic compounds (VOCs) on the separation of air and VOCs using PDMS membranes. They conclude that their simple model is able to predict the separation well although the membrane material swells at elevated feed pressures and applying increased VOC concentrations. Al-Juaied and Koros [140] have reported on the impact of heavy hydrocarbons (in ppm range) on the permeance of CO_2 and CH_4 in hollow fiber polyimide membranes. They found that permeances significantly

Table 3.3: Membrane module properties.

| Model parameters | Unit | Value |
|--------------------------|---------------|-------|
| Outer fiber diameter | μm | 415 |
| Porous support thickness | μm | 74 |
| Fiber length | m | 0.2 |
| Module diameter | m | 0.038 |
| Number of fibers | [-] | 3380 |

increases when toluene is exposed to the membrane at low temperatures only.

A fourth non-ideal effect may be pressure losses at the entry and the exit ports of the module. Such effect need to be accounted for by measuring the friction factor belonging to specific module geometry. They can easily be included in the presented model by adding pressure loss correlations to the overall module related pressure loss.

3.5 Application of the model in process simulation

The Aspen Custom Modeler[®] model can easily be integrated into the process simulator Aspen Plus[®]. The parameters of the model can be selected individually to cover the various non-ideal effects. The user should carefully select an appropriate set of equations which characterizes the separation task to be investigated.

3.6 Membrane module

The permeances applied in this simulation study were obtained from pure gas measurements. In order to determine the pure gas permeances, the gas permeation module was operated in dead end mode by closing the retentate valve. Both, the pressure on the feed side and the pressure on the permeate side as well as the permeate flow rate were measured. Hence, the permeance is the ratio of the flow rate and the product of transmembrane pressure difference and membrane area.

Furthermore, experimental mixed gas data was obtained with an industrial hollow fiber polyimide gas permeation module (Ube industries, LTD.). Used here was a gas permeation test facility allowing the simulatenous mixing and analysis of seven different gases. The gas permeation module was placed in a heating cabinet to control the feed temperature and module temperature. Subsequently, the simulation data which uses pure gas permeances was compared to the data of the mixed gas experiments. Various feed flow rates were specified, and the flow rates as well as the mole fractions

Table 3.4: Parameters applied for model validation.

| Variable | Value | Unit |
|-----------------------------|-------|------|
| Feed pressure | 3 | bar |
| Feed temperature | 50 | °C |
| Feed mole fraction C_3H_8 | 0.5 | |

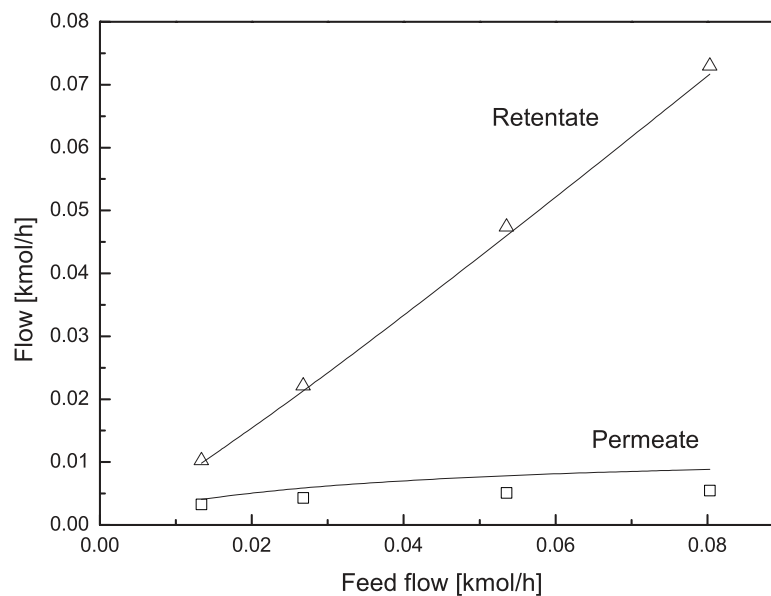


Figure 3.4: Separation of CO_2/C_3H_8 . The retentate and permeate flow are presented as a function of the feed flow rate. The curves present the simulation results. The symbols represent the empirical data points. The temperature is $50^\circ C$, the feed side pressure is 3 bar, the permeate side pressure is 1 bar, the CO_2 permeance is 203 GPU and the C_3H_8 permeance is 0.23 GPU, respectively.

were measured. A detailed description of the gas permeation test facility as well as information on the measurement procedure was published for the separation of carbon monoxide and argon [141]. Table 3.3 summarizes the module properties. The fiber diameters were measured microscopically and the number of fibers were counted. The module diameter and the fiber length could be measured.

3.7 Results and discussion

3.7.1 Model validation

For the system CO_2/C_3H_8 we would like to evaluate how the model data and experimental data agree. CO_2 permeates selectively over the membrane enriching in the permeate. Figure 3.4 shows that the experimental results for the retentate flow rate vs. feed flow agree well with the simulation curve for the system CO_2/C_3H_8 . For the permeate, however, the experimental data are different

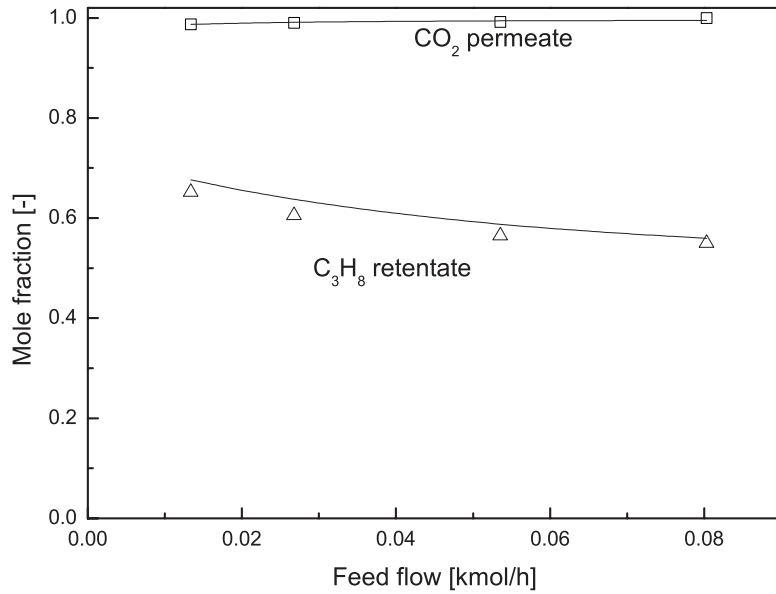


Figure 3.5: Separation of $\text{CO}_2/\text{C}_3\text{H}_8$. The retentate mole fraction of C_3H_8 and permeate CO_2 mole fractions are shown as a function of feed flow. The curves illustrate the simulation results and the symbols represent the empirical data points. The temperature is 50°C , the feed side pressure is 3 bar, the permeate side pressure is 1 bar, the CO_2 permeance is 203 GPU and the C_3H_8 permeance is 0.23 GPU, respectively.

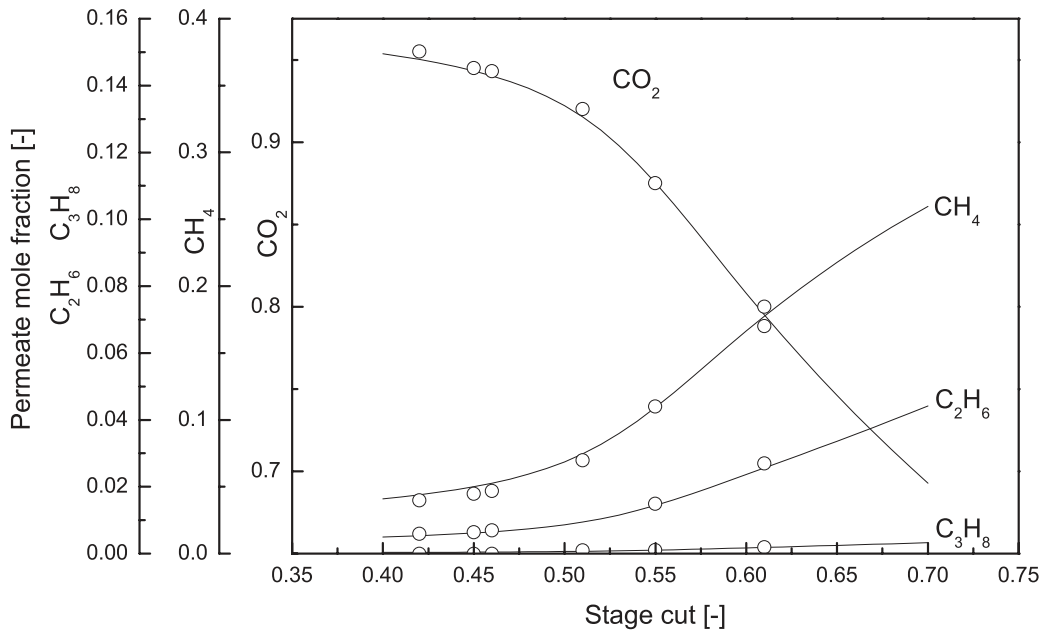


Figure 3.6: Comparing the model to experimental data reported by Pan [129]. The lines represent the simulation results obtain by the presented model. The dots indicate the experimental data by Pan. Feed temperature is 10°C , the feed pressure is 35.28 bar, the permeate pressure is 0.928 bar and the feed composition is 0.485 CO_2 , 0.279 CH_4 , 0.1626 C_2H_6 and 0.0734 C_3H_8 , respectively. Permeances (GPU): 40.05 CO_2 , 1.11 CH_4 , 0.31 C_2H_6 and 0.06 C_3H_8 .

from the simulated ones. This maybe within the accuracy of measurement. Since flow rate of the permeate is low, the experimental data for permeate flow may be inaccurate. A second reason may well be a strong pressure- and concentration-dependence of the permeance due to the glassy nature of the polymer which is addressed in the paragraph on additional non-ideal effects. Figure 3.5 depicts the C_3H_8 mole fraction in the retentate and the CO_2 mole fraction in the permeate for both simulation as well as experimental data. It can be seen that in both cases the simulations agree very well with the empirical data.

In order to demonstrate the applicability of the model for applications in which high pressures (> 35 bar) as well as multiple components are to be separated, the model was compared to experimental data published by Pan [129]. Figure 3.6 shows the permeate mole fraction of CO_2 , CH_4 , C_2H_6 and C_3H_8 as a function of stage cut. Regarding the model data as well as the experimental data, the model predicts the experimental data well.

3.7.2 Case studies to evaluate model performance

In order to investigate the effect of non-ideal module operation, two case studies were performed analyzing the separation of C_3H_8 and CO_2 and the separation of CH_4 and CO_2 . Both studies compare ideal and real module conditions. In the latter case, all aforementioned non-ideal effects were taken into account. To analyze the influence of the non-ideal effects individually, the ideal module operation was simulated respectively with each single non-ideal effect. Both systems, the separation of C_3H_8 and CO_2 as well as the separation of CH_4 and CO_2 , are selected such that Joule-Thomson cooling and real gas behavior are pronounced.

The separation of C_3H_8 and CO_2

Table 3.5 summarizes the parameters applied in the simulation of the separation of CO_2 and C_3H_8 , which were obtained from pure gas measurements. The heat transfer coefficient and the ratios of the activation energy and the universal gas constant $\frac{E}{R}$ were estimated based on data provided by Melin and Rautenbach [13]. Moreover, Table 3.3 shows the module properties for the polyimide gas permeation module. Figure 3.7 shows the retentate CO_2 mole fraction for ideal module operation and for the real module operation where the considered non-ideal effects are accumulated. The latter case is referred to as accumulated effects. Since the difference between the individual non-ideal effects and ideal module operation is not pronounced, all the effects (i.e. concentration polarization, the Joule-Thomson Effect, pressure losses and real gas behavior) are considered as a whole. Here, the curves depicting the Joule-Thomson Effect and real gas behavior are congruent with the curve showing the accumulated effects. Analogously, the curves for concentration polarization and pressure losses are congruent with the curve for ideal operation.

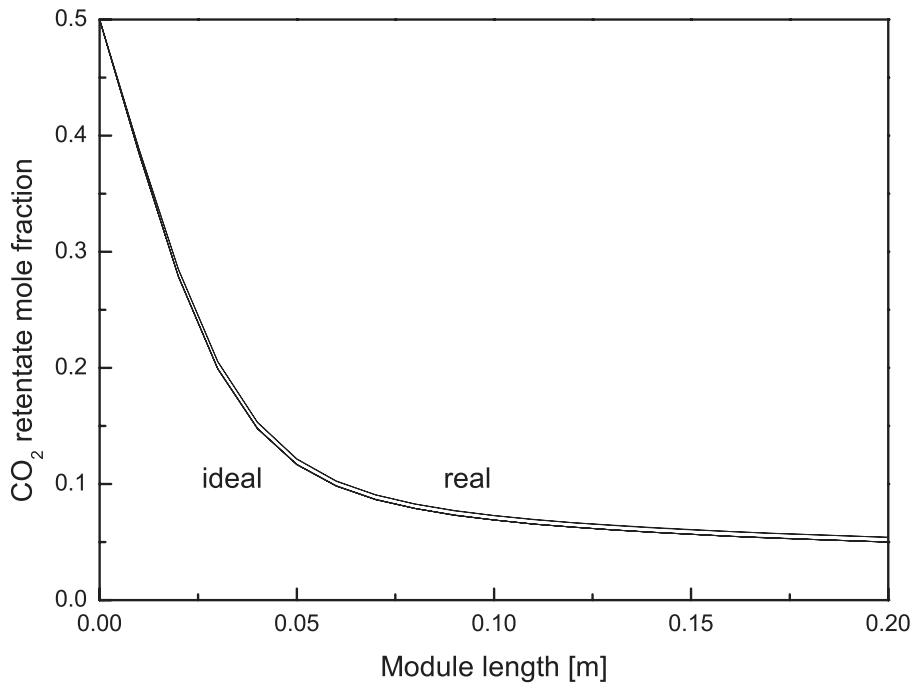


Figure 3.7: Separation of CO₂/C₃H₈. Ideal and real mole fraction of CO₂ on the retentate side of the gas permeation module as a function of module length.

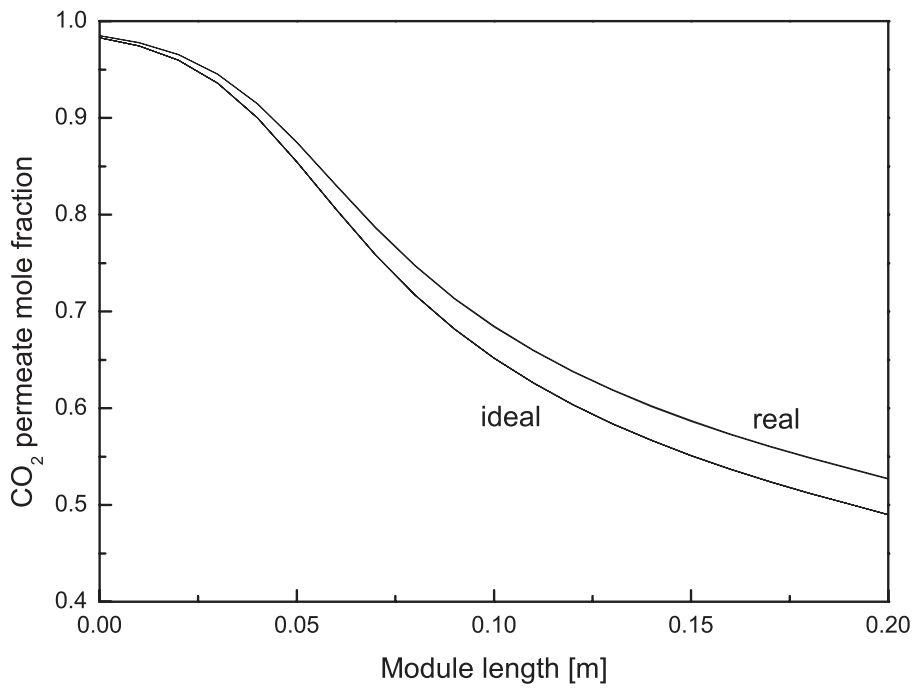


Figure 3.8: Separation of CO₂/C₃H₈. Ideal and real mole fraction of CO₂ on the permeate side of the gas permeation module as a function of module length.

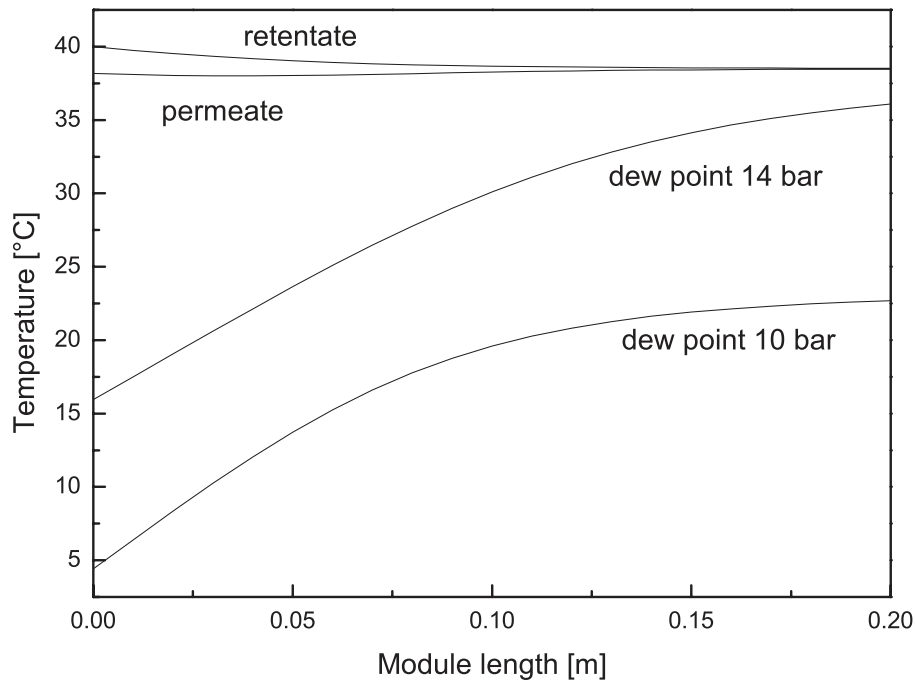


Figure 3.9: Separation of $\text{CO}_2/\text{C}_3\text{H}_8$. Gas temperature for the retentate and the permeate side as well as the dew point temperature on the retentate side at a feed pressure of 14 bar and a feed pressure of 10 bar as a function of module length.

Table 3.5: Parameters applied for simulation in the separation of CO_2 and C_3H_8 using a polyimide hollow fiber membrane module.

| Variable | Value | Unit |
|---|-------|---------------------------------------|
| Feed pressure | 10 | bar |
| Feed temperature | 40 | °C |
| Heat transfer coefficient | 4 | $\frac{\text{W}}{\text{m}^2\text{K}}$ |
| Feed mole fraction C_3H_8 | 0.5 | |
| Permeance CO_2 | 203 | GPU |
| Permeance C_3H_8 | 0.23 | GPU |
| $\frac{E}{R} \text{CO}_2$ | 1000 | K |
| $\frac{E}{R} \text{C}_3\text{H}_8$ | 2000 | K |

Figure 3.8 presents the permeate CO₂ mole fraction for ideal module operation and the accumulated effects module operation. Compared to Figure 3.7 the difference between both operation conditions is more pronounced. However, the CO₂ mole fraction at the permeate outlet is almost equal for both ideal module operation and the accumulated effects module operation. Thus, here the difference between both operation conditions is insignificant. Consequently, in this case the simple model assuming ideal gas behavior and neglecting non-ideal effects may be applied in process simulation. However, an appropriate mass transfer equation is required in order to describe the influence of feed pressure, feed temperature and gas composition on the permeance.

Figure 3.9 shows the temperature distribution as well as the dew point temperature for the retentate side of the hollow fiber gas permeation module. Since the dew point temperature on the permeate side is lower than - 87 °C and condensation of the respective gases is not expected, the dew point temperature curves are not shown in Figure 3.9. C₃H₈ and CO₂ have a distinct Joule-Thomson coefficient; hence the feed gas cools down along the length of the module. However, the gas temperatures are not lower than the dew point and condensation does not occur, even at feed pressures as high as 14 bar.

The separation of CH₄ and CO₂

The separation of CO₂ and CH₄ was investigated by analyzing whether non-ideal effects influence the mole fraction of CO₂ on the retentate and the permeate side. Table 3.6 summarizes the simulation parameters. The heat transfer coefficient and the ratios of the activation energy and the universal gas constant $\frac{E}{R}$ were assumed based on published experimental data [13]. Table 3.3 presents the properties of a polyimide gas permeation module applied in the simulation.

Figure 3.10 presents the CO₂ mole fraction on the retentate side of the gas permeation module as a function of module length. Here, the non-ideal effects are more marked, whereas the effect of pressure loss and concentration polarization are negligible as the respective curves are congruent with the curve for ideal operation. It can be seen that the real gas behavior has the strongest impact on the separation performance. The Joule-Thomson cooling also has an impact on the CO₂ mole fraction but it is less pronounced.

Figure 3.11 illustrates the CO₂ mole fraction on the permeate side of the gas permeation module as a function of module length. The impact of concentration polarization and pressure losses can be neglected here. Compared to Figure 3.10 the difference between ideal module operation and the accumulated effects module operation is more pronounced. The most important contribution to non-ideal module operation is observed for the Joule-Thomson Effect and for the real gas behavior. As the various non-ideal effects are interdependent, the curves for the individual effects cannot be summed up to obtain the curve in which all the aforementioned effects are taken into account (accumulated effects case). Hence, the superposition principle cannot be applied.

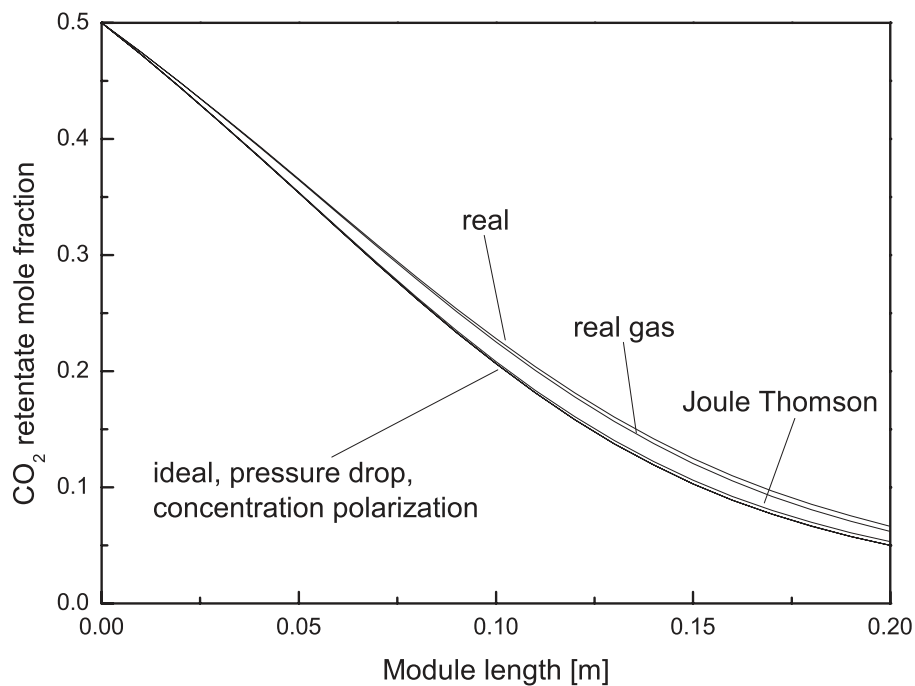


Figure 3.10: Mole fraction of CO₂ on the retentate side as a function of module length. The distribution of CO₂ is presented for the various non-ideal effects as well as for the ideal module operation and the accumulated effects module operation, separating CO₂ and CH₄.

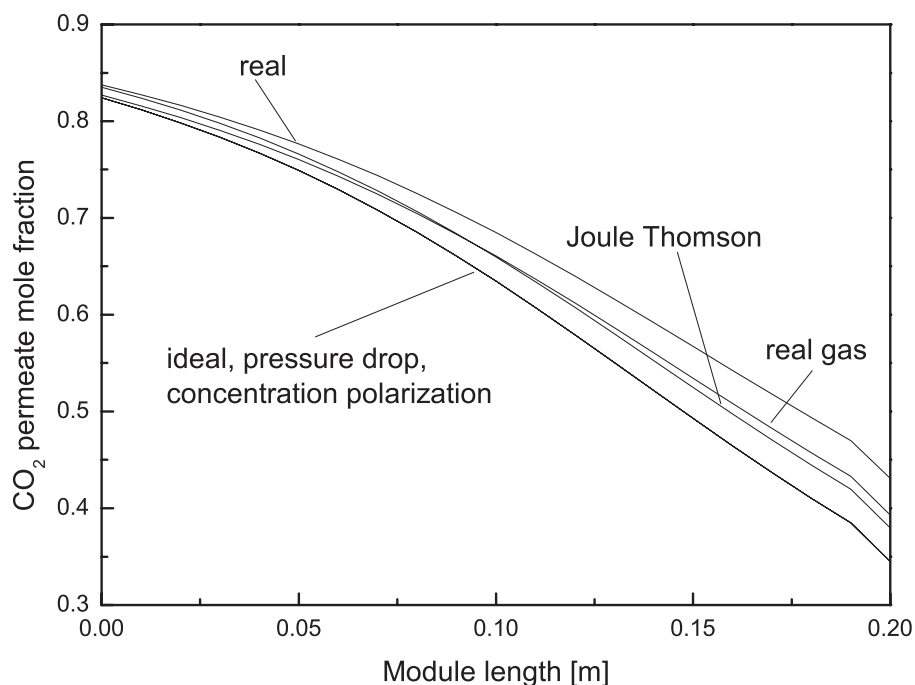


Figure 3.11: Mole fraction of CO₂ on the permeate side as a function of module length. The distribution of CO₂ is presented for the various non-ideal effects as well as for the ideal module operation and the accumulated effects module operation, separating CO₂ and CH₄.

Table 3.6: Parameters applied for simulating the separation of CO₂ and CH₄ using a polyimide hollow fiber membrane module.

| Variable | Value | Unit |
|------------------------------------|-------|------------------|
| Feed pressure | 10 | bar |
| Feed temperature | 40 | °C |
| Heat transfer coefficient | 4 | $\frac{W}{m^2K}$ |
| Feed mole fraction CH ₄ | 0.5 | |
| Permeance CO ₂ | 203 | GPU |
| Permeance CH ₄ | 10 | GPU |
| $\frac{E}{R}$ CO ₂ | 1000 | K |
| $\frac{E}{R}$ CH ₄ | 2000 | K |

3.8 Pressure dependent permeance

In general, the feed pressure and in particular the partial pressure of CO₂ influences the permeation of the gas molecules through the membrane material [107] and hence, a pressure dependent permeance is analyzed separately in this paragraph. Here, the separation of CO₂ and C₃H₈ is considered. Figure 3.12 depicts the permeance of CO₂ and C₃H₈ as a function of feed pressure. The characteristics of the permeance are based on theoretical consideration. At low pressure competitive sorption will reduce permeance whereas at high pressures plasticization becomes significant resulting in an increased permeance. It is assumed that due to competitive sorption the permeance is reduced by 20 % at a pressure of 12 bar compared to the permeances at a pressure of 1 bar. Furthermore, it is assumed, that the permeances increase by 20 % at a feed pressure of 30 bar. Hence, the permeance can be described by a second order polynomial [107]. In addition, the selectivity is assumed to be constant. However, this assumption is rather unrealistic [107]. It is essential to include an adequate description of the pressure-dependent permeation equation in order to account for the pressure and the temperature influence as well as the impact of the permeating components.

To compare the different feed pressure levels the pressure ratio across the membrane is kept constant at 10. Two different cases were considered in which one assumes constant permeances and one calculates the module performance with a pressure dependent permeance. Figure 3.13 shows the CO₂ mole fraction in the retentate as a function of module length for feed pressures of 10 bar, 30 bar and 50 bar. At low feed pressure the difference between constant and pressure dependent simulations is less pronounced. At pressures of more the 30 bar the differences between the case in which constant permeances are assumed and the pressure dependent case becomes significant. In Figure 3.14 the CO₂ mole fraction in the permeate is illustrated as a function of module length

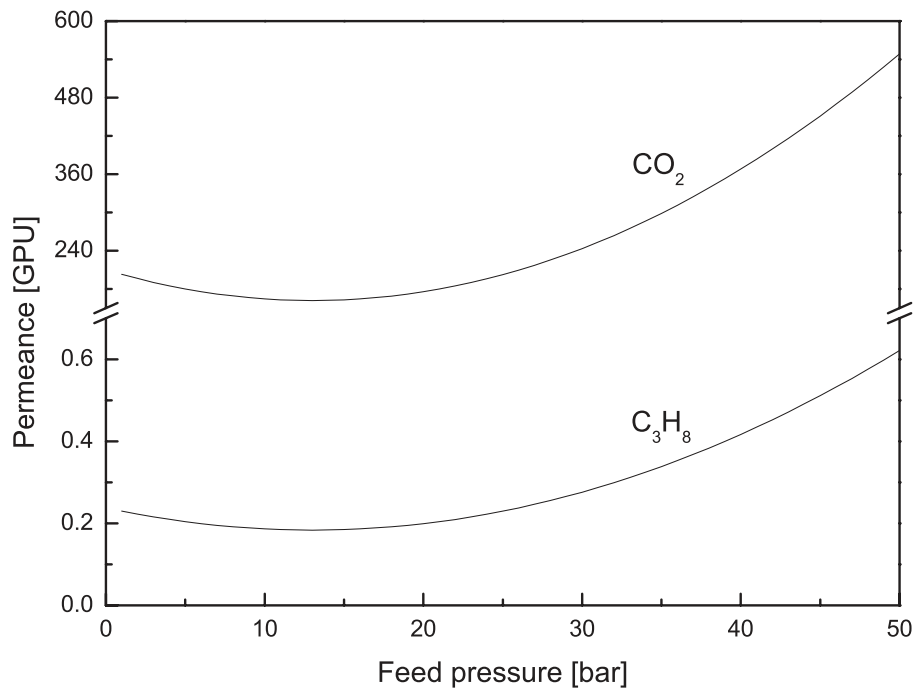


Figure 3.12: Permeances of CO_2 and C_3H_8 as a function of feed pressure. The selectivity is assumed to be constant.

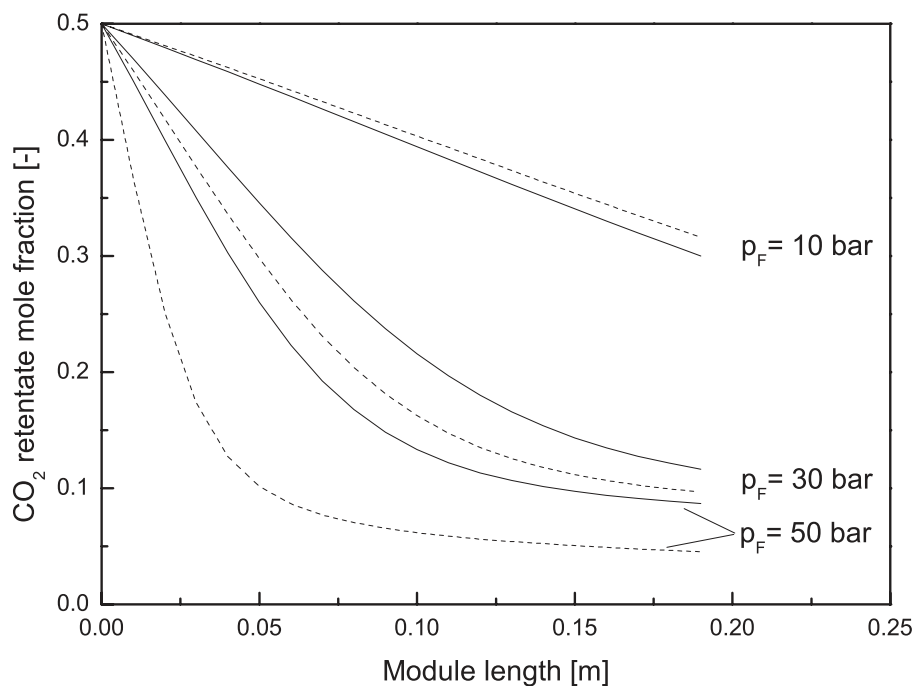


Figure 3.13: Mole fraction of CO_2 in the retentate as a function of module length. The solid lines represent the case in which constant permeances are assumed. The dashed lines illustrate the case in which pressure dependent permeances are applied in the simulation. The feed pressure is varied between 10 bar and 50 bar, whereby the pressure ratio across the membrane is fixed at 10.

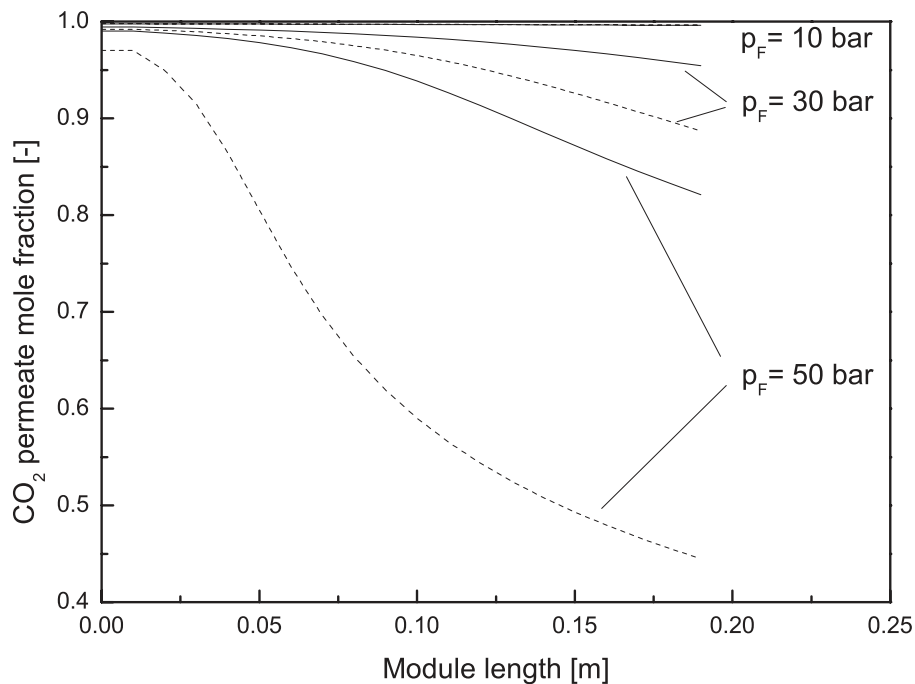


Figure 3.14: Mole fraction of CO_2 in the permeate as a function of module length. The solid lines represent the case in which constant permeances are assumed. The dashed lines illustrate the case in which pressure dependent permeances are applied in the simulation. The feed pressure is varied between 10 bar and 50 bar, whereby the pressure ratio across the membrane is fixed at 10.

for feed pressures of 10 bar, 30 bar and 50 bar. For pressures of more than 30 bar the difference between both cases is pronounced.

According to the simulation results an appropriate description of the mass transfer through the membrane is essential which requires a detailed experimental investigation to determine the mixed gas permeances at elevated pressures. However, complex mass transfer equations can easily be incorporated in the existing model.

Compared to the aforementioned non-ideal effects (Joule-Thomson Effect, concentration polarization, pressure losses, real gas behavior) the temperature and pressure dependence of the permeance may even have a more pronounced effect on module performance. Hence, the interaction between non-ideal effects related to the permeation through the membrane material as well as non-ideal effects related to module operation need to be considered for an adequate description of module performance.

3.9 Conclusions

The presented model of a hollow fiber gas permeation module programmed in Aspen Custom Modeler[®] predicts experimental data under non-ideal conditions. Whereas conventional gas perme-

ation models generally focus on individual non-ideal effects, our model links as a whole concentration polarization, the Joule-Thomson Effect, pressure losses and real gas behavior.

In particular, the separation of CH_4 and CO_2 exhibits non-ideal behavior (a) through the Joule-Thomson cooling along the length of the module and (b) through real gas behavior. Thus, these effects have to be taken into account for large-scale process design where multiple membrane stages are integrated or different unit operations are combined in hybrid processes. As the case studies on separating CH_4/CO_2 and $\text{C}_3\text{H}_8/\text{CO}_2$ demonstrate, it is important that the process designer chooses the appropriate set of equations for non-ideal effects as well as their respective parameters that depend on the separation task at hand. We anticipate the effect of the complex permeation properties in glassy polymers at very low as well as at high feed pressure to be significant.

Ultimately, the presented model represents more realistically gas permeation behavior in large-scale hollow fiber modules and potential for future application in gas separation, in particular, for flue gas treatment, biogas upgrading and natural gas purification.

Chapter 4

Structural optimization of a membrane based biogas upgrading process

4.1 Introduction

Biogas will considerably contribute to future energy supply as it is a renewable resource. Biogas upgrading refers to the separation of CH_4 and CO_2 , where a CH_4 rich gas is polished so that it can be used as natural gas substitute [2]. Gas permeation membranes are well known for separating CO_2 and CH_4 [49, 93, 114]. Their application in biogas upgrading offers several advantages over conventional gas separation techniques. First the gas permeation operates with the upgraded product gas being at an elevated pressure so that it can directly be injected into the natural gas grid [2]. Secondly gas permeation modules are robust and the process is simple, which is particularly suitable for on-farm application.

The objective of the study at hand is to design a membrane based biogas upgrading process based on structural process optimization. Here, (i) the optimal process configuration, (ii) the required membrane areas in the various stages and (iii) the pressure to drive the gas permeation process for a commercial membrane material are determined simultaneously. In a further step the selectivity of the membrane material is optimized together with the process layout and the process conditions. Process design often relies on heuristics and experience [31] which may result in suboptimal process configurations. The application of systematic methods for process design ensures the identification of the most profitable process configuration. Although superstructure optimization provides a systematic framework for the design of membrane based separation processes only limited work has been published. Sargent and Gaminibandara were the first who introduced the concept of structural optimization in designing distillation sequences [142]. This concept has been adapted by El-Hawagi and Manousiouthakis who optimized mass exchange networks [143].

In the optimization of gas permeation processes Uppaluri et al. [29] studied the enriched oxygen production, hydrogen recovery from synthesis gas, and hydrogen recovery from refinery streams. They obtained new process designs which reduces the costs by 20 % compared to process designs previously reported in literature. They applied stochastic optimization using a simulated annealing algorithm.

Qi and Henson [27, 144] report on CO_2/CH_4 separation in natural gas treatment and enhanced oil recovery. Here, only recycle compressors are investigated as the raw gas is already pressurized. They used the General Algebraic Modeling System (GAMS) along with the DICOPT++ algorithm to solve the mixed integer non-linear program (MINLP). They even introduced discrete variables to account for a more realistic process design as membrane modules are available with fixed active membrane areas. They identified a four stage gas permeation process as the process configuration with the lowest gas treatment costs for natural gas polishing. For enhanced oil recovery they also determined a four stage process as optimal process configuration as it has the lowest costs. However, the permeator model used in this study is limited to binary mixtures. In an additional publication [27] they extend the binary model to a multicomponent model. The separation of CH_4 , CO_2 , H_2S and heavier hydrocarbons in natural gas treatment as well as the separation of CH_4 , CO_2 , H_2S , C_2H_6

and heavier hydrocarbons in enhanced oil recovery were investigated.

Kookos [28] does not only optimize the process layout and process conditions, but he also determines the best selectivity along with the best permeance for the production of nitrogen and oxygen from air. The upper bound correlation published by Robeson is applied to account for the membrane material performance. For the production of oxygen the comparison of an optimized membrane material and a commercial membrane material leads to the conclusion that impressive cost reductions are obtained.

Yeomanns and Grossmann [19] introduced a framework of superstructure optimization for process synthesis. Two fundamental superstructure representations are reported: the state task network and the state equipment network. Both superstructures involve the transfers of mass, energy and momentum. This kind of approach can be applied to any synthesis problem to identify the optimal process layout. The state task network initially introduced by Kondili et al. [145] involves the determination of states and tasks while the equipment is assigned subsequently. The state equipment network initially developed by Smith [146] includes the determination of states and the involved equipment in a first step while the tasks which take place in the equipment are determined in a second step. Linke and Kokossis [147] used a superstructure based method to optimize integrated reaction and separation processes. They distinguished between reactor/mass exchangers and separation task units.

We adapt the structural optimization approach to identify the most profitable membrane based biogas upgrading system. The optimization model is implemented in the General Algebraic Modeling System (GAMS). In a first step commercial gas permeation membranes are applied to the process optimization. The best process layout together with the optimal membrane areas and process conditions were calculated. In a second step the membrane's selectivity is an additional optimization parameter. The relation between selectivity and CO₂ permeance is determined according to the upper bound published by Robeson [148]. In contrast to Kookos [28], we applied the updated data for the upper bound correlation published in 2008. A three stage process is the optimal process configuration for the commercial membrane materials while a two stage process is the best layout for optimal membrane materials. Two questions arise when optimizing the membrane properties: what is the optimal CO₂/CH₄ selectivity and process configuration for a process in which a single type of membrane material is used in all membrane stages? What is the optimal CO₂/CH₄ selectivity and process configuration for a process in which the membrane properties are optimized for each membrane stage individually? The process model can easily be adapted to other gas separation problems such as helium production from natural gas, natural gas upgrading or air separation to determine the most profitable process configuration.

Table 4.1: Feed and product gas conditions of a common biogas upgrading process. The permeances of the polymeric membrane materials are also listed. PI - polyimide; CA - cellulose acetate

| | Unit | Value |
|------------------------------|----------------------|-------|
| Raw gas mole fraction CH_4 | - | 0.6 |
| Raw gas mole fraction CO_2 | - | 0.4 |
| Raw gas flow rate | $\frac{m^3(STP)}{h}$ | 150 |
| Raw gas temperature | $^{\circ}C$ | 20 |
| Raw gas pressure | bar | 1 |
| Product pressure | bar | 16 |
| Product mole fraction CH_4 | - | 0.96 |
| CH_4 permeance PI | GPU | 1 |
| CO_2 permeance PI | GPU | 60 |
| CH_4 permeance CA | GPU | 3 |
| CO_2 permeance CA | GPU | 60 |

4.2 Process model

Commonly, gas permeation processes include multiple membrane stages to achieve high gas purities and recoveries simultaneously. Favre [14] reported that more than three stages are usually not installed in industrial applications since these processes seem to be less efficient and cost demanding. In biogas upgrading it is rather unsuitable to use more than three stages as the complexity of the system increases rapidly and the application of such a system at a biogas site seems to be less robust. The process model implemented here is not limited to any number of membrane stages, but for the optimization of the biogas upgrading process a maximum number of three membrane stages is defined.

The gas permeation modules considered in the simulations are equipped with polymeric membrane materials to separate CO_2 and CH_4 . CO_2 will permeate faster through the membrane so that the permeate is enriched in CO_2 . Thus, CH_4 is enriched on the retentate side of the membrane which is particularly advantageous in biogas upgrading as the product gas is pressurized and can thereby directly be injected into the natural gas grid. Table 4.1 lists the raw gas conditions and the product gas requirements. A membrane CO_2/CH_4 selectivity of 60 is assumed based on the patent of Evonik [113] for a polyimide membrane material. However, no information is given on the permeances of such a membrane material and we assume a CO_2 permeance of 60 GPU. In addition, a membrane material with selectivities reflecting the characteristics of a cellulose acetate membrane is investigated since these materials have been widely used in gas permeation. The permeances are

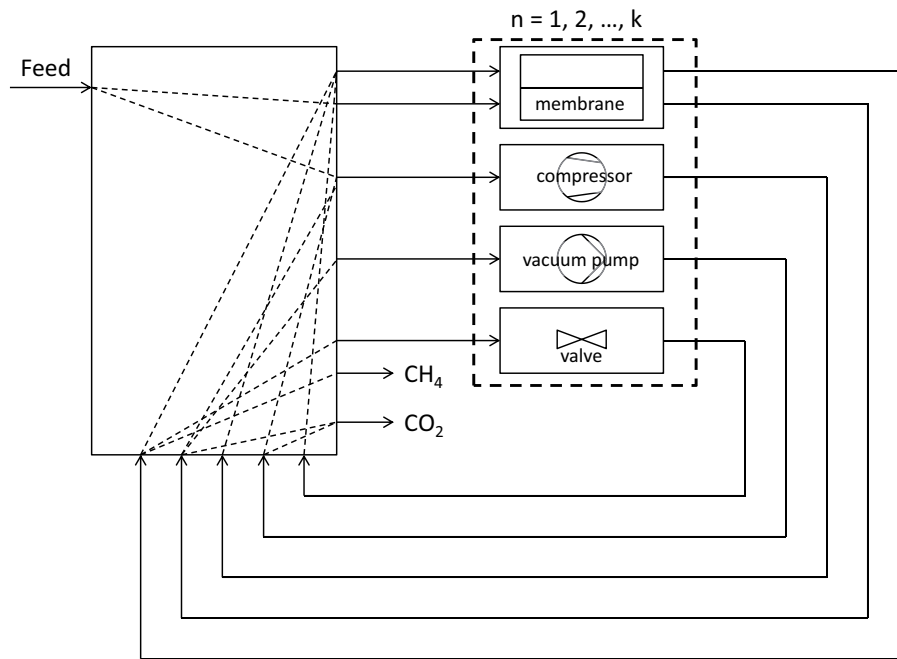


Figure 4.1: Superstructure approach to optimize a membrane based biogas upgrading plant. Note that not all possible connections between the various unit operations are presented.

also listed in Table 4.1.

The objective of the optimization is to maximize the profit of the biogas upgrading process. Four different types of unit operations are implemented and could be used in the process model. These are a gas permeation module to perform the separation and the equipment to generate the driving force of permeation by compressors, vacuum pumps, and pressure control valves. Figure 4.1 shows the respective unit operations and illustrates potential connections of the individual unit operation with other unit operations. Here, only selected connections are presented. For the gas permeation model it is also possible to use a sweep gas on the permeate side. At the inlet (bottom) of the so called distribution box each stream can be split and connected to all available outlet ports of the distribution box. The inlets are splitters while the various outlet ports on the right side of the distribution box are mixers. Each unit operation can be selected several times, so that multistage processes can be optimized with the process model.

The gas permeation module itself is the most important piece of process equipment as it performs the separation. The driving force can either be generated by compressing the feed gas, by applying sub-ambient pressure on the permeate side or by diluting the permeate with a sweep gas. The solver selects the compression equipment based on the operational and investment costs since the driving force method determines the pressure levels as well as the recycle flow rates.

The superstructure model including the models for the unit operations and their connections were programmed in the General Algebraic Modeling System (GAMS). In GAMS the mathematical problem is programmed independently of the solver. Various algorithms are available to solve linear programs (LP), nonlinear programs (NLP) and mixed integer nonlinear programs (MINLP). Opti-

mizing the biogas upgrading process is a MINLP as the connections between the unit operations are of integer type and nonlinear equations (e.g. capital cost calculation) are solved.

The Branch-And-Reduce Optimization Navigator (BARON) is used which is a branch and bound type global optimization solver. With this kind of solver, identification of the global optimum is guaranteed even if fairly general assumptions are made [24].

4.2.1 Unit operation models

The gas permeation module is built as a short cut model based on the fundamental equations for conservation of mass and a simple mass transfer equation. The mole balances of the feed side and the permeate side are:

$$\dot{n}_{R,j} = \dot{n}_j + \dot{n}_{R,j+1} \quad (4.1)$$

$$\dot{n}_{P,j} = \dot{n}_j + \dot{n}_{P,j+1} \quad (4.2)$$

Here, $\dot{n}_{R,j}$ refers to the flow rate on the feed side and $\dot{n}_{P,j}$ is the flow rate on the permeate side, respectively. The mass transfer through the membrane \dot{n} is determined by the partial pressure difference, the permeance of the gas species Q_j and the active membrane area A :

$$\dot{n}_j = Q_j \cdot (x_j p_F - y_j p_P) \cdot A \quad (4.3)$$

Simplifying assumptions have been made: (i) no pressure losses are considered, (ii) isothermal operation, (iii) concentration polarization is neglected, (iv) constant permeances and (v) ideal gas behavior are assumed.

The compressors and the vacuum pumps are modeled as single stage isentropic compression units without interstage cooling. The isentropic outlet temperature T_{out} is determined by:

$$T_{out} = T_{in} \cdot \left(\frac{p_{out}}{p_{in}} \right)^{\frac{\kappa-1}{\kappa}} \quad (4.4)$$

The isentropic exponent κ is 1.3. T_{in} and p_{in} delineate the inlet temperature and pressure, and p_{out} is the compressor's discharge pressure. The real outlet temperature T_{real} is calculated by:

$$\eta_{isent} = \frac{T_{out} - T_{in}}{T_{real} - T_{in}} \quad (4.5)$$

The isentropic efficiency η_{isent} of the compressor is 0.72. Vacuum equipment has isentropic efficiencies of less than 0.5, in case of a jet pump it is only 0.1 [111]. Thus, we assume an isentropic

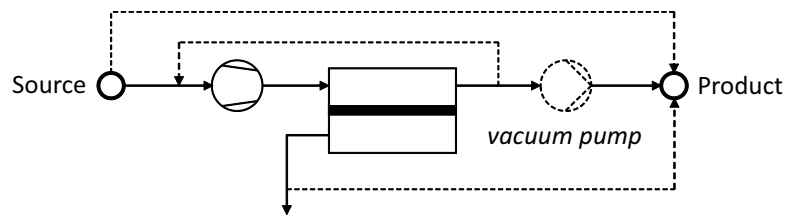


Figure 4.2: Connections which are excluded from the optimization. Excluded connections are labelled with dashed lines.

efficiency of 0.5 for the vacuum equipment. The net power e , which is the energy supplied to the gas stream, is determined by:

$$e = \dot{m} \cdot c_p \cdot (T_{real} - T_{in}) \quad (4.6)$$

Whereby, \dot{m} is the mass flow rate through the compression equipment and c_p is the specific heat capacity of the gas ($34.77 \frac{J}{molK}$). A simple constraint for the pressure control valve was implemented. Here, the upstream pressure has to be higher than the downstream pressure:

$$p_{in} \geq p_{out} \quad (4.7)$$

Compared to the costs for compressors and vacuum pumps the costs for a pressure valve can be neglected. Generally, any outlet of an unit operation can be connected to any inlet of all available unit operations. Therefore, it is possible to optimize membrane cascades including recycle streams. To mix the different process streams the pressure of the streams have to be equal. In case of different stream pressures these are either increased by a compressor or reduced by a pressure control valve. To reduce the number of process configurations and the calculation effort some connections can be precluded which do not contribute to the separation process or even have a negative impact on process performance. Figure 4.2 illustrates some of these connections which are not considered in the optimization. These connections are for instance:

- Recycling of a retentate stream and mixing this stream with the feed stream of the same membrane stage
- Direct connection of the feed and the product stream
- Mixing of permeate streams with the product stream
- Connection of a retentate outlet stream and a vacuum pump inlet

Table 4.2: Economic parameters used for optimization of a membrane based biogas upgrading plant.

| Costs | Unit | Value |
|---------------------------|--------------------|-------|
| Membrane module costs | $\frac{Euro}{m^2}$ | 55 |
| Electrical costs | $\frac{Euro}{kWh}$ | 0.08 |
| Comission of purified gas | $\frac{Euro}{m^3}$ | 1.2 |
| Membrane lifetime | year | 4 |
| Annual operation | h | 8000 |
| Interest rate | - | 0.09 |
| Amortization period | years | 8 |

4.2.2 Economics

To optimize the process it is more appropriate to determine the economic optimum rather than the energetic optimum, since the membrane based biogas upgrading process has to compete economically with well established gas separation techniques. The energetic optimum can be fairly different from the economic optimum. In this study we determine the most profitable process configuration by taking both, operational cost, mainly caused by electrical energy consumption, and investment costs for the compression equipment and the membrane modules into account. The membranes lifetime is 4 years and the membranes have to be replaced after this operation period. Table 4.2 summarizes the economic parameters chosen for the optimization simulation.

Investment costs for the compressor and the vacuum pump can be estimated with Guthrie's method [110, 149]. This method enables the calculation of investment costs based on the size of the compression equipment and the process conditions. The method roughly estimates investment cost with an error of $\pm 25\%$ [110].

In a first step the bare module costs (BC) are determined:

$$BC = C_0 \cdot \left(\frac{S}{S_0}\right)^\alpha \quad (4.8)$$

Where C_0 are reference costs for the equipment, S is a variable taking the size of the respective equipment into account and S_0 is a reference size of the equipment. In case of compression S is the required compression duty and S_0 is the reference compression duty. The parameter α considers the cost increase with increasing equipment size. Here, the economy of scale is taken into account since α is generally lower than 1. The required values for C_0 and S_0 are tabulated in Biegler et al. [110]. To determine the investment costs the reference costs have to be updated as the values were

Table 4.3: Parameters to estimate the investment costs for the compression equipment with Guthrie's method [110]. *bhp - brake horse power

| Parameter | Symbol | Unit | Value |
|--|----------|----------------|--------|
| Update factor 2011 | UF | | 4.91 |
| Material and pressure factor | MPF | | 2.9 |
| Module factor | MF | | 5.11 |
| Conversion bhp* in kW | | kW/bhp | 0.746 |
| Reference costs for compressor in 1968 | C_0 | US Dollar | 23000 |
| Reference compressor size | S_0 | bhp | 100 |
| Cost function exponent | α | | 0.77 |
| Conversion US Dollar in Euro | | US Dollar/Euro | 1.2719 |

determined for the reference year 1969. In addition, the capital costs of the equipment depend on the operating conditions and the materials used. Thus, the investment costs IC are calculated by:

$$IC = UF \cdot BC \cdot (MPF + MF - 1) \quad (4.9)$$

Here, UF delineates the update factor which takes the current price level into account. MPF is the material and pressure factor accounting for the material of the equipment. The module factor MF additionally considers the size of the equipment. Hirschberg [150] suggests that 2 should be added to this factor to realistically reflect today's investment costs. The Guthrie parameters used here are listed in Table 4.3.

4.2.3 Robeson Plot

Many efforts are made to develop new membrane materials which have improved selectivities and permeances. From an operational point of view the application of these membranes in gas permeation processes is limited. High selectivities together with high permeances induce concentration polarization significantly limiting the separation performance of the gas permeation modules. Thus, the driving force for the retained gas species increases while the driving force for the fast permeating species is reduced [45, 101]. However, the effect of concentration polarization is not accounted for in the model but it is remarkable for membranes with selectivities and permeances as high as 100 and 1000 GPU, respectively [101].

Furthermore, for gas permeation processes high pressure ratios have to be provided to take advantage of high membrane selectivities [9]. The trade-off between permeability and selectivity is well known [148]. In terms of process design low selectivities increase the amount of the retained gas

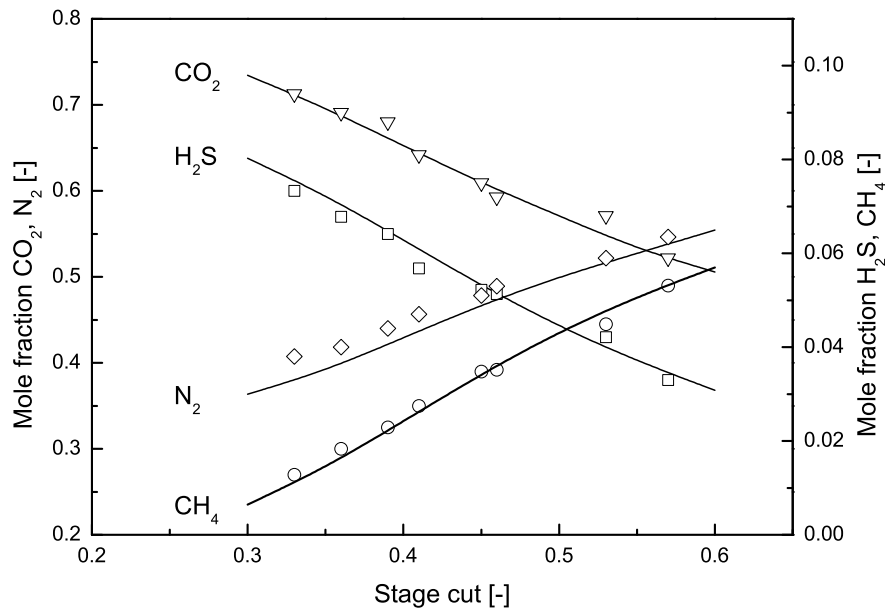


Figure 4.3: Permeate mole fractions as a function of stage cut. The model data (lines) is compared to data reported by Pan (symbols) [129].

species which permeates through the membrane resulting in increased compression duty. For high selectivity, permeance drops which increases the required membrane area remarkably. As a consequence higher investment costs and membrane replacement costs reduce the profitability of the upgrading process.

Robeson [148] introduced a correlation to determine the permeability as a function of the selectivity for upper bound materials. We implemented the upper bound correlation into the superstructure model to determine the most profitable selectivity simultaneously with the optimal process layout, the membrane areas and pressures. For CO_2 and CH_4 Robeson published the following correlation:

$$P_{\text{CO}_2} = 5369140 (\alpha_{\text{CO}_2/\text{CH}_4})^{-2.636} \text{ Barrer} \quad (4.10)$$

Assuming a membrane thickness of 30 nm transforms permeability into permeance.

$$Q_{\text{CO}_2} = 33.77 \cdot 5369140 (\alpha_{\text{CO}_2/\text{CH}_4})^{-2.636} \text{ GPU} \quad (4.11)$$

Where, $\alpha_{\text{CO}_2/\text{CH}_4}$ is the selectivity:

$$\alpha_{\text{CO}_2/\text{CH}_4} = \frac{Q_{\text{CO}_2}}{Q_{\text{CH}_4}} \quad (4.12)$$

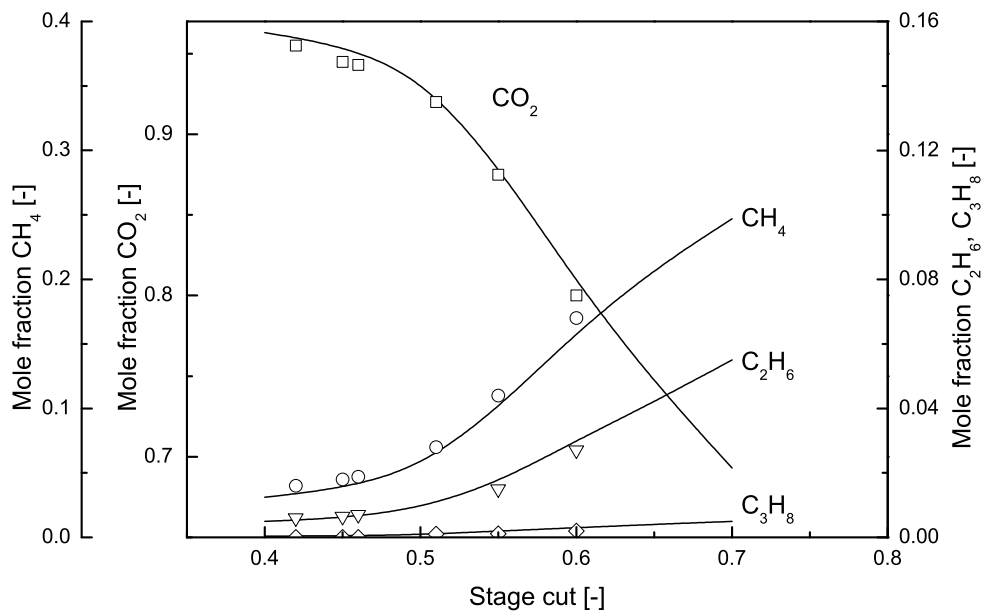


Figure 4.4: Permeate mole fractions as a function of stage cut. The model data (lines) is compared to data reported by Pan (symbols) [129].

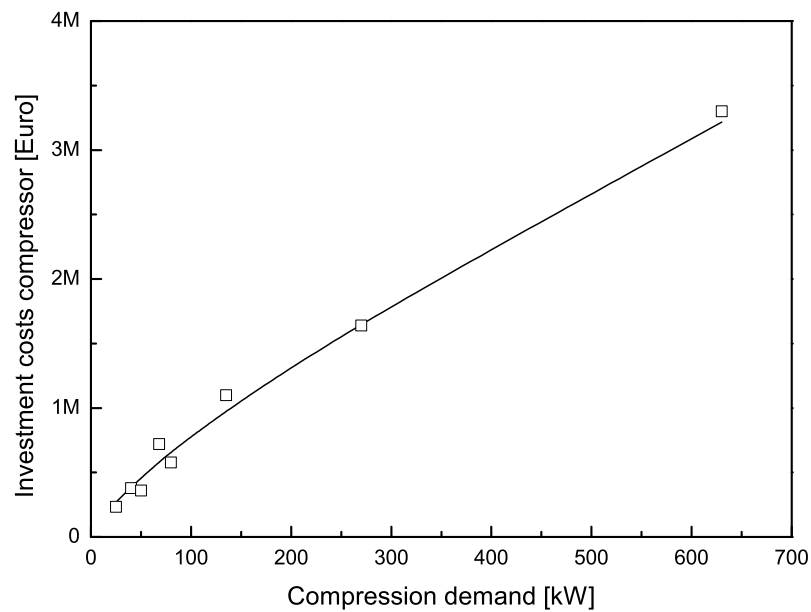


Figure 4.5: Comparison of real investment costs for compressor (symbols) and investment costs estimated by Guthrie's method as a function of the compression demand.

4.3 Results and Discussion

4.3.1 Model validation

Pan [129] reported experimental data on the separation of CO₂, N₂, H₂S and CH₄, and for the separation of CO₂, CH₄, C₂H₆ and C₃H₈. We compared this data to the simulation results of the gas permeation model. Figure 4.3 shows the mole fractions of CO₂, N₂, H₂S and CH₄ as a function of the stage cut. For a wide range of stage cuts the model applied here reflects the experimental data. Analogously, Figure 4.4 show the mole fraction of CO₂, CH₄, C₂H₆ and C₃H₈ as a function of stage cut. Here, the model results agree with the published data.

Figure 4.5 depicts the investment costs for a compressor as a function of the compression demand. The line refers to the data obtained by Guthrie's method, while the squares represent data provided by a compressor manufacturer, who does not want to be mentioned here. The difference between the estimated costs and the real compressor costs are less than 20 %. In general, Biegler et al. [110] report an error of ± 25 % for Guthrie's method. It has to be noted that for low compression duties the investment costs for compressors might fluctuate significantly. Compressors with a low discharge pressure can be single stage, while a slight increase in the discharge pressure results in an additional compression stage which increases the costs for the compressor. However, we apply Guthrie's investment cost estimation method to determine investment costs in the superstructure optimization model.

4.3.2 Superstructure optimization with commercial membranes

In this section two commercial membrane materials are compared. One with a CO₂/CH₄ selectivity of 60 which is typical for polyimide type of materials and a second material reflecting the properties of cellulose acetate membranes with a selectivity of 20. While the cellulose acetate membrane is well established in the gas permeation applications [69], the polyimide membranes considered have recently be launched. Both types of membranes are considered to investigate the impact of selectivity on the process performance. In the optimization a product gas purity of at least 96 % together with a CH₄ recovery of more than 95 % and 99.5 %, respectively, have to be met.

Figure 4.6 shows the optimal process layout together with the process parameters for a membrane material with a CO₂/CH₄ selectivity of 60 and a CO₂ permeance of 60 GPU. A three stage membrane process using a single compressor is identified to be the best process configuration. The raw gas is compressed to pipeline pressure of 16 bar and fed to the first membrane stage. The first stage performs a bulk separation of CO₂ and CH₄ and significant amounts of CH₄ also permeate through the gas permeation membrane. The retentate of the first stage is fed to a second stage in which the final product purity is obtained. The permeate of the second stage is recycled and mixed with the raw gas stream to enhance the CH₄ recovery. The third stage polishes the permeate of the first

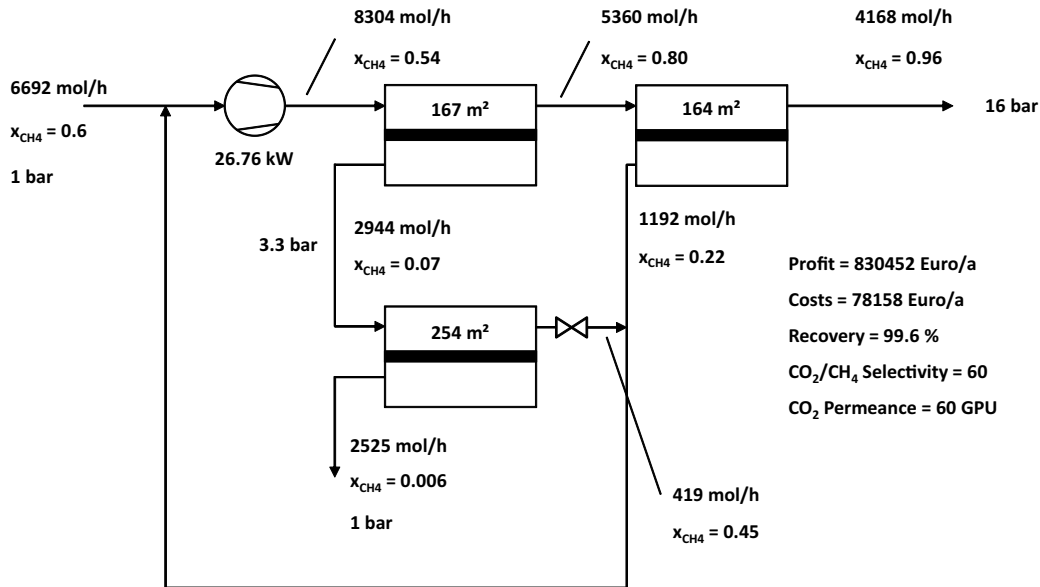


Figure 4.6: Optimal process design and process conditions for gas permeation membranes with a CO_2/CH_4 selectivity of 60 and a CO_2 permeance of 60 GPU.

stage and the retentate of the third stage is also recycled to further increase the CH_4 recovery of the process. The pressure valve on the retentate outlet of the third stage controls the feed pressure in the third stage, hence, it provides the driving force for permeation. Accordingly, the elevated pressure on the permeate side of the first stage reduces the driving force in the first stage. The optimal feed pressure in the third membrane stage is 3.3 bar.

By using this process a CH_4 recovery of 99.6 % can be obtained, which is slightly higher than the required recovery of 99.5 %. Unsurprisingly, the same process layout as well as the process conditions are chosen for the case in which the lower bound of CH_4 recovery is set to 95 %. An annual profit of approximately 830000 Euro can be realized along with annual upgrading costs of approximately 78000 Euro. A compressor with a compression duty of 26.76 kW is required to drive the process, which translates to a specific electrical energy demand of 0.178 kWh/m³(STP) with respect to the raw gas flow rate. A total membrane area of 585 m² has to be installed. This area results in a specific area demand of 3.9 m²h/m³(STP). Assuming a gas permeation module size of 25 m² per module, 24 modules have to be installed.

For a membrane reflecting the characteristics of a cellulose acetate membrane with a CO_2/CH_4 selectivity of 20 the results are depicted in Figure 4.7. In Figure 4.7(a) the lower bound for CH_4 recovery is set to 95 %. However, a higher CH_4 recovery of 98.7 % is identified to be optimal. The process layout does not change compared to the case in which more selective membrane materials are applied. An annual profit of approximately 810000 Euro is obtained and annual costs of approximately 90000 Euro have to be paid. While the total membrane area (524 m²) is almost constant compared to the process using more selective membranes, the compression demand increases significantly due to the increased recycle flow rate. A specific electrical compression demand of

0.22 kWh/m³(STP) together with a specific area demand of 3.5 m²h/m³(STP) are required. 21 gas permeation modules have to be installed in case that a single module contains 25 m² membrane area.

By demanding a CH₄ recovery of at least 99.5 %, the profit for a process using membranes with selectivities of 20 drops significantly. The optimal process is still the three stage process describe for the better selective material, while the areas to be installed in the three stages differ remarkably. However, the high recovery can only be obtained on cost of an increased recycle flow rate. The recycle flow rate (9024 mol/h) is even higher than the raw gas flow rate (6692 mol/h). This translates to a high compression demand and a high specific energy demand of 0.34 kWh/m³(STP). Since large amounts of gas are recycled, large membrane area is also required to obtain the required product gas purity. The total membrane area of 1739 m² results in a specific area demand of 11.6 m²h/m³(STP) with respect to the raw gas. Assuming a module size of 25 m² per module, 70 modules have to be installed. This poor performance results in low profitability (\approx 762000 Euro/a) and high annual upgrading cost (\approx 145000 Euro/a).

Although the solver can select a vacuum pump to generate the driving force for permeation, for each set of parameters considered here, the compression of the feed side is preferred. In any case the gas has to meet the natural gas grid pressure of 16 bar, so that at least a single compressor is needed to provide the natural gas grid pressure. In general, the investment costs for the membranes are 10 % of the total investment costs. This agrees well with the data published by Baker [9].

Comparing these results to conventional upgrading techniques such as amine absorption ($e_{elec} = 0.15$ kWh/m³(STP), $e_{therm} = 0.3-0.8$ kWh/m³(STP)) and pressurized water scrubbing ($e_{elec} = 0.25$ kWh/m³(STP)) clearly shows that the gas permeation process can compete with these established technologies [2, 5]. Please note that the energy demands for the conventional techniques are obtained at a gas grid pressure of 7 bar while the energy demand determined here refers to a grid pressure of 16 bar. In addition, the application of a multistage compressor would further reduce the electrical energy demand for the gas permeation processes.

4.3.3 Identifying the optimal selectivity and permeance

As material development aims for high selectivities and permeances, we used both parameters in process optimization. Hence, not only the process layout, the membrane area and the pressures are optimized, but also the optimal selectivity is determined. The optimal CO₂ permeance is calculated with the characteristic of the upper bound correlation of Robeson. For the processes considered here, the CH₄ recovery should be at least 99.5 % to minimize the environmental impact caused by extensive CH₄ losses. Two cases are investigated. In the first case a single selectivity is determined for all membrane stages while in the second case an optimal selectivity is calculated for each individual membrane stage.

Figure 4.8(a) shows the optimal process flowsheet for the first case in which only a single selectivity

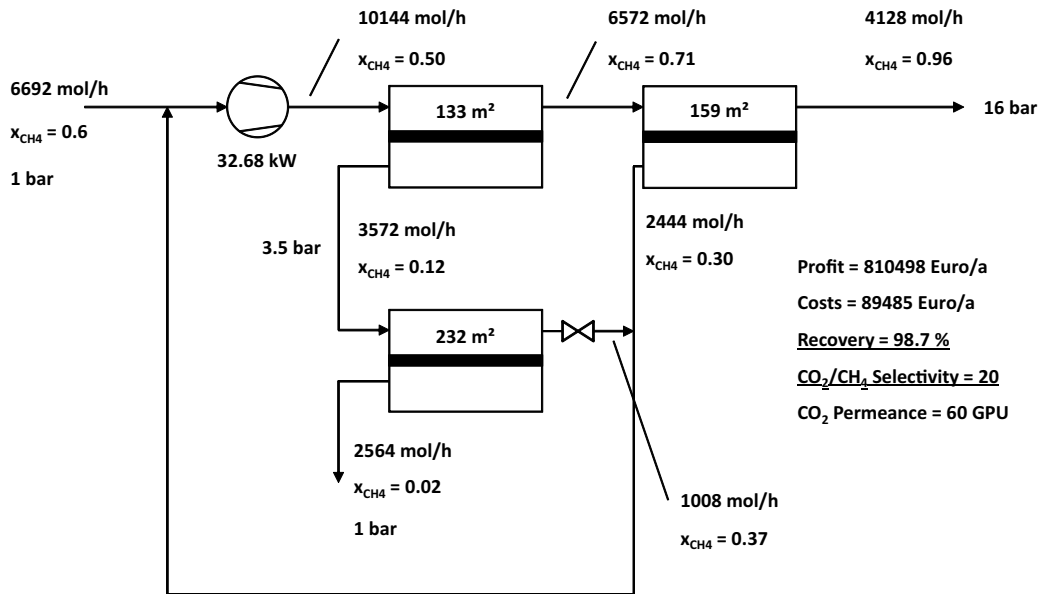
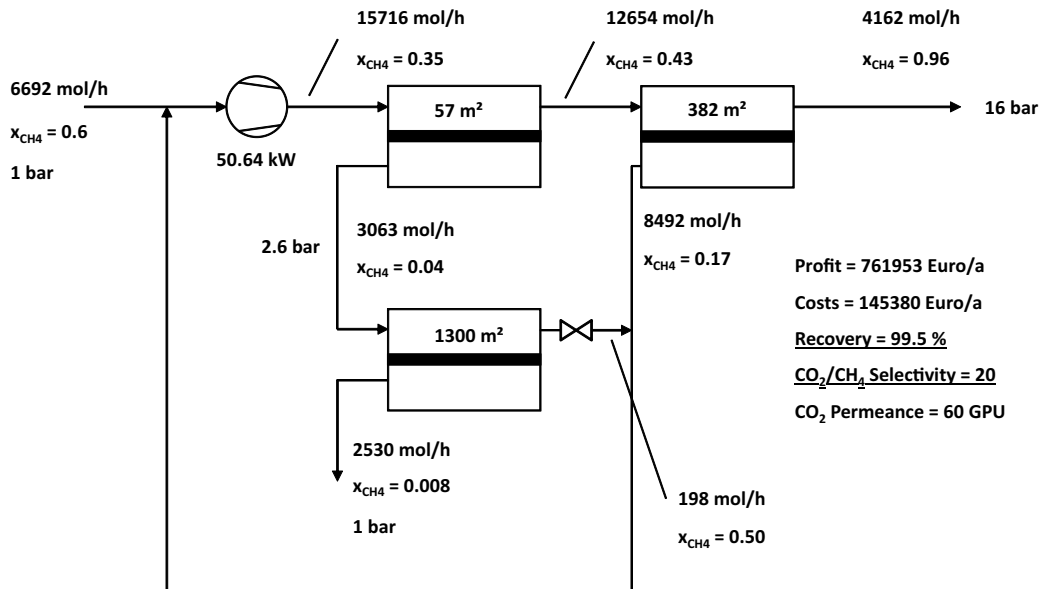
(a) The required CH_4 recovery is higher than 95 %.(b) The required CH_4 recovery is higher than 99.5 %.

Figure 4.7: Optimal process design and process conditions for gas permeation membranes with a CO_2/CH_4 selectivity of 20 and a CO_2 permeance of 60 GPU.

is applied to all membrane stages. Here, an optimal CO_2/CH_4 selectivity of 123 together with a CO_2 permeance of 555 GPU is determined. Compared to the processes in which a commercial gas permeation material is applied, the optimal process only consists of two membrane stages. This process design is similar to the three stage process presented in Section 4.3.2. However, the stage for final product gas purification is not required as the first stage already polishes the raw gas to product grade without generating large CH_4 losses in the permeate. Due to the Robeson's upper bound characteristic the required membrane area reduces significantly compared to the commercial

membranes ($585 \text{ m}^2 \rightarrow 127 \text{ m}^2$). Hence, only 5 gas permeation modules are required, assuming a module size of 25 m^2 . Interestingly, the energy demand to drive the process is similar to the case in which commercial materials are applied. Here, a specific energy demand of $0.161 \text{ kWh/m}^3(\text{STP})$ is required. Hence, the optimization of the membrane material has the strongest impact on the membrane area rather than on the energy demand. In terms of energy demand the commercial membrane with a CO_2/CH_4 selectivity requires similar energies to drive the gas permeation process (compare Section 4.3.2). An annual profit of approximately 842000 Euro with annual cost of approximately 65000 Euro can be obtained.

Figure 4.8(b) illustrates the process layout for the process optimization in which the membrane properties for each stage are determined individually. Although the selectivities and permeances differ significantly from the case in which only a single selectivity is optimized for all stages, the annual profit as well as the annual upgrading costs are almost constant. A small reduction in the energy demand is compensated by providing more membrane area.

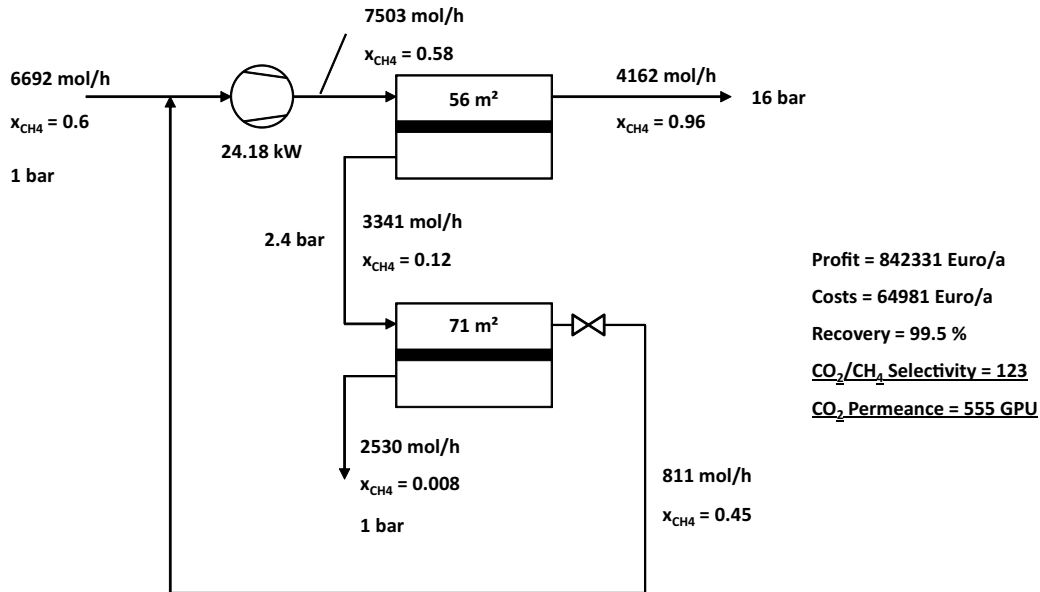
Changing the CH_4 feed mole fraction

In this section the impact of the CH_4 feed mole fraction on the process layout and selectivity is analyzed. Here, two effects have to be accounted for. On the one hand the CO_2 driving force increases with increasing CO_2 level in the feed gas. On the other hand, the higher the CH_4 mole fraction in the feed gas the less CO_2 has to be removed to meet the gas grid standard.

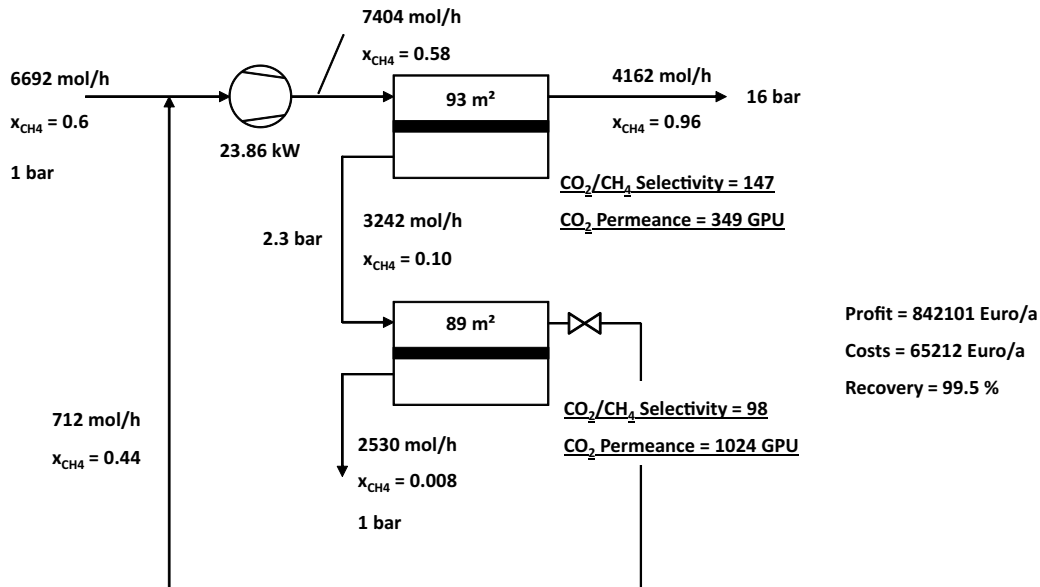
Figure 4.9 shows the optimal selectivity and the permeance of CO_2 as a function of the CH_4 mole fraction in the feed gas. Here, selectivity and CO_2 permeance follow the correlation of Robeson's upper bound. Although the feed mole fraction of CH_4 changes considerably from 50 % to 70 % the optimal selectivity is in the range between 118 and 123. The resulting CO_2 permeance ranges between 560 and 600 GPU. Regarding their selectivity polypyrrolones might be an adequate polymer of choice with a selectivity of 130 [148, 151].

The maximum in selectivity and as a consequence the minimum in permeance are caused by a trade-off between recycle ratio and driving force. The recycle ratio, which is the ratio of the recycle flow rate to the feed flow rate, increases with increasing CH_4 feed mole fraction. Increasing the selectivity steers against the increase in recycle ratio. On the other hand driving force decreases with increasing CH_4 feed mole fraction. Thus, larger membrane areas are required to compensate the loss in driving force. To reduce the required membrane area higher permeances have to be applied resulting in reduced selectivities.

The impact of the CH_4 feed mole fraction on annual profit is depicted in Figure 4.10. Since the product gas flow rate increases with an increased CH_4 feed mole fraction at a fixed CH_4 recovery, the profit also increases linearly with increasing CH_4 feed mole fraction.



(a) A single optimal selectivity is determined for all membrane stages.



(b) Individual optimal selectivities are calculated for each stage.

Figure 4.8: Optimal process design and process conditions for a gas permeation material inherent Robeson's upper bound characteristics.

Changing the required CH_4 product purity

Figure 4.11 shows the optimal CO_2/CH_4 selectivity as a function of the required CH_4 mole fraction in the product gas for a CH_4 feed mole fraction of 0.6 considering the case in which only a single selectivity is optimized for all membrane stages. Selectivity increases with increasing product purity. Increasing the CH_4 level in the product gas results in increased permeation of CH_4 in the first gas permeation stage which increases the recycle flow rate. As a consequence the energy demand to

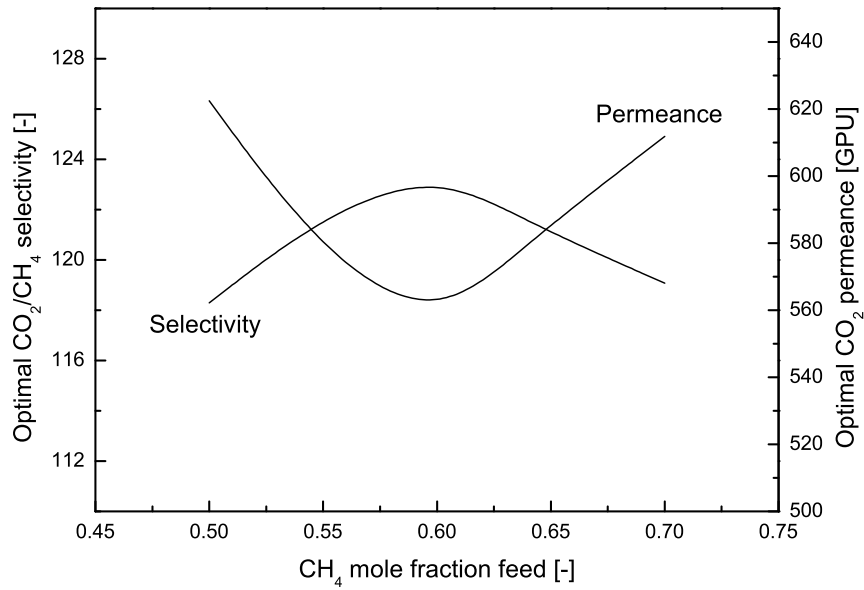


Figure 4.9: Optimal selectivity and CO₂ permeance as a function of the CH₄ mole fraction in the feed gas.

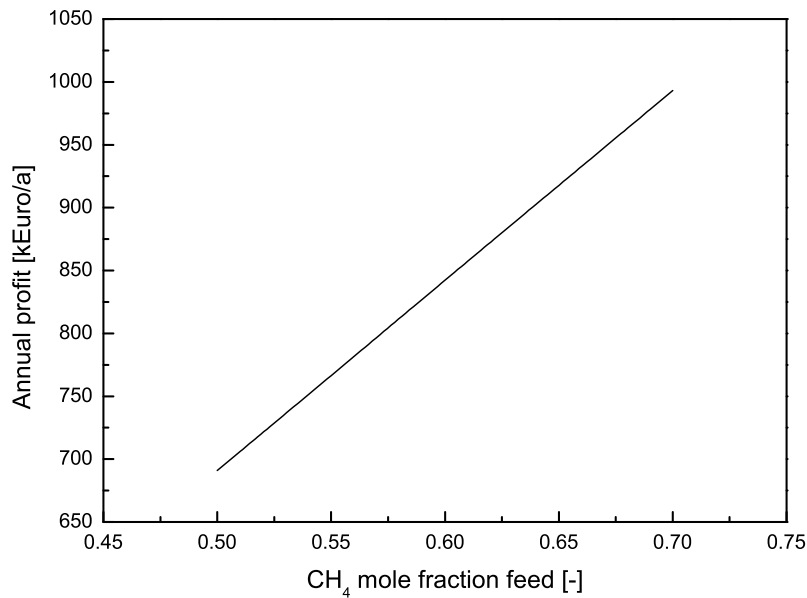


Figure 4.10: Profit as a function of the CH₄ mole fraction in the feed gas for an optimal selectivity and CO₂ permeance following the Robeson upper bound.

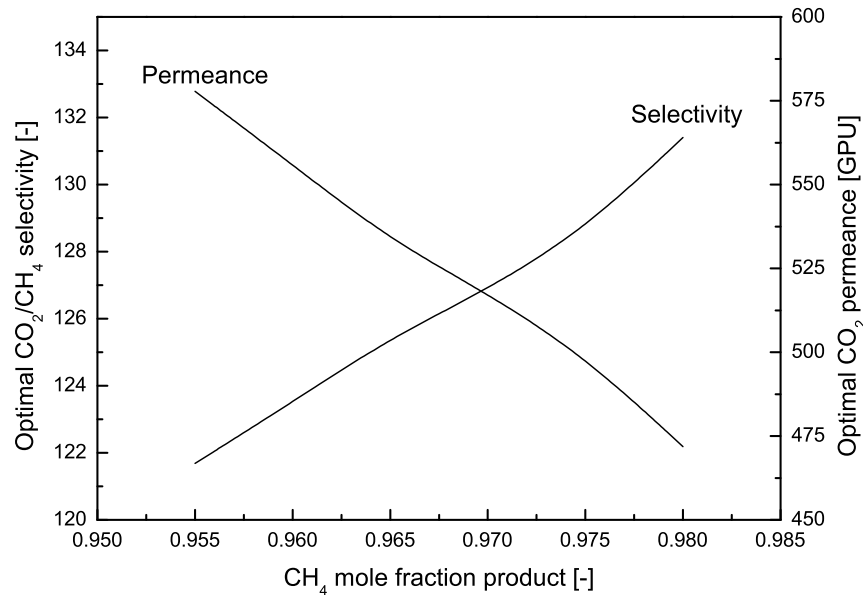


Figure 4.11: Optimal selectivity and CO₂ permeance as a function of CH₄ mole fraction of the product gas. The feed mole fraction of CH₄ is 60 %.

drive the compressor increases. To reduce the recycle flow rate selectivity increases which translates to lower permeances.

Compared to the change in the CH₄ feed mole fraction the change in the required CH₄ mole fraction of the product gas is more pronounced. The impact of the required product purity on optimal selectivity is more pronounced than the impact of the CH₄ feed mole fraction since the selectivity drops by more than 8 % while only increasing the CH₄ mole fraction of the product gas by 3.5 % (compare to Figure 4.9). This typically reflects the characteristic of gas permeation processes which are good in performing a bulk separation but need extensive efforts for providing high purities. Consequently, the required product purity has to be chosen carefully, since it has a tremendous impact on the process performance and only the required natural gas standard should be met. Figure 4.12 illustrates the annual profit as a function of CH₄ mole fraction of the product gas. Due to an increase in the recycle flow rate and required membrane area the annual profit decreases by 3.2 %.

Does the process benefit from higher selectivity and permeance?

From a technical point of view the process benefits from a better membrane material inherent upper bound characteristics. However, the profit for a process in which the CH₄ product mole fraction of 96 % and a CH₄ recovery of 99.5 % are achieved is 830000 Euro for a commercial membrane material ($Q_{CO_2}=60$ GPU, $\alpha_{CO_2/CH_4}=60$) and 842000 Euro for a material of the upper

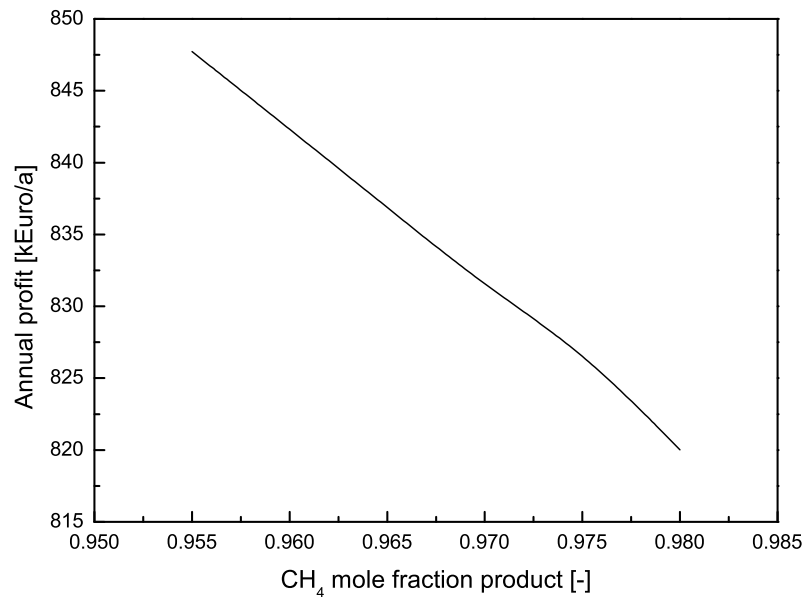


Figure 4.12: Profit for an optimal gas permeation process as a function of CH₄ mole fraction of the product gas. The feed mole fraction of CH₄ is 60 %.

bound ($Q_{CO_2}=580$ GPU, $\alpha_{CO_2/CH_4}=120$), respectively. Hence, the profit is increased by less than 2 %. The annual upgrading costs can be reduced from 78000 Euro for a current membrane material to 65000 Euro for an optimal material. Thus, the annual costs decrease by approximately 16 %. Ultimately, the optimal membrane material has only a minor impact on the process profitability. Taking the material development costs into account and considering that this material has to be manufactured in large quantities it is unlikely that the increase in profitability justifies the effort for material development for this particular separation process. In addition, Baker [9] reported that only nine polymeric membrane materials play a role in large scale application of gas permeation membranes. Furthermore, for selectivities as high as 100 and permeances exceeding 1000 GPU concentration polarization will have an impact on the module performance. Most likely the increase in profitability will be diminished by concentration polarization.

4.4 Conclusions

A process model for structural optimization of gas permeation processes is presented and applied to the separation of CH₄ and CO₂ in biogas upgrading. Short cut models for a gas permeation module, a compressor, a vacuum pump and a pressure valve have been implemented in GAMS. Both, commercial membrane materials as well as optimal membrane materials have been investigated. For the commercial gas permeation membranes a three stage gas permeation process using only a

single compressor is most profitable. Comparing two types of commercial membrane materials the process equipped with membrane materials with CO_2/CH_4 selectivity of 60 has a higher profit and lower costs than the process with low selective membranes. Regarding the specific energy demand, the optimized gas permeation processes can compete with established gas separation techniques for biogas upgrading. The simple process layout and the robustness of the process would even favor the application of gas permeation technology in biogas upgrading.

Moreover, we investigated the impact of optimal selectivity on the process performance where the membrane material follows the correlation for Robeson's upper bound. Two cases have been investigated in which a two stage process is identified to be most profitable. First a single optimal selectivity for all gas permeation stages have been determined ($\alpha_{\text{CO}_2/\text{CH}_4}=120$). Subsequently, the selectivity is optimized for each membrane stage individually. Here, a high selective stage ($\alpha_{\text{CO}_2/\text{CH}_4}=147$) is combined with a stage in which high permeances ($\text{CO}_2 = 1024 \text{ GPU}$) are required.

However, the impact of optimized membrane materials on profitability is low, as the CH_4 recovery of the three stage process using commercial membrane modules is already high. Hence, the product gas flow rate cannot be increased significantly. The choice of the membrane material has an impact on the upgrading costs. For the optimal membrane material it is questionable if development and product launching costs justify the application of such a material. Ultimately, the application of a three stage gas permeation process with current commercial membranes already shows good performance.

4.5 Appendix

In order to facilitate the application of the superstructure model implemented in GAMS, a graphical user interface (GUI) has been developed in Microsoft-Excel as most engineers are familiar with MS-Excel. An example input data sheet for MS-Excel is presented in Figure 4.13. Key parameters such as permeances, costs for membrane and pressure, feed conditions and product requirements have to be specified. In addition, the maximum number of membrane stages as well as the maximum number of compressors and vacuum pumps have to be defined.

Figure 4.14 illustrates the output data sheet from MS-Excel. The optimal process flowsheet is displayed showing the number of unit operations and their connections. Furthermore, key performance indicators such as membrane area or compression demand can be displayed.

However, it might be possible to develop a web-based interface, so that external users can use the GAMS tool, without having GAMS installed on their machine. Thus, a first evaluation of membrane technology for a separation task can easily be performed without having a strong background in membrane science and technology.

| Feed | | Membran | | Kosten | |
|-------------------|--|--------------------------------|--|---------------------|-----------------------|
| Volumenstrom: | 200 Nm ³ /h | Anzahl: | 2 | Strompreis: | 0,08 €/kWh |
| Zusammensetzung: | 50,00% CH ₄ 50,00% CO ₂ | Kosten: | 55 €/m ² | Wärmepreis: | 0,5 €/MWh |
| Permeatdruck: | 1 bar | Permeanz: | 0,0439 GPU (CH ₄) 2,1960 GPU (CO ₂) | Zinssatz: | 8% |
| Feeddruck: | 16 bar | CO ₂ -Selektivität: | 50 | Abschreibungsdauer: | 15 Jahre |
| Mindest Ausbeute: | 98,00% | Verdichter: | 1 | Standzeit: | 4 Jahre |
| | | | | Verguetung: | 0,8 €/Nm ³ |

| Produkt | | Module | | Verdichter | |
|----------------------------|--------------------------|--------|-----------------------------------|------------|--------------------|
| CH ₄ -Reinheit: | 97,0% Soll 97,0% Ist | Fläche | Kosten | Leistung | Kosten |
| Volumenstrom: | 75,78 Nm ³ /h | M1 | 196,82 m ² 18.698,81 € | V2 | 0,0 kW 2.486,79 € |
| | | M2 | 143,16 m ² 18.698,81 € | V1 | 36,1 kW 2.486,79 € |
| | | M3 | 0,00 m ² 18.698,79 € | | |

| Prozess | | Solver Reports | |
|---------------------|--------------------------|-----------------|--------------|
| Ausbeute: | 98,01% | Gams Version: | 23,9 |
| Rezirkulationsrate: | 8% | Modelstatus: | 2 |
| Spezifische Kosten: | 9,00 ct./Nm ³ | Lokal Optimal?: | |
| Investitionskosten: | 140.328,89 € | Solverstatus: | 1 |
| Einnahmen: | 485.013,44 € | Normal: | |
| Kosten: | 54.578,37 € | Benötigte Zeit: | 1,7 Sekunden |
| Gewinn: | 430.435,07 € | | |

| |
|----------------|
| GO ! |
| Reset |
| Element Editor |

Figure 4.13: GUI for GAMS programmed with Visual Basic in MS-Excel: Input sheet.

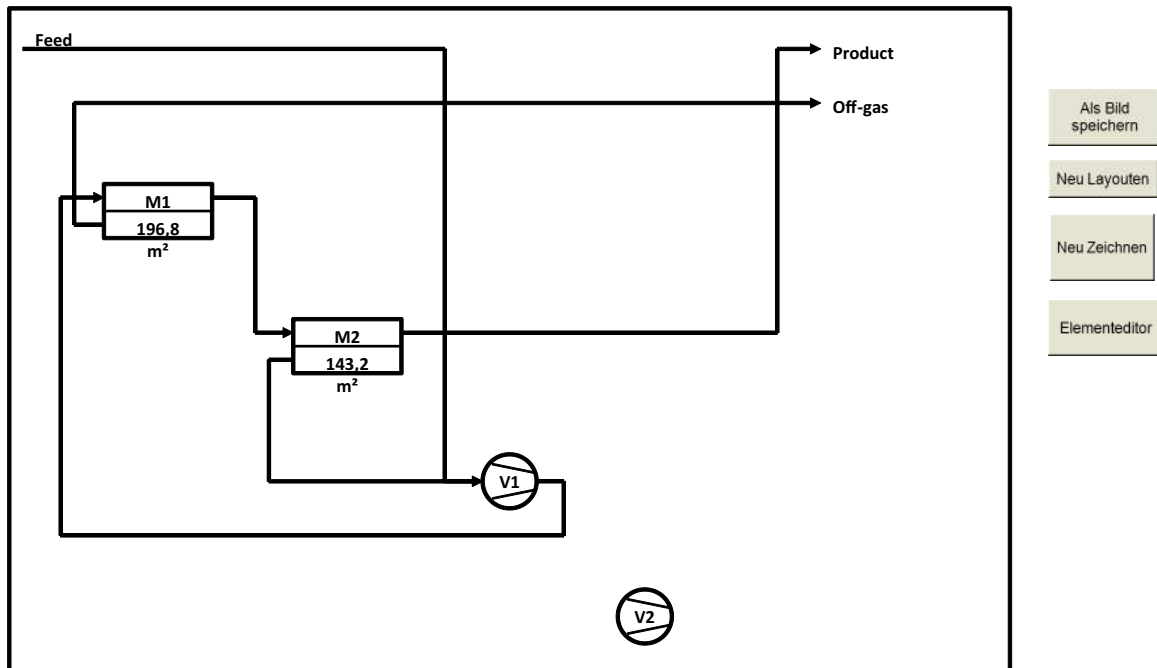


Figure 4.14: GUI for GAMS programmed with Visual Basic in MS-Excel: Output sheet showing an example of an optimal process flowsheet.

Chapter 5

Dynamic simulation and control of a membrane based biogas upgrading process

5.1 Introduction

Commonly, gas permeation processes are modelled and analyzed in the steady state mode because it is valid for a large variety of separation processes. However, some processes show a distinct dynamic behavior where a dynamic analysis is required [152]. Furthermore, the initial operation in the start-up and the shut down of a process is dynamic which can be analyzed with dynamic models. In particular, variations in the feed conditions have a decisive impact on the separation performance of gas permeation processes. In this work at hand, we investigate the impact of changing feed flow rates and compositions as well as the start-up on the separation performance of a membrane based biogas upgrading process [2, 15, 87, 97, 153].

In order to maintain the product purity of the upgraded biogas at pipeline specifications various control schemes are proposed. Here, two simple but effective control structures are investigated in detail by analyzing the product purity as a function of time for modified feed gas conditions. In this work we present a three stage gas permeation process with partial decompression to upgrade biogas which is presented in Chapter 4. This process is able to achieve both, high CH₄ purities as well as high CH₄ recoveries by using only a single compressor.

A dynamic model of a hollow fiber gas permeation module was programmed and applied to the dynamic process simulation. The process analysis was performed by using Aspen Engineering Suite [32]. The dynamic model of the gas permeation module was programmed in Aspen Custom Modeler. Subsequently, the biogas upgrading process was implemented in Aspen Plus using the Aspen Custom Modeler gas permeation model which was presented in Chapter 3. The flowsheet was exported to Aspen Plus Dynamics to perform dynamic simulations of the biogas upgrading process. In order to maintain the product gas purity a control scheme was implemented to adjust changes in the feed conditions.

Literature on the dynamic modeling of classical membrane processes such as reverse osmosis, pervaporation and gas permeation is limited. Typically, these processes are modelled in steady state. However, in gas permeation two interesting studies have been reported by Bouton and Luyben [154] and Katoh et al.[41]. Bouton and Luyben [154] analyzed the dynamic behavior of a hydrodealkylation process (HDA) using a single gas permeation module. They programmed a gas permeation model in Aspen Custom Modeler and applied it to the dynamic process simulation (Aspen Plus Dynamics) to identify the economic optimum. Katoh et al. [41] programmed a dynamic multicomponent gas permeation model to analyze the separation of H₂, CH₄, C₂H₆ and C₃H₈ as well as the separation of CH₄, CO₂ and H₂. Here, hollow fiber gas permeation modules have been modelled.

In this study we present a model to investigate the dynamic behaviour of a multistage gas permeation process. The process analysis facilitates the application of process controllers to maintain stable product gas conditions. We also present two new process control schemes which are not limited to the separation of CO₂ and CH₄.

Table 5.1: Permeances and feed composition of the biogas components.

| Parameter | Unit | Value |
|-------------------------------|------------------|-------|
| Feed mole fraction CH_4 | - | 0.5 |
| Feed mole fraction CO_2 | - | 0.5 |
| Feed flow rate | $\frac{kmol}{h}$ | 11.72 |
| Feed temperature | $^{\circ}C$ | 20 |
| Feed pressure | bar | 1 |
| Product pressure | bar | 16 |
| CH_4 mole fraction product | - | 0.96 |
| CH_4 permeance | GPU | 1 |
| CO_2 permeance | GPU | 60 |
| Permeate pressure first stage | bar | 4 |

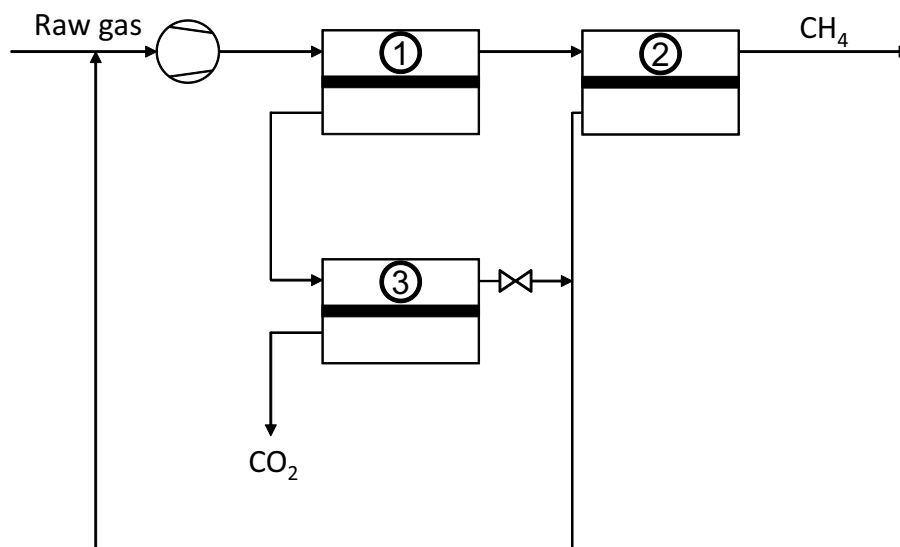


Figure 5.1: Flowsheet of a three stage gas permeation process to upgrade biogas and labelling of the respective membrane stages. Both, high CH_4 purities and high CH_4 recoveries can be obtained simultaneously.

5.2 Upgrading process

Biogas mainly consists of CH_4 and CO_2 . Hence, CO_2 has to be removed from CH_4 to obtain an upgraded gas with an increased heating value which can be used as natural gas substitute. Several trace compounds like H_2S or H_2O are also present in the biogas and these components have to be removed as well due to their corrosive nature. However, in this study we focus on the separation of CO_2 and CH_4 as it is the most important separation for biogas upgrading as a consequence of the high CO_2 load in the feed gas. Hence, all trace components are not considered here. It is a well

known fact that gas permeation membranes are an excellent technology to separate CO₂ and CH₄ [2, 93, 117]. Single stage gas permeation processes can be used to generate a CH₄ rich product gas, though significant CH₄ losses are observed in the permeate.

Figure 5.1 illustrates the flowsheet of the three stage gas permeation process [155]. Here, the CH₄ is supplied at natural gas grid grade and high CH₄ recoveries are obtained. No additional compression equipment is required, since the upgraded biogas is supplied at pipeline pressure. In this study the pipeline pressure is assumed to be 16 bar. The gas permeation process consists of three membrane stages. The first stage is connected to the compression unit and the retentate of the first stage is the feed of the second stage. The retentate of the second membrane stage is the product, thus the upgraded biogas. The permeate of the second stage is recycled and mixed with the feed stream to increase the CH₄ recovery. The permeate of the first stage is fed to a third membrane stage. Here, the retentate stream of the third stage, which is rich in CH₄ is recycled and mixed with the feed stream to further increase the CH₄ recovery. The permeate stream of the third stage is the exhaust gas stream of the process which is enriched in CO₂. The driving force of permeation in the third membrane stage is generated by using a pressure valve at the retentate outlet of the third membrane stage which also increases the permeate pressure in the first membrane stage. Hence, only a single stage compressor is required to drive the upgrading process.

The separation of CO₂ and CH₄ can be done by utilizing glassy polymeric membrane materials. Table 5.1 shows the typical permeances of the biogas components for such a membrane material as well as the process conditions applied to the dynamic simulations.

5.3 Process model

The model of a hollow fiber gas permeation module was presented in Chapter 3. This model was adapted and the dynamic terms were added to the mass balance equations. The mass balances are the basic equations to be solved. The balance for substances on the retentate side for counter current flow is:

$$0 = \frac{\partial n_{R,j}}{\partial t} + \frac{\partial \dot{n}_{R,j}}{\partial x} dx + \dot{n}_{M,j} \quad (5.1)$$

Here, $n_{R,j}$ is the amount of component i on the retentate side and $\dot{n}_{R,j}$ is the molar flow rate of component i on the retentate side. The term $\dot{n}_{M,j}$ delineates the molar flow rate through the gas permeation membrane. The respective balance for the permeate side of the module in counter current flow is:

$$0 = \frac{\partial n_{P,j}}{\partial t} + \frac{\partial \dot{n}_{P,j}}{\partial x} dx + \dot{n}_{M,j} \quad (5.2)$$

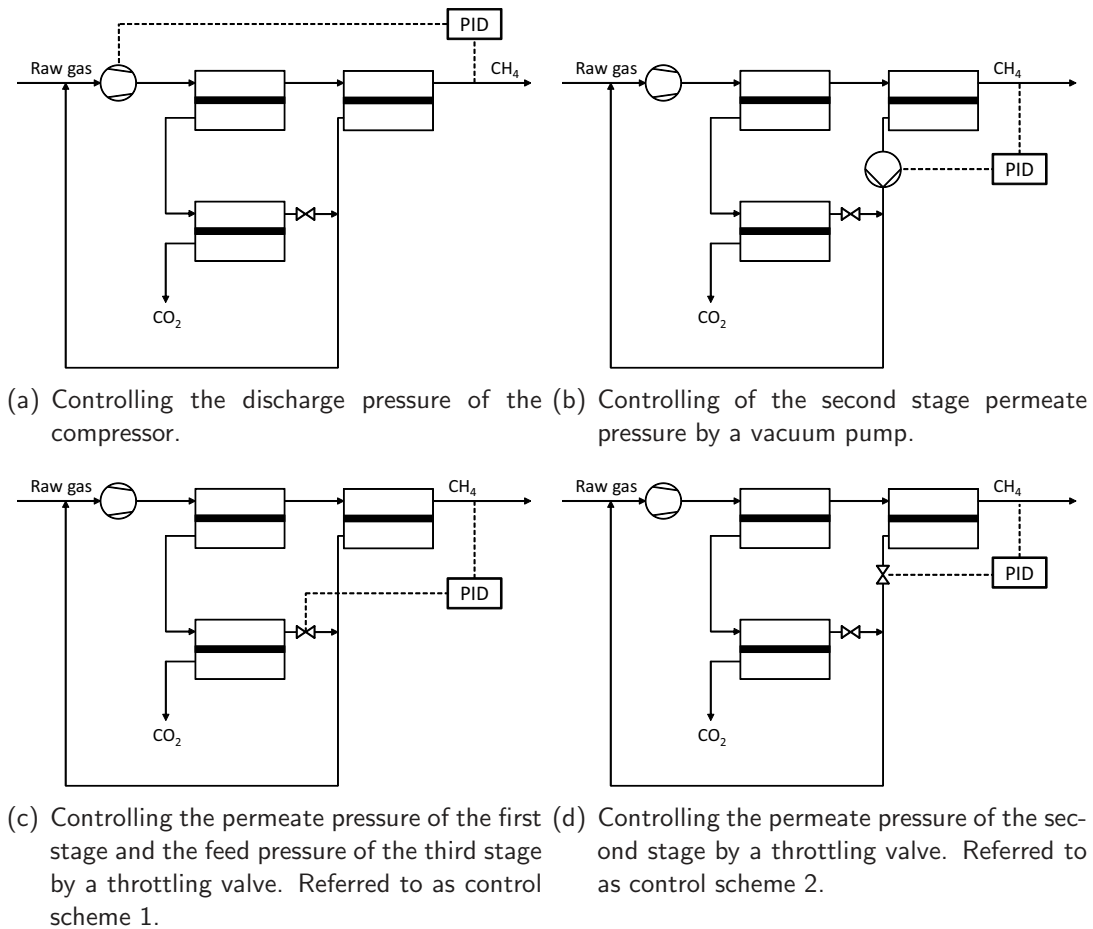


Figure 5.2: Process control schemes for a three stage membrane based biogas upgrading process to maintain the CH_4 mole fraction in the product gas for variations in the feed conditions.

Simplifying assumptions are made to reduce the model complexity and to enhance the robustness of the model for dynamic simulation. These simplifying assumptions are: (i) constant permeances, (ii) isothermal operation and neglecting Joule-Thomson Effect, (iii) neglecting concentration polarization, (iv) ideal gas behavior, (v) plug flow on lumen and shell side of the module, and (vi) laminar flow on both sides of the membrane.

Pressure losses are calculated by Hagen-Poiseuille equation. The gas permeation model was programmed in Aspen Custom Modeler where dynamic simulations can be performed. Subsequently, the model was exported to the Aspen Plus process simulation engine. Here, the gas permeation model can be combined with conventional unit operations such as compressors and a flowsheet of the biogas upgrading process is set up, so that steady state process simulations can be performed. In order to conduct dynamic simulations of the biogas upgrading process the Aspen Plus flowsheet was exported to Aspen Plus Dynamics. In Aspen Plus Dynamics process control equipment is available and used for the biogas upgrading process.

Table 5.2: Process parameters for both control schemes investigated.

| | Unit | Control 1 | Control 2 |
|---------------------------------------|----------------|-----------|-----------|
| Membrane area 1. stage | m ² | 520 | 520 |
| Membrane area 2. stage | m ² | 520 | 1382 |
| Membrane area 3. stage | m ² | 780 | 700 |
| Permeate pressure 1. stage | bar | 4 | 4 |
| Permeate pressure 2. stage | bar | 1 | 3 |
| CH ₄ mole fraction product | - | 0.96 | 0.96 |
| Initial CH ₄ recovery | - | 0.995 | 0.995 |

Table 5.3: Parameters for the PID controller applied here.

| Parameter | Unit | Value |
|-------------------|------|-------|
| Proportional gain | - | 1 |
| Integral gain | min | 20 |
| Derivative gain | min | 0 |

5.4 Process control schemes

Figure 5.2 illustrates possible process control schemes to maintain a CH₄ mole fraction of 96 % in the product gas. The control structure illustrated in Figure 5.2(a) measures the product purity and adjusts the discharge pressure of the compressor. In case that the CH₄ purity decreases the discharge pressure of the compressor increases and vice versa. However, this control scheme is limited. On the one hand it is inefficient in case of compensating low product purities since the discharge pressure of the compressor is higher than the required injection pressure for the natural gas grid. Hence, the energy demand to drive the process increases. On the other hand if the product purity is higher than the required injection purity lowering the compressors discharge pressure is limited to the injection pressure of the natural gas grid, here 16 bar. Thus, controlling the product purity by manipulating the feed gas compressor is inefficient. However, it is reasonable to note that no additional process equipment is required.

Figure 5.2(b) shows a process in which the CH₄ level of the product gas is controlled by the pressure on the permeate side of the second membrane stage. By lowering the pressure on the permeate side the mole fraction of CH₄ increases. The additional vacuum pump results in additional investment costs as well as increasing operating costs. However, the permeate flow rate of the second membrane stage is low, hence the costs for the vacuum equipment might be insignificant.

The process control scheme presented in Figure 5.2(c) operates without any additional process

equipment, so that additional investment costs do not emerge. In this particular process the permeate pressure of the first membrane stage, which is also the feed pressure of the third stage, is controlled by a PID controller adjusting the pressure valve opening. This process control design is simple and since the permeate is at elevated pressure anyway, the process performance does not change significantly compared to a process without a controller.

Figure 5.2(d) illustrates a second process control scheme which operates by changing the permeate pressure of the second stage. Commonly, the second membrane stage is operated with a permeate pressure of approximately 1 bar to obtain the highest possible driving force. However, for the process control design proposed here, a lower driving force is accepted and the permeate pressure is increased up to 3 bar. The loss of separation performance is compensated by providing additional membrane area in the second membrane stage to enhance the CH₄ recovery. The process operating with an elevated permeate pressure in the second stage has similar characteristics like the process control using a vacuum pump on the permeate side of the second stage (see Figure 5.2(b)). This particular process design has the advantage of operating close to the control factor which is the CH₄ mole fraction in the product gas. Hence, the process control scheme should be able to compensate changes in the feed conditions faster than the aforementioned process control schemes.

Aspen Plus Dynamics facilitates the application of conventional process control equipment. Hence, it is possible to implement a control scheme keeping the product purity at specification when changing feed conditions influence the plant performance.

Two different effects have to be considered when the product gas conditions deviate from the gas quality specifications. First, the product purity decreases and the product gas cannot be supplied to the natural gas grid. Second, the change in feed conditions will increase the product purity and the gas can be supplied to the natural gas grid. However, it is inefficient to supply upgraded biogas with concentrations significantly higher than the required product purity. Consequently, more energy is consumed and the CH₄ recovery decreases which directly reduces the plants' profitability.

A PID controller is used to operate the upgrading process since it is the most flexible controller. The PID controller can be used as a P-, PI- or PD controller by zeroizing the respective controller parameters. Both process control schemes, which are presented in Figure 5.2(c) and Figure 5.2(d) are analyzed in detail. Table 5.2 and Table 5.3 present the parameters applied in the dynamic process simulation.

5.5 Results and Discussion

In this section the impact of changes in the feed conditions on the CH₄ mole fraction of the product gas, which is referred to as product purity, is analyzed. Here, dynamic simulations with and without a controller, that maintains the product purity, are performed to demonstrate the positive effect of the controller on the performance of the gas permeation process. Four different scenarios are analyzed

which are (i) the reduction and (ii) the increase in the feed flow rate as well as (iii) the reduction and (iv) the increase in the CH₄ mole fraction of the feed gas. The changes in these respective variables are enforced in a S-shape course. The two different control schemes are analyzed in detail, where the feed conditions, the product purity, the recycle flow rates and the pressure controlling the product purity are recorded and shown in the following figures.

5.5.1 Control scheme 1 (see Figure 5.2(c))

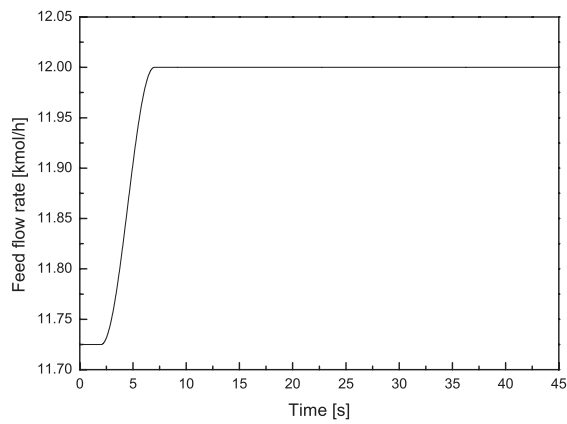
Increasing the feed flow rate

Figure 5.3 illustrates the performance of the biogas upgrading process for an increase in the feed flow rate. In this case, the flow rate is changed from 11.72 kmol/h to 12 kmol/h within 5 seconds.

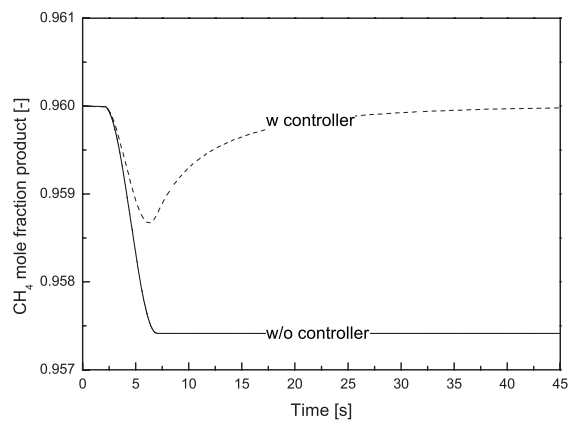
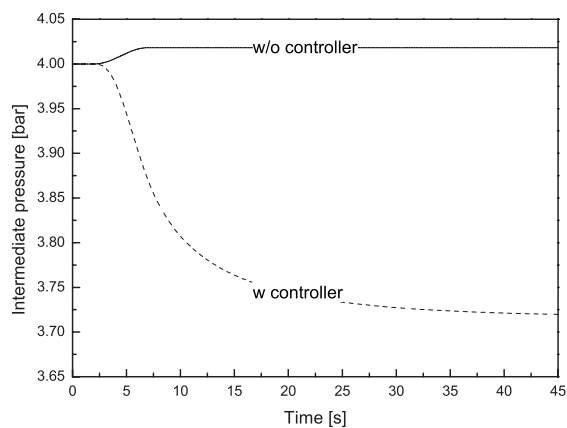
Figure 5.3(a) shows the feed flow rate as a function of time causing the changes of the other variables in the system. Figure 5.3(b) illustrates the mole fraction of CH₄ in the product stream. For the process without a controller maintaining the product purity, the mole fraction drops under the gas grid specifications. The changes in the product gas due to changes in the feed conditions are observed almost instantly in the product gas. Manipulating the feed pressure by applying a controller to the third membrane stage, the product purity decreases but not as significantly as in the case without controller. In addition, the controller is able to increase the product purity by increasing the feed pressure in the third membrane stage (see Figure 5.3(c)). Figure 5.3(b) shows that the required level of the CH₄ mole fraction in the product gas is reached within 45 s.

The feed pressure of the third membrane stage, which is also the permeate pressure of the first stage, is decreased in order to enhance the driving force for CO₂ permeation in the first stage. Hence, the stage cut in the first gas permeation stage is increased. However, the CH₄ recovery of the upgrading process decreases. The slight increase in the feed pressure of the third stage for a system without a controller occurs due to a slight increase in the stage cut of the first membrane stage as a consequence of the changed concentration profile within the first stage. The increased flux in the first stage increases the flow rate through the pressure control valve. Here, the valve opening is constant and hence, the pressure upstream of the valve increases. The increased pressure in the third stage forces more gas through the membrane so that the recycle stream is almost constant for a system without a controller (see Figure 5.3(d)).

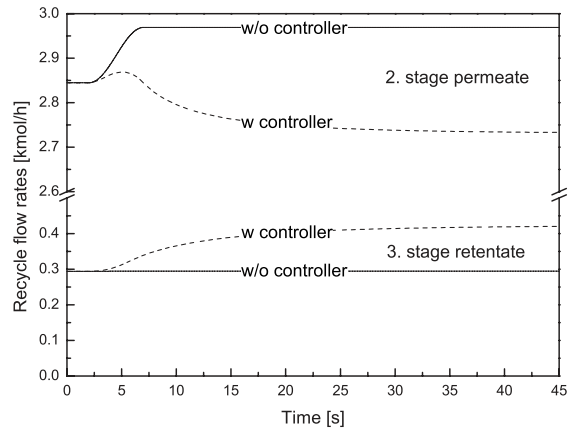
In Figure 5.3(d) the recycle flow rates of the second stage permeate and the third stage retentate are presented as a function of time and as a response to the changed feed flow rate. For a system without controller the recycle of the second stage increases due to an increased CO₂ level on the feed side of the second stage. By applying a controller the recycle flow rate of the second stage decreases since more CO₂ is removed in the first membrane stage which results in a lower CO₂ concentration at the inlet of the second stage. The recycle flow rate of the third stage is constant for a system in which no controller is used. By using the controller the recycle flow rate increases



(a) Feed flow rate as a function of time.

(b) CH₄ mole fraction in the product gas as a function of time and as a response to the change in the feed conditions.

(c) The intermediate pressure, which is the feed pressure of the third membrane stage, is shown as a function of time.



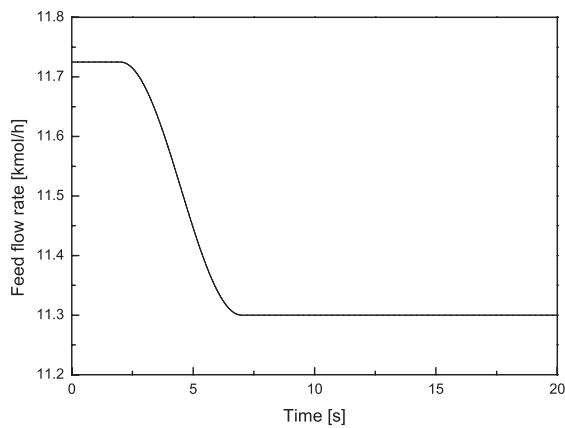
(d) The two recycle flow rates are illustrated as a function of time and as a response to changing feed conditions.

Figure 5.3: Control scheme 1 - The performance of the biogas upgrading process is illustrated for an increase in the feed flow rate. Both the performance with and without a controller maintaining the product purity are presented. The dashed lines represent the flow rate for a process with a control scheme and the full lines illustrate the flow rates for a process without controller.

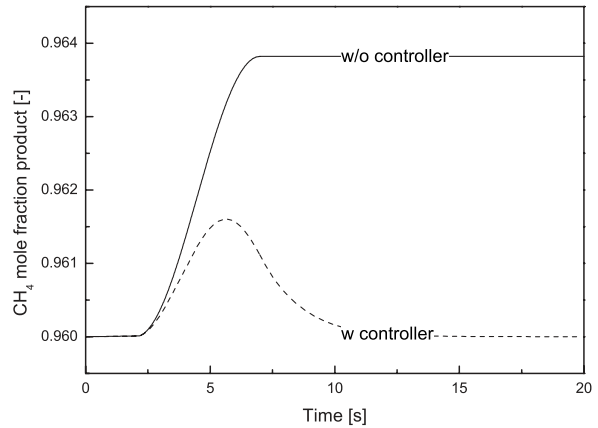
due to a driving force reduction as a consequence of the lower pressure on the feed side of the third stage.

Reducing the feed flow rate

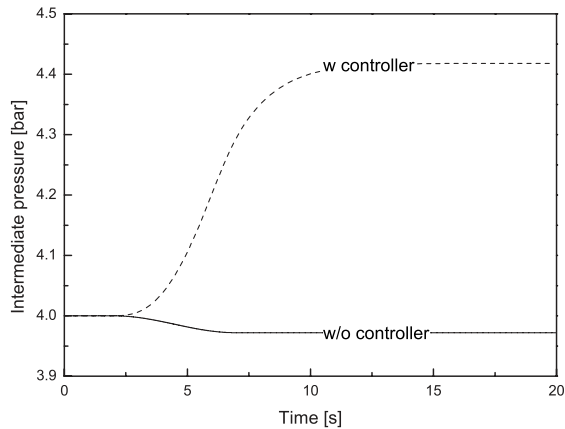
Figure 5.4 illustrates the performance of the gas permeation process for a reduced feed flow rate which is decreased from 11.72 kmol/h to 11.3 kmol/h within 5 seconds (see Figure 5.4(a)). Figure 5.4(b) shows the CH₄ mole fraction of the product gas as a function of time and as a response to the reduced



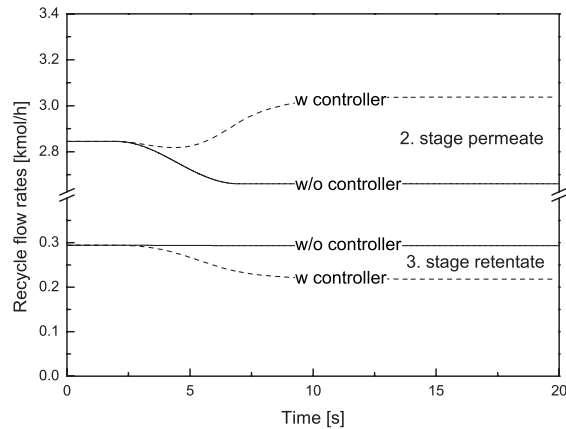
(a) Feed flowrate as a function of time.



(b) CH₄ mole fraction in the product gas as a function of time and as a response to the change in the feed conditions.



(c) The intermediate pressure, which is the feed pressure of the third membrane stage, is shown as a function of time.



(d) The two recycle flow rates are illustrated as a function of time and as a response to the change in the feed conditions.

Figure 5.4: Control scheme 1 - The performance of the biogas upgrading process is illustrated for a reduction in the feed flow rate. Both the performance with and without a controller maintaining the product purity are presented. The dashed lines represent the flow rate for a process with a control scheme and the full lines illustrate the flow rates for a process without controller.

feed flow rate. By decreasing the feed flow rate the product gas purity increases. Technically the injection of biogas to the natural gas grid is not affected by a higher CH₄ purity. However, it is more economic for the biogas supplier to only provide gas at the required product gas purity.

For a gas permeation process without controller the CH₄ mole fraction of the product gas increases to 96.4 %. By applying the controller the CH₄ purity reaches a maximum value of approximately 96.15 % and the target purity of 96 % is reached after the short period of 15 s.

Figure 5.4(c) presents the feed pressure of the third membrane stage as a response to the reduced feed flow rate. For the operation without controller, less mass permeates through the first stage

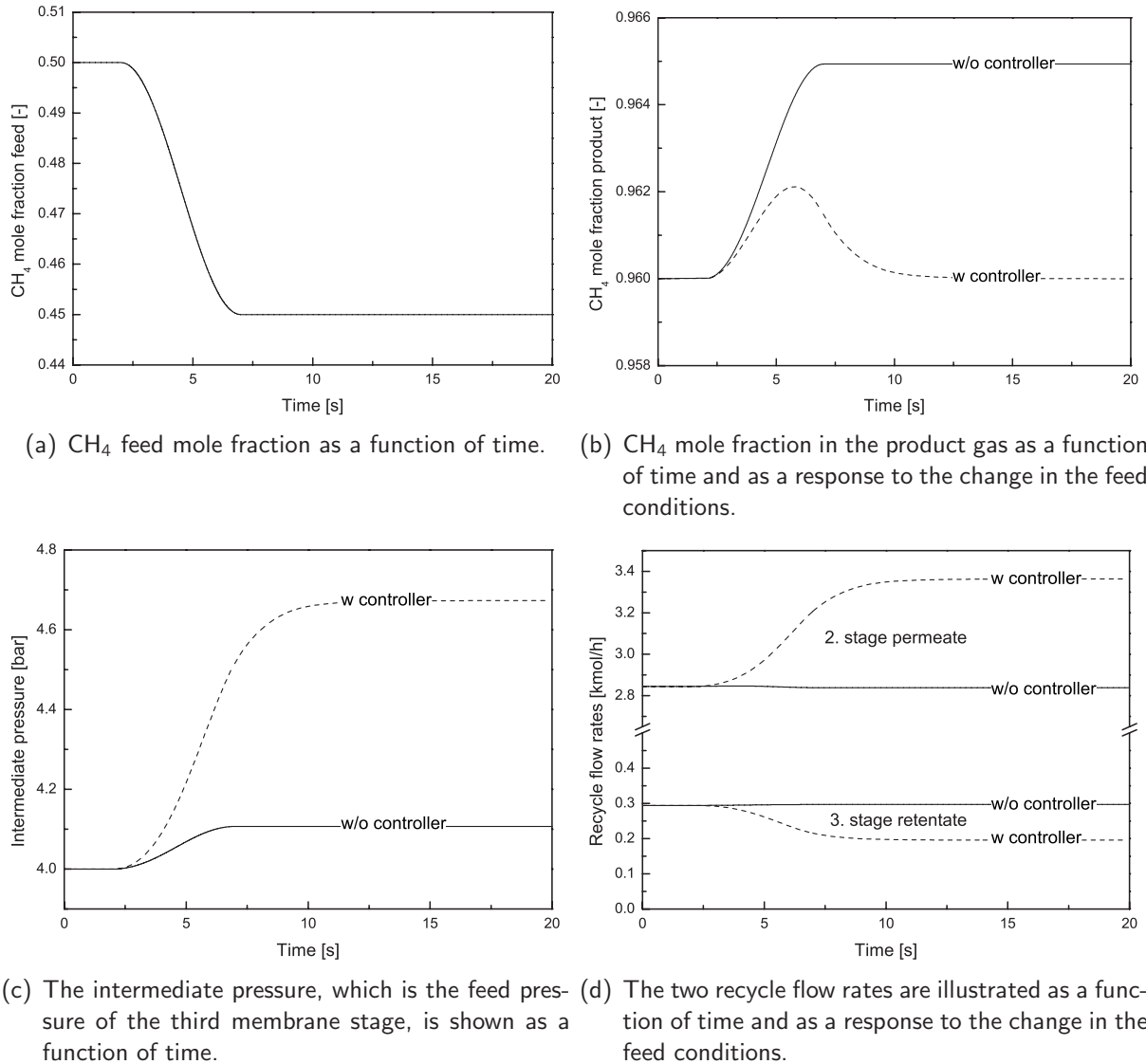


Figure 5.5: Control scheme 1 - The performance of the biogas upgrading process is illustrated for a reduction of the CH₄ mole fraction in the feed gas. Both the performance with and without a controller maintaining the product purity are presented. The dashed lines represent the flow rate for a process with a control scheme and the full lines illustrate the flow rates for a process without controller.

when reducing the feed flow rate. As the valve opening is constant, the reduced flow rate in the feed of the third stage results in a decrease of the feed pressure of the third stage. In order to maintain the product purity using a controller it is expedient to increase the pressure on the permeate side of the first membrane stage. Hence, the stage cut decreases and the CH₄ mole fraction in the product gas decreases as well. The pressure is increased from 4 bar to 4.4 bar.

In Figure 5.4(d) the recycle flow rates of the second and third stage are shown as a function of time. Similarly to the increase in the feed flow rate, the reduction in the feed flow rate does not affect the flow rate of the third stage recycle which is due to the selfcompensating effect of the increased

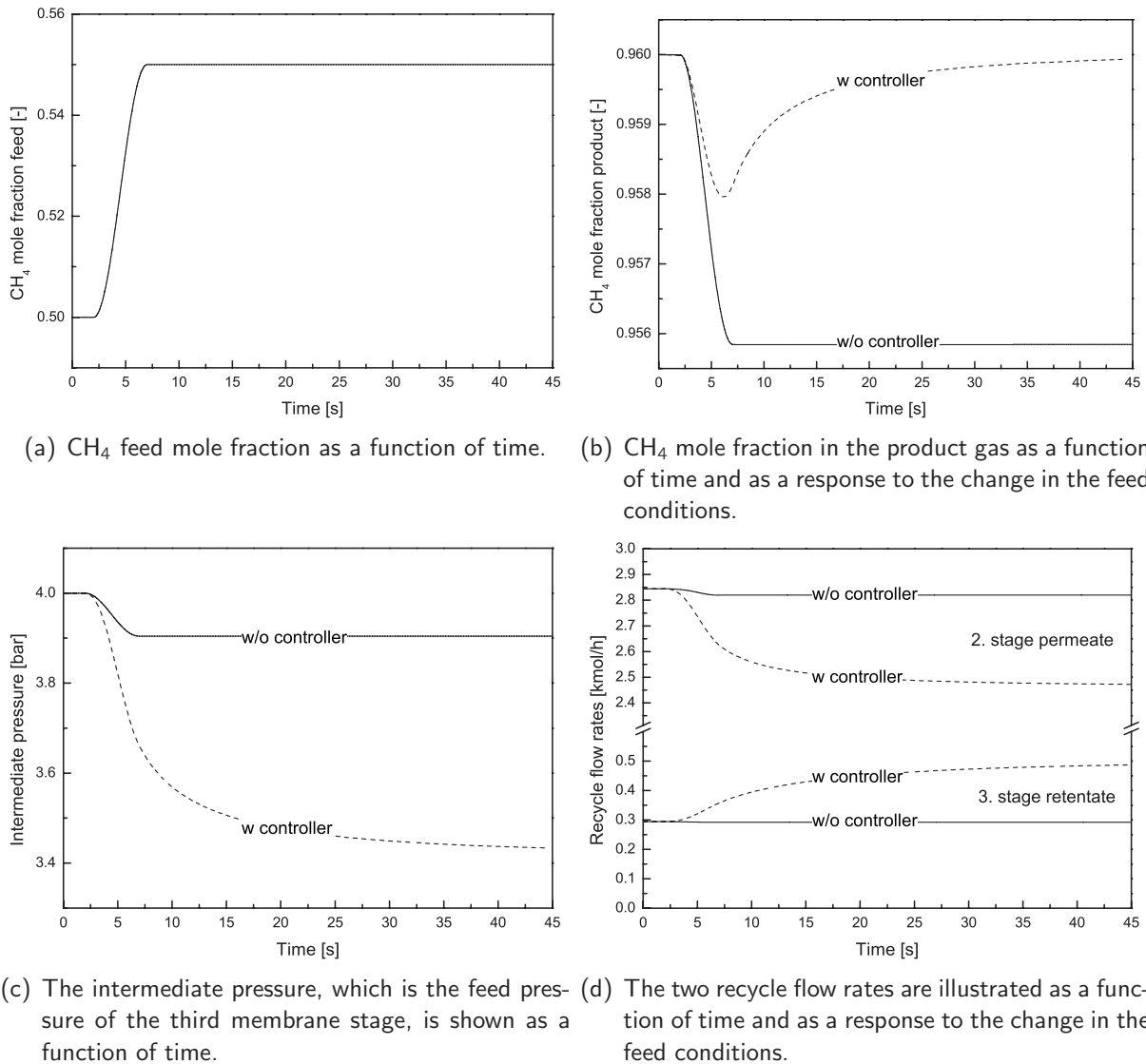


Figure 5.6: Control scheme 1 - The performance of the biogas upgrading process is illustrated for an increase of the CH₄ mole fraction in the feed gas. Both the performance with and without a controller maintaining the product purity are presented. The dashed lines represent the flow rate for a process with a control scheme and the full lines illustrate the flow rates for a process without controller.

pressure on the feed side of the third stage. The flow rate of the second stage recycle decreases since the inlet mole fraction of CO₂ in the second stage is lowered by reducing the feed flow rate. By applying the controller which increases the permeate pressure of the first stage the recycle flow rate of the second module increases due to an increase in the CO₂ level at the feed of the second stage. Hence, the driving force for CO₂ permeation increases as well. The increased pressure on the feed side of the third membrane stage results in a reduced recycle flow rate of the third membrane stage. In contrast to the increase in the feed flow rate for the reduction of the feed flow rate the change in product purity can be compensated faster (only 15 s).

Reducing the CH₄ level in the feed gas

Figure 5.5 presents the decrease of the CH₄ level in the feed gas as well as the response of the biogas upgrading process to this change. In Figure 5.5(a) the CH₄ mole fraction in the feed gas is illustrated as a function of time which is reduced from 50 % to 45 % while the CO₂ level is increased simultaneously from 50 % to 55 %.

Surprisingly, the mole fraction of CH₄ in the product gas increases while reducing the CH₄ level in the feed gas when no controller is applied (see Figure 5.5(b)). This is due to the increased driving force for CO₂ permeation in the first stage. However, by applying a controller to manipulate the feed pressure of the third membrane stage the required CH₄ mole fraction in the product gas of 96 % is obtained after the short period of 15 s. In addition, the maximum level of CH₄ mole fraction in the product gas is 96.2 %, while the CH₄ level for the process without a controller reaches 96.5 %.

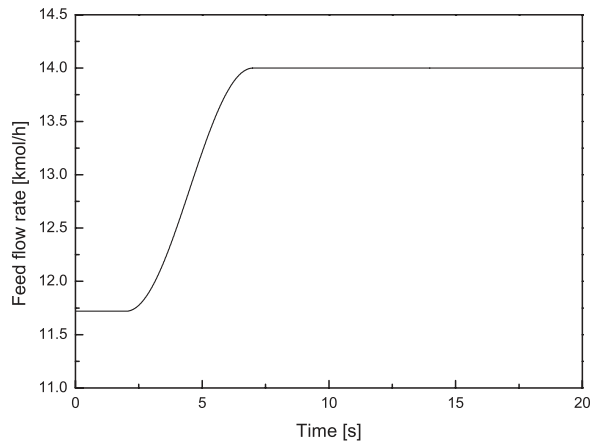
Figure 5.5(c) shows the permeate pressure of the first gas permeation stage, which is also the feed pressure of the third stage, as a response to the reduced CH₄ level in the feed gas. For the process without a controller the pressure increases due to the increased permeate flow rate of the first membrane stage. Here, the valve opening remains constant so that an increased flow rate results in an increased pressure. By using a controller the pressure upstream of the throttling valve is manipulated. In order to reduce the CH₄ purity of the product gas the permeate pressure of the first stage is increased from 4 bar to 4.7 bar to reduce the stage cut in the first stage.

In Figure 5.5(d) the recycle flow rates are presented as a function of time and as a response to the reduction of CH₄ content in the feed gas. For the process without the controller the recycle flow rates remain almost constant since the system adapts the feed pressure of the third stage. Applying the controller to increase the permeate pressure of the first stage, the stage cut in the first membrane stage significantly decreases. This effect is even stronger than the increased driving force as a consequence of the elevated pressure on the feed side of the third stage and the flow rate of the third stage recycle decreases.

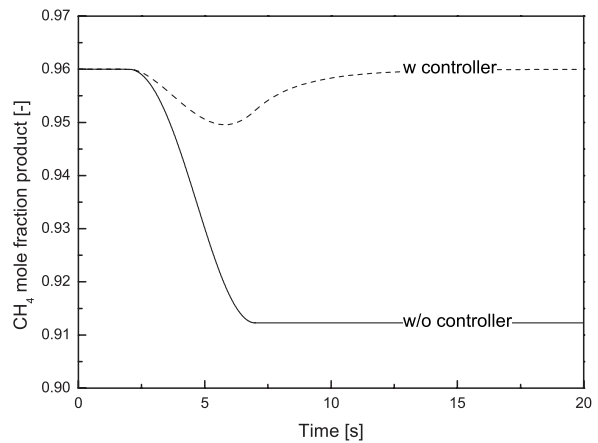
Increasing the CH₄ level in the feed gas

In Figure 5.6 the response of the biogas upgrading process to the change in the feed conditions are illustrated for an increase in the feed gas CH₄ mole fraction. Figure 5.6(a) shows the CH₄ feed mole fraction as a function of time. Here, the CH₄ level is increased from 50 % to 55 % within 5 s while CO₂ is balanced at the same time.

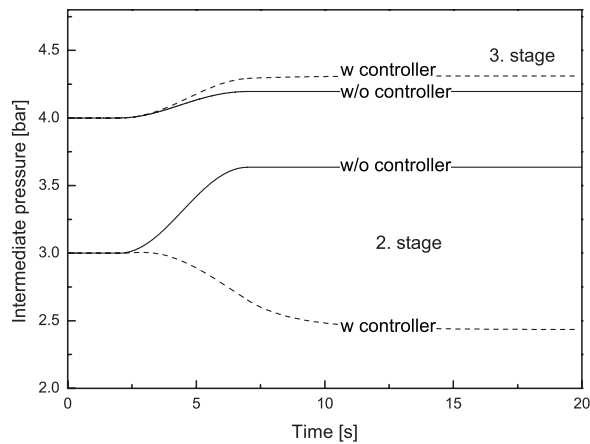
In Figure 5.6(b) the CH₄ purity of the product gas is illustrated as a response to the change in the feed mole fraction. By increasing the CH₄ in the feed gas the CH₄ purity of the product gas declines. This results from the reduced driving force for CO₂ permeation in the first membrane stage. Hence, the stage cut in the first stage decreases while the CO₂ level of the second stage feed increases which results in a decreased product purity. In order to enhance the product purity to the specification of



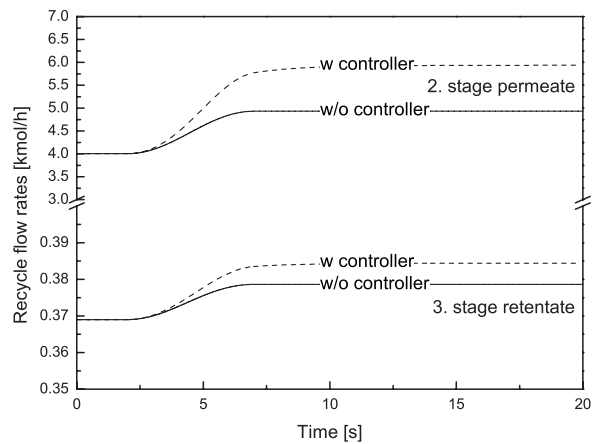
(a) Feed flow rate as a function of time.



(b) CH₄ mole fraction in the product gas as a function of time and as a response to the change in the feed conditions.



(c) The intermediate pressure, which is the feed pressure of the third membrane stage, is shown as a function of time.



(d) The two recycle flow rates are illustrated as a function of time and as a response to the change in the feed conditions.

Figure 5.7: Control scheme 2 - The performance of the biogas upgrading process is illustrated for an increase in the feed gas flow rate. Both the performance with and without a controller maintaining the product purity are presented. The dashed lines represent the flow rate for a process with a control scheme and the full lines illustrate the flow rates for a process without a controller.

96 % CH₄ the feed pressure of the third membrane stage is adjusted. By using the controller the CH₄ level of 96 % in the product gas can be reached after 45 s while the deviation from the initial purity is less distinct.

Figure 5.6(c) shows the feed pressure of the third membrane stage as a function of time. Here, both the pressure with and without a controller are presented. For the process without the controller the pressure decreases due to the reduced permeate flow rate of the first membrane stage and a constant valve opening. When applying process control, the controller reduces the permeate pressure of the first stage in order to increase the stage cut of the first stage. Here, the controller sets the

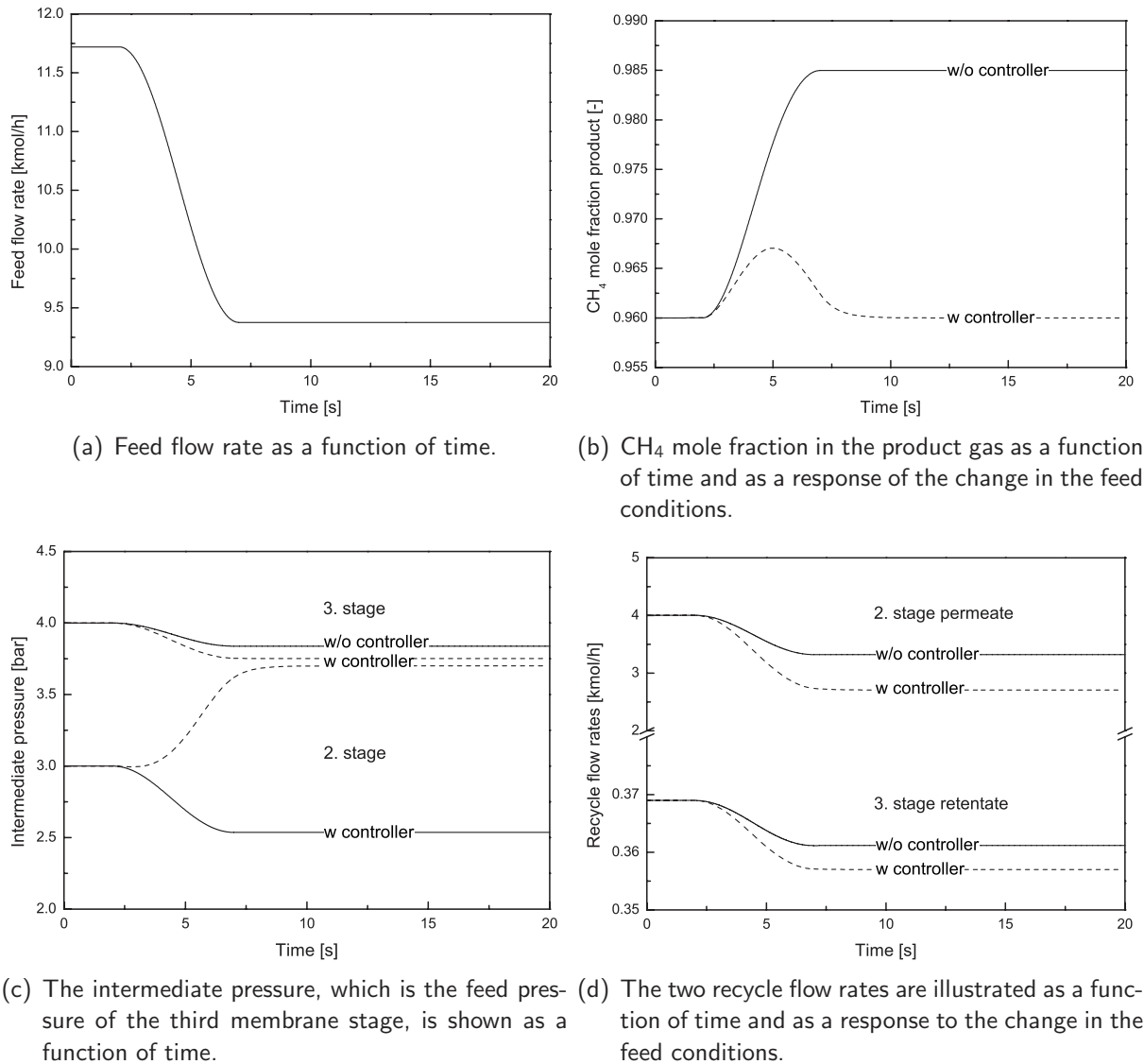


Figure 5.8: Control scheme 2 - The performance of the biogas upgrading process is illustrated for a reduction of the feed gas flow rate. Both the performance with and without a controller maintaining the product purity are presented. The dashed lines represent the flow rate for a process with a control scheme and the full lines illustrate the flow rates for a process without controller.

pressure to approximately 3.4 bar. The recycle flow rates for the process without process control are almost constant (see Figure 5.6(d)). Only for the second stage recycle a marginal decrease in the flow rate is observed. This is due to the decreased permeate pressure in the first stage which results in a reduced driving force for CO₂ permeation in the second stage. Applying the controller the flow rate of the second stage decreases as a consequence of the reduced CO₂ level in the feed gas of the second membrane stage. Figure 5.6(d) also illustrates the recycle flow rate of the third membrane stage as a response to the increase of the CH₄ feed mole fraction. Here, the recycle flow rate increases due to the lower feed pressure of the third stage.

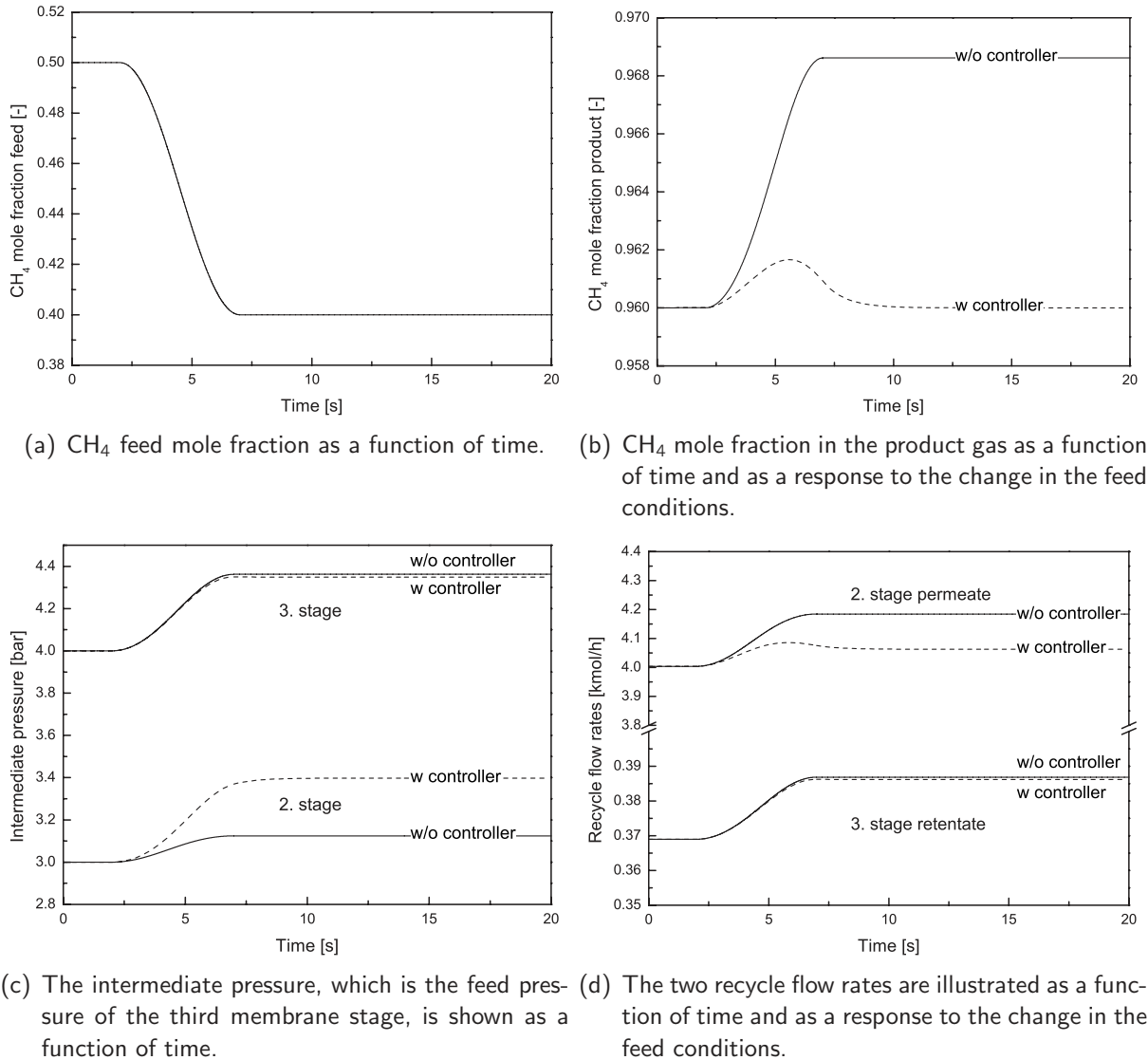


Figure 5.9: Control scheme 2 - The performance of the biogas upgrading process is illustrated for a reduction of the CH₄ mole fraction in the feed gas. Both the performance with and without a controller maintaining the product purity are presented. The dashed lines represent the flow rate for a process with a control scheme and the full lines illustrate the flow rates for a process without controller.

5.5.2 Control scheme 2 (see Figure 5.2(d))

In this section the performance of the process control scheme depicted in Figure 5.2(d) is analyzed in detail. In contrast to process control scheme 1 which is presented in Figure 5.2(c) the permeate pressure of the second membrane stage is manipulated by the controller in order to maintain the CH₄ mole fraction of 96 % in the product gas.

Figure 5.7 shows the impact of an increase in the feed flow rate while Figure 5.8 presents the effect of a reduced feed flow rate. In principle, the impact on the product mole fraction and the recycle flow rates is similar to the impact on these variables for process control scheme 1.

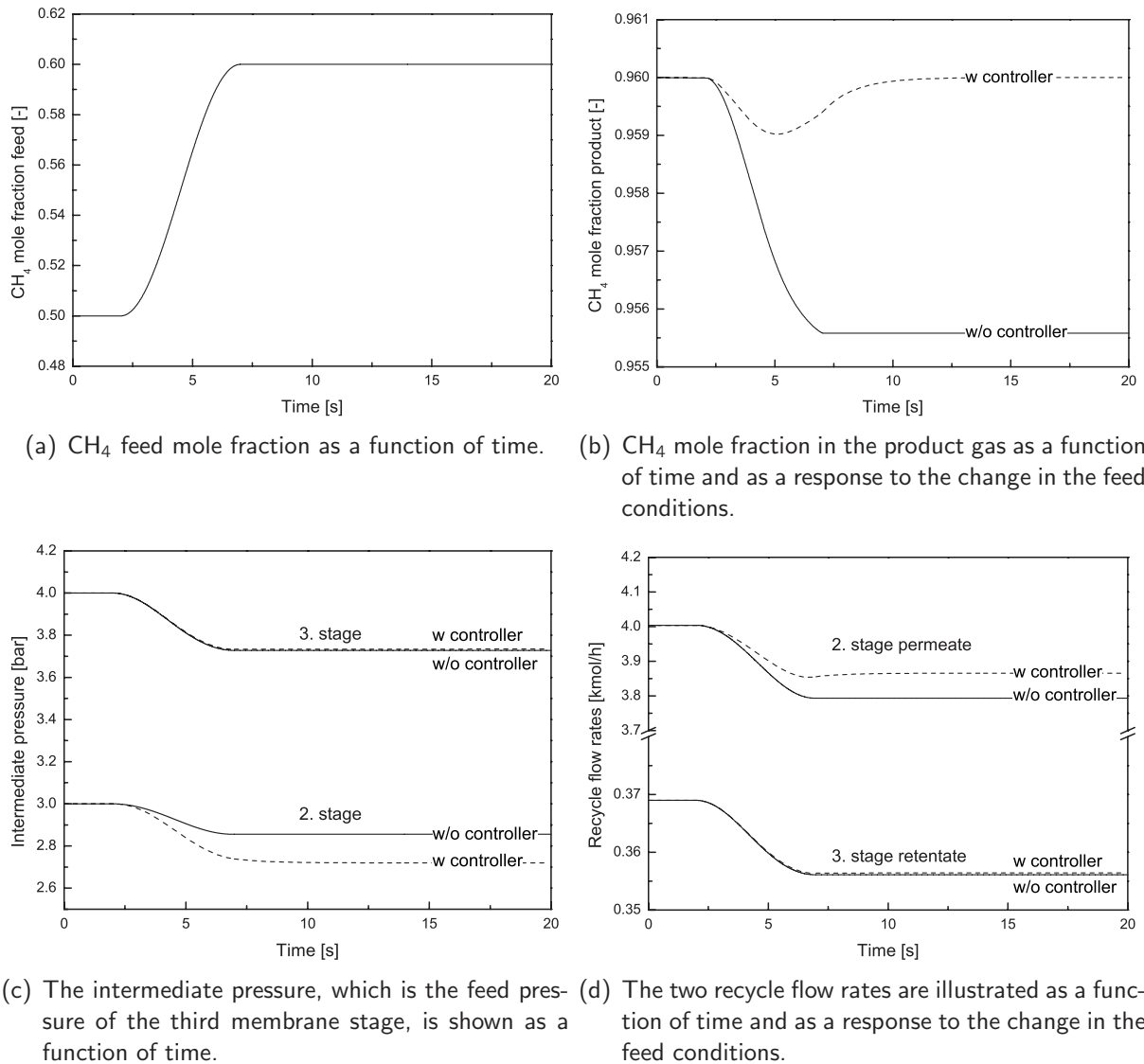


Figure 5.10: Control scheme 2 - The performance of the biogas upgrading process is illustrated for an increase in the CH₄ mole fraction in the feed gas. Both the performance with and without a controller maintaining the product purity are presented. The dashed lines represent the flow rate for a process with a control scheme and the full lines illustrate the flow rates for a process without controller.

For the increased feed flow rate the permeate pressure of the second stage increases significantly for a system operating without a controller. Here, the valve opening in the second stage recycle stream remains constant. As a result of the increased feed flow rate the driving force for CO₂ permeation in the second stage enhances. Hence, the permeate flow rate increases resulting in an increased permeate pressure due to the constant valve opening. By applying a controller the permeate pressure of the second stage is reduced. Here, the reduced driving force due to the low level of CO₂ in the second stage feed gas has to be compensated. The increased driving force results in an increased recycle flow rate of the second stage. The process where the feed flow rate is reduced shows exactly

Table 5.4: Comparison of both control schemes for the initial conditions as well as for the steady state after changed feed conditions.

| | Control scheme 1 | | | Control scheme 2 | | |
|-----------------------------|------------------|---------------|---------------|------------------|---------------|---------------|
| | p | η_{CH_4} | Recycle ratio | p | η_{CH_4} | Recycle ratio |
| | bar | % | - | bar | % | - |
| Initial state | 4.00 | 99.50 | 0.267 | 3.00 | 99.50 | 0.372 |
| Increasing \dot{n}_{Feed} | 3.73 | 99.53 | 0.263 | 2.44 | 99.67 | 0.452 |
| Reducing \dot{n}_{Feed} | 4.42 | 98.80 | 0.288 | 3.60 | 99.21 | 0.331 |
| Increasing $x_{CH_4,Feed}$ | 3.48 | 99.62 | 0.253 | 2.72 | 99.56 | 0.360 |
| Reducing $x_{CH_4,Feed}$ | 4.67 | 98.80 | 0.303 | 3.40 | 99.53 | 0.380 |

the converse behavior as the process with an increase in the feed flow rate.

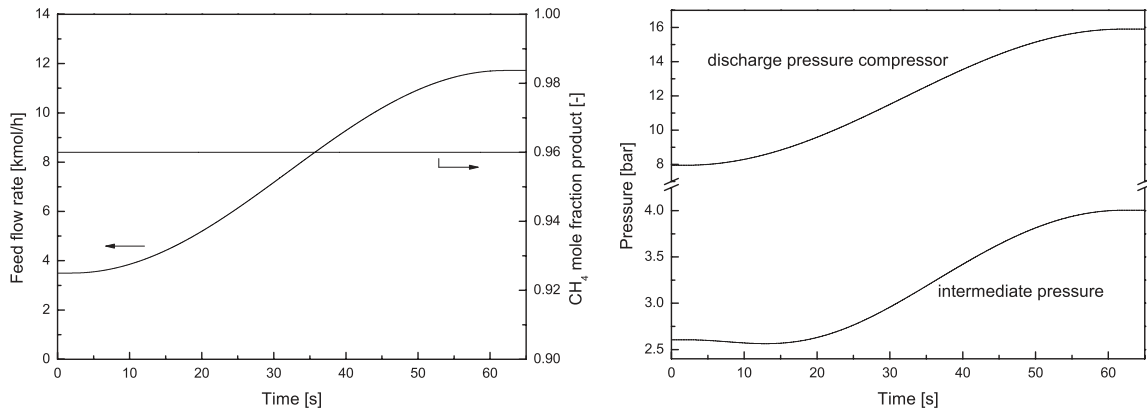
In Figure 5.10 and Figure 5.9 the impact of changed CH_4 mole fractions in the feed gas is presented as a function of time. The responses of the CH_4 mole fraction in the product gas, the pressures on the permeate of the second stage as well as the pressure on the feed side of the third membrane stage, and the recycle flow rates to the changed feed mole fraction are reported. The system shows a similar behavior as described for process control scheme 1. Hence, the effects discussed in Section 5.5.1 are also valid for control scheme 2.

5.5.3 Comparing control scheme 1 and scheme 2

Both control schemes are able to maintain the CH_4 mole fraction in the product gas for variations in the feed conditions and have a simple structure. Furthermore, both control schemes do not require any additional process equipment to operate the upgrading process. However, process control scheme 1 has the advantage that the operating conditions remain unchanged compared to a process with conventional control structure such as manipulating the compressor's discharge pressure.

Anyway process control scheme 2 is an excellent alternative to control scheme 1 though the increased permeate pressure in the second stage requires additional membrane area in the second gas permeation stage. Process control scheme 2 reacts faster (less than 10 s) and can handle even strong variations in the feed conditions which are approximately $\pm 20\%$ in the feed flow rate as well as $\pm 20\%$ in the CH_4 mole fraction of the feed gas. Table 5.4 compares both control schemes in terms of CH_4 recovery and recycle ratio as an indicator for the energy demand. The recycle ratio is defined as:

$$recycle\ ratio = \frac{\sum \dot{n}_{recycles}}{\dot{n}_{feed}} \quad (5.3)$$



(a) Feed flow rate and product gas purity as a function of time.

(b) Compressor discharge pressure and

Figure 5.11: Two advanced control schemes are presented which combine a conventional controller with a model predictive controller.

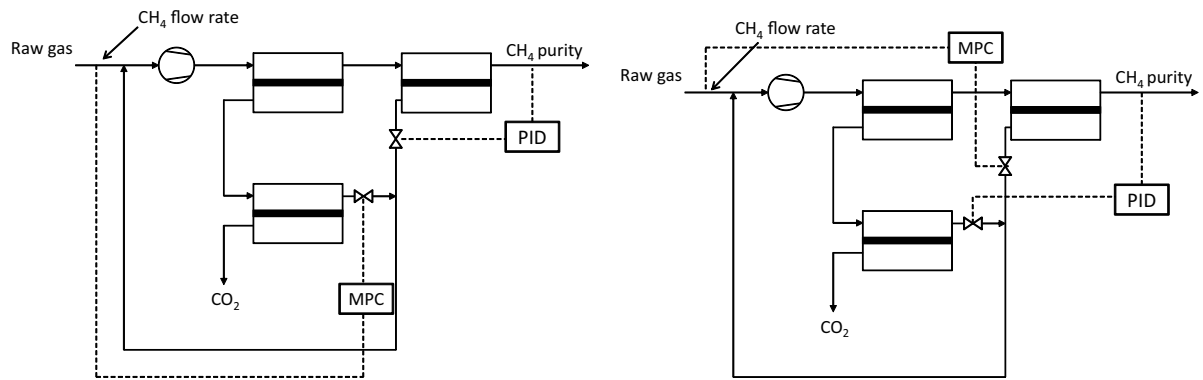
In general, the impact of changes in the feed conditions on CH₄ recovery is more pronounced for process control scheme 1. The CH₄ recovery in process control scheme 2 is only insignificantly influenced by changes in the feed. However, control scheme 2 operates with a significantly higher recycle ratio. It is reasonable to note that the CH₄ recovery for process control scheme 2 is almost constant although the changes in the feed conditions are more pronounced compared to control scheme 1.

5.5.4 Start up of the process

Commonly biogas processes operate continuously. The shut down and start up of the process is unavoidable for maintenance intervals. In addition, driving biogas upgrading processes might support the smoothing of peaks in the electrical grid by discontinuous operation when a surplus of renewable energy is available (see Chapter 8).

Figure 5.11(a) depicts the feed flow rate and the CH₄ product gas mole fraction as a function of time for a start of a biogas upgrading process. The feed flow rate is increased from 3.75 kmol/h to the working point flow rate of 11.72 kmol/h within a period of 60 seconds. At the same time the discharge pressure of the compressor is increased from 8 bar to 16 bar (see Figure 5.11(b)). In order to maintain the product gas purity, control scheme 1 is applied, in which the permeate pressure of the first membrane stage is manipulated. This intermediate pressure, which is also the feed pressure of the third membrane stage, is shown in Figure 5.11(b) as a function of time.

Using control scheme 1 a product gas with the required CH₄ mole fraction of 96 % can be provided at any time. However, the product gas pressure for grid injection is met after 60 seconds. Hence, a buffer gas storage tank is required to collect the first gas produced during the start of the processes and continuous operation can be performed when the product gas pressure is at 16 bar. In contrast



(a) Model predictive controller (MPC) sets the pres- (b) Model predictive controller (MPC) sets the pres-
 sure of the first stage permeate. sure of the second stage permeate.

Figure 5.12: Two advanced control schemes are presented which combine a conventional controller with a model predictive controller.

to other biogas upgrading techniques, such as amine absorption, the gas permeation process can be started and shut down in short periods.

5.6 Advanced control schemes

An advanced method to control the product purity of the biogas upgrading process involves the application of model predictive controllers combined with the control schemes proposed in this current study. Here, the conditions in the feed gas are measured online. In case of changed feed gas conditions the controller immediately sets the pressures in the system. Hence, the controller reacts on the changed conditions before the purity of the product gas is affected by these changes. A system operating with this kind of control scheme seems to be more stable and operates faster than conventional systems measuring the product purity.

Figures 5.12(a) and 5.12(b) show two examples of such a control scheme. In Figure 5.12(a) the model predictive controller measures the raw gas conditions and sets the feed pressure of the third stage. A common PID controller measures the product gas purity and adjusts the permeate pressure of the second stage. Figure 5.12(b) presents a control scheme which operates similarly to the control scheme presented in Figure 5.12(a). Here, the changes in the feed gas conditions are controlled by a model predictive controller setting the permeate pressure of the second membrane stage while the product gas purity is maintained by a controller which adjusts the feed pressure of the third stage. However, these advanced process control schemes require reliable process models to predict the system's behavior. The complexity of the control structure might be a drawback.

5.7 Conclusion

The presented model of a hollow fiber gas permeation module enables the analysis of dynamic process behavior which is particularly interesting for processes with varying feed conditions. Biogas upgrading, which is the separation of CO₂ and CH₄, is a dynamic process as the feed flow rate as well as the feed concentrations of CO₂ and CH₄ might change during operation.

In this study a three stage biogas upgrading process is presented which delivers upgraded biogas at natural gas grade and achieves high CH₄ recoveries at the same time. Two new process control schemes are presented which do not require additional process equipment to maintain the product gas purity. Both proposed control structures compensate changing feed conditions within a few seconds. Due to the deviation from the design point, lower CH₄ recoveries and/or increased recycle flow rate are inevitable. However, particularly for process control scheme 2 the difference in the CH₄ recovery between the initial operation and for changed feed conditions is insignificant.

The presented dynamic gas permeation model is not limited to the biogas upgrading process and can also handle multicomponent gas mixtures. Processes such as natural gas treatment and air separation can benefit from the proposed process control schemes presented here.

Also it could be used to investigate the impact of material degradation on the gas permeation process on a large time scale. In this case, the optimal moment for replacing the membrane modules can be determined. In addition, combinations of batch reactors and gas permeation modules could be analyzed.

Chapter 6

Membrane hybrid processes for biogas upgrading

6.1 Introduction

Upgraded biogas serves as a natural gas substitute which can be used for energy supply and as feedstock for chemical synthesis. Commonly, biogas upgrading is done by absorption or adsorption techniques. Basically four different technologies are applied in biogas upgrading which are (i) amine scrubbing, (ii) pressurized water scrubbing, (iii) pressure swing adsorption and (iv) gas permeation [53]. In principle, it is also possible to use cryogenic technology to separate CO₂ and CH₄ [156] but due to the extensive energy demand it is not commercially applied in biogas upgrading. Recently a hybrid process combining membrane technology and cryogenic equipment was commercialized by Pentair. Combining gas permeation membranes with established separation processes in so called membrane hybrid processes merges the advantages of both technologies [157]. In this study we provide a techno-economic analysis of membrane hybrid processes for biogas upgrading. In general, two different process configurations are investigated. In the first configuration the membrane performs the bulk separation while the conventional gas separation equipment polishes the biogas to natural gas grade. In the second case the membrane produces the upgraded biogas in a single stage while CH₄ in the permeate is recovered by conventional gas separation techniques.

The on-farm application of gas separation equipment requires robust and low cost operation. The fusion of gas permeation membranes and established technologies support low operation costs. Membrane hybrid processes have been of strong interest in research and development [158–160]. In particular, pervaporation or vapor permeation processes combined with conventional separation equipment have been analyzed extensively [20, 161–168]. In gas separation particularly natural gas treatment with membrane hybrid processes [69, 79, 169] and hybrid processes for post-combustion CO₂ capture were investigated [108, 170]. Various studies have been performed where membranes are combined with adsorption technology [43, 171–174]. However, this study at hand focuses on a combination of liquid and low temperature separation techniques with gas permeation membranes. We analyzed different process configuration with Aspen Plus and performed a full cost calculation. This includes the determination of investment and operational costs. Due to the lack of data for investment costs we applied Guthrie's method [110, 149, 150] for investment cost estimation.

The data for the individual absorption processes obtained from the process simulations coincide with the data published in literature demonstrating the reliability of the process models [5]. For pressurized water scrubbing (PWS) processes the combination with membrane technology offers advantages over the single PWS process, since both process configurations have lower upgrading costs compared to the conventional process. The amine scrubbing process only benefits from the combination with a gas permeation stage in the process where the membrane performs the bulk separation. The impact of the membrane on the separation process is most remarkable for the cryogenic process. The specific upgrading costs reduce to only 9 % of the costs for the conventional process so that the hybrid process competitive to established upgrading techniques.

6.2 Upgrading process

In biogas upgrading primarily CO_2 has to be removed from CH_4 to enhance the heating value of the product gas which is supplied to the natural gas grid. The CH_4 mole fraction in the raw gas of 60 % has to be increased to more than 96 % in order to meet the natural gas grid requirements. Several trace components are present in the raw biogas. Table 6.1 shows these components and their respective mole fraction in the raw gas.

The product gas is supplied to the natural gas grid at elevated pressures (4 to 70 bar) by using a multistage compressor. In this current study, we assume that the biogas is delivered at 16 bar. In order to compare the various processes, the product gas pressure is set to 16 bar even if the process commonly operates at ambient pressure such as the amine absorption process.

6.3 Process description

In principle, two different process configurations are analyzed here. One in which the membrane is used for the bulk removal of CO_2 and the conventional separation equipment performs the final purification. And a second configuration where the conventional separation technology is used to enhance the CH_4 recovery by separating CO_2 and CH_4 in the permeate stream of the gas permeation stage. The flowsheets presented here only contain the most important unit operations. Pumps as well as pressure valves which are extensively used in the absorption processes are not illustrated to keep the flowsheets simple. However, the process conditions for the different unit operations are given in the flowsheets (see Figure 6.1 - Figure 6.4).

6.3.1 Hybrid process with pressurized water scrubbing

Figure 6.1 shows two hybrid processes in which a single gas permeation stage is combined with a pressurized water scrubbing vessel. The upgraded biogas leaving the absorption column is saturated with water and might contain traces of H_2S . Hence, a drying step and a fine desulfurization unit are installed prior to grid injection. In both processes the loaded solvent enters a flash vessel at a pressure of 3 bar. Here, the CH_4 rich vapor is recycled to the absorption column to increase the CH_4 recovery. The liquid leaving the flash is fed to a stripping column in which air is used as a stripping gas to remove CO_2 . The lean water is recycled and fed to the absorption column.

In Figure 6.1(a) the retentate of the gas permeation stage enters the absorption column. Here, a significant fraction of CH_4 permeates through the membrane and leaves the process as exhaust gas.

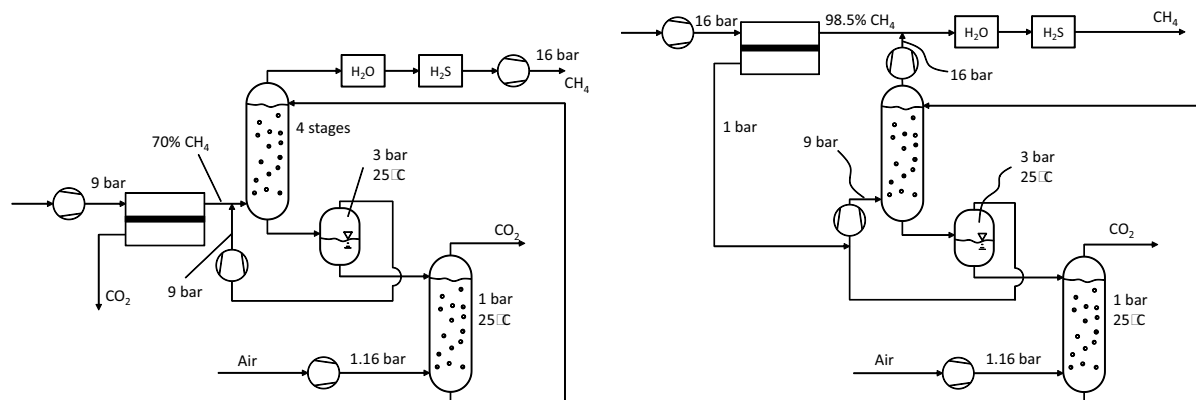
Table 6.1: Feed and product gas conditions for a typical biogas upgrading process. The permeances of the polymeric membrane material are also presented.

| | Unit | Value |
|---------------------------------------|------------------------|------------|
| Raw gas mole fraction | | |
| CH ₄ | - | 0.6 |
| CO ₂ | - | 0.367 |
| H ₂ O | - | 0.031 |
| H ₂ S | - | 0.002 |
| Raw gas flow rate | m ³ (STP)/h | 150 - 2000 |
| Raw gas temperature | °C | 20 |
| Raw gas pressure | bar | 1 |
| Product pressure | bar | 16 |
| Product mole fraction CH ₄ | - | 0.96 |
| Permeate pressure | bar | 1 |
| Permeance | | |
| CH ₄ | GPU | 1 |
| CO ₂ | GPU | 60 |
| H ₂ O | GPU | 300 |
| H ₂ S | GPU | 100 |

Figure 6.1(b) shows a process flowsheet in which the gas permeation stage provides a product gas with the required gas grid specifications. However, as significant amounts of CH₄ are lost in the permeate, this particular stream is fed to the absorption column of a water scrubbing process. The purified gas from the absorption vessel has to be compressed to meet the natural gas grid pressure.

6.3.2 Hybrid process with amine scrubbing

Figure 6.2 illustrates two different hybrid processes in which a gas permeation membrane is connected with an amine absorption process. Various process configurations are reported for regenerating the loaded solvent [5]. Here, we use a three step desorption process in which the solvent leaving the absorption column is heated by the recycle streams of downstream purification steps. The hot solvent enters a first flash vessel operating at 9 bar. The liquid leaving this vessel is fed to a second flash which has a pressure of 10 bar. Both vapor streams, from the first and the second flash vessel, are mixed and fed to a third flash to recover the CH₄ in the vapor phase. The third flash operates at 9 bar and a temperature of 20 °C. The gas phase leaving this flash is the exhaust gas of the



(a) Membrane hybrid process in which the retentate stream of the membrane is fed to a pressurized water scrubbing absorber which is referred to as *PWS 1*.

(b) Membrane hybrid process in which the permeate stream of the membrane is fed to a pressurized water scrubbing absorber which is referred to as *PWS 2*.

Figure 6.1: Two membrane hybrid processes are presented in which gas permeation technology is combined with pressurized water scrubbing equipment.

process mainly containing CO_2 . The liquid streams of the second and third flash are recycled to the absorption column and they are used for heat integration to increase the temperature of the inlet stream of the first flash. Since the amine solution is able to strongly bind H_2S molecules the regeneration of the solvent is extremely expensive when H_2S is fed to the amine process. Hence, a desulfurization unit is installed upstream of the absorption column. The gas leaving the absorption column is saturated with water requiring a drying step prior to gas grid injection.

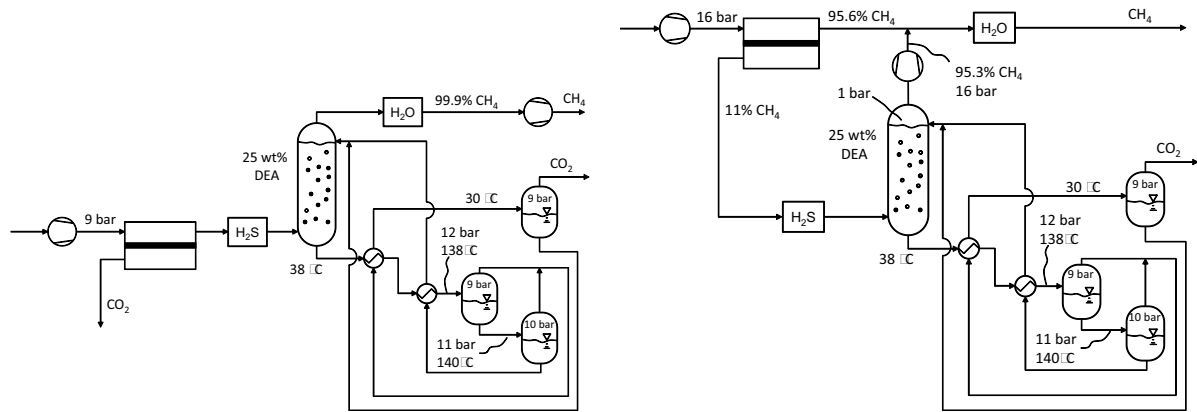
In Figure 6.2(a) the gas permeation stage is used to perform the bulk separation of CO_2 and CH_4 . The final polishing of the biogas is performed by the amine absorption process. The permeate of the membrane stage as well as the vapor stream of the third flash vessel leave the process as exhaust gases. Particularly, the permeate stream of the membrane stage might contain significant amounts of CH_4 which reduces the CH_4 recovery of this process configuration.

Figure 6.2(a) depicts a process configuration where the amine absorption column is applied to recover the CH_4 from the permeate stream of the membrane stage. Hence, the raw biogas is polished in the membrane stage to natural gas grade, while the permeate is separated into a CH_4 rich gas at the column top and a CO_2 rich gas at the third flash vessel outlet.

6.3.3 Hybrid process with cryogenic separation

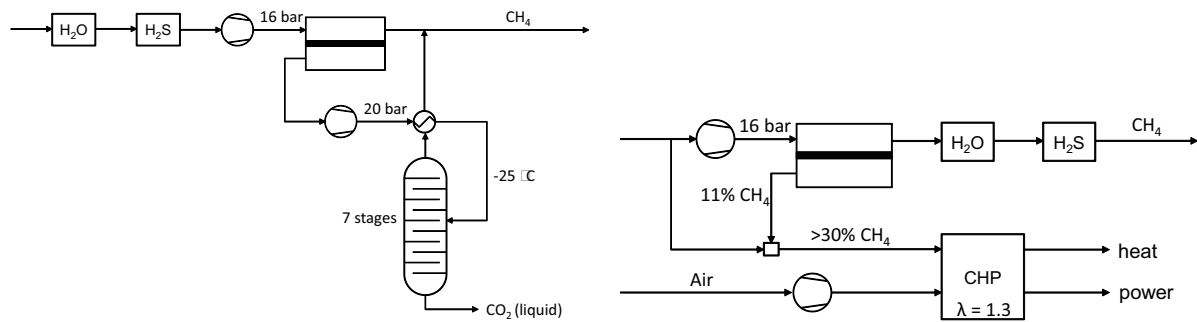
Figure 6.3(a) illustrates a process in which gas permeation technology is combined with cryogenic separation. This particular process configuration is analyzed here, because it has recently been commercialized by Pentair. Since the CO_2 is obtained at high purity and in liquid phase it could be sold increasing the profitability of the process.

The permeate stream of the gas permeation stage is compressed to 20 bar, pre-cooled to a temper-



(a) Membrane hybrid process in which the retentate stream of the membrane is fed to an amine scrubbing absorber. This process is referred to as *Amine 1*.
 (b) Membrane hybrid process in which the permeate stream of the membrane is fed to an amine scrubbing absorber. This process is referred to as *Amine 2*.

Figure 6.2: Two membrane hybrid processes are presented in which gas permeation technology is combined with amine scrubbing equipment.



(a) Membrane hybrid process in which the permeate of the gas permeation membrane is compressed and separated in a low temperature distillation column. This process is referred to as *Cryogen*.
 (b) Gas permeation process connected to an engine which used the permeate stream as well as air and a fraction of the raw biogas to provide both, heat and power. This process is referred to as *CHP*.

Figure 6.3: Two entirely different membrane hybrid processes are presented. A cryogenic separation which separates the gases resulting from the permeate stream of the membrane module. And a second process in which the permeate of the membrane stage is used to drive a combined heat and power engine.

ature of $-25\text{ }^{\circ}\text{C}$ and fed to a low temperature distillation column. In the distillation column a pure CH_4 stream is obtained at the column top and CH_4 recoveries of almost 100 % can be achieved. A drying and a desulfurization step are installed upstream of the membrane stage as H_2O and H_2S will accumulate on the permeate side of the membrane stage reducing the purity of the gas streams in the distillation column.

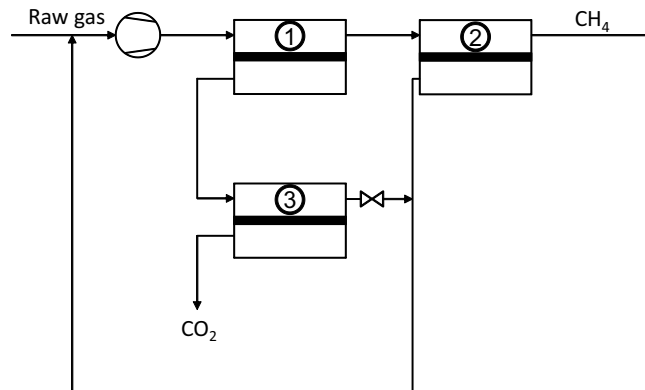


Figure 6.4: Three stage gas permeation process in which the permeate pressure of the first stage is elevated to drive the permeation in the third membrane stage. This process is referred to as *3 stage GP*.

6.3.4 Combination of a gas permeation process and a combined heat and power engine

A combined heat and power engine which uses the permeate of the membrane stage as feedstock is depicted in Figure 6.3(b). This particular process design serves as a benchmark, since it is highly efficient in case that the produced heat can be utilized. The raw biogas is upgraded to the required grade in a single stage membrane process. Here, a significant fraction of CH₄ permeates through the membrane and mole fractions as high as 7 % can be found in the permeate stream. Since this CH₄ is too low to drive the gas engine, a fraction of the raw gas is mixed with the permeate stream to adjust a CH₄ level of 30 % [114]. In addition, air is fed to the gas engine. The gas engine supplies both, heat and electrical energy. The latter can directly be used to drive the compressor for the membrane separation.

6.3.5 Benchmark processes

The stand alone processes of amine absorption, pressurized water scrubbing and a three stage gas permeation process (see Figure 6.4) serve as a benchmark for the membrane hybrid processes. The membrane process operates at elevated permeate pressures in the first gas permeation stage to provide the driving force of permeation in the third stage. A detailed overview on the process equipment applied in the investigated processes is given in Table 6.2 and it summarizes the number of process equipment for each hybrid process.

Table 6.2: Number of unit operations applied in the different hybrid processes.

| | PWS 1 | PWS 2 | Amine 1 | Amine 2 | Cryogen | CHP | 3 stage GP |
|-----------------------|-------|-------|---------|---------|---------|-----|------------|
| Compressors / blowers | 3 | 3 | 2 | 2 | 2 | 1 | 1 |
| Pumps | 1 | 1 | 3 | 3 | - | - | - |
| Flash vessels | 1 | 1 | 3 | 3 | - | - | - |
| Columns | 2 | 2 | 1 | 1 | 1 | - | - |
| Heat exchangers | 1 | 1 | 7 | 7 | 2 | - | - |
| Membrane stages | 1 | 1 | 1 | 1 | 1 | 1 | 3 |
| Gas engines | - | - | - | - | - | 1 | - |

Table 6.3: Physical properties methods applied in the Aspen Plus simulations.

| | base method | exception |
|----------------------------|--------------------------------|--------------------------|
| PWS 1 / PWS 2 | Predictive Soave-Redlich-Kwong | GP = Soave-Redlich-Kwong |
| Amine 1 / Amine 2 | AMINES | GP = Soave-Redlich-Kwong |
| Cryogen / CHP / 3 stage GP | Soave-Redlich-Kwong | - |

6.4 Process model

6.4.1 Unit operation models and model parameters

Flowsheets for the different process configurations are set up in Aspen Plus. The processes are built by applying models for absorption columns, distillation columns, flashes, compressors and gas permeation modules. All these models are built-in models in Aspen Plus.

Only the gas permeation model is not part of the Aspen Plus model library. Hence, we implemented a model for a gas permeation module in Aspen Custom Modeler and incorporated it into the Aspen Plus environment. The equations and the model validation are reported in Chapter 3. In this study at hand, we assume that the module operates isothermal and that effects such as concentration polarization, real gas behavior and pressure losses can be neglected. Equilibrium models are applied to determine the performance and the number of theoretical separation stages of the absorption columns. The built-in multistage compressor model is applied as operating pressures of more than 9 bar and 16 bar, respectively, have to be provided. Isentropic compression is assumed with an isentropic efficiency of 0.72, while the mechanical and the electrical efficiency are 0.9 and 0.99, respectively.

Table 6.3 presents the physical property methods for the different hybrid processes. The base method refers to the property method applied to the entire process and the column exceptions summarizes the equipment which rely on a different property method. Table 6.2 indicates that the hybrid

Table 6.4: Parameters for investment cost estimation using Guthrie's method for the different unit operations.

| | MPF | MF | d_0 | l_0 | C_0 | S_0 | α | β |
|---|------|------|-------|-------|----------|---------------------|----------|---------|
| Compressors | 1.29 | 5.11 | - | - | 23000 \$ | 100 bhp | 0.77 | - |
| Blowers | 1.00 | 5.11 | - | - | 23000 \$ | 100 bhp | 0.77 | - |
| Absorber | 3.67 | 6.23 | 3 ft | 4 ft | 1000 \$ | - | 0.81 | 1.05 |
| Desorber | 3.67 | 6.23 | 3 ft | 4 ft | 1000 \$ | - | 0.81 | 1.05 |
| Distillation column | 3.67 | 6.23 | 3 ft | 4 ft | 1000 \$ | - | 0.81 | 1.05 |
| Flash vessel (< 10 bar) | 4.22 | 6.23 | 3 ft | 4 ft | 1000 \$ | - | 0.81 | 1.05 |
| Flash vessel (\geq 10 bar) | 4.40 | 6.23 | 3 ft | 4 ft | 1000 \$ | - | 0.81 | 1.05 |
| Pumps | 2.89 | 5.38 | - | - | 650 \$ | 2000 gpm psi | 0.36 | - |
| Heat exchanger (< 100 ft ²) | 2.08 | 3.83 | - | - | 300 \$ | 5.5 ft ² | 0.024 | - |
| Heat exchanger (\geq 100 ft ²) | 3.08 | 5.29 | - | - | 5000 \$ | 400 ft ² | 0.65 | - |

processes are complex in terms of the number of process equipment. The hybrid process involving the combined heat and power engine as well as the three stage gas permeation process include only a limited number of unit operations which makes them less prone to incidents.

6.4.2 Economic parameters

In order to evaluate the different process configurations an economic analysis is performed. Both operating and investment costs are taken into account. Operating costs considered here are cost for electricity, for heat, for cooling and costs for chemical substances presented in Table 6.6. The investment costs are estimated by Guthrie's method [110, 149, 150]. The general approach is to determine the investment costs IC by:

$$IC = UF \cdot BC \cdot (MPF + MF - 1) \quad (6.1)$$

UF is the update factor taking the current price level into account. Here, an update factor of 4.91 (valid in 2011) is assumed. MPF is the material and pressure correction factor, and MF is the module factor accounting for the size of the equipment. The bare module costs BC are calculated with an exponential approach

$$BC = C_0 \cdot \left(\frac{S}{S_0}\right)^\alpha \quad (6.2)$$

Table 6.5: Investment and operational costs for additional process equipment.

| | | [m ³ (STP)/h] | 150 | 500 | 1000 | 2000 |
|-----------------------------|----------|--------------------------|--------|--------|--------|--------|
| Rough desulfurisation [175] | | | | | | |
| Investment costs | [Euro] | | 159000 | 159000 | 159000 | 159000 |
| Operating costs | [Euro/a] | | 2674 | 7890 | 15800 | 31500 |
| Fine desulfurisation [175] | | | | | | |
| Investment costs | [Euro] | | 16000 | 16000 | 16000 | 16000 |
| Operating costs | [Euro/a] | | 7651 | 24200 | 47957 | 95400 |
| Adsorptive drying [175] | | | | | | |
| Investment costs | [Euro] | | 16873 | 20500 | 22663 | 25500 |
| Operating costs | [Euro/a] | | 2575 | 8740 | 17158 | 34300 |
| Off-gas treatment [176] | | | | | | |
| Investment costs | [Euro] | | 173241 | 200000 | 250000 | 265000 |
| Operating costs | [Euro/a] | | 6000 | 6000 | 6000 | 6000 |

Table 6.6: Parameters for operation costs.

| | Unit | Costs |
|-------------|---------------------|-------|
| Electricity | Euro/kWh | 0.08 |
| Water | Euro/m ³ | 2 |
| Heat | Euro/kWh | 0.046 |
| Amine | Euro/t | 2150 |

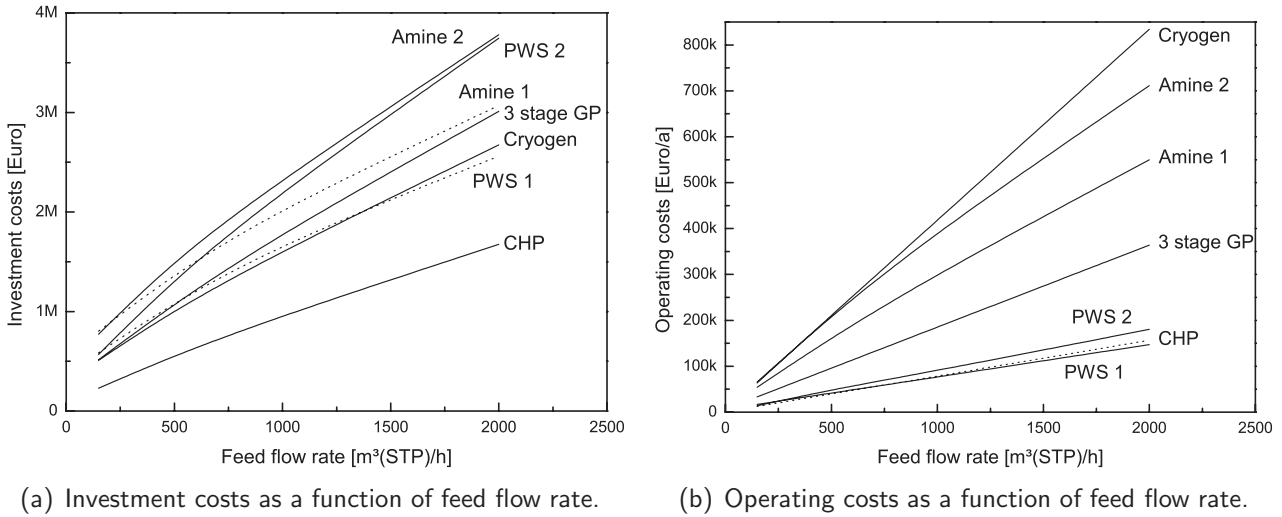


Figure 6.5: Investment and operational costs for plant sizes ranging from 150 to 2000 $m^3(STP)/h$ feed flow rate. The investment costs are given in Mio. Euros while the operating costs are depicted in 1000 Euros.

for equipment such as compressors, heat exchangers and pumps. Whereby, S characterizes the size of the equipment. C_0 and S_0 are the reference costs as well as the reference characteristic value, respectively. The exponent α is often less than 1 to take the economy of scale effect into account. For absorption columns and pressure vessels both, the height l as well as the diameter d , determine the investment costs. Both contribute individually to the costs by using a different exponent to account for the size of the equipment:

$$BC = C_0 \cdot \left(\frac{l}{l_0}\right)^\alpha \cdot \left(\frac{d}{d_0}\right)^\beta \quad (6.3)$$

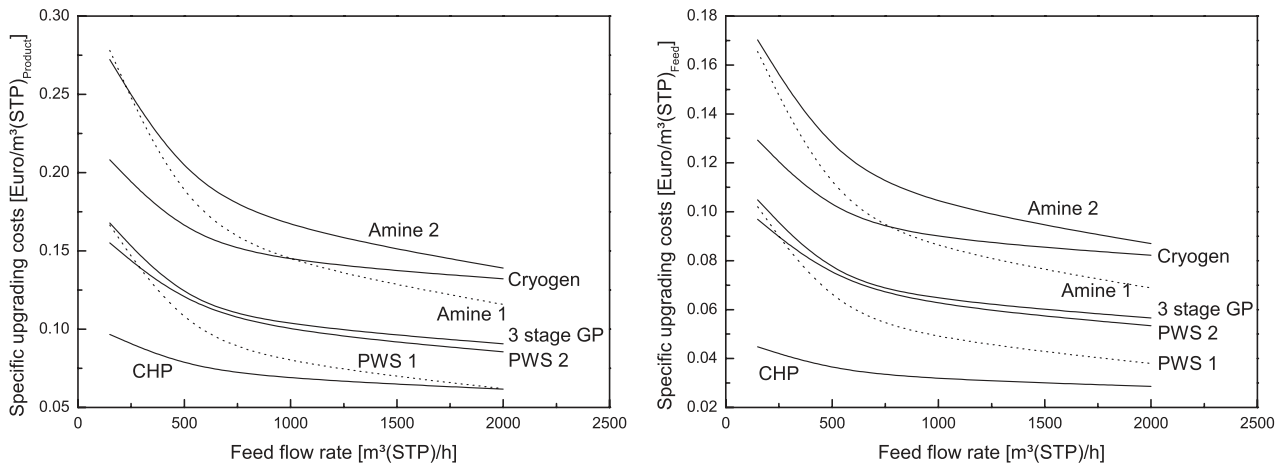
The complete set of parameters to be applied using the Guthrie method including MPF, MF, α , β and the reference values for C_0 , S_0 , l_0 , as well as d_0 , are presented in Table 6.4.

The lifetime of the membrane is assumed to be 4 years. The specific membrane module costs including peripheral equipment, such as piping and control devices, are assumed to be 102.30 Euro/m². The costs to replace the membrane after 4 years operation is assumed to be 55 Euro/m².

An annual operation of 8000 h is used in the economic evaluation. Furthermore, an amortization period of 8 years and an interest rate of 9 % are assumed. Additional investment and operational costs for drying, desulfurization and exhaust gas treatment are summarized in the Table 6.5.

6.5 Results and discussion

In this section the different hybrid processes are compared to each other as well as to conventional separation technologies which only use an individual process such as amine scrubbing without the



(a) Comparison of the different hybrid processes with respect to the specific upgrading costs which are presented as a function of feed flow rate. Here, the upgrading costs refer to the product flow rate.
 (b) Comparison of the different hybrid processes with respect to the specific upgrading costs which are presented as a function of feed flow rate. Here, the upgrading costs refer to the feed flow rate.

Figure 6.6: The specific upgrading costs are presented for the different hybrid process configurations as a function of the feed flow rate.

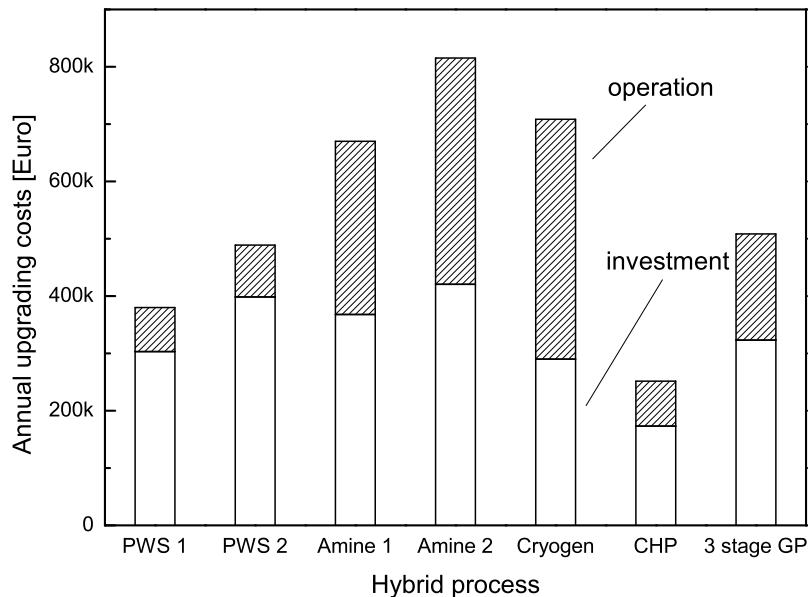


Figure 6.7: Annual operation costs splitted in annual operation costs and annual costs for investment. The data is shown for a feed flow rate of 1000 m³(STP)/h.

application of a membrane. The CHP process is different to the other processes since a significant fraction of the raw gas is mixed with the permeate from the gas permeation stage to enhance the heating value of this gas mixture. Here a CH₄ content of at least 30 % is required to drive the gas engine. In the CHP process the focus is not only providing an upgraded biogas, but also electricity and heat from the gas engine. Therefore, only low CH₄ recoveries can be achieved while the other hybrid processes operate by supplying a gas with a high CH₄ mole fraction and drive the process with CH₄ recoveries as high as 99.9 %. This exception of the CHP process has to be taken into account while reviewing the following graphs.

6.5.1 Investment costs

Figure 6.5(a) presents the investment costs for the membrane hybrid processes as a function of feed flow rate. The investment costs for the CHP process are lowest. For the hybrid processes where high CH₄ recoveries are obtained the PWS 1 and the cryogenic process have the lowest investment costs. For processes with feed flow rate of more than 1500 m³(STP)/h the PWS 1 has the lowest investment costs. In case that the feed flow rate is less than 1500 m³(STP)/h the cost for investment are lowest for the hybrid cryogenic process. Interestingly, the three stage membrane processes has particularly low investment costs for a process with a feed flow rate of 150 m³(STP)/h. The gas permeation process has similar investment costs as the cryogenic process. The slope of the curve illustrating the investment costs for the gas permeation process is strongest due to the economy of scale effect. The investment costs for the membrane modules increase linearly with increasing feed flow rate. The economy of scale effect is remarkable for the absorption processes as the costs for vessels, heat exchanger, pumps and columns show a distinct dependency on equipment size indicated by the α in Table 6.4.

6.5.2 Operating costs

Figure 6.5(b) depicts the annual operating cost for the hybrid processes as a function of the feed flow rate. While the investment cost for the hybrid cryogenic are low the operating costs are highest for the whole range of feed flow rates. Both hybrid processes involving the pressurized water scrubbing technology have the lowest operating costs. For the PWS processes the regeneration of loaded solvent is less expensive compared to the amine absorption as only air is fed to the stripping column without introducing large amounts of heat to dissolve the CO₂ from the solvent. In addition, the compression duty is lower compared to the 3 stage gas permeation process, since no recycle stream is used in PWS 1 nor in PWS 2. However, the CH₄ recovery of PWS 1 is low.

In Figure 6.7 the annual upgrading costs are presented for the hybrid processes at a raw gas flow rate of 1000 m³(STP)/h. Both, annual operation costs and annual interest payments due to investment

costs are included. For the processes using pressurized water scrubbing technology, for the CHP process and for the 3 stage membrane process the investment costs dominate the annual operation costs. For the amine processes and for the hybrid cryogenic separation the operating costs are equal or higher than the investment related costs.

6.5.3 CH₄ recovery

In Figure 6.8 the CH₄ recovery is presented for the membrane hybrid processes. The CH₄ recovery of the CHP process is remarkably lower than that of the other processes since a major fraction of the raw gas is used to drive the gas engine. For the processes focusing on upgrading two types of processes are distinguished. First, the processes in which a single gas permeation membrane performs the bulk separation and the conventional process equipment is used for final purification are analyzed. Here, significant CH₄ losses via the permeate of the membrane stage result in low CH₄ recoveries.

Figure 6.10 presents the CH₄ loss as a function of feed pressure of the membrane stage for PWS 1 and Amine 1. For both processes the CH₄ loss decreases with increasing feed pressure since the membrane module operates in the pressure ratio controlled region. Hence, the operation at higher pressure ratios facilitates the production of a purer permeate, resulting in reduced CH₄ losses. The CH₄ loss is more pronounced for the PWS 1 process. This is due to the unavoidable CH₄ losses in the pressurized water scrubbing process and the losses in the permeate of the membrane stage, which add up to the total CH₄ loss. For process configuration PWS 2 the CH₄ loss is low as only a small fraction of the CH₄ present in the raw gas are fed to the absorption process while for PWS 1 the major fraction of the CH₄ is in contact with the solvent.

In Figure 6.11 the CH₄ loss as well as the required membrane area for PWS 1 are presented as a function of the CH₄ mole fraction in the retentate of the membrane stage at a feed pressure of 16 bar and a flow rate of 1000 m³(STP)/h. The retentate mole fraction is an indicator for the ratio of the separation performed by the membrane stage and by the pressurized water scrubbing process. The higher the retentate mole fraction the higher the fraction of the bulk separation performed by the membrane. The required membrane area increases drastically with increasing CH₄ purity in the retentate since the driving force for CH₄ permeation strongly decreases. By providing more membrane area, more CH₄ permeates through the membrane resulting in extensive CH₄ losses. Hence, the ratio of the separation performed by the membrane stage and separation performed by the absorption process has to be chosen carefully as it directly determines the CH₄ loss.

The second process type is characterized by a single stage membrane which is combined with conventional gas separation equipment to recover the CH₄ from the membrane stage permeate. For this process configuration CH₄ recoveries of more than 99.5 % are realized. This is particularly important as for biogas injection in Germany additional gratuities are paid for processes with CH₄ recoveries of more than 99.5 %. The individual amine absorption process has CH₄ recoveries as high

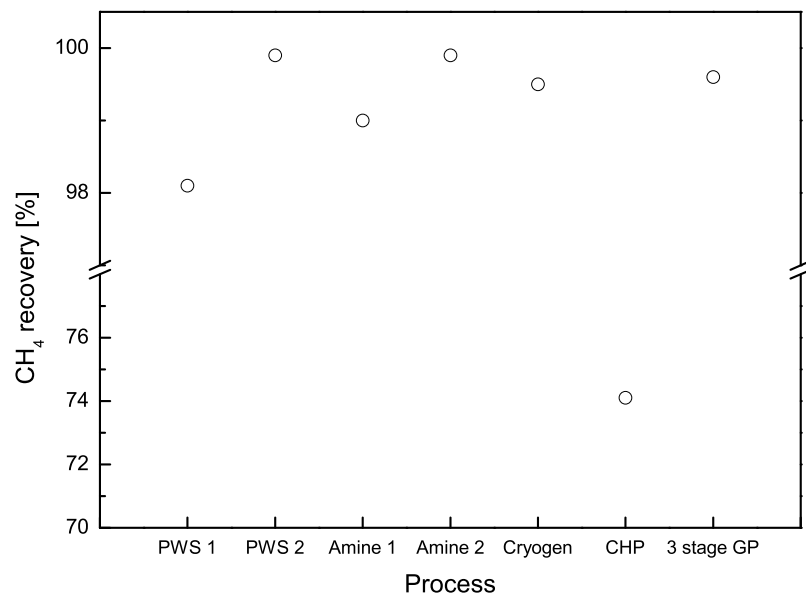


Figure 6.8: The CH₄ recovery is illustrated for the different hybrid processes at a feed flow rate of $1000 \text{ m}^3(\text{STP})/\text{h}$. The CH₄ recovery of the hybrid combined heat and power process (CHP) is significantly lower compared to the other process configuration. A significant fraction of the raw gas is used to increase the CH₄ level in the feed for the gas engine.

Table 6.7: Energy demand and generation for a combined heat and power engine.

| | $\text{m}^3(\text{STP})/\text{h}$ | 150 | 500 | 1000 | 2000 |
|--|-----------------------------------|-----|-----|------|------|
| Electrical energy demand (compression) | kWh | 17 | 58 | 116 | 233 |
| Electrical energy produced | kWh | 93 | 309 | 618 | 1231 |
| Electrical energy produced netto | kWh | 72 | 239 | 478 | 949 |

as 99.9 % while the pressurized water scrubbing process only obtains CH₄ recoveries of 98 % [5, 177].

6.5.4 Specific upgrading costs

Figure 6.6(a) and Figure 6.6(b) show the specific upgrading costs as a function of feed flow rate with respect to the product and the feed, respectively. Both calculations are presented as the specific upgrading costs reported in literature [5] are often presented either with respect to the product or feed flow rate.

The absolute value of the specific upgrading costs is higher in the case where it is related to the product flow rate. However, the general result which is the order of the processes from the cheapest to the most expensive process does not change for both calculations.

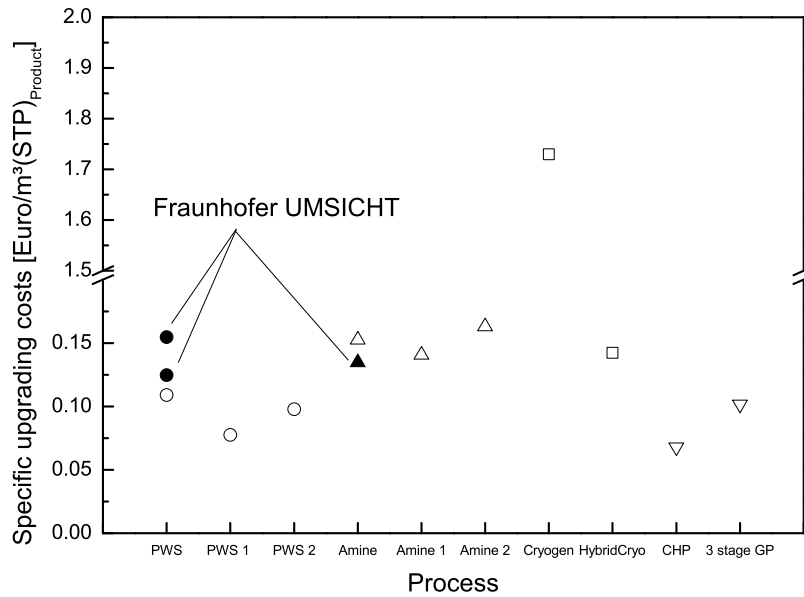


Figure 6.9: Comparison of the different hybrid processes in term of the specific upgrading costs. Here, the upgrading costs are presented with respect to the product flow rate. The data is shown for a feed flow rate of $1000 \text{ m}^3(\text{STP})/\text{h}$. The filled symbols refer to published data for the amine and the pressurized water scrubbing process [5].

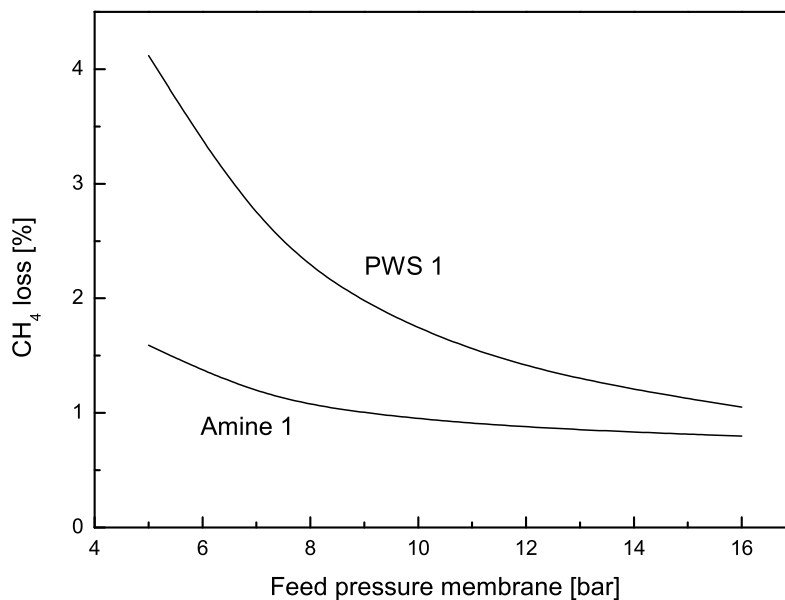


Figure 6.10: CH_4 loss as a function of the membrane feed pressure for a feed flow rate of $1000 \text{ m}^3(\text{STP})/\text{h}$. Comparison of PWS 1 and Amine 1.

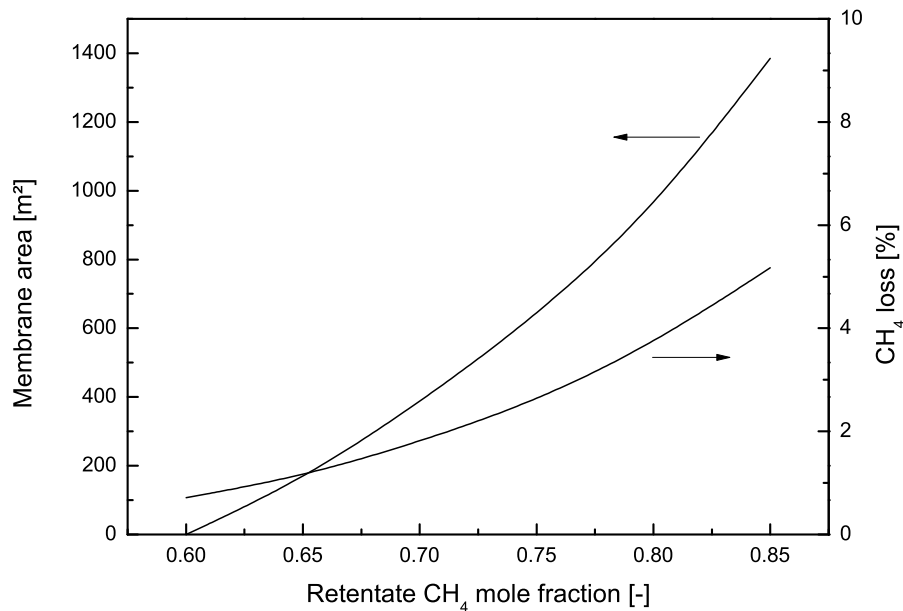


Figure 6.11: PWS 1 Membrane area and CH₄ loss as a function of CH₄ retentate mole fraction. The data is shown for a feed flow rate of 1000 m³(STP)/h and a feed pressure of 16 bar.

Two groups of processes can be identified. The first group include both hybrid amine systems as well as the hybrid cryogenic process. Here, the level of the specific upgrading costs is significantly higher than that of the second group which includes the water scrubbing processes and the three stage membrane process. As the CHP process has the lowest investment costs as well as low operational costs the specific upgrading costs are least significant.

The sharp decrease of the specific upgrading costs with increasing feed flow rates is attributed to the investment costs for peripheral equipment such as exhaust gas treatment and desulfurization (see Table 6.5). Here, the investment costs for rough desulfurization as well as for exhaust gas treatment do not change significantly with increasing feed flow rate. Hence, this impact is more pronounced in case of low feed flow rates. In addition, the economy of scale effect reduces the influence of the feed flow rate on the upgrading costs for large feed flow rates.

6.5.5 Comparison to conventional technologies

Figure 6.9 shows the specific upgrading costs for the hybrid processes investigated here as well as the costs for the individual processes operating without a gas permeation. The unfilled symbols refer to data obtained from the simulations while the filled symbols refer to real process data reported by Fraunhofer UMSICHT [5]. In general, the calculated data agrees well with the published data for both, the water scrubbing and the amine absorption process.

Table 6.8: Plant profit as a function of feed flow rate.* Electrical energy revenue and heat sales are not taken into account. This would enhance the performance of the CHP plant.

| Feed flow rate $m^3(STP)/h$ | PWS 1 | PWS 2 | Amine 1 | Amine 2 | Cryogen | CHP* | 3 stage GP |
|--------------------------------|-----------|-------|---------|---------|---------|------|------------|
| | 1000 Euro | | | | | | |
| 150 | 392 | 408 | 301 | 320 | 366 | 335 | 398 |
| 500 | 1477 | 1461 | 1255 | 1266 | 1340 | 1156 | 1458 |
| 1000 | 3050 | 3010 | 2663 | 2687 | 2773 | 2342 | 2990 |
| 2000 | 6256 | 6145 | 5563 | 5613 | 5647 | 4738 | 6091 |

The pressurized water scrubbing process benefits by applying a gas permeation membrane. The specific upgrading costs are lower for the hybrid processes compared to the conventional scrubbing process operating without a membrane. For the amine absorption process only the process configuration in which the membrane performs the bulk separation and the scrubber does the final gas polishing seems to be better than the conventional amine absorption process. The application of a gas permeation membrane has a paramount impact on the cryogenic separation processes. The upgrading costs reduce to less than 9 % by operating a membrane hybrid process instead of an individual cryogenic process. The specific upgrading costs for the combined heat and power process are lowest as it operates self-sustaining. Table 6.7 indicates that only 20 % of the electrical energy supplied by the gas engine are required to drive the compressor for the membrane process. The excess energy can be fed into the electrical grid. However, this process is only efficient in case that the produced heat can be utilized. It has to be noted that the CH₄ recovery is low (see Figure 6.8). The specific upgrading costs for the three stage gas permeation process are lower than the upgrading costs for all conventional upgrading technologies. Compared to the hybrid processes only the two processes in which gas permeation membranes are combined with a pressurized water scrubbing process have lower upgrading costs than the individual gas permeation process. However, operating PWS 1 results in significant CH₄ losses. In general, the PWS hybrid processes include lots of different equipment which is less robust than the three stage gas permeation system as it is only equipped with a multistage compressor and membrane modules in the three membrane stages.

6.6 Conclusion

Membrane hybrid processes in which gas permeation technology is combined with established gas separation techniques such as pressurized water scrubbing, amine absorption and cryogenic separation are attractive for biogas upgrading. These hybrid processes were primarily investigated in terms of upgrading costs using Aspen Plus. Investment costs are accounted for by Guthrie's method for

equipment cost estimation.

Comparing the hybrid processes to the established separation techniques clearly shows that established upgrading processes would benefit from a combination with membrane technology. Solely the amine hybrid process in which the permeate of the membrane stage is fed to the amine absorber has higher upgrading costs than an individual amine absorption process. The application of a gas permeation stage is paramount for the cryogenic separation. Only the membrane cryogenic hybrid process is competitive to established separation techniques while the upgrading costs for an individual cryogenic process are an order of magnitude higher than the costs for established upgrading processes. Linking a gas engine to the permeate of a single gas permeation stage is particularly attractive when the heat produced along with the electricity can be utilized. Due to the low CH₄ recovery it is not recommended to built such a plant in case that the heat is unused. Ultimately, a non-hybrid three stage gas permeation process was investigated which also shows low upgrading costs and operates with high CH₄ recoveries. Due to its simple process layout, only involving a single compressor, this process seems to be highly attractive. The robustness of this process makes it particularly suitable for on-farm operation in small and medium scale biogas upgrading plants.

Chapter 7

Superstructure optimization of biogas upgrading processes

7.1 Introduction

In biogas upgrading CO_2 , H_2S and H_2O have to be removed from CH_4 to inject the upgraded gas into the natural gas grid. Various technologies are available to remove the single compounds individually from CH_4 . Combining these three purifying steps leads to numerous combinations of the different unit operations. Furthermore, the operation of the different design alternatives can be done at different process conditions and a straight forward evaluation of all combinations is impossible. Hence, we present a superstructure optimization model which supports the selection of the most profitable process configuration for biogas upgrading. For specified economic parameters and the feed gas conditions the optimization model determines the most profitable process configuration by selecting and sizing the unit operations, specifying their sequence and by determining the process conditions, mainly the pressures.

In biogas upgrading process conditions and parameters remarkably influence the profitability of the upgrading process. Costs of electricity and steam are key process parameters and they play an important role in determining the operating costs of upgrading processes. Prices for utilities may differ significantly for different biogas sites and an individual survey is required to determine the most profitable upgrading technique for a specific biogas site. In this work at hand the state equipment approach is applied to determine the optimal process configuration for a biogas upgrading process.

7.2 Process equipment for biogas purification

Table 7.1 lists the unit operations and indicates for which separation the equipment is used in this study. The most important equipment in biogas upgrading are technologies to remove CO_2 as it is the bulk component to be removed from CH_4 . Here, three different technologies are considered in the optimization model which are: (i) a three stage gas permeation process, (ii) an amine absorption process and (iii) a pressurized water scrubbing process. These technologies have to be combined with desulfurization and gas drying equipment to provide a biogas which can be injected into the natural gas grid. Pressure swing adsorption is an established technique to adsorb CO_2 but due to its low CH_4 recovery ($< 96\%$) it is not considered here [5].

For rough desulfurization, iron chelates in aqueous solution (RedOx) are applied to remove H_2S . 99.9 % of H_2S can be removed and a load of 0.1 - 3 mol-% H_2S in the raw gas can be treated with such a system. The rough desulfurization is important for the amine absorption process since the amines strongly bind H_2S and regenerating the solvent is expensive. Fine desulfurization is achieved with adsorption on activated carbon.

Four methods to dry the biogas are considered here. Water vapor condenses in the compression equipment at elevated pressures and low temperatures. A significant amount of water condenses in the heat exchanger downstream of the compressor so that only a fine drying step is required which

Table 7.1: Unit operations for desulfurization, drying and CO₂ removal in biogas upgrading processes.

| H ₂ S | H ₂ O | CO ₂ |
|------------------|-------------------|------------------------------|
| RedOx | Condensation | Amine absorption |
| Activated carbon | Silica gel | Gas permeation |
| | Activated carbon | Pressurized water absorption |
| | Glycol absorption | |

Table 7.2: Feed gas conditions and product gas requirements.

| | Unit | Feed | Product |
|------------------|-------|-------|----------|
| CH ₄ | mol-% | 60 | > 96 |
| CO ₂ | mol-% | 35 | < 4 |
| H ₂ O | mol-% | 3 | < 0.08 |
| H ₂ S | mol-% | 2 | < 0.0003 |
| Pressure | bar | 1.013 | 16 |

can be accomplished by glycol absorption, adsorption on activated carbon or silica gel.

7.3 Process model

The superstructure model which is based on physical and economic equations facilitates the fast determination of the most profitable biogas upgrading process. Short cut models for the involved unit operations are used in a superstructure optimization. The model equations and a detailed summary of the parameters for the unit operations are reported in the Appendix 7.6.

Table 7.2 presents the feed gas conditions and product gas requirements. The feed gas mainly consists of CH₄ and CO₂. However, strict quality requirements of the product gas have to be met to

Table 7.3: Economic parameters and process conditions for a base case and the parameter ranges which are used in the sensitivity analysis.

| | Unit | Base case | Range | Increment | Reference |
|------------------------------------|---|-----------|-------------|-----------|-----------|
| Electricity cost | $\frac{\text{Euro}}{\text{kWh}}$ | 0.08 | 0.04 - 0.36 | 0.04 | [178] |
| Steam cost | $\frac{\text{Euro}}{\text{t}}$ | 20 | 10 - 40 | 10 | [178] |
| Water cost | $\frac{\text{Euro}}{\text{m}^3}$ | 0.08 | 0.04 - 0.36 | 0.04 | [178] |
| Feed flow rate | $\frac{\text{m}^3(\text{STP})}{\text{h}}$ | 1000 | 500 - 2000 | 500 | [2] |
| Feed mole fraction CH ₄ | - | 0.6 | 0.5 - 0.7 | 0.1 | [2] |

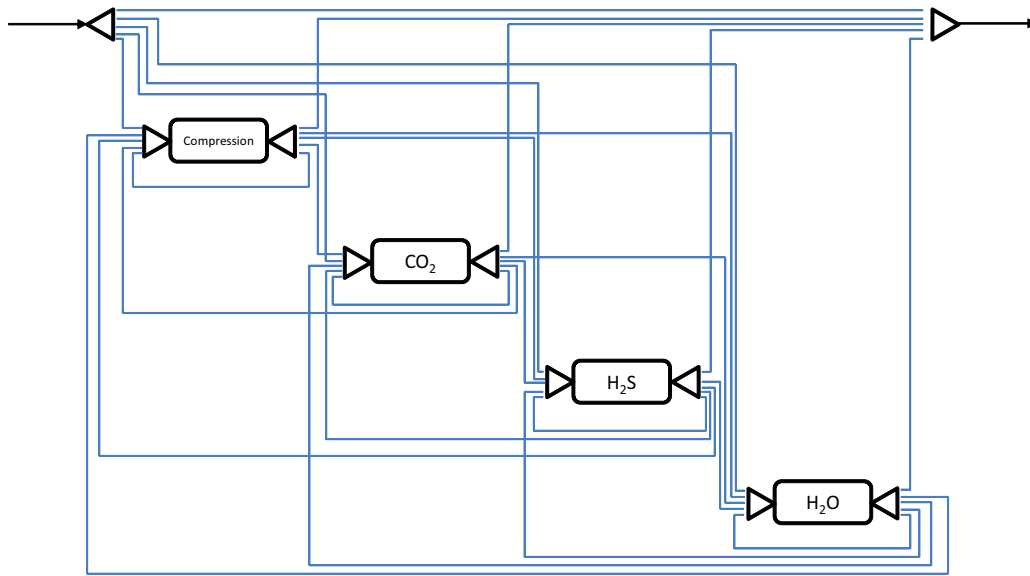
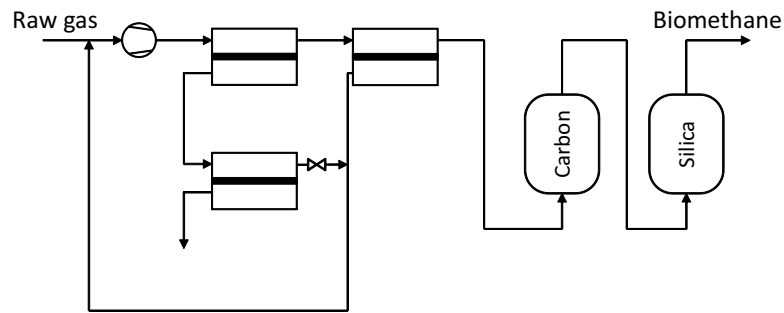


Figure 7.1: Superstructure optimization approach used to determine the optimal biogas upgrading process. All possible connections between the involved unit operations are illustrated.

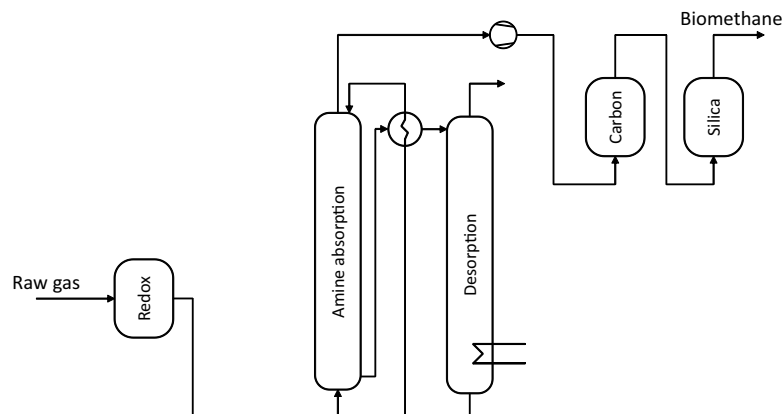
provide the gas at natural gas grade. Obviously, the H_2O and H_2S levels are very low (see Table 7.2). In addition, the product gas has to be compressed to meet the natural gas grid pressure which is set to 16 bar.

Investment and operational costs have to be considered for evaluating the biogas upgrading process. The investment costs are estimated according to Guthrie [149] and the parameters for the cost model are given in the Appendix 7.6. The utility costs which are accounted for are: (i) cost for electricity to drive compressors, blowers and pumps, (ii) costs for low pressure steam which is used in the regeneration of the amine absorption process and (iii) costs for cooling water. In addition, the feed conditions severely influence the process performance and profitability. The impact of the feed flow rate and the mole fraction of CH_4 are investigated in a sensitivity analysis.

Table 7.3 lists the utility costs and the feed gas conditions for a base case. Furthermore, a range of these parameters is given which is used in a sensitivity analysis to determine the process performance. Since a full evaluation of all parameters including the large number of their combinations is demanding, each parameter is investigated while the other parameters are kept at their base case value. A detailed analysis of electricity and steam costs including their combinations is performed since both parameters have a remarkable impact on the process configuration and the profitability. The schematic overview on the process model is depicted in Figure 7.1. In general, four steps have to be performed in biogas upgrading: (i) compression of the gas, (ii) CO_2 removal, (iii) desulfurization and (iv) gas drying. The different blocks (see Figure 7.1) represent a set of unit operations which can be selected by the solver. The unit operations are presented in Table 7.1. Each block outlet can be connected to any other block inlet, so that the sequence of the different unit operations is not predefined and the process configuration can be determined by the solver. Figure 7.1 also indicates that different unit operations from one single block can be used at the same time. Hence, it is



(a) Process flowsheet of the optimal gas permeation process for CO₂ removal. Since the membrane system cannot meet the natural gas grade in terms of H₂S and H₂O level, a desulfurization and drying equipment operate downstream of the membrane process.



(b) Process flowsheet of the optimal upgrading process based on amine absorption. A rough desulfurization is installed before the amine absorption process. A fine desulfurization and drying equipment operate downstream of the absorption column.

Figure 7.2: Optimal process configurations in biogas upgrading including desulfurization and gas drying.

possible that the solver selects a hybrid process to be the most profitable process configuration. The process optimization model was implemented in the General Algebraic Modeling System (GAMS). The Branch And Reduce Optimization Navigator (BARON) solver was applied to solve the optimization problem. This particular solver guarantees to identify the global optimum and a model initialization is not required.

7.4 Results and discussion

7.4.1 Base case

For the base case the membrane based upgrading process is the most profitable process configuration. This process including the desulfurization and drying equipment is presented in Figure 7.2(a).

Table 7.4: Process parameters and equipment sizes for the base case.

| | Unit | Value |
|-------------------------------|---------------------------|-----------|
| CH ₄ recovery | - | 0.998 |
| Annual revenue | Euro/a | 5 979 766 |
| Annual profit | Euro/a | 5 576 731 |
| Annual operating costs | Euro/a | 184 692 |
| Annual costs (total) | Euro/a | 403 035 |
| Membrane area (Stage 1) | m ² | 950 |
| Membrane area (Stage 2) | m ² | 1319 |
| Membrane area (Stage 3) | m ² | 1100 |
| Feed pressure (Stage 3) | bar | 3.1 |
| Silica mass | kg | 56 |
| Silica adsorber cross section | m ² | 0.133 |
| Silica adsorber height | m | 0.732 |
| Silica adsorber pressure | bar | 16 |
| Carbon mass | kg | 167 |
| Carbon adsorber cross section | m ² | 0.133 |
| Carbon adsorber height | m | 3.132 |
| Carbon adsorber pressure | bar | 16 |
| Compression demand | kW | 203 |
| Specific upgrading costs | Euro/m ³ (STP) | 0.08 |

In the gas permeation process three membrane stages are combined to obtain high CH₄ purities together with high CH₄ recoveries. Firstly, the raw gas is compressed to provide the driving force for permeation and the elevated pressure for natural gas grid injection at the same time. Although the membrane is even more permeable for H₂O and H₂S two additional units for fine desulfurization and gas drying are required. Due to their low mole fractions in the raw gas and, as a consequence, their low driving forces, the gas permeation process is not able to achieve the demanding levels of H₂O and H₂S for grid injection. However, a significant amount of H₂O is removed by the compressor due to interstage cooling. The bulk of H₂S is removed with the permeate of the gas permeation process. Table 7.4 presents the process characteristics for the base case process including the size of the adsorber vessels and the required membrane areas in the different stages. A high CH₄ recovery of 99.8 % is achieved with this process. Assuming a membrane module size of 25 m² the membrane area translates to the application of 135 membrane modules. Small adsorption vessels for H₂S and H₂O removal are required.

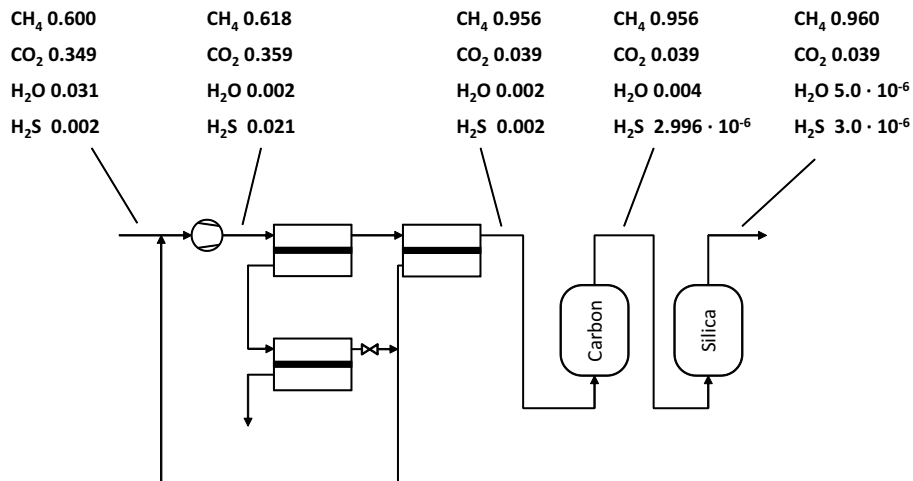


Figure 7.3: The flowsheet depicts the mole fractions of CH₄, CO₂, H₂O and H₂S for the base case.

Table 7.5: Depletion rate of H₂O and H₂S in the different unit operations for the base case process.

| Depletion | H ₂ O | H ₂ S |
|-------------------|------------------|------------------|
| Compressor | 0.937 | - |
| Membrane | 0.022 | 0.929 |
| Carbon adsorption | - | 0.071 |
| Silica adsorption | 0.075 | - |

The flowsheet illustrated in Figure 7.3 gives a review on the mole fractions of all components for the inlet and outlet of each unit operation. While the membrane process is mainly dedicated to remove CO₂, significant quantities of H₂S are removed along with CO₂. The activated carbon and the silica adsorber are used to remove H₂S and H₂O, respectively, so that natural gas standard is obtained. Table 7.5 shows the depletion rate of both trace components, H₂S and H₂O. The compressor which increases the pressure from 1 bar to 16 bar is equipped with a heat exchanger at the outlet which operates at a temperature of 25 °C. Hence, more than 90 % of the water condenses at the outlet of the compression unit which leads to a low water content of the gas entering the gas permeation process. As a consequence, the driving force for water permeation is also low and only 2 % of the total amount of water are removed by gas permeation membranes. The activated carbon adsorption does not contribute to the drying of the product gas. In contrast, since the chemical adsorption of H₂S is accompanied by the production of H₂O, it is added to the product gas stream. Hence, a final drying is required which is done by silica adsorption. 8 % of H₂O from the feed are removed. H₂S is mainly removed by the gas permeation process (93 %). However, the required H₂S level for grid injection is not met and a final desulfurization is performed by the activated carbon adsorption. This adsorption removes approximately 7 % of the H₂S present in the raw biogas.

Figure 7.4 depicts the investment costs for the different unit operations at base case conditions.

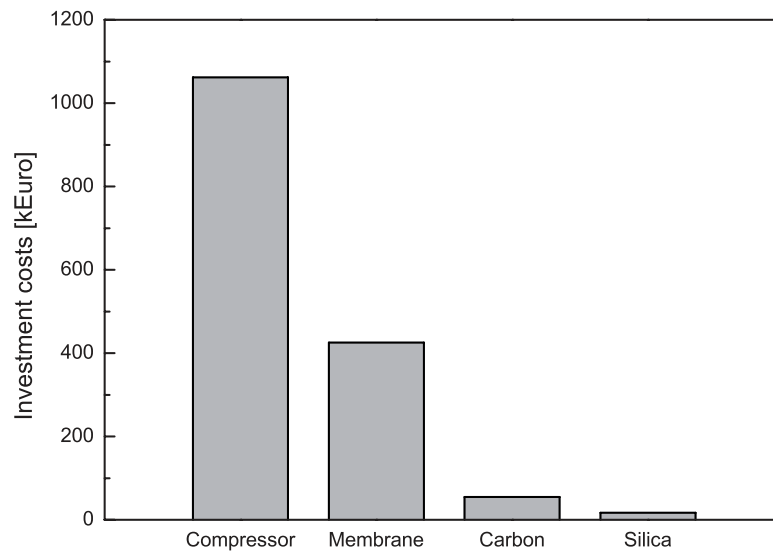


Figure 7.4: Investment costs for the different unit operations for the base case scenario.

The compressor is the most expensive unit operation which accounts for 68 % of the total investment costs. The membrane modules contribute with 27 % to the total investment costs while the contributions of the activated carbon adsorption (4 %) and silica adsorption (1 %) are insignificant. In the following, the influence of operational parameters on the process configuration and the profitability are presented. Here, only one single parameter is changed while the other parameters are kept at their base case conditions.

Figure 7.5 shows the annual profit for the optimal process configuration as a function of electricity costs. For electricity costs less than 0.13 Euro/kWh the membrane process illustrated in Figure 7.2(a) is the best process configuration. In case that the electricity costs are higher, the amine process generates higher profits than the membrane process. The intersection of both trendlines indicates the conditions where a change in the optimal process configuration is observed.

In Figure 7.6 the annual upgrading costs are depicted as a function of electricity costs. In contrast to Figure 7.5 the change in the most profitable process configuration is observed at electricity costs of 0.14 Euro/kWh. While the costs include the investment and the operational costs, the annual profit (see Figure 7.5) includes the product gas flow rate which is higher for the amine process due to a high CH₄ recovery.

Figure 7.7 depicts the annual profit and the annual upgrading costs as a function of the feed flow rate. Both, the annual profit and the upgrading costs increase with increasing feed flow rate. The increase in annual profit is due to the increased gas sales. The increase in the upgrading costs is caused by the larger process equipment and the increased cost for utilities. In particular, the costs to drive the compressors increase with increasing feed flow rate. However, the feed flow rate does not have an impact on the process configuration for the boundary conditions considered here. The membrane process is the most profitable process configuration for all considered feed flow rates.

In Figure 7.8 the annual profit and the annual upgrading costs are presented as a function of the feed

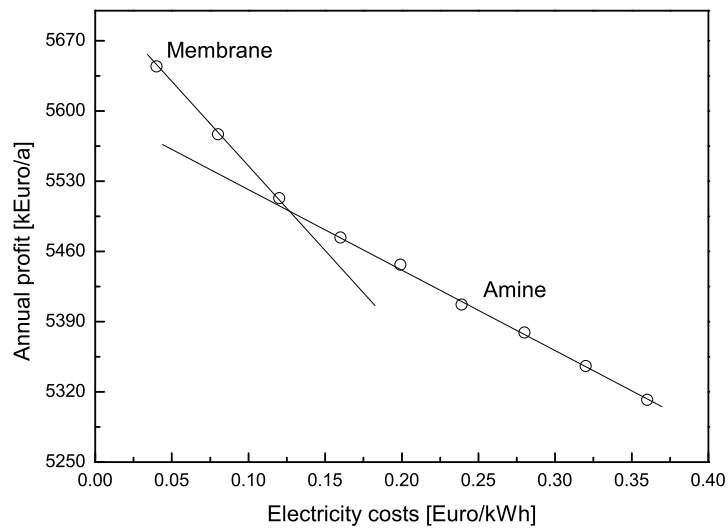


Figure 7.5: Annual profit as a function of electricity costs. For electricity costs lower than 0.13 Euro/kWh the membrane process is the most profitable configuration.

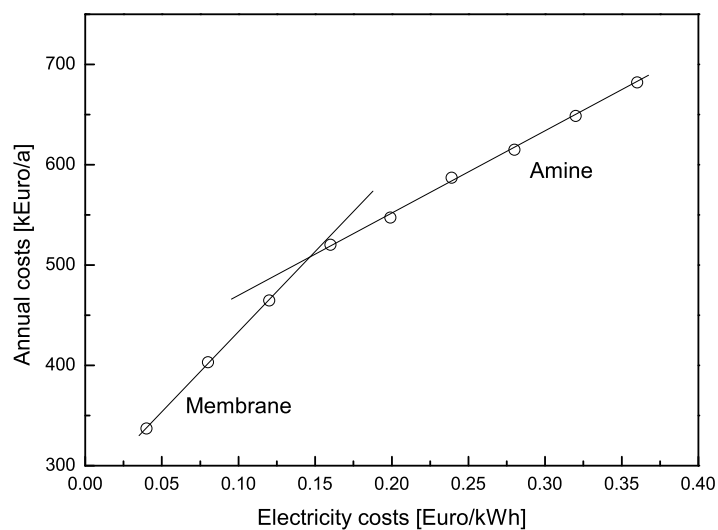


Figure 7.6: Annual costs as a function of electricity costs. For electricity costs lower than 0.14 Euro/kWh the membrane process is the most profitable configuration.

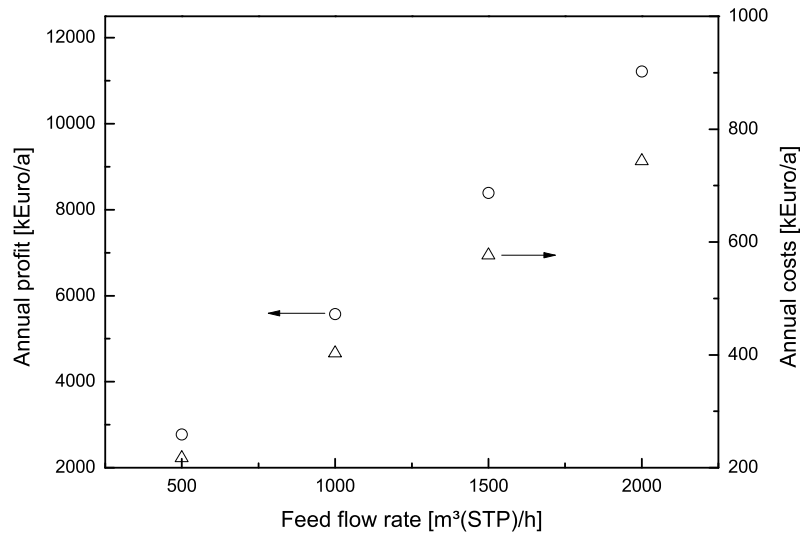


Figure 7.7: Annual profit and annual upgrading costs as a function of feed flow rate.

mole fraction of CH_4 . The annual upgrading costs decrease with increasing CH_4 feed mole fraction since less CO_2 has to be removed from the bulk of CH_4 . Both, investment costs and operational costs decrease. The annual profit increases due to two phenomena. First, the product gas flow rate increases with increasing CH_4 content in the raw gas. This directly translates to increased gas sales. Second, the annual upgrading costs decrease which further increases the annual profit. Here, the membrane process including the adsorption on activated carbon and the final drying with silica gel is also the most profitable process configuration for the entire range of CH_4 feed mole fractions.

Figure 7.9 presents the annual profit for the optimized process configuration as a function of the membrane costs. For the base case the membrane costs are 55 Euro/ m^2 and the membrane process is the most profitable process configuration. Increasing the membrane costs up to 80 Euro/ m^2 results in a reduced annual profit as a consequence of increased investment and operational costs. Membrane replacement costs are taken into account for operational costs. However, further increasing the membrane costs results in a change in the optimal process configuration. For membrane costs of more than 80 Euro/ m^2 the amine absorption process is most profitable. Reducing the membrane costs below 55 Euro/ m^2 would linearly increase the annual profit.

In Figure 7.10 the impact of CO_2/CH_4 membrane selectivity on the annual profit is illustrated. For selectivities less than 40 the amine process should be applied. For low membrane selectivities the annual profit drops considerably caused by a drastic increase in the recycle flow rate to achieve high CH_4 recoveries. For the base case ($\alpha_{\text{CO}_2/\text{CH}_4} = 60$) the CH_4 recovery is at 99.8 % and a low recycle flow rate is required. Hence, further increasing the membrane selectivity does not reduce the recycle flow rate significantly which only translates to a low increase in profitability.

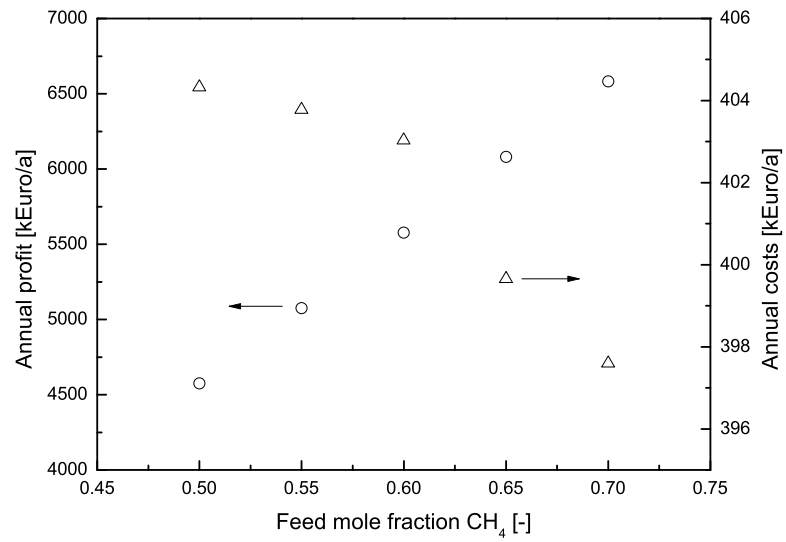


Figure 7.8: Annual profit and annual upgrading costs as a function of CH₄ feed mole fraction.

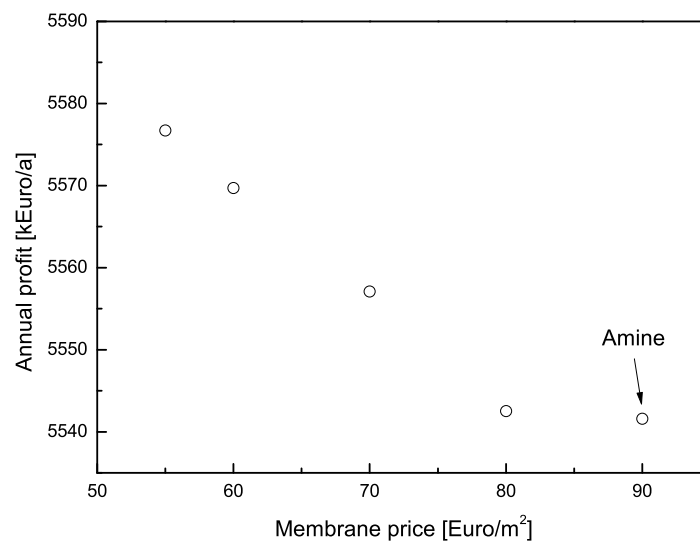


Figure 7.9: Annual profit as a function of membrane price.

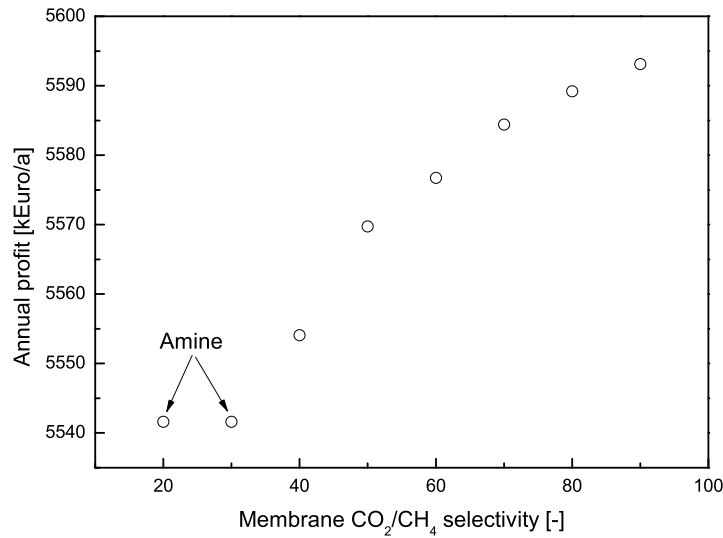


Figure 7.10: Annual profit as a function of membrane CO₂/CH₄ selectivity.

7.4.2 Amine process

When using the amine process the raw gas enters a redox unit (see Section 7.6) first for rough desulfurization. Subsequently, the gas is injected into the amine absorption column where mainly CO₂ is removed. Since the amine absorption and the redox unit operate at ambient pressure the upgraded gas is fed to a compressor which provides the driving force for the fine desulfurization and the final drying as well as the natural gas injection pressure at the same time. After compression the gas enters an adsorber filled with activated carbon to remove traces of H₂S. Finally, the gas is fed to a silica adsorption unit which removes H₂O and the gas is fed to the natural gas grid.

Table 7.6 gives an example of the size of the equipment involved in the amine absorption process which is also equipped with a rough desulfurization using iron chelates (redox) and a fine desulfurization with activated carbon as well as a final product gas drying with silica adsorption. The annual revenue is similar for both processes, the membrane and the amine process, due to their high CH₄ recovery. The economic parameters cannot be compared as the data for the membrane process are obtained with electrical energy costs of 0.08 Euro/kWh while the amine process presents data for a scenario in which the electricity costs are set to 0.16 Euro/kWh. However, the amine requires less electrical energy. Since the CO₂ removal in the amine process is performed at ambient pressure and the gas compression is downstream of the absorption process, only the purified CH₄ rich product gas has to be compressed. However, the desorption process requires a heat duty of 337 kW. The size of the activated carbon adsorber is reduced due to the rough desulfurization which is performed prior to the amine absorption process. Consequently, less H₂O is generated in the fine desulfurization step which results in a reduced size of the silica adsorption vessel.

Table 7.6: Process parameters and equipment sizes for an example amine process (elect. 16 ct / kWh).

| | Unit | Value |
|--------------------------------|---------------------------|-----------|
| CH ₄ recovery | - | 1 |
| Annual revenue | Euro/a | 5 994 240 |
| Annual profit | Euro/a | 5 473 937 |
| Annual operating costs | Euro/a | 318 183 |
| Annual costs (total) | Euro/a | 520 303 |
| Amine absorber cross section | m ² | 0.099 |
| Amine absorber height | m | 8.1 |
| Amine desorber cross section | m ² | 0.217 |
| Amine desorber height | m | 6.0 |
| Amine reboiler duty | kW | 337 |
| Redox H ₂ S removal | kmol/h | 0.848 |
| Silica mass | kg | 38 |
| Silica adsorber cross section | m ² | 0.133 |
| Silica adsorber height | m | 0.493 |
| Silica adsorber pressure | bar | 16 |
| Carbon mass | kg | 76 |
| Carbon adsorber cross section | m ² | 0.133 |
| Carbon adsorber height | m | 1.43 |
| Carbon adsorber pressure | bar | 16 |
| Compression demand | kW | 104 |
| Specific upgrading costs | Euro/m ³ (STP) | 0.104 |

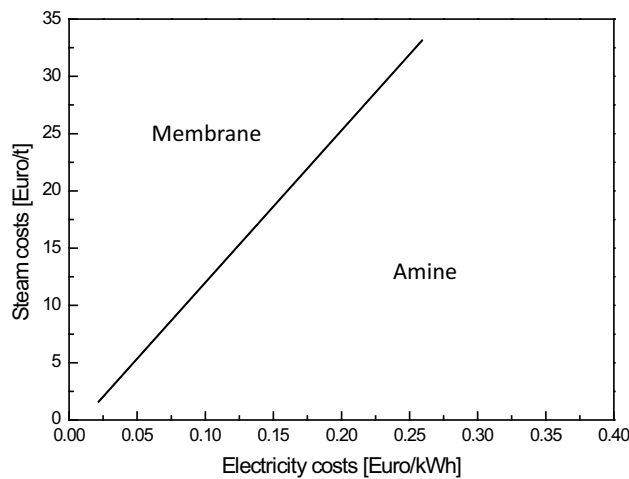


Figure 7.11: Schematic illustration of the region in which the gas permeation and the amine process should be applied to upgrade biogas.

7.4.3 Combined simulation

Figure 7.11 schematically illustrates the effect of electricity and steam costs on the choice of CO₂ removal technology for biogas upgrading. For a set of electricity and steam costs the diagram facilitates the selection of an optimal upgrading process. The line indicates the boundary where a transition from the membrane process to the amine process is observed. The application of the amine process is favorable when steam prices are low while the membrane process should be applied in case that electrical energy is inexpensive.

7.4.4 Remarks

The costs for process water do not have an impact on the process performance. Even in the case where the water is free of charge the pressurized water scrubbing process is never identified to be the best equipment for CO₂ removal. Hence, a sensitivity analysis for water costs is not presented here. Although it is possible that the solver selects different unit operations for H₂S and H₂O removal, activated carbon and silica adsorption are always determined to be the most profitable unit operations.

7.5 Conclusion

A process optimization model is presented which rapidly evaluates the most profitable process configuration for a biogas upgrading process. The model extracts the most promising design alternative from the vast number of possible process configurations by determining (i) the process layout, (ii)

the type of equipment which should be applied in the separation, (iii) the size of the involved equipment and (iv) the process conditions. The gas separation of CO₂ is investigated together with desulfurization and gas drying to supply a biogas with natural gas grade ready for grid injection. For CO₂ removal gas permeation membranes, amine absorption and pressurized water scrubbing are possible candidates. Desulfurization can be achieved by adsorption on activated carbon or using a redox reaction based on iron chelates. Gas drying can be done by condensation, adsorption on silica gel or absorption in glycols. Short cut models for all these unit operations have been implemented in a superstructure optimization model.

A techno-economic evaluation is performed which includes the calculation of investment and operational costs. For a base case scenario a process involving a three stage gas permeation process for CO₂ removal, an activated carbon adsorption for desulfurization and a silica adsorption for gas drying is the most profitable process configuration. Key parameters such as electricity costs, CO₂/CH₄ membrane selectivity and membrane costs have a remarkable impact on the process configuration and profitability. For high electricity costs the optimal process design is a process which first removes the bulk of H₂S in a redox reaction with iron chelates. The H₂S lean gas is fed to an amine absorption column and a final desulfurization is performed using activated carbon. A final gas drying is done with adsorption on silica gel.

In order to verify the results from the superstructure optimization, a detailed process analysis is mandatory. The software tool at hand facilitates the selection of the most profitable process configuration for biogas upgrading. The toolbox could be extended with unit operation such as pressure swing adsorption to apply the model to other separation processes.

7.6 Appendix

The model equations presented here have been developed within the frame of the diploma thesis of Ludger Wolff [179].

7.6.1 Absorption processes

Short cut models for different absorption processes to remove CO₂ and H₂O have been implemented. Pressurized water scrubbing and amine scrubbing for the separation of CO₂ as well as drying by dehydrating liquids such as triethyleneglycol are considered. Typically, the absorption process consists of an absorption column in which the washing liquid flows in countercurrent mode to the raw gas. The column may be designed as spray, tray or packed column [180]. A desorber or stripper regenerates and recycles the washing liquid. Desorption can be accomplished by heating the loaded solvent, by reducing the pressure and by stripping the solvent with an inert gas. Two different models are commonly applied to predict mass transfer in absorption processes: kinetic and equilibrium models [180]. In this work the two film model (kinetic approach) is used and column dimensioning is done with the HTU (height of transfer unit) - NTU (number of transfer units) model.

Kinetic model: Two Film Theory

In the two film model the boundary layers at the gas liquid interface determine the mass transfer resistance while the bulk phases are ideally mixed. Assuming equilibrium at the gas liquid interface, the mass transfer is:

$$\dot{n} = A_i \beta_G (C_G - C_{Gi}) = A_i \beta_L (C_{Li} - C_L) \quad (7.1)$$

Here, A_i is the interface area and β_G and β_L are the mass transfer coefficients of the gas side and the liquid side, respectively. When introducing the distribution coefficient m_C :

$$m_C = \frac{C_G}{C_L}, \quad (7.2)$$

the liquid phase concentration is converted into a hypothetical gas phase concentration C_G^* to erase the discontinuity in the concentration profile. Thus, the unknown concentrations at the interface can be determined and the molar flow through the interface can be described with respect to the gas phase only:

$$\dot{n} = A_i K_G (C_G - C_G^*) = A_i K_G (C_G - m_C C_L) \quad (7.3)$$

K_G is the overall mass transfer coefficient which is related to the individual gas phase and liquid phase mass transfer coefficients β_G and β_L through

$$\frac{1}{K_G} = \frac{1}{\beta_G} + \frac{m_C}{\beta_L}. \quad (7.4)$$

Sherwood correlations are used to calculate the mass transfer coefficients [180–183]:

$$Sh = Sh(Re_G, Re_L, Sc_G, geometry). \quad (7.5)$$

Commonly volumetric overall mass transfer coefficients $K_G a$ or $K_L a$ are used accounting for the specific surface a :

$$a = \frac{A_i}{V_{Pack}} \quad (7.6)$$

where V_{Pack} is packing volume. This translates to:

$$\dot{n} = V(K_G a)(C_G - m_C C_L). \quad (7.7)$$

Henry's law can describe the gas liquid equilibrium

$$p_j^* = H_j x_j \quad (7.8)$$

which relates the partial pressure of the component j in the gas phase p_j^* to the mole fraction x_j of this component in the liquid phase through the Henry constant H_j . In general, Henry's law is valid only for diluted solutions. Applying activity coefficients would account for non-idealities in the liquid. H_j strongly depends on temperature and solubility decreases with increasing temperature. For modeling chemical absorption, it is common practice to apply the equations derived for physical absorption (see Equation 7.3, 7.4) and consider corrected mass transfer coefficients considering the chemical reaction [184].

Dimensioning absorption columns

Dimensioning both, the absorption and desorption column, the column diameters and heights are calculated and an appropriate type of column internal is chosen [180, 184].

The column diameter D is specified by the pressure drop as a result of the column internal design and the gas and liquid flow rates because the column should neither be flooded nor starting to foam. Typical pressure drops are in the range of 0.2 to 0.33 $\frac{\text{kPa}}{\text{m}}$ for non-foaming and 0.08 to 0.2 $\frac{\text{kPa}}{\text{m}}$ for

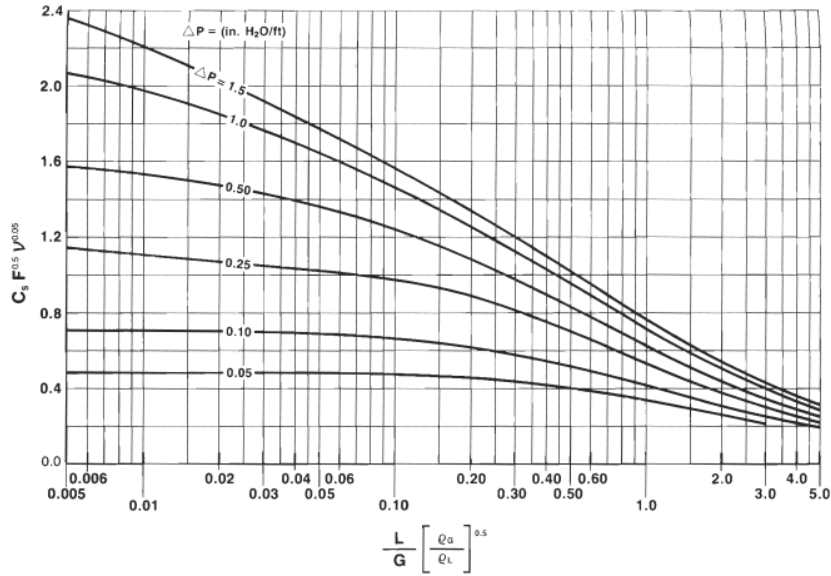


Figure 7.12: Absorption characteristic adapted from [184].

foaming systems [184]. Defining the pressure drop, the mass balances have to be solved and the type of column internals has to be chosen to firstly specify geometric factors. The superficial gas velocities \bar{v}_G are determined by the diagram presented in Figure 7.12. The abscissa, the so-called flow parameter

$$X = \frac{L}{G} \sqrt{\left(\frac{\rho_G}{\rho_L}\right)} \quad (7.9)$$

is the square root of the ratio of liquid kinetic energy to gas kinetic energy [184]. L and G are the liquid and gas mass flow rates and ρ_L and ρ_G are the densities of the liquid and gas phase, respectively. The diagrams ordinate

$$Y = C_s F^{0.5} \nu^{0.05} \quad (7.10)$$

relates the capacity factor C_s , the packing factor F (an empirical factor) and the kinematic viscosity ν (in cp). The resulting superficial gas velocity \bar{v}_G is calculated by obtaining the capacity factor from the diagram and using:

$$C_s = \bar{v}_G \sqrt{\frac{\rho_G}{\rho_L - \rho_G}} \quad (7.11)$$

Consequently the column diameter is determined by:

$$D = \sqrt{\frac{4\dot{V}}{\pi \bar{v}}} \quad (7.12)$$

The column height results from the packing height H_{Pack} where an additional height of 15 % for liquid distributors and the liquid drainage is added. The packing height is determined by the required packing volume and the column's cross sectional area:

$$H = 1.15H_{Pack} = 1.15 \frac{4V_{Pack}}{\pi D^2} \quad (7.13)$$

The mass transfer model determines the packing volume V_{Pack} . According to Strigle [184], the packing volume based on the HTU-NTU concept can be calculated through:

$$V_{Pack} = \max_i \left(\frac{\dot{n}_i}{K_{G,i} a \Delta p_{LM,i}} \right) \quad (7.14)$$

Here, \dot{n}_i is the transferred molar flow rate, $K_{G,i}$ is the mass transfer coefficient, a is the specific wetted area and $\Delta p_{LM,i}$ is the logarithmic mean of the driving pressure difference of component i . Using partial pressures instead of concentrations in Equation 7.7, integrating along the column height and assuming a logarithmic concentration profile along the column results in Equation 7.14. The logarithmic mean (LM) of the driving pressure differences is calculated by:

$$\Delta p_{LM,i} = \frac{\Delta p_{i,bottom} - \Delta p_{i,top}}{\ln \left(\frac{\Delta p_{i,bottom}}{\Delta p_{i,top}} \right)} \quad (7.15)$$

where $\Delta p_{i,bottom}$ and $\Delta p_{i,top}$ are the differences between the component i 's gas phase pressure and its pressure in equilibrium at the bottom and top of the column.

Alternatively to this approach, the column height can directly be calculated by the HTU-NTU-model:

$$H_{Pack} = \underbrace{\frac{4G}{\pi D^2 K_G a p_{system}}}_{HTU} \int_{y_{in}}^{y_{out}} \underbrace{\frac{dy}{y - y^*}}_{NTU} \quad (7.16)$$

G is the molar raw gas flow rate, D the column diameter and p_{system} the system pressure. y_{in} and y_{out} are the mole fractions in the gas phase at the column inlet and outlet, respectively [180]. Assuming a linear relationship for the equilibrium, Kremser's equation applies for estimating the number of transfer units:

$$NTU = \ln \left[\frac{y_{in} - y_{out}^*}{y_{in} - y_{out}^*} \left(1 - \frac{1}{A} \right) + \frac{1}{A} \right] \frac{1}{\ln(A)} \quad (7.17)$$

Here, A is the absorption factor which considers the equilibrium constant $K = \frac{y}{x}$:

$$A = \frac{L}{GK} \quad (7.18)$$

The same set of equations can be derived for gas stripping processes, where the liquid is depleted along the column. Hence, the number of required transfer units is determined by

$$NTU = \ln \left[\frac{x_{out} - x_{in}^*}{x_{in} - x_{in}^*} \left(1 - \frac{1}{S} \right) + \frac{1}{S} \right] \frac{1}{\ln(S)} \quad (7.19)$$

using the stripping factor S which is defined through:

$$S = \frac{GK}{L} = \frac{1}{A} \quad (7.20)$$

7.6.2 Pressurized water scrubbing

In pressurized water scrubbing CO_2 and H_2S are physically absorbed in water while hydrophobic, nonpolar hydrocarbons such as CH_4 do not absorb. The water absorption column is equipped with random dumped packings and operates at pressures of 5 to 12 bar and temperatures of 3 to 30 °C [53]. The elevated pressure and the low temperature allow for an adequate loading capacity of the washing water.

In a desorption column the rich solvent is stripped with air at ambient pressure. To overcome the column pressure drop, the air is pressurized to 150 mbarg before entering the column. In order to recycle and reuse the water in the absorption process, the lean water is cooled and re-pressurized. The short cut model for the pressurized water scrubbing process includes the calculation of the absorber, the stripper, the pump and the cooler dimensions. The costs to drive the stripping gas blower can be neglected as they are low compared to the costs for other equipment.

Absorption column

Equations 7.12 and 7.14 are applied to size the absorption column. The maximum loading of the rich solvent at the bottom outlet of the absorption column was chosen in the way that the equilibrium pressure of CO_2 is 80 % of the partial pressure of CO_2 in the entering gas stream [184]:

$$p_{\text{CO}_2}^* = 0.8 p_{\text{CO}_2}^{\text{gas in}} \quad (7.21)$$

The lean liquid was defined to be loaded as much that the equilibrium pressure of CO_2 is 50 % of the partial pressure of CO_2 in the leaving gas stream [184]:

$$p_{\text{CO}_2}^* = 0.5 p_{\text{CO}_2}^{\text{gas out}} \quad (7.22)$$

The required washing water flow rate is obtained from the overall mass balance. Ceramic Raschig Rings (70 mm) were used in random dump packings due to their high packing factor ($F = 37$) as

well as their resistance against sulfur bearing acids. Assuming a pressure drop of $0.33 \frac{\text{kPa}}{\text{m}}$ results in a superficial gas velocity of $v_G = 0.05 \frac{\text{m}}{\text{sec}}$ (see Figure 7.12). However, this considerably low superficial gas velocity is determined by the high liquid flow rate as a consequence of the low solubility of CO_2 in water. Onda [180] reported on correlations to determine the specific wetted area and the required mass transfer coefficients. Since the mass transfer is controlled by the liquid phase boundary layer resistance [184], only the liquid mass transfer coefficients have to be taken into account:

$$a_w = a_t \left[1 - \exp \left\{ -1.45 \left(\frac{\sigma_C}{\sigma} \right)^{0.75} Re^{0.1} Fr^{-0.05} We^{0.2} \right\} \right] \quad (7.23)$$

$$k_L = 0.0051 \left(\frac{\eta_L g}{\rho_L} \right)^{\frac{1}{3}} \left(\frac{\dot{L}''}{a_w \eta_L} \right)^{\frac{2}{3}} \left(\frac{\eta_L}{\rho_L D_L} \right)^{-\frac{1}{2}} (a_t d_p)^{0.4} \quad (7.24)$$

$$Re = \frac{\dot{L}''}{a_t \eta_L} \quad (7.25)$$

$$Fr = \frac{\dot{L}''^2 a_t}{\rho_L^2 g} \quad (7.26)$$

$$We = \frac{\dot{L}''^2}{\rho_L \sigma a_t} \quad (7.27)$$

Table 7.7 lists process conditions and parameters for the pressurized water scrubbing process. The costs for a vertical column and the column internal contribute to the investment costs of the absorber. Assuming that the vessel is clad with stainless steel and that it operates at pressures of up to 13 bar the material and pressure factor is $MPF = F_m F_p = 2.25 \cdot 1.15 = 2.6$. Hence, the base costs are [110]:

$$BC_{\text{vessel}} = 1\text{k\$} \left(\frac{H}{4\text{ft}} \right)^{0.81} \left(\frac{D}{3\text{ft}} \right)^{1.05} \quad (7.28)$$

The updated bare module costs (UBMC) which are the investment costs result from:

$$\begin{aligned} UBMC &= UF \cdot BC_{\text{vessel}} \cdot (MPF + MF - 1) + V_{\text{Pack}} BC_{\text{Pack}} \\ &= 4.91 \cdot BC \cdot (2.6 + 4.23 - 1) + V_{\text{Pack}} BC_{\text{Pack}} \end{aligned} \quad (7.29)$$

Stripper

The stripper operates at a pressure of 1 bar to facilitate the desorption process. The short cut model is based on the HTU-NTU model. The required stripping gas flow rate is assumed to be 1.5 times

Table 7.7: Model parameters for the absorber of the pressurized water scrubbing model.

| | Parameter | Unit | Value | Reference |
|----------------------------|---------------------------|-----------------------------------|-----------------------|------------|
| Absorption Conditions | pressure | [bar] | 9 | |
| | temperature | [°C] | 25 | |
| Column Internals | random packing | Raschig rings, ceramic, 70mm | | |
| | packing factor F | [-] | 37 | [184] |
| | specific surface area | [m ² /m ³] | 60 | |
| | specific wetted area | [m ² /m ³] | 57.5 | calculated |
| | pressure drop | [kPa/m] | 0.33 | [184] |
| | superficial gas velocity | [m/sec] | 0.05 | calculated |
| | Henry Coefficients | $H(\text{CH}_4)$ | [bar] | 39200 |
| $H(\text{CO}_2)$ | | [bar] | 1635 | [182] |
| $H(\text{H}_2\text{S})$ | | [bar] | 543 | [182] |
| Diffusion Coefficients | $D_L(\text{CH}_4)$ | [m ² /sec] | $1.88 \cdot 10^{-9}$ | [182] |
| | $D_L(\text{CO}_2)$ | [m ² /sec] | $1.91 \cdot 10^{-9}$ | [182] |
| | $D_L(\text{H}_2\text{S})$ | [m ² /sec] | $1.61 \cdot 10^{-9}$ | [182] |
| Mass Transfer Coefficients | $k_L(\text{CH}_4)$ | [mol/(m ² sec bar)] | $1.48 \cdot 10^{-3}$ | calculated |
| | $k_L(\text{CO}_2)$ | [mol/(m ² sec bar)] | $35.88 \cdot 10^{-3}$ | calculated |
| | $k_L(\text{H}_2\text{S})$ | [mol/(m ² sec bar)] | $99.24 \cdot 10^{-3}$ | calculated |
| Cost Calculation | MPF | [-] | 2.6 | [110] |

the minimal stripping gas flow rate which results from the inlet and outlet concentrations and the equilibrium data. The superficial gas velocity, the mass transfer coefficients and the material and pressure factor are assumed to be equal to those of the absorber (see Table 7.7). The costs of the desorption column are determined in the same way as for the absorber.

Pump

The recirculation pump has to pressurize the lean solvent to the operating pressure of the absorption column. The required energy demand P is obtained by:

$$P = \dot{V}_{\text{washing liquid}} \Delta p \frac{1}{\eta_P} \quad (7.30)$$

with $\eta_P = 0.9$ as pump efficiency. The energy demand determines the size of the pump and as a consequence its investment as well as its operational costs. The base costs are obtained through [110]

$$BC = 0.39\text{k\$} \left(\frac{P}{10\text{gpm} \cdot \text{psi}} \right)^{0.17} \quad (7.31)$$

Assuming that the pump material is stainless steel and that it operates at a maximum pressure of 11 bar, a material and pressure factor of $MPF = F_m \cdot F_o = 1.93 \cdot 1.5 = 2.9$ was used. The *UBMC* are given by [110]

$$UBMC = UF \cdot BC \cdot (MPF + MF - 1) = 4.91 \cdot BC \cdot (2.9 + 3.38 - 1) \quad (7.32)$$

Cooler

The cooler's temperature change of $\Delta T = 0.17\text{K}$ was estimated based on data reported by Falß [185]. The transferred heat is:

$$\dot{Q} = \dot{m}_{\text{washing liquid}} c_p \Delta T \quad (7.33)$$

Assuming a heat transfer coefficient of $U = 1277 \frac{\text{W}}{\text{m}^2\text{K}}$ [110] and a logarithmic temperature difference of $\Delta T_{In} = 10\text{K}$ allows for the determination of the heat transfer area:

$$A = \frac{\dot{Q}}{U \Delta T_{In}} \quad (7.34)$$

Hence, the base costs can be estimated [110]:

$$BC = 0.3\text{k\$} \left(\frac{A}{5.5\text{ft}^2} \right)^{0.024} \quad (7.35)$$

Assuming a fixed tube sheet made of stainless steel results in a material and pressure factor of $MPF = 0.8 \cdot 2.5 = 2$ which allows for the calculation of the *UBMC*:

$$UBMC = UF \cdot BC \cdot (MPF + MF - 1) = 4.91 \cdot BC \cdot (2 + 1.83 - 1) \quad (7.36)$$

7.6.3 Amine scrubbing

Amine absorption can remove CO₂ and H₂S simultaneously in a chemical absorption process. The acid gases react reversible with the amines and the gas molecules are bounded stronger compared to physical absorption, which allows for higher gas loadings in the amine process together with higher CO₂/CH₄ selectivities [53]. As a consequence more energy is required to regenerate the rich solvent [53].

Commonly used amines are monoethanolamine (MEA) and diethanolamine (DEA). In both of these solutions, a maximum of $\frac{1}{2}$ mol of acid gas combines with 1 mol amine [184]. While MEA has the advantage of a higher loading capacity and to be less expensive in comparison to DEA, it is more toxic, tends to foam and to be more corrosive than DEA. Due to the higher loading capacity MEA is used in this study. Typically, an amine concentration of 18 wt-% was used which has inlet and outlet loadings of $0.12 \frac{\text{molCO}_2}{\text{molMEA}}$ and $0.43 \frac{\text{molCO}_2}{\text{molMEA}}$, respectively.

For the amine absorption process commonly structured packings are applied and the absorption column operates at ambient pressure. The temperature of the amine solution increases from 35 °C at the inlet to approximately 51 °C at the solvent outlet, due to the exothermal reaction of the acid gases with the amine. At the same time the gas temperature increases from 16 °C to approximately 35 °C [184].

Upstream of the desorption column the loaded solution is preheated to 87-99 °C while a reboiler in the desorption column provides the heat of reaction which is $1907 \frac{\text{kJ}}{\text{kgCO}_2}$ to increase the solutions temperature to 113 to 118 °C [184]. To avoid thermal decomposing, the temperature should not exceed 121 °C.

To recover MEA and H₂O from the vapor leaving the top of the desorber, these vapor components are condensed. The temperature of the lean solvent ($0.12 \frac{\text{molCO}_2}{\text{molMEA}}$) is decreased and the solvent is fed to the absorption column. The economic evaluation includes the cost for the absorber, the desorber with its reboiler and condenser, the heat exchanger and the cooler while the investment costs for the pump can be neglected.

Absorber

The calculations for the absorber include the following aspects:

1. The specified inlet and outlet concentrations of moles acid gas per mole amine and the knowledge of the acid gas stream which has to be removed allow for the determination of the required flow rate of washing liquid.
2. The absorber diameter is calculated with a superficial gas velocity of $3 \frac{\text{m}}{\text{sec}}$ [186].
3. The absorber height is determined through the required packing volume and the absorber diameter. The calculation of the packing volume is based on overall $k_G a$ values reported by

Strigle [184]: The overall $k_G a$ results from a "basic"- $k_G a$ of a test system which is corrected with respect to the absorbent, the absorbate, the absorbate flux L , the absorbent concentration, the temperature and the pressure. This can be written in the form:

$$k_G a = k_G a|_{\text{base system}} C_{\text{absorbate}} C_{\text{absorbent}} C_L C_{\text{concentration}} C_{\text{temperature}} C_{\text{pressure}}. \quad (7.37)$$

For MEA absorption, the following relations are applied for the correction factors [184]:

- $k_G a|_{\text{base system}}$: For an Intalox[®] Structured Packing 3T $k_G a|_{\text{NaOH}}^{\text{CO}_2} = 2.76 \frac{\text{lb-mol}}{\text{h}\cdot\text{ft}^3\cdot\text{atm}}$ holds.
- $C_{\text{absorbate}}$: $k_G a|_{\text{MEA}}^{\text{CO}_2} = 2k_G a|_{\text{NaOH}}^{\text{CO}_2}$
- $C_{\text{absorbent}}$: $k_G a|_{\text{MEA}}^{\text{H}_2\text{S}} = 2.5k_G a|_{\text{MEA}}^{\text{CO}_2}$
- $C_L = \left(\frac{L}{10 \frac{\text{gpm}}{\text{ft}^2}} \right)^{0.3}$
- $C_{\text{concentration}} = 1.375 - 2.5 \cdot C \left[\frac{\text{mol acid gas}}{\text{mol MEA}} \right]$
- $C_{\text{temperature}}^{\text{CO}_2} = \exp\{0.013(T - 75^\circ\text{F})\}$
- $C_{\text{temperature}}^{\text{H}_2\text{S}} = \exp\{0.013(T - 75^\circ\text{F})\}$

Assuming a washing liquid flux of $27 \frac{\text{gpm}}{\text{ft}^2}$, inlet and outlet loadings of $0.12 \frac{\text{mol CO}_2}{\text{mol MEA}}$ and $0.43 \frac{\text{mol CO}_2}{\text{mol MEA}}$, top and bottom temperatures of $T_{\text{top}} = 35^\circ\text{C}$ and $T_{\text{bottom}} = 51^\circ\text{C}$ and a pressure of $p = 1 \text{ bar}$ leads to the $k_G a$ values presented in Table 7.8.

4. The UBMC were calculated for an absorber vessel clad with stainless steel ($MPF = F_m F_p = 2.25 \cdot 1 = 2.25$). Hence, the following cost equations were applied:

$$BC_{\text{vessel}} = 1\text{k\$} \left(\frac{H}{4\text{ft}} \right)^{0.81} \left(\frac{D}{3\text{ft}} \right)^{1.05} \quad (7.38)$$

$$\begin{aligned} UBMC &= UF \cdot BC_{\text{vessel}} \cdot (MPF + MF - 1) + V_{\text{Pack}} BC_{\text{Pack}} \\ &= 4.91 \cdot BC_{\text{vessel}} \cdot (2.25 + 4.23 - 1) + V_{\text{Pack}} BC_{\text{Pack}} \end{aligned} \quad (7.39)$$

Table 7.8 summarizes the parameters for the amine absorber model.

Desorber

The desorber was designed on basis of the following assumptions:

1. The desorber diameter is determined through a washing liquid flux of $73 \frac{\text{m}^3}{\text{h}\cdot\text{m}^2}$ [184].
2. Due to lack of data, the desorber height was assumed to be the same as the absorber height.
3. The desorber costs are calculated analogously to the absorber costs.

Table 7.8: Model parameters for the absorber of the amine scrubbing model.

| | Parameter | Unit | Value | Reference |
|-----------------------|---------------------------|-------------------------------|------------|------------|
| Absorption Conditions | pressure | [bar] | 1 | [184] |
| | mean temperature | [°C] | 25 | assumed |
| Column Internals | structured packing | | Intalox 3T | |
| | superficial gas velocity | [m/sec] | 3 | [186] |
| Mass Transfer | $k_L(\text{CO}_2)$ | [kmol/(m ³ h atm)] | 143 | calculated |
| Coefficients | $k_L(\text{H}_2\text{S})$ | [kmol/(m ³ h atm)] | 185 | calculated |
| Cost Calculation | MPF | [-] | 2.25 | [110] |

Reboiler

The reboiler supplies the energy for the reverse reaction of acid gases and MEA. For CO₂, this energy amounts to $1907 \frac{\text{kJ}}{\text{kg}_{\text{CO}_2}}$ [184] which results in a reboiler duty \dot{Q}_{Reb} of:

$$\dot{Q}_{Reb} = \dot{m}_{\text{CO}_2} \cdot 1907 \frac{\text{kJ}}{\text{kg}_{\text{CO}_2}} \quad (7.40)$$

The reboiler temperature of 117 °C is provided by steam with a temperature of 140 °C. Using a heat transfer coefficient of $U = 1420 \frac{\text{W}}{\text{m}^2\text{K}}$ [110] and a logarithmic temperature difference of $\Delta T_{In} = 23 \text{ K}$ the required heat transfer area is:

$$A = \frac{\dot{Q}_{Reb}}{U \Delta T_{In}} \quad (7.41)$$

Hence, the base costs are [110]:

$$BC = 5 \text{ k\$} \left(\frac{A}{400 \text{ ft}^2} \right)^{0.65} \quad (7.42)$$

Assuming a fixed tube sheet constructed of stainless steel with a material and pressure factor of $MPF = 0.8 \cdot 2.5 = 2$ results in UBMC of:

$$UBMC = UF \cdot BC \cdot (MPF + MF - 1) = 4.91 \cdot BC \cdot (2 + 1.83 - 1) \quad (7.43)$$

Condenser

The condenser recovers water vapor and MEA by separating these components from the overhead vapor. Assuming a composition of $y_{top}^{CO_2} = 30$ mol-% and $y_{top}^{water/MEA} = 70$ mol-% [184], a superficial gas velocity of $v_G = 1 \frac{m}{sec}$ [186], a water/MEA vapor density of $\rho = 0.59 \frac{kg}{m^3}$ and an enthalpy of evaporation of $\Delta h_V = 2257 \frac{kJ}{kg}$ [187] enables to calculate the condenser duty:

$$\dot{Q}_{Cond} = \frac{\pi D_{desorber}^2}{4} v_G y_{top}^{water/MEA} \rho \Delta h_V \quad (7.44)$$

The heat transfer coefficient is $U = 4000 \frac{W}{m^2K}$ [110] and the cooling water temperature increase $10^\circ C$ (from $15^\circ C$ to $25^\circ C$). The heat transfer area and the investment costs can be calculated:

$$A = \frac{\dot{Q}_{Reb}}{U \Delta T_{In}} \quad (7.45)$$

$$BC = 0.3 \text{ k\$} \left(\frac{A}{5.5 \text{ ft}^2} \right)^{0.024} \quad (7.46)$$

$$UBMC = UF \cdot BC \cdot (MPF + MF - 1) = 4.91 \cdot BC \cdot (2 + 1.83 - 1) \quad (7.47)$$

Heat exchanger

The heat exchanger recovers energy from the lean solvent and as a consequence this energy can be saved in the reboiler and the cooler. Determination of the investment costs include:

1. The exchanged heat was determined through:

$$\dot{Q} = c_p \dot{m} \Delta T \quad (7.48)$$

2. With a heat transfer coefficient of $U = 1136 \frac{W}{m^2K}$ [110] and a logarithmic temperature difference of $\Delta T_{In} = 14$ K the heat transfer area is:

$$A = \frac{\dot{Q}}{U \Delta T_{In}} \quad (7.49)$$

3. The costs are calculated analogously to the reboiler:

$$BC = 5 \text{ k\$} \left(\frac{A}{400 \text{ ft}^2} \right)^{0.65} \quad (7.50)$$

$$\begin{aligned} UBMC &= UF \cdot BC \cdot (MPF + MF - 1) \\ &= 4.91 \cdot BC \cdot (2 + 1.83 - 1) \end{aligned} \quad (7.51)$$

Cooler

The cooler is calculated analogously to the heat exchanger. The inlet and outlet temperatures of 65 °C and 35 °C result in a transferred heat of 552 kW. The logarithmic temperature difference is assumed to be 27 K.

7.6.4 Glycol scrubbing

The use of triethyleneglycol (TEG) is an established technology to dehydrate natural gases. The raw gas is dehydrated in a counter current absorption column at ambient temperature and a pressure of 20 to 40 bar [184]. The column is filled with structured metal packings (HTU=1.3 to 2 m, liquid recirculation rate: $3 \frac{\text{t}_{\text{TEG}}}{\text{m}^2\text{h}}$) or bubble-cap trays (tray efficiency: 25 %, bubbling area: 1.7 m^2 per $\frac{\text{m}^3(\text{STP})}{\text{h}}$ entering gas) [184]. The triethyleneglycol flow rate is in the range of 25 to 50 $\frac{\text{t}_{\text{TEG}}}{\text{kg}_{\text{H}_2\text{O}}}$ which was reported by [188] and [184].

The rich solvent stream first enters a flash vessel operating at ambient pressure and the solvent degasses. After being preheated, the solvent enters the regeneration column at a temperature of 150 °C. The water is desorbed at a temperature of 200 °C [189]. A condenser is installed at the head of the column to recover TEG. The lean solvent is cooled down and recycled to the absorber. The short cut model includes the calculation of the absorber, the desorber with its reboiler, the heat exchanger and the cooler. The pump and the condenser can be neglected with respect to the investment costs.

Absorber

The absorber is equipped with a structured packing. Its diameter was calculated using a solvent flux of $3 \frac{\text{t}_{\text{TEG}}}{\text{m}^2\text{h}}$. The inlet and outlet loadings of the washing liquids are assumed to be $0.11 \frac{\text{kmol}_{\text{H}_2\text{O}}}{\text{kmol}_{\text{TEG}}}$ and $0.3 \frac{\text{kmol}_{\text{H}_2\text{O}}}{\text{kmol}_{\text{TEG}}}$, respectively. This correlates to a TEG flux of $33 \frac{\text{t}_{\text{TEG}}}{\text{kg}_{\text{H}_2\text{O}}}$. The absorber height is calculated by the number of transfer units according to equation 7.17 and a HTU of 2 m. Table 7.9 lists the absorber parameters.

The UBMC were calculated for an absorber vessel clad with stainless steel ($MPF = F_m F_p = 2.25 \cdot 1.45 = 3.26$) which results in:

$$BC_{\text{vessel}} = 1\text{k\$} \left(\frac{H}{4\text{ft}} \right)^{0.81} \left(\frac{D}{3\text{ft}} \right)^{1.05} \quad (7.52)$$

$$\begin{aligned} UBMC &= UF \cdot BC_{\text{vessel}} \cdot (MPF + MF - 1) + V_{\text{Pack}} BC_{\text{Pack}} \\ &= 4.91 \cdot BC_{\text{vessel}} \cdot (3.26 + 4.23 - 1) + V_{\text{Pack}} BC_{\text{Pack}} \end{aligned} \quad (7.53)$$

Table 7.9: Model parameters for the absorber of the glycol scrubbing model.

| | Parameter | Unit | Value | Reference |
|-----------------------|-------------------------|---|-------|-----------|
| Absorption Conditions | pressure | [bar] | 30 | [184] |
| | mean temperature | [°C] | 65 | assumed |
| | loading lean solvent | [kmol _{H₂O} / kmol _{TEG}] | 0.11 | assumed |
| | loading rich solvent | [kmol _{H₂O} / kmol _{TEG}] | 0.3 | assumed |
| Column Internals | structured packing | | | |
| | HTU | [m] | 2 | [184] |
| Henry Coefficients | $H(\text{CH}_4)$ | [bar] | 1845 | [190] |
| | $H(\text{CO}_2)$ | [bar] | 122 | [190] |
| | $H(\text{H}_2\text{S})$ | [bar] | 15 | [190] |
| | $H(\text{H}_2\text{O})$ | [bar] | 0.052 | [188] |
| Cost Calculation | MPF | [-] | 3.26 | [110] |

Desorber

As in amine scrubbing, the desorber was designed based on the following assumptions:

1. The desorber diameter is determined through a liquid flux of $1.4 \frac{\text{m}^3}{\text{h m}^2}$.
2. The desorber height was assumed to be 2.4 m. Equilibrium data show that the required purity can be obtained in a single stage.
3. The desorber costs are calculated analogously to the absorber costs but a material and pressure factor of only $MPF = F_m F_p = 2.25 \cdot 1 = 2.25$ is used due to the low pressure in the desorber.

Reboiler

The reboiler provides the energy for heating the mixture from 150 °C to 204 °C and for evaporating the absorbed water:

$$\dot{Q}_{Reb} = \dot{m}_{TEG} c_p^{TEG} \Delta T + \dot{m}_{H_2O} \Delta H_V^{H_2O}$$

The steam temperature is 230 °C and as a consequence a logarithmic temperature difference of $\Delta T_{In} = 37$ K is obtained. The required heat transfer area is

$$A = \frac{\dot{Q}_{Reb}}{U\Delta T_{In}} \quad (7.54)$$

for a heat transfer coefficient of $U = 2200 \frac{W}{m^2K}$ [110]. Hence, the base costs are [110]:

$$BC = 0.3 \text{ k\$} \left(\frac{A}{5.5 \text{ ft}^2} \right)^{0.024} \quad (7.55)$$

Assuming a fixed tube sheet made of stainless steel leads to a material and pressure factor of $MPF = 0.8 \cdot 2.5 = 2$ which is used for calculating the UBMC:

$$UBMC = UF \cdot BC \cdot (MPF + MF - 1) = 4.91 \cdot BC \cdot (2 + 1.83 - 1) \quad (7.56)$$

Heat exchanger

The heat exchanger serves the saving of energy for the reboiler and the cooler and the investment costs are determined by the following steps:

1. The exchanged heat is:

$$\dot{Q} = c_p^{TEG} \dot{m}_{TEG} \Delta T \quad (7.57)$$

2. With an assumed heat transfer coefficient of $U = 1136 \frac{W}{m^2K}$ [110] and a logarithmic temperature difference of $\Delta T_{In} = 54$ K the heat transfer area is:

$$A = \frac{\dot{Q}}{U\Delta T_{In}} \quad (7.58)$$

3. The cost are calculated analogously to the reboiler:

$$BC = 0.3 \text{ k\$} \left(\frac{A}{5.5 \text{ ft}^2} \right)^{0.024} \quad (7.59)$$

$$\begin{aligned} UBMC &= UF \cdot BC \cdot (MPF + MF - 1) \\ &= 4.91 \cdot BC \cdot (2 + 1.83 - 1) \end{aligned} \quad (7.60)$$

Cooler

The cooler is again calculated analogously to the heat exchanger. The inlet and outlet temperatures of 119 °C and 65 °C result in a transferred heat of 28 kW with a logarithmic temperature difference of 54 K.

7.6.5 Membrane process

CO₂, H₂O and H₂S permeate through the membrane much faster than CH₄ leading to a separation of those components. Assuming ideal gas behavior, the driving force in gas permeation processes is the partial pressure difference of the components between retentate and permeate side. The solution diffusion model is applied to predict mass transfer through the membrane.

$$\dot{n}_j'' = P_j(p_{Fj,F} - p_{Pj,P}) \quad (7.61)$$

A three stage gas permeation process, identified to be optimal in Chapter 4, is used here. In the short cut model, a logarithmic mean concentration on the feed side of the membrane stages and a free flow of the permeate is determined. The UBMC are calculated dependent on the membrane area A_{mem} :

$$UBMC = A_{mem}BC_{mem} \quad (7.62)$$

BC_{mem} are the specific membrane costs. Table 7.10 lists the most important parameters applied in the gas permeation model.

Table 7.10: Model parameters for the membrane model.

| | Parameter | Unit | Value | Reference |
|------------------|---------------------------|------------------------|-------|-----------|
| Pressure Levels | inlet pressure | [bar] | 16 | - |
| | outlet pressure retentate | [bar] | 16 | - |
| | outlet pressure permeate | [bar] | 1 | - |
| Permeances | $P(\text{CH}_4)$ | [GPU] | 1 | - |
| | $P(\text{CO}_2)$ | [GPU] | 60 | - |
| | $P(\text{H}_2\text{S})$ | [GPU] | 60 | - |
| | $P(\text{H}_2\text{O})$ | [GPU] | 300 | - |
| Cost Calculation | BC | [Euro/m ²] | 55 | - |
| | membrane lifetime | years | 4 | - |

7.6.6 Adsorption processes

A short cut method following Bathen [191] is applied to size the adsorption equipment. This method works with a rough estimation of the adsorbent's loading and the superficial gas velocity. The calculation consists of the following steps:

1. The adsorbent's loading X is estimated from isotherm data.
2. A superficial gas velocity $v_{G,Ads}$ is specified. Typical velocities are in the range of 0.1 to $0.5 \frac{m}{sec}$.

3. The cross sectional area A can be calculated through

$$A = \frac{\dot{V}}{v_{G,Ads}} \quad (7.63)$$

with \dot{V} as the volume flow rate of the entering gas stream.

4. The adsorption time t_{ads} has to be specified. For continuous operation, multiple adsorbers are installed in parallel.
5. The required adsorbent mass M_{ads} is calculated through:

$$M_{adsorbent} = \frac{\dot{m}_{adsorbate} t_{ads}}{X} \quad (7.64)$$

Here, $\dot{m}_{adsorbate}$ is the mass flux of adsorbate which has to be adsorbed.

6. The adsorber height H results from

$$H = \frac{M_{adsorbent}}{A \rho_{app}}, \quad (7.65)$$

with ρ_{app} as apparent density of the adsorbent.

For adsorption processes in which the bed can be regenerated, hot gas is applied to the packed bed to desorb the gas molecules from the solid surface. In order to determine the amount of hot inert gas for regeneration as well as the regeneration period, Bathen [191] proposes the following method:

1. Define the desorption temperature T_{Des} . Typical temperatures are in the range of 120 to 200 °C.
2. Estimate the energy demand E for the desorption. Here, the desorption energy and the heating of the packed bed are considered:

$$E_{Des} = M_{adsorbent} [X \Delta h_{Ads} + c_{p,ads} (T_{Des} - T_0)] \quad (7.66)$$

$c_{p,ads}$ is the specific heat capacity of the adsorbent, T_0 is the temperature at which the adsorption takes place and Δh_{ads} is the specific adsorption enthalpy. If no data for the adsorption enthalpy is available, it can be estimated with the help of the specific enthalpy of evaporation of the adsorbate, Δh_V :

$$\Delta h_{Ads} \approx 1.5 \Delta h_V. \quad (7.67)$$

3. Calculate the required mass of hot gas purge M_{inert} :

$$M_{inert} = \frac{E_{Des}}{c_{p,inert}(T_{Des} - (T_0 + 10K))} \quad (7.68)$$

with $c_{p,inert}$ as specific heat capacity of the hot gas. Here, a minimum temperature difference of 10K was considered.

4. Specify a superficial gas velocity $v_{G,Des}$ which is typically in the range of 0.3 to 1 $\frac{m}{sec}$.
5. Determine the desorption time t_{Des} through

$$t_{Des} = \frac{M_{inert}}{\rho_{inert} v_{G,Des} A} \quad (7.69)$$

with ρ_{inert} as the density of the hot gas.

6. Calculate the time required for cooling the adsorber to its operating temperature, t_{cool} which is done with a cold inert gas.

Continuous operation is realized by using multiple adsorption vessels in parallel. The number N_{Abs} of absorber vessels is:

$$N_{Abs} = \frac{t_{Des} + t_{cool}}{t_{Ads}} + 1 \quad (7.70)$$

Bathen [191], Goedecke [180] and Perry [182] provide detailed analyses of adsorption processes.

7.6.7 Drying with silica gel

Silica gel (SiO_2) is widely applied to dry humid gases. However, it is important to note that not only H_2O is adsorbed but also H_2S . Here, silica pellets with a diameter of 2 to 8 mm [191] in a packed bed are applied. Two adsorbers are installed in parallel to facilitate continuous operation. The adsorption operates at a pressure of 8 bar and ambient temperature [53]. A maximum load of $X = 0.35 \frac{kg_{adsorbate}}{kg_{SiO_2}}$ was chosen. The superficial gas velocity $v_{G,Ads}$ was estimated through the F-Factor:

$$F_{Ads} = v_{G,Ads} \sqrt{\rho_G} \approx 0.2 \dots 0.4 \sqrt{Pa} \quad (7.71)$$

The desorption operates at a pressure of 1 bar and a purge gas temperature of 150 °C. The specific adsorption enthalpy was estimated through the specific enthalpy of evaporation (see Equation 7.67) and air is used as purge gas.

The investment costs for the two vessels are estimated with Guthrie's method [110]:

$$BC_{Vessels} = 2 \cdot 1 \text{ k\$} \left(\frac{H}{4 \text{ ft}} \right)^{0.81} \left(\frac{D}{3 \text{ ft}} \right)^{1.05} \quad (7.72)$$

The vessels are clad with stainless steel and have to withstand pressures of up to 13 bar. Hence, the material and pressure factor is $MPF = F_m F_p = 2.25 \cdot 1.15 = 2.6$. The UBMC result from the costs for the vessels and the packed bed:

$$\begin{aligned} UBMC &= UF \cdot BC_{Vessels} \cdot (MPF + MF - 1) + M_{Packing} \cdot BC_{Packing} \\ &= 4.91 \cdot BC \cdot (2.6 + 4.23 - 1) + M_{Packing} \cdot 2 \frac{\text{Euro}}{\text{kg}} \end{aligned} \quad (7.73)$$

Table 7.11 lists the parameters for both adsorption and desorption.

Table 7.11: Model parameters for the silica adsorption.

| | Parameter | Unit | Value | Reference |
|-----------------------|------------------------|--|-------|-----------|
| Adsorption Conditions | pressure | [bar] | 8 | [53] |
| | temperature | [°C] | 25 | [53] |
| | F-Factor | [-] | 0.3 | [191] |
| | X_{max} | [kg _{adsorbat} /kg _{SiO₂}] | 0.35 | |
| Desorption Conditions | pressure | [bar] | 1 | [53] |
| | temperature | [°C] | 150 | [191] |
| | $v_{G,Des}$ | [m/sec] | 1 | [191] |
| | $\Delta h_{Ads,H_2S}$ | [kJ/kg] | 637 | estimated |
| | $\Delta h_{Ads,H_2O}$ | [kJ/kg] | 3668 | estimated |
| Packing | packed bed | pellets | | [53] |
| | apparent density | [kg/m ³] | 425 | [191] |
| | specific heat capacity | [kJ/(kg K)] | 0.96 | [191] |
| Cost Calculation | pellet price | [Euro/kg] | 2 | [191] |
| | MPF | [-] | 2.6 | [110] |

7.6.8 Desulfurization with iron chelates

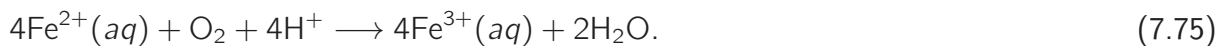
Rough desulfurization can be accomplished with iron chelates. Aqueous solution of Fe³⁺-ions in a bubble column reactor react with H₂S:



Table 7.12: Model parameters for the adsorption on activated carbon.

| | Parameter | Unit | Value | Reference |
|-----------------------|-----------------------------|--|-------|-----------|
| Adsorption Conditions | pressure | [bar] | 16 | |
| | temperature | [°C] | 25 | [193] |
| | F-Factor | [-] | 0.3 | [191] |
| | X_{max} | [kg _{H₂S} /kg _{Adsorbent}] | 0.25 | |
| Packing | packed bed | pellets | | [191] |
| | apparent density | [kg/m ³] | 400 | [191] |
| Cost Calculation | pellet costs $BC_{Packing}$ | [Euro/kg] | 2.5 | [191] |
| | MPF | [-] | 2.6 | [110] |
| | t_{ads} | [hours] | 24 | |

The generated elemental sulfur is separated through decantation or sedimentation. The Fe²⁺ is regenerated by oxidation in a subsequent reactor [192]:



The desulfurization with iron chelates is also known commercially as LO-CAT process. Sulfur depletion rates of more than 99.9 % are obtained for gases containing 0.1-3 mol-% H₂S [192]. Due to limited data reported on this particular process, a short cut model which takes the feed flow rate into account determines investment and operational costs:

$$UBMC = \frac{160 \text{ k\$}}{500 \frac{\text{m}^3}{\text{h}}} \cdot \dot{V}^{feed} \quad (7.76)$$

$$AOC = \frac{24 \text{ k\$}}{500 \frac{\text{m}^3}{\text{h}}} \cdot \dot{V}^{feed} \quad (7.77)$$

The investment reference costs were taken from [193] whereas the reference costs for the AOC were adjusted since the amount of H₂S to be removed in the reference plant is only a third of the amount to be removed in the process considered here. Hence, a factor of three is taken into account. Details about the removal of H₂S with chelated iron are reported in [192], [193] and [185].

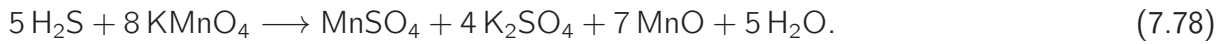
7.6.9 Desulfurization with activated carbon

H₂S can be removed through an adsorption on activated carbon which is additionally impregnated with KMnO₄. This adsorption is based on an irreversible chemical reaction of H₂S with the impreg-

Table 7.13: Model parameters for the compressor model.

| | Parameter | Unit | Value | Reference |
|------------|-----------------------------|--------------------|----------|-----------|
| Compressor | pressure | [bar] | 0.8-16 | |
| | κ | [-] | 1.3 | [187] |
| | η_{isent} | [-] | 0.72 | [111] |
| | MPF | [-] | 1 | [110] |
| | MF | [-] | 5.11 | [150] |
| Cooler | $C_p^{cooling\ water}$ | $[\frac{kJ}{kgK}]$ | 4.18 | [187] |
| | $\Delta T_{cooling\ water}$ | [°C] | 25-15=10 | |
| | MPF | [-] | 1 | [110] |
| | MF | [-] | 5.11 | [150] |

nating compound [193]:



This reaction runs at temperatures of 20 to 100 °C [193]. The achievable purity is $5 \frac{\text{mg}}{\text{m}^3}$ [193] and the maximum loading is assumed to be in the range of $0.25 \frac{\text{kg}_{\text{H}_2\text{S}}}{\text{kg}_{\text{Adsorbent}}}$. As no regeneration is possible, the expensive adsorbent has to be exchanged regularly. Hence, this process is worthwhile only for fine desulfurization. The *UBMC* are calculated analogously to the adsorption on silica gel. Again, two adsorbers have to be installed in parallel to enable a continuous operation. The annual operating costs are estimated through the costs evolving from the exchange of the adsorbent:

$$AOC = M_{\text{Adsorbent}} BC_{\text{Carbon}} \frac{t_a}{t_{\text{ads}}}. \quad (7.79)$$

Table 7.12 summarizes the used parameters for the adsorption on activated carbon.

7.6.10 Compressor

The compressor is calculated as a single stage compressor with after-cooling using a separate heat exchanger. The compressor power P_{Comp} is:

$$P_{\text{Comp}} = \dot{m} c_p (T_{\text{out}} - T_{\text{in}}) \quad (7.80)$$

The outlet temperature T_{out} is determined by the isentropic outlet temperature $T_{\text{out,isent}}$ and the isentropic efficiency η_{isent} ($= 0.72$):

$$T_{\text{out}} = T_{\text{in}} + \frac{(T_{\text{out,isent}} - T_{\text{in}})}{\eta_{\text{isent}}} \quad (7.81)$$

The isentropic outlet temperature is calculated by

$$T_{out,isent} = T_{in} \left(\frac{p_{out}}{p_{in}} \right)^{\frac{\kappa-1}{\kappa}} \quad (7.82)$$

where the isentropic coefficient κ is 1.3. The compressor base costs are determined through [110]:

$$BC = 23 \text{ k\$} \left(\frac{P_{Comp}}{745.7 \text{ W}} \right)^{0.77} \quad (7.83)$$

With a material and pressure factor of $MPF = 1.00$ for a centrifugal compressor [110], a module factor of $MF = 5.11$ [150] and an update factor of $UF = 4.91$ the UBMC are calculated through:

$$UBMC = UF \cdot BC \cdot (MPF + MF - 1) \quad (7.84)$$

The heat exchanger costs are calculated for heat exchangers made of stainless steel with fixed tube sheets and a maximum pressure of $p = 21$ bar. This results in a material and pressure factor of $MPF = F_m(F_p + F_d) = 1.54 \cdot (0.1 + 0.8) = 1.4$. The required shell and tube area is determined for cooling with water and a temperature increase from 15°C to 25°C . Table 7.13 lists the parameters used for the compressor short cut model.

Chapter 8

Conclusion and outlook

8.1 Summary biogas upgrading

In this thesis membrane based biogas upgrading processes are analyzed and optimized. In Germany, most biogas plants operate on-farm in the agricultural production. Hence, the raw gas flow rates are low compared to large scale gas separations in natural gas treatment for example. Commercial polymeric gas permeation membranes are applied for separating CO₂ and CH₄.

In order to develop and optimize a gas permeation process a rigorous gas permeation model was implemented in Aspen Custom Modeler. This model is able to calculate multicomponent mixtures in counter current flow. Non-ideal effect such as concentration polarization, pressure losses, temperature changes and real gas behavior are taken into account. The permeance of glassy polymers can remarkably be affected by high partial pressures of CO₂. Phenomena such as competitive sorption and plasticization can have a tremendous effect on the separation performance on gas permeation modules. The ACM model was exported to Aspen Plus and Aspen Plus Dynamics to perform steady state as well as dynamic process simulations.

For structural process optimization a short cut model was implemented in GAMS. A three stage gas permeation process, using only a single compressor and commercial membranes, is the most profitable process configuration for biogas upgrading. This particular process design provides the upgraded biogas at the natural gas grid pressure. Hence, the driving force for upgrading and the required pressure for grid injection are provided at the same time. In addition, the membrane material is optimized taking Robeson's upper bound correlation into account. Two different cases were investigated. First, a single material is determined for all stages. An optimal CO₂/CH₄ selectivity of 123 with a CO₂ permeance of 555 GPU is the most profitable material property. Second, the optimal material properties are determined for each gas permeation stage individually. Here, a two stage process with a high selective membrane in the first stage ($\alpha_{CO_2/CH_4}=147$; CO₂ = 349 GPU) is combined with a highly permeable stage ($\alpha_{CO_2/CH_4}=98$; CO₂ = 1024 GPU). Since the CH₄ recovery is already high for the process using commercial membranes the impact of optimal membrane materials on the profit is low. Membranes with CO₂/CH₄ selectivities of more than 100 are available, which are for example polypyrrole 6FDA/PMDA (25/75)-TAB and PVSH doped polyaniline [148]. However, Baker reported that only nine polymer materials are commercially applied in gas permeation [9]. Hence, a number of criteria have to be met by a commercial membrane material: (i) it has to be inexpensive, (ii) it has to be manufactured in large quantities and (iii) it has to be thermally and chemically stable. The effect of pressure dependent permeance should only influence the separation performance of the first membrane stage due to high CO₂ partial pressures. In the second stage the CO₂ feed mole fraction is low while in the third stage only low pressure are applied. Thus, the separation performance of these stage can be considered as ideal.

A flowsheet of the three stage gas permeation process was set up in Aspen Plus Dynamics to investigate the dynamic behavior of the upgrading process. Variations in the feed conditions were analyzed and two process control schemes are proposed to efficiently maintain the product gas purity even if

strong changes in the feed gas conditions are enforced. Both control schemes are able to overcome the impact of changed feed conditions within less than 30 seconds and both do not require additional process equipment such as compressors or vacuum pumps.

Membrane hybrid processes often demonstrate a superior behavior compared to the individual gas separation processes. Here, we investigated membrane hybrid processes in which the gas permeation membrane is used for bulk separation and the conventional equipment performs the final purification. In a second configuration the conventional gas separation equipment is used to recover CH_4 from the membrane stage permeate. Pressurized water scrubbing, amine absorption, cryogenic separation and the combination of a membrane and a combined heat and power engine were analyzed. In general, the individual, conventional processes would benefit from a combination with membrane technology since the specific upgrading costs are reduced. For the cryogenic separation the use of a membrane is mandatory since its application reduces the upgrading costs drastically so that this technology becomes competitive to other separation techniques in biogas upgrading.

The three stage gas permeation process was included into an entire process optimization in which the removal of CO_2 together with desulfurization and gas drying was investigated. Various unit operations for each separation step have been implemented. For a base case scenario the three stage gas permeation process combined with an activated carbon adsorber for desulfurization and a silica adsorption for gas drying is the most profitable process configuration. By increasing the electricity costs, the costs for the membrane or by reducing CO_2/CH_4 membrane selectivity, the gas permeation process is replaced by an amine absorption process. For this particular process a rough desulfurization is required prior to the amine absorption. A fine desulfurization using activated carbon and a gas drying with silica have to be installed downstream of the amine absorption. However, for a wide range of parameter the three stage membrane process seems to be the best process configuration.

Ultimately, membrane based gas permeation using a process configuration in which high CH_4 recoveries are achieved can compete and even outperform existing biogas upgrading techniques. However, the profitability of the upgrading process strongly depends on the process conditions and the costs for utilities.

8.2 Summary process design

Within the frame of this work, various process and optimization models have been developed and implemented. For process simulation the AspenTech platform was used, in particular, Aspen Custom Modeler, Aspen Plus and Aspen Dynamics have been applied. Process optimization has been done with the General Algebraic Modeling System (GAMS) in combination with the BARON solver.

The rigorous model of a hollow fiber gas permeation module presented in Chapter 3 includes various non-ideal effects which influence the operation of such a gas permeation module. The model equa-

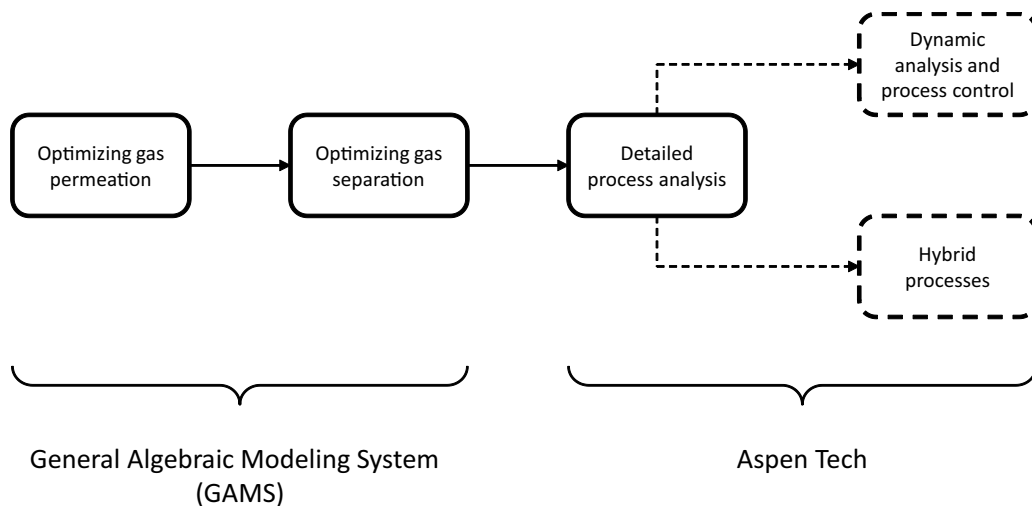


Figure 8.1: Simulation and optimization tools developed within the frame of this work.

tions have been implemented independently of the applied gas mixture so that this model can easily be applied to any other gas mixture. The model has been applied to simulate various other gas permeation processes including: argon recovery from process synthesis gas, olefin-paraffin separation, enthalpy recovery for air conditioning, dehydration of supercritical CO_2 , and siloxane removal from process exhaust gases.

Two optimization models have been implemented into GAMS, one which is dedicated to optimize gas permeation processes and the second which was implemented to optimize gas separation processes. The model for optimization of gas permeation processes can be used to optimize any gas permeation process. Since models for all driving force generation methods have been accounted for a broad range of different processes can be investigated and the optimization is not limited to the separation of CH_4 and CO_2 . However, material properties such as permeances or selectivities have to be specified in case that the Robeson Plot is not used in the optimization.

The model for optimizing gas separation processes in general, includes chemical and physical absorption, adsorption and gas permeation processes to remove H_2S , CO_2 and H_2O from CH_4 . However, the general formulation of all model equations allows for applying the optimization model to other gas separation than biogas upgrading. It has to be noted that numerous parameters for the various processes have to be provided and that the variable bounds have to be adapted.

The simulation and optimization models developed here, provide a framework for systematic design and evaluation of gas permeation processes (see Figure 8.1). Both short cut optimization models allow for a quick but reliable identification of the most promising process layout including process parameters. The rigorous model (Aspen) facilitates a detailed analysis of the optimal process layout. Even dynamic simulations can be performed for gas separations with fluctuating feed conditions or product gas requirements. Furthermore, complex process configurations where gas permeation stages are combined with conventional process equipment can be analyzed.

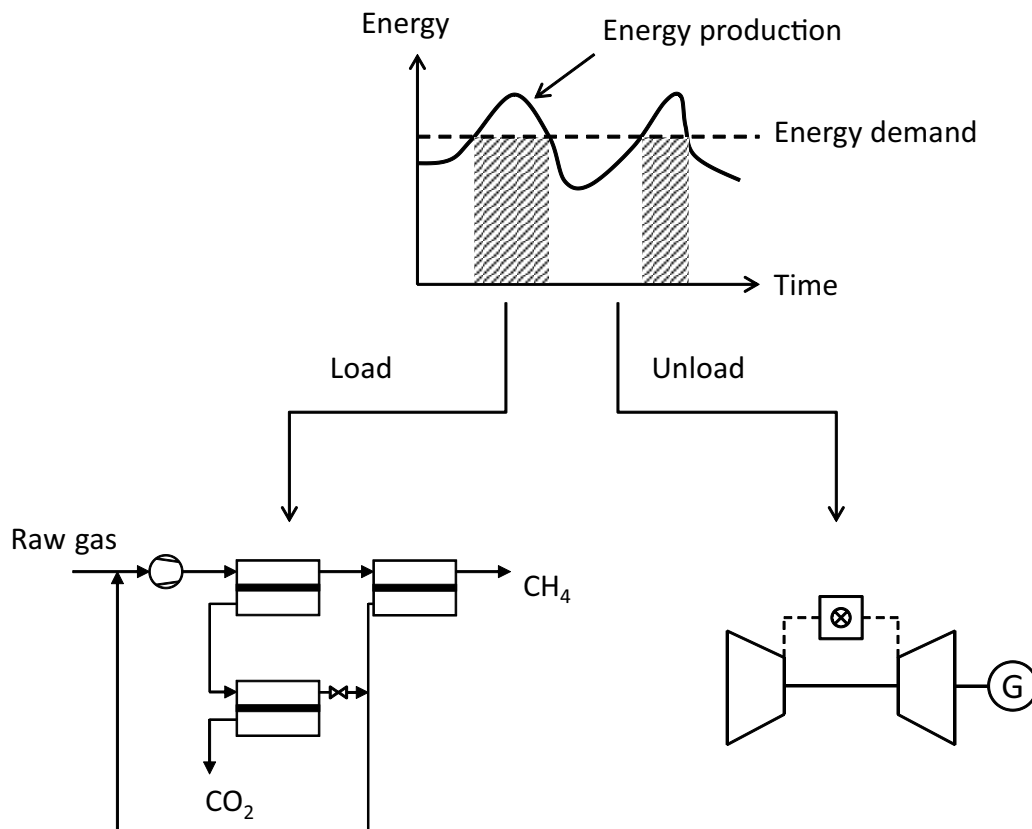


Figure 8.2: Illustration of the three stage gas permeation process which can be used to provide negative electrical control energy when a surplus of solar and wind power is produced. When the electrical base demand cannot be covered by solar and wind power, the prior injected biogas provides the electrical energy by driving gas turbines.

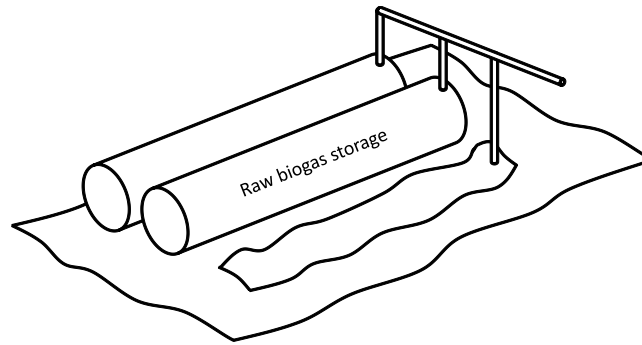


Figure 8.3: Raw biogas storage to decouple the biogas upgrading from the biogas production process.

8.3 Outlook

In general, membrane processes are easy to operate and can start and shut down in short periods. Thus, the three stage gas permeation process is particularly interesting for smoothening peaks in the electrical grid. Here, the bioas upgrading process only operates when excessive solar and wind power is available. In case that solar and wind power cannot cover the electrical base demand, the biogas prior injected to the natural gas grid can efficiently be converted into electrical energy by driving gas turbines or large combined heat and power cycles. Figure 8.2 illustrates such a process configuration. To operate this process large raw gas storage tanks are required. Concepts to store large quantities of raw gas are under investigation. For example, long robust polymer tubes with diameters of less than 2 m and a length of approximately 30 m have been installed on underused areas in the agricultural production (see Figure 8.3). Vertical constructions would even reduce the footprint of such systems.

Biogas upgrading processes do not only provide a CH_4 rich product but also an exhaust gas stream enriched in CO_2 . The CO_2 mole fraction in the exhaust gas can be as high as 99 % which is attractive for chemical processes where CO_2 is used as a feedstock to supply carbon. One interesting example is the production of formic acid [194] which is a base chemical with a world production of 517000 tons/a (2003) [195].

Together with H_2 , CO_2 can be used as feedstock for methanation [196]. This is particularly interesting for biogas upgrading due to a further increase in the CH_4 yield. The reaction equation is [197]:

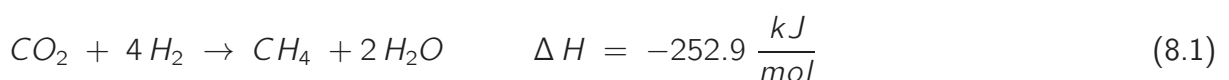


Figure 8.4 shows a process in which the permeate of the third membrane stage is fed to a methanation reactor. The H_2 required for the methanation can be provided by electrolysis of water (17 $\text{MJ}/\text{m}^3(\text{STP})$) [178]. For H_2 capacities of more than 500 $\frac{\text{m}^3(\text{STP})}{\text{h}}$ H_2 is commonly produced by

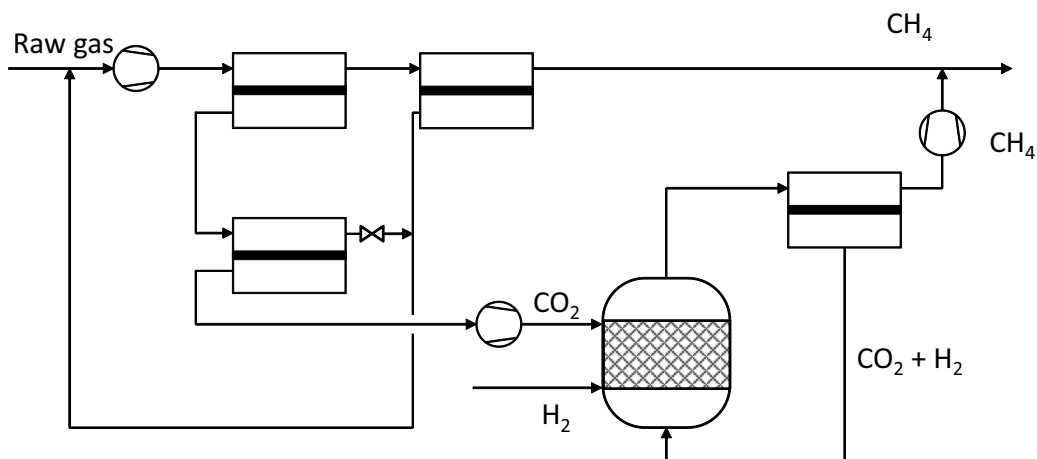


Figure 8.4: Three stage biogas upgrading process which is combined with a methanation reactor. Here, the CO₂ in the exhaust gas of the upgrading process is the feed stock for methanation reaction. The product gas from the methanation contains CH₄, CO₂ and H₂. An additional gas permeation unit upgrades the CH₄ content and recycles the unreacted CO₂ and H₂ to the methanation reactor.

steam reforming of natural gas or naphtha with a downstream pressure swing adsorption unit to separate H₂ and CO [198]. However, in case that electrical energy is inexpensively available from renewable sources, electrolysis of water can be applied for large scale H₂ production.

Bibliography

- [1] G. Erdmann and P. Zweifel. *Energieökonomik: Theorie und Anwendungen*. Springer, 2008.
- [2] M. Scholz, T. Melin, and M. Wessling. Transforming biogas into biomethane using membrane technology. *Renewable and Sustainable Energy Reviews*, 2012.
- [3] M. Specht, F. Baumgart, B. Feigl, V. Frick, B. Stürmer, U. Zuberbühler, M. Sterner, and G. Waldstein. Biogas upgrading with hydrogen a new concept for storing bio energy and renewable power in the natural gas grid. Biogasaufbereitung zu Biomethan 2010, Bad Hersfeld, Germany, 2010.
- [4] DVGW-Arbeitsblatt. Nr. 262 Nutzung von Gasen aus regenerativen Quellen in der öffentlichen Gasversorgung. 2004.
- [5] E. Weidner, W. Urban, K. Girod, and H. Lohmann. Technologien und Kosten der Biogasaufbereitung und Einspeisung in das Erdgasnetz. Ergebnisse der Markterhebung 2007 - 2008. Technical report, 2008.
- [6] P. Weiland. Biogas production: current state and perspectives. *Applied microbiology and biotechnology*, 85(4):849–860, 2010.
- [7] M. Poschl, S. Ward, and P. Owende. Evaluation of energy efficiency of various biogas production and utilization pathways. *Applied Energy*, 87(11):3305–3321, 2010.
- [8] Y. Yampolskii, I. Pinnau, and B.D. Freeman. *Materials science of membranes for gas and vapor separation*. Wiley Online Library, 2006.
- [9] R. Baker. Future directions of membrane gas-separation technology. *Membrane Technology*, 2001(138):5–10, 2001.
- [10] M. Mulder. *Basic principles of membrane technology*. Springer, 1996.
- [11] R.L. Burns and W.J. Koros. Defining the challenges for C_3H_6/C_3H_8 separation using polymeric membranes. *Journal of Membrane Science*, 211(2):299–309, 2003.
- [12] M. Scholz, M. Wessling, and J. Balster. *Membrane Engineering for the Treatment of Gases: Gas-separation Problems with Membranes*. Royal Society of Chemistry, 2010.

- [13] T. Melin and R. Rautenbach. *Membranverfahren*. Springer, 2004.
- [14] E. Drioli and L. Giorno. *Comprehensive Membrane Science and Engineering*. Elsevier Science, 2010.
- [15] S.A. Stern, B. Krishnakumar, S.G. Charati, W.S. Amato, A.A. Friedman, and D.J. Fues. Performance of a bench-scale membrane pilot plant for the upgrading of biogas in a wastewater treatment plant. *Journal of Membrane Science*, 151(1):63–74, 1998.
- [16] T. Visser, N. Masetto, and M. Wessling. Materials dependence of mixed gas plasticization behavior in asymmetric membranes. *Journal of Membrane Science*, 306(1-2):16–28, 2007.
- [17] A. Struck. *Untersuchung und Optimierung von Hohlfasermusername für die Stickstoffanreicherung durch Gaspermeation*. PhD thesis, RWTH Aachen University, 1998.
- [18] L.T. Biegler. Advances in computer-aided process design. *Analytica Chimica Acta*, 210:97–108, 1988.
- [19] H. Yeomans and I.E. Grossmann. A systematic modeling framework of superstructure optimization in process synthesis. *Computers and Chemical Engineering*, 23(6):709–731, 1999.
- [20] J. Bausa and W. Marquardt. Shortcut design methods for hybrid membrane/distillation processes for the separation of nonideal multicomponent mixtures. *Industrial & Engineering Chemistry Research*, 39(6):1658–1672, 2000.
- [21] H. Chang and W.C. Hou. Optimization of membrane gas separation systems using genetic algorithm. *Chemical Engineering Science*, 61(16):5355–5368, 2006.
- [22] L.T. Biegler and I.E. Grossmann. Retrospective on optimization. *Computers & Chemical Engineering*, 28(8):1169–1192, 2004.
- [23] R.E. Rosenthal and A. Brooke. *GAMS: a user's guide*. GAMS Development Corporation, 2007.
- [24] N. Sahinidis and M. Tawarmalani. Baron solver manual. *GAMS Development Corporation, Washington, DC, USA*, 2009.
- [25] J. Marriott and E. Sørensen. The optimal design of membrane systems. *Chemical Engineering Science*, 58(22):4991–5004, 2003.
- [26] A.K. Datta and P.K. Sen. Optimization of membrane unit for removing carbon dioxide from natural gas. *Journal of Membrane Science*, 283(1-2):291–300, 2006.
- [27] R. Qi and M.A. Henson. Membrane system design for multicomponent gas mixtures via mixed-integer nonlinear programming. *Computers & Chemical Engineering*, 24(12):2719–2737, 2000.

- [28] I.K. Kookos. A targeting approach to the synthesis of membrane networks for gas separations. *Journal of Membrane Science*, 208(1-2):193–202, 2002.
- [29] R.V.S. Uppaluri, R. Smith, P. Linke, and A.C. Kokossis. On the simultaneous optimization of pressure and layout for gas permeation membrane systems. *Journal of Membrane Science*, 280(1-2):832–848, 2006.
- [30] H. Lababidi, G.A. Al-Enezi, and H.M. Ettouney. Optimization of module configuration in membrane gas separation. *Journal of Membrane Science*, 112(2):185–197, 1996.
- [31] W.D. Seider, J.D. Seader, and D.R. Lewin. *Product & Process Design Principles: Synthesis, Analysis And Evaluation*. Wiley, 2009.
- [32] Inc. Aspen Technology. Aspen one, 2006.
- [33] K. Ohlrogge, J. Wind, C. Scholles, and T. Brinkmann. Membranverfahren zur Abtrennung organischer Dämpfe in der chemischen und petrochemischen Industrie. *Chemie Ingenieur Technik*, 77(5):527–537, 2005.
- [34] D.T. Coker, T. Allen, B.D. Freeman, and G.K. Fleming. Nonisothermal model for gas separation hollow-fiber membranes. *AIChE Journal*, 45(7):1451–1468, 1999.
- [35] J.I. Marriott, E. Sørensen, and I.D.L. Bogle. Detailed mathematical modelling of membrane modules. *Computers & Chemical Engineering*, 25(4-6):693–700, 2001.
- [36] J. Marriott and E. Sørensen. A general approach to modelling membrane modules. *Chemical Engineering Science*, 58(22):4975–4990, 2003.
- [37] S.P. Kaldis, G.C. Kapantaidakis, T.I. Papadopoulos, and G.P. Sakellariopoulos. Simulation of binary gas separation in hollow fiber asymmetric membranes by orthogonal collocation. *Journal of Membrane Science*, 142(1):43–59, 1998.
- [38] S.P. Kaldis, G.C. Kapantaidakis, and G.P. Sakellariopoulos. Simulation of multicomponent gas separation in a hollow fiber membrane by orthogonal collocation–hydrogen recovery from refinery gases. *Journal of Membrane Science*, 173(1):61–71, 2000.
- [39] S. Giglia, B. Bikson, J.E. Perrin, and A.A. Donatelli. Mathematical and experimental analysis of gas separation by hollow fiber membranes. *Industrial & Engineering Chemistry Research*, 30(6):1239–1248, 1991.
- [40] R.A. Davis. Simple gas permeation and pervaporation membrane unit operation models for process simulators. *Chemical Engineering & Technology*, 25(7):717–722, 2002.

- [41] T. Katoh, M. Tokumura, H. Yoshikawa, and Y. Kawase. Dynamic simulation of multicomponent gas separation by hollow-fiber membrane module: Nonideal mixing flows in permeate and residue sides using the tanks-in-series model. *Separation and Purification Technology*, 2010.
- [42] A. Makaruk and M. Harasek. Numerical algorithm for modelling multicomponent multipermeator systems. *Journal of Membrane Science*, 344(1-2):258–265, 2009.
- [43] I. Esteves and JPB Mota. Simulation of a new hybrid membrane/pressure swing adsorption process for gas separation. *Desalination*, 148(1-3):275–280, 2002.
- [44] R. Rautenbach, R. Knauf, A. Struck, and J. Vier. Simulation and design of membrane plants with Aspen Plus. *Chemical Engineering & Technology*, 19(5):391–397, 1996.
- [45] M. Scholz, T. Harlacher, T. Melin, and M. Wessling. Modeling gas permeation by linking non-ideal effects. *Industrial & Engineering Chemistry Research*, 2012.
- [46] R. Pielke, T. Wigley, and C. Green. Dangerous assumptions. *Nature*, 452(7187):531–532, 2008.
- [47] A. Petersson and A. Wellinger. Biogas upgrading technologies—developments and innovations. *IEA-Task*, 37:20, 2009.
- [48] T. Bley, C. Kirsten, and M.D. Weitze. Bioenergie in Deutschland. *Biotechnologische Energieumwandlung*, pages 13–35, 2009.
- [49] L. Deng and M.B. Hägg. Techno-economic evaluation of biogas upgrading process using CO₂ facilitated transport membrane. *International Journal of Greenhouse Gas Control*, 2010.
- [50] J. Markard, M. Stadelmann, and B. Truffer. Prospective analysis of technological innovation systems: Identifying technological and organizational development options for biogas in Switzerland. *Research Policy*, 38(4):655–667, 2009.
- [51] J.R.H. Ross, A.N.J. Van Keulen, M.E.S. Hegarty, and K. Seshan. The catalytic conversion of natural gas to useful products. *Catalysis today*, 30(1-3):193–199, 1996.
- [52] R. Raven and K.H. Gregersen. Biogas plants in denmark: successes and setbacks. *Renewable and Sustainable Energy Reviews*, 11(1):116–132, 2007.
- [53] F. Hofmann and A. Plaettner. Einspeisung von Biogas in das Erdgasnetz. Technical report, 2006.
- [54] C. Anderson. Landfill gas upgrading to pipeline quality in the US. World Congress of Bioenergy 2011, Dalian, China, 2011.

- [55] G. Resch, A. Held, T. Faber, C. Panzer, F. Toro, and R. Haas. Potentials and prospects for renewable energies at global scale. *Energy Policy*, 36(11):4048–4056, 2008.
- [56] P. Moriarty and D. Honnery. What is the global potential for renewable energy? *Renewable and Sustainable Energy Reviews*, 16(1):244 – 252, 2012.
- [57] P. McKendry. Energy production from biomass (part 1): overview of biomass. *Bioresource Technology*, 83(1):37–46, 2002.
- [58] A. Jess. What might be the energy demand and energy mix to reconcile the world 's pursuit of welfare and happiness with the necessity to preserve the integrity of the biosphere? *Energy Policy*, 38(8):4663–4678, 2010.
- [59] J.B. Holm-Nielsen, T. Al Seadi, and P. Oleskowicz-Popiel. The future of anaerobic digestion and biogas utilization. *Bioresource Technology*, 100(22):5478–5484, 2009.
- [60] S. Sumathi, S.P. Chai, and A.R. Mohamed. Utilization of oil palm as a source of renewable energy in malaysia. *Renewable and Sustainable Energy Reviews*, 12(9):2404–2421, 2008.
- [61] J.F.K. Akinbami, M.O. Ilori, T.O. Oyebisi, I.O. Akinwumi, and O. Adeoti. Biogas energy use in nigeria: current status, future prospects and policy implications. *Renewable and Sustainable Energy Reviews*, 5(1):97–112, 2001.
- [62] R. Arthur, M.F. Baidoo, and E. Antwi. Biogas as a potential renewable energy source: A ghanaian case study. *Renewable Energy*, 2010.
- [63] M. Berglund and P. Borjesson. Assessment of energy performance in the life-cycle of biogas production. *Biomass and Bioenergy*, 30(3):254–266, 2006.
- [64] S. Rasi, A. Veijanen, and J. Rintala. Trace compounds of biogas from different biogas production plants. *Energy*, 32(8):1375–1380, 2007.
- [65] S. Rasi, J. Lantelä, and J. Rintala. Trace compounds affecting biogas energy utilisation - A review. *Energy Conversion and Management*, 52(12):3369–3375, 2011.
- [66] T. Patterson, S. Esteves, R. Dinsdale, and A. Guwy. An evaluation of the policy and techno-economic factors affecting the potential for biogas upgrading for transport fuel use in the UK. *Energy Policy*, 2011.
- [67] Deutscher Verein des Gas und Wasserfaches e.V. DVGW Gas. Arbeitsblatt G 260 Gasbeschaffenheit, 2000.
- [68] M.M. Foss and C.E.E. Head. Interstate natural gas–quality specifications & interchangeability. *Center for Energy Economics, Bureau of Economic Geology, University of Texas at Austin, December*, 2004.

- [69] R.W. Baker and K. Lokhandwala. Natural Gas Processing with Membranes: An Overview. *Industrial & Engineering Chemistry Research*, 47(7):2109–2121, 2008.
- [70] H. Yang, Z. Xu, M. Fan, R. Gupta, R.B. Slimane, A.E. Bland, and I. Wright. Progress in carbon dioxide separation and capture: A review. *Journal of Environmental Sciences*, 20(1):14–27, 2008.
- [71] S. Cavenati, C.A. Grande, A.E. Rodrigues, C. Kiener, and U. Müller. Metal Organic Framework Adsorbent for Biogas Upgrading. *Industrial & Engineering Chemistry Research*, 47(16):6333–6335, 2008.
- [72] C.A. Grande and A.E. Rodrigues. Layered Vacuum Pressure-Swing Adsorption for Biogas Upgrading. *Industrial & Engineering Chemistry Research*, 46(23):7844–7848, 2007.
- [73] A. Alonso-Vicario, J.R. Ochoa-Gómez, S. Gil-Río, O. Gómez-Jiménez-Aberasturi, C.A. Ramírez-López, J. Torrecilla-Soria, and A. Domínguez. Purification and upgrading of biogas by pressure swing adsorption on synthetic and natural zeolites. *Microporous and Mesoporous Materials*, 134(1-3):100–107, 2010.
- [74] W. Kast. Adsorption aus der Gasphase Grundlagen und Verfahren. *Chemie Ingenieur Technik*, 53(3):160–172, 1981.
- [75] R.A. Waldo and J.R. Burkinshaw. Distillation plus membrane processing of gas streams, June 26 1990. US Patent 4,936,887.
- [76] G. Göttlicher and R. Pruscsek. Comparison of CO₂ removal systems for fossil-fuelled power plant processes. *Energy Conversion and Management*, 38:S173–S178, 1997.
- [77] E. Ryckebosch, M. Drouillon, and H. Vervaeren. Techniques for transformation of biogas to biomethane. *Biomass and Bioenergy*, 2011.
- [78] S. Tessendorf, R. Gani, and M.L. Michelsen. Modeling, simulation and optimization of membrane-based gas separation systems. *Chemical Engineering Science*, 54(7):943–955, 1999.
- [79] B.D. Bhide, A. Voskericyan, and S.A. Stern. Hybrid processes for the removal of acid gases from natural gas. *Journal of Membrane Science*, 140(1):27–49, 1998.
- [80] J. Hao, P.A. Rice, and S.A. Stern. Upgrading low-quality natural gas with H₂S- and CO₂-selective polymer membranes Part I. Process design and economics of membrane stages without recycle streams. *Journal of Membrane Science*, 209(1):177–206, 2002.
- [81] K.A. Lokhandwala, I. Pinnau, Z. He, K.D. Amo, A.R. DaCosta, J.G. Wijmans, and R.W. Baker. Membrane separation of nitrogen from natural gas: A case study from membrane synthesis to commercial deployment. *Journal of Membrane Science*, 346(2):270–279, 2010.

- [82] D. Chinn, S. Okeowo, J.D. Euhus, and S. Husain. Process for upgrading natural gas with improved management of CO_2 , 2009. US Patent App. 12/361,961.
- [83] T. Brinkmann, J. Wind, and K. Ohlrogge. Membranverfahren in der Erdgasaufbereitung. *Chemie Ingenieur Technik*, 75(11):1607–1611, 2003.
- [84] M. Harasimowicz, P. Orluk, G. Zakrzewska-Trznadel, and A.G. Chmielewski. Application of polyimide membranes for biogas purification and enrichment. *Journal of Hazardous Materials*, 144(3):698–702, 2007.
- [85] S.G. Kimura and G.E. Walmet. Fuel gas purification with permselective membranes. *Separation Science and Technology*, 15(4):1115–1133, 1980.
- [86] M.M. Qiu, S.T. Hwang, and Y.K. Kao. Economic evaluation of gas membrane separator designs. *Industrial & Engineering Chemistry Research*, 28(11):1670–1677, 1989.
- [87] R. Rautenbach and K. Welsch. Treatment of landfill gas by gas permeation—pilot plant results and comparison to alternatives. *Desalination*, 90(1-3):193–207, 1993.
- [88] R. Rautenbach and W. Dahm. Gas permeation—module design and arrangement. *Chemical Engineering and Processing*, 21(3):141–150, 1987.
- [89] S. Jäschke. Evaluierung der Gaspermeation zur Einspeisung von Biogas ins Erdgasnetz. *Diploma Thesis RWTH Aachen University*, 2006.
- [90] K. Simons, K. Nijmeijer, and M. Wessling. Gas–liquid membrane contactors for CO_2 removal. *Journal of Membrane Science*, 340(1-2):214–220, 2009.
- [91] S.A.M. Marzouk, M.H. Al-Marzouqi, M.H. El-Naas, N. Abdullatif, and Z.M. Ismail. Removal of carbon dioxide from pressurized $\text{CO}_2\text{-CH}_4$ gas mixture using hollow fiber membrane contactors. *Journal of Membrane Science*, 2010.
- [92] R. Faiz and M. Al-Marzouqi. Mathematical modeling for the simultaneous absorption of CO_2 and H_2S using MEA in hollow fiber membrane contactors. *Journal of Membrane Science*, 342(1-2):269–278, 2009.
- [93] S. Basu, A.L. Khan, A. Cano-Odena, C. Liu, and I.F.J. Vankelecom. Membrane-based technologies for biogas separations. *Chemical Society Reviews*, 39(2):750–768, 2009.
- [94] S. Li, J.G. Martinek, J.L. Falconer, R.D. Noble, and T.Q. Gardner. High-pressure CO_2/CH_4 separation using SAPO-34 membranes. *Industrial & Engineering Chemistry Research*, 44(9):3220–3228, 2005.

- [95] S. Li, J.L. Falconer, R.D. Noble, and R. Krishna. Modeling Permeation of CO₂/CH₄, CO₂/N₂, and N₂/CH₄ Mixtures Across SAPO-34 Membrane with the Maxwell- Stefan Equations. *Industrial & Engineering Chemistry Research*, 46(12):3904–3911, 2007.
- [96] S. Li, M.A. Carreon, Y. Zhang, H.H. Funke, R.D. Noble, and J.L. Falconer. Scale-up of SAPO-34 Membranes for CO₂/CH₄ Separation. *Journal of Membrane Science*, 2010.
- [97] S. Jäschke, M. Ajhar, and T. Melin. Evaluierung der Gaspermeation zur Einspeisung von Biogas ins Erdgasnetz. *Energie, Wasser-Praxis*, 2008.
- [98] H. Gorissen. Temperature changes involved in membrane gas separations. *Chemical Engineering and Processing*, 22(2):63–67, 1987.
- [99] K. Welsch. *Gaspermeation - Membranwerkstoffe, Stofftransport und Anwendungsbeispiele*. PhD thesis, RWTH Aachen University, 1992.
- [100] R. Rautenbach, A. Struck, and M.F.M. Roks. A variation in fiber properties affects the performance of defect-free hollow fiber membrane modules for air separation. *Journal of Membrane Science*, 150(1):31–41, 1998.
- [101] A. Mourgues and J. Sanchez. Theoretical analysis of concentration polarization in membrane modules for gas separation with feed inside the hollow-fibers. *Journal of Membrane Science*, 252(1-2):133–144, 2005.
- [102] R.W. Baker, J.G. Wijmans, A.L. Athayde, R. Daniels, J.H. Ly, and M. Le. The effect of concentration polarization on the separation of volatile organic compounds from water by pervaporation. *Journal of Membrane Science*, 137(1-2):159–172, 1997.
- [103] A. Alpers, B. Keil, O. Ludtke, and K. Ohlrogge. Organic vapor separation: Process design with regards to high-flux membranes and the dependence on real gas behavior at high pressure applications. *Industrial & Engineering Chemistry Research*, 38(10):3754–3760, 1999.
- [104] T. Visser, G.H. Koops, and M. Wessling. On the subtle balance between competitive sorption and plasticization effects in asymmetric hollow fiber gas separation membranes. *Journal of Membrane Science*, 252(1-2):265–277, 2005.
- [105] T. Visser and M. Wessling. Auto and mutual plasticization in single and mixed gas C₃ transport through Matrimid-based hollow fiber membranes. *Journal of Membrane Science*, 312(1):84–96, 2008.
- [106] S. Kanehashi, T. Nakagawa, K. Nagai, X. Duthie, S. Kentish, and G. Stevens. Effects of carbon dioxide-induced plasticization on the gas transport properties of glassy polyimide membranes. *Journal of Membrane Science*, 298(1-2):147–155, 2007.

- [107] A. Bos, I.G.M. Pünt, M. Wessling, and H. Strathmann. Plasticization-resistant glassy polyimide membranes for CO₂/CH₄ separations. *Separation and Purification Technology*, 14(1-3):27–39, 1998.
- [108] T.C. Merkel, H. Lin, X. Wei, and R. Baker. Power plant post-combustion carbon dioxide capture: An opportunity for membranes. *Journal of Membrane Science*, 359(1-2):126–139, 2010.
- [109] D.T. Coker, B.D. Freeman, and G.K. Fleming. Modeling multicomponent gas separation using hollow-fiber membrane contactors. *AIChE Journal*, 44(6):1289–1302, 1998.
- [110] L.T. Biegler, I.E. Grossmann, and A.W. Westerberg. Systematic methods for chemical process design. 1997.
- [111] P.M. Follmann. *Membrane Gas Separation Processes for Post Combustion CO₂ Capture from Coal Fired Power Plants*. PhD thesis, RWTH Aachen University, 2010.
- [112] R.W. Baker. *Membrane technology and applications*. Wiley, 2004.
- [113] M. Ungerank, G. Baumgarten, M. Priske, and H. Roegl. Process for separation of gases, 2012. WO Patent WO 2012/00727.
- [114] A. Makaruk, M. Miltner, and M. Harasek. Membrane biogas upgrading processes for the production of natural gas substitute. *Separation and Purification Technology*, 74(1):83–92, 2010.
- [115] R. Rautenbach and K. Welsch. Treatment of landfill gas by gas permeation—pilot plant results and comparison to alternatives. *Journal of Membrane Science*, 87(1-2):107–118, 1994.
- [116] M. Miltner, A. Makaruk, and M. Harasek. Investigation of the long-term performance of an industrial-scale biogas upgrading plant with grid supply applying gas permeation membranes. *Chemical Engineering*, 21, 2010.
- [117] E. Favre, R. Bounaceur, and D. Roizard. Biogas, membranes and carbon dioxide capture. *Journal of Membrane Science*, 328(1-2):11–14, 2009.
- [118] S.S. Kapdi, V.K. Vijay, S.K. Rajesh, and R. Prasad. Biogas scrubbing, compression and storage: perspective and prospectus in Indian context. *Renewable Energy*, 30(8):1195–1202, 2005.
- [119] S. Iniyand K. Sumathy. An optimal renewable energy model for various end-uses. *Energy*, 25(6):563–575, 2000.

- [120] S. Iniyar, L. Suganthi, and T.R. Jagadeesan. Renewable energy planning for India in 21st century. *Renewable Energy*, 14(1-4):453–457, 1998.
- [121] T. Bond and M.R. Templeton. History and future of domestic biogas plants in the developing world. *Energy for Sustainable Development*, 2011.
- [122] L.C. Martins das Neves, A. Converti, and T.C. Vessoni Penna. Biogas production: New trends for alternative energy sources in rural and urban zones. *Chemical Engineering & Technology*, 32(8):1147–1153, 2009.
- [123] N. Kuwahara, M.D. Berni, and S.V. Bajay. Energy supply from municipal wastes: The potential of biogas-fuelled buses in Brazil. *Renewable Energy*, 16(1):1000–1003, 1999.
- [124] K.R. Salomon and E.E. Silva Lora. Estimate of the electric energy generating potential for different sources of biogas in Brazil. *Biomass and Bioenergy*, 33(9):1101–1107, 2009.
- [125] K. Ohlrogge, K. Ebert, B. Krause, H. Göhl, and F. Wiese. *Membranen*. Wiley-VCH, Weinheim, 2006.
- [126] M.J. Thundiyil and W.J. Koros. Mathematical modeling of gas separation permeators – for radial crossflow, countercurrent, and cocurrent hollow fiber membrane modules. *Journal of Membrane Science*, 125(2):275–291, 1997.
- [127] M.H. Murad Chowdhury, X. Feng, P. Douglas, and E. Croiset. A new numerical approach for a detailed multicomponent gas separation membrane model and AspenPlus simulation. *Chemical Engineering & Technology*, 28(7), 2005.
- [128] R. Wang, S.L. Liu, T.T. Lin, and T.S. Chung. Characterization of hollow fiber membranes in a permeator using binary gas mixtures. *Chemical Engineering Science*, 57(6):967–976, 2002.
- [129] C.Y. Pan. Gas separation by high-flux, asymmetric hollow-fiber membrane. *AIChE Journal*, 32(12):2020–2027, 1986.
- [130] E.C. Carlson. Don't gamble with physical properties for simulations. *Chemical Engineering Progress*, 92(10):35–46, 1996.
- [131] P.J. Linstrom, W.G. Mallard, National Institute of Standards, and Technology (US). NIST Chemistry WebBook, 1997.
- [132] W.J. Koros and G.K. Fleming. Membrane-based gas separation. *Journal of Membrane Science*, 83(1):1–80, 1993.
- [133] R. Rautenbach, A. Struck, T. Melin, and M.F.M. Rokhs. Impact of operating pressure on the permeance of hollow fiber gas separation membranes. *Journal of Membrane Science*, 146(2):217–223, 1998.

- [134] R. Bird, W. Stewart, and E. Lightfoot. *Transport Phenomena—Second Edition*, 2002.
- [135] M. Al-Juaied and W.J. Koros. Frame of reference effects on the performance of hollow fiber membranes. *Industrial & Engineering Chemistry Research*, 44(10):3648–3654, 2005.
- [136] R.T. Chern, W.J. Koros, and P.S. Fedkiw. Simulation of a hollow-fiber gas separator: the effects of process and design variables. *Industrial & Engineering Chemistry Process Design and Development*, 24(4):1015–1022, 1985.
- [137] M. Das and W.J. Koros. Performance of 6FDA–6FpDA polyimide for propylene/propane separations. *Journal of Membrane Science*, 365(1):399–408, 2010.
- [138] M. Pourafshari Chenar, M. Soltanieh, T. Matsuura, A. Tabe-Mohammadi, and K.C. Khulbe. The effect of water vapor on the performance of commercial polyphenylene oxide and Cardo-type polyimide hollow fiber membranes in CO₂/CH₄ separation applications. *Journal of Membrane Science*, 285(1-2):265–271, 2006.
- [139] L. Gales, A. Mendes, and C. Costa. Removal of acetone, ethyl acetate and ethanol vapors from air using a hollow fiber PDMS membrane module. *Journal of Membrane Science*, 197(1-2):211–222, 2002.
- [140] M. Al-Juaied and W.J. Koros. Performance of natural gas membranes in the presence of heavy hydrocarbons. *Journal of Membrane Science*, 274(1-2):227–243, 2006.
- [141] T. Harlacher, M. Scholz, T. Melin, and M. Wessling. Optimizing argon recovery: Membrane separation of carbon monoxide at high concentrations via the water gas shift. *Industrial & Engineering Chemistry Research*, 51(38):12463–12470, 2012.
- [142] R.W.H. Sargent and K. Gaminibandara. Optimum design of plate distillation columns. *Optimization in action*, pages 267–314, 1976.
- [143] M.M. El-Halwagi and V. Manousiouthakis. Synthesis of mass exchange networks. *AIChE Journal*, 35(8):1233–1244, 1989.
- [144] R. Qi and M.A. Henson. Optimal design of spiral-wound membrane networks for gas separations. *Journal of Membrane Science*, 148(1):71–89, 1998.
- [145] E. Kondili, C.C. Pantelides, and R.W.H. Sargent. A general algorithm for short-term scheduling of batch operations - I. MILP formulation. *Computers & Chemical Engineering*, 17(2):211–227, 1993.
- [146] E.M. Smith. *On the optimal design of continuous processes*. PhD thesis, Imperial College London (University of London), 1996.

- [147] P. Linke and A. Kokossis. Attainable reaction and separation processes from a superstructure-based method. *AIChE journal*, 49(6):1451–1470, 2003.
- [148] L.M. Robeson. The upper bound revisited. *Journal of Membrane Science*, 320(1):390–400, 2008.
- [149] H.M. Guthrie. Capital cost estimation for the chemical and process industries. *Chemical Engineering*, 32:463, 1969.
- [150] H.G. Hirschberg. *Handbuch Verfahrenstechnik und Anlagenbau: Chemie, Technik und Wirtschaftlichkeit*. Springer, 1999.
- [151] C.M. Zimmerman and W.J. Koros. Polypyrrolones for membrane gas separations. I. Structural comparison of gas transport and sorption properties. *Journal of Polymer Science Part B: Polymer Physics*, 37(12):1235–1249, 1999.
- [152] U. Hommerich and R. Rautenbach. Design and optimization of combined pervaporation/distillation processes for the production of MTBE. *Journal of Membrane Science*, 146(1):53–64, 1998.
- [153] H.E. Ehresmann. *Untersuchungen zur Methananreicherung von Biogas durch Gaspermeation*. PhD thesis, RWTH Aachen University, 1990.
- [154] G.R. Bouton and W.L. Luyben. Optimum Economic Design and Control of a Gas Permeation Membrane Coupled with the Hydrodealkylation (HDA) Process. *Industrial & Engineering Chemistry Research*, 47(4):1221–1237, 2008.
- [155] F. Borgmann. *Modellierung und Optimierung von Gaspermeationsanlagen*. Master's thesis, RWTH Aachen University, 1990.
- [156] M. Tuinier and M. van Sint Annaland. Biogas purification using cryogenic packed bed technology. 2012.
- [157] D.E. Gottschlich and D.L. Roberts. Energy minimization of separation processes using conventional/membrane hybrid systems. Technical report, EG and G Idaho, Inc., Idaho Falls, ID (USA), 1990.
- [158] E.W. Crabtree, M.M. El-Halwagi, and R.F. Dunn. Synthesis of hybrid gas permeation membrane/condensation systems for pollution prevention. *Journal of the Air & Waste Management Association*, 48(7):616–626, 1998.
- [159] T. Burdyny and H. Struchtrup. Hybrid membrane/cryogenic separation of oxygen from air for use in the oxy-fuel process. *Energy*, 35(5):1884–1897, 2010.

- [160] P. Shao, M. Dal-Cin, A. Kumar, H. Li, and D.P. Singh. Design and economics of a hybrid membrane–temperature swing adsorption process for upgrading biogas. *Journal of Membrane Science*, 2012.
- [161] M.F.J. Dijkstra, S. Bach, T. Brinkmann, K. Ebert, and K. Ohlrogge. Hybridverfahren zur Trennung von Methanol/Isopropanol/Wasser-Gemischen. *Chemie Ingenieur Technik*, 75(11), 2003.
- [162] K. Kraemer, A. Harwardt, R. Bronneberg, and W. Marquardt. Separation of butanol from acetone-butanol-ethanol fermentation by a hybrid extraction-distillation process. *Computer Aided Chemical Engineering*, 28:7–12, 2010.
- [163] F. Lipnizki, R.W. Field, and P.K. Ten. Pervaporation-based hybrid process: a review of process design, applications and economics. *Journal of Membrane Science*, 153(2):183–210, 1999.
- [164] W. Marquardt, S. Kossack, and K. Kraemer. A framework for the systematic design of hybrid separation processes. *Chinese Journal of Chemical Engineering*, 16(3):333–342, 2008.
- [165] R.W. Baker, J.G. Wijmans, and J.H. Kaschemekat. The design of membrane vapor-gas separation systems. *Journal of Membrane Science*, 151(1):55–62, 1998.
- [166] J.B. Haelssig, A.Y. Tremblay, and J. Thibault. A new hybrid membrane separation process for enhanced ethanol recovery: Process description and numerical studies. *Chemical Engineering Science*, 68(1):492–505, 2012.
- [167] Y. Huang, R.W. Baker, and L.M. Vane. Low-energy distillation-membrane separation process. *Industrial & Engineering Chemistry Research*, 49(8):3760–3768, 2010.
- [168] J.A. Caballero, I.E. Grossmann, M. Keyvani, and E.S. Lenz. Design of hybrid distillation- vapor membrane separation systems. *Industrial & Engineering Chemistry Research*, 48(20):9151–9162, 2009.
- [169] W.I. Echt. Hybrid systems-combining technologies leads to more efficient gas conditioning. In *Proceedings of the Laurance Reid gas conditioning conference*, 2002.
- [170] B. Belaissaoui, Y. Le Moullec, D. Willson, and E. Favre. Hybrid membrane cryogenic process for post-combustion CO₂ capture. *Journal of Membrane Science*, 2012.
- [171] X. Feng, C.Y. Pan, J. Ivory, and D. Ghosh. Integrated membrane/adsorption process for gas separation. *Chemical Engineering Science*, 53(9):1689–1698, 1998.
- [172] X. Feng, C.Y. Pan, and J. Ivory. Pressure swing permeation: novel process for gas separation by membranes. *AIChE Journal*, 46(4):724–733, 2000.

- [173] P. Bernardo, E. Drioli, and G. Golemme. Membrane gas separation: a review/state of the art. *Industrial & Engineering Chemistry Research*, 48(10):4638–4663, 2009.
- [174] P. Bernardo, A. Criscuoli, G. Clarizia, G. Barbieri, E. Drioli, G. Fleres, and M. Picciotti. Applications of membrane unit operations in ethylene process. *Clean Technologies and Environmental Policy*, 6(2):78–95, 2004.
- [175] W. Althaus and W. Urban. Analyse und Bewertung der Nutzungsmöglichkeiten von Biomasse - Band 3: Biomassevergasung, Technologien und Kosten der Gasaufbereitung und Potentiale der Biogaseinspeisung in Deutschland. Technical report, Fraunhofer Institut UMSICHT, 2005.
- [176] W. Urban, H. Lohmann, and K. Giro. Beseitigung technischer, rechtlicher und ökonomischer Hemmnisse bei der Einspeisung biogener Gase in das Erdgasnetz zur Reduzierung klimarelevanter Emissionen durch Aufbau und Anwendung einer georeferenzierten Datenbank. Band 4: Technologien und Kosten der Biogasaufbereitung und Einspeisung in das Erdgasnetz. Abschlussbericht für das BMBF-Verbundprojekt "Biogaseinspeisung" (Version 4.17). Technical report, Fraunhofer-Institut für Umwelt-, Sicherheits- und Energietechnik UMSICHT, 2009.
- [177] M. Reppich, S. Datzmann, X. Li, S. Rosenbauer, C. Schlecht, and S. Tschepur. Vergleich verschiedener Aufbereitungsverfahren von Biogas zur Einspeisung in das Erdgasnetz. *Chemie Ingenieur Technik*, 81(3):211–223, 2009.
- [178] M. Baerns, A. Behr, A. Brehm, J. Gmehling, H. Hofmann, U. Onken, and A. Renken. *Technische Chemie*. WILEY-VCH, 2006.
- [179] L. Wolff. Model based structural optimization of biogas upgrading processes. *RWTH Aachen University*, 2012. Diploma Thesis.
- [180] R. Goedecke. *Fluidverfahrenstechnik: Grundlagen, Methodik, Technik, Praxis*, volume 1. Wiley-VCH Verlag GmbH, 2006.
- [181] W.R.A. Vauck and H.A. Müller. *Grundoperationen chemischer Verfahrenstechnik*. VEB Deutscher Verlag für Grundstoffindustrie, 2000.
- [182] R.H. Perry and D.W. Green. *Perry's chemical engineers' handbook*. McGraw-Hill New York, 2008.
- [183] G.Q. Wang, X.G. Yuan, and K.T. Yu. Review of mass-transfer correlations for packed columns. *Industrial & engineering chemistry research*, 44(23):8715–8729, 2005.
- [184] R.F. Strigle. *Packed tower design and applications: random and structured packings*. Gulf Publishing Company, 1994.

- [185] S. Falss. Biogas upgrading: Simulation and economic evaluation of different processes. Technical report, RWTH Aachen University, Studienarbeit, 2011.
- [186] L.E. Øi. Removal of CO₂ from exhaust gas.
- [187] K. Lucas. *Thermodynamik*. Springer DE, 2007.
- [188] L. Polák. Modeling absorption drying of natural gas. *NTNU, May*, 2009.
- [189] L.E. Øi and E. Tyvand Selstø. Process simulation of glycol regeneration. In *GPA Europe's meeting in Bergen*, 2002.
- [190] A. Bahadori and H.B. Vuthaluru. Simple methodology for sizing of absorbers for TEG (triethylene glycol) gas dehydration systems. *Energy*, 34(11):1910–1916, 2009.
- [191] D. Bathen and M. Breitbach. *Adsorptionstechnik*. Springer Verlag, 2001.
- [192] S. Klinski. Einspeisung von Biogas in das Erdgasnetz. *Hrsg.: Fachagentur Nachwachsende Rohstoffe eV, Gülzow*, 2, 2006.
- [193] S. Ramesohl, K. Arnold, M. Kaltschmitt, F. Scholwin, F. Hofmann, A. Plättner, M. Kalies, S. Lulies, G. Schröder, W. Althaus, et al. Analyse und Bewertung der Nutzungsmöglichkeiten von Biomasse. Endbericht: Band 3: Biomassevergasung, Technologien und Kosten der Gasaufbereitung und Potenziale der Biogaseinspeisung in Deutschland. 2005.
- [194] W. Leitner. Carbon dioxide as a raw material: the synthesis of formic acid and its derivatives from CO₂. *Angewandte Chemie International Edition in English*, 34(20):2207–2221, 1995.
- [195] H.J. Arpe. *Industrielle Organische Chemie*. WILEY-VCH, 2006.
- [196] T. Trost, S. Horn, M. Jentsch, and M. Sterner. Erneuerbares Methan: Analyse der CO₂-Potenziale für Power-to-Gas Anlagen in Deutschland. *Zeitschrift für Energiewirtschaft*, 36(3):173–190, 2012.
- [197] W. Wei and G. Jinlong. Methanation of carbon dioxide: an overview. *Frontiers of Chemical Science and Engineering*, 5(1):2–10, 2011.
- [198] Air Liquide. Wasserstoff On-Site, June 2013.

Curriculum vitae

Marco Scholz

Born April 10th 1983 in Dortmund

| | |
|------------|---|
| 1999–2002 | Mallinckrodt-Gymnasium, Dortmund |
| 2002–2003 | Civilian service Lebenshilfe, Dortmund |
| 2003–2005 | Basic studies in mechanical engineering at RWTH Aachen |
| 2005–2008 | Advanced studies in chemical engineering at RWTH Aachen |
| 2005–2013 | Advanced studies in economics at RWTH Aachen |
| 2006 | Advanced studies abroad at NTNU Trondheim, Norway |
| since 2009 | Chair for Chemical Process Engineering RWTH Aachen |

December 30, 2013